UNIVERSITY OF SOUTHAMPTON

FACULTY OF ENGINEERING, SCIENCE & MATHEMATICS

School of Chemistry

Investigations into Lipoic Acid Biosynthesis

by

Penny Bryant

Thesis for the degree of Doctor of Philosophy

September 2007

UNIVERSITY OF SOUTHAMPTON

<u>ABSTRACT</u>

FACULTY OF ENGINEERING, SCIENCE AND MATHEMATICS

SCHOOL OF CHEMISTRY

<u>Doctor of Philosophy</u>

INVESTIGATIONS INTO LIPOIC ACID BIOSYNTHESIS

by Penny Bryant

The protein lipoyl synthase (LipA) is essential for lipoic acid biosynthesis via sulfur insertions at the C6 and C8 positions of a protein-bound octanoyl group. LipA from *Escherichia coli* binds two $[4Fe-4S]^{1+/2+}$ and is a member of the radical SAM superfamily of proteins. To facilitate mechanistic investigations into LipA dependent lipoyl synthesis, a novel *in vitro* assay has been developed which makes use of synthetic peptide substrates. These peptides contain an N(ε)-octanoyl lysine residue, corresponding in sequence to the lipoyl binding domain of the E2 subunit of pyruvate dehydrogenase. The activity LipA from *Sulfolobus solfataricus* was measured using these substrate analogues.

The optimal temperature for the *S. solfataricus* LipA dependent formation of the lipoyl group was found to be 60 °C. Time dependent activity of LipA has been investigated over a wide range of temperatures (23-60 °C) and rate constants approximated for the observed rates of loss of octanoyl starting material and lipoyl formation at each temperature. This has allowed calculation of rate constants for the overall rate. kinetic analysis over a range of temperatures has allowed the activation energy for overall lipoyl formation (47.2 ± 5.4 kJ/mol) and for sulfur insertion at C6 (38.3 ± 4.9 kJ/mol) and C8 (46.9 ± 5.7 kJ/mol) to be determined

In all experiments using of *S. solfataricus* LipA, reconstitution with exogenous iron and sulfide was found to be essential for activity and spectroscopic studies have been carried out which show that *S. solfataricus* LipA can bind two $[4Fe-4S]^{1+/2+}$ and therefore closely resembles *E. coli* LipA. The mechanistic roles of these clusters have been investigated and EPR spectroscopy suggested that SAM bound to at least one of

the clusters. Biochemical studies have also indicated that one cluster may act as the source of sulfur during lipoyl formation.

Contents

Appendix 1

Scripts used for fitting timecourse data using DYNAFIT

List of Figures

List of Schemes

List of tables

Acknowledgements

I would like to warmly thank Peter Roach his enthusiastic supervision throughout this work and help in the process of writing this thesis. I am grateful for his interesting thoughts and ideas throughout the project and for his practical advice.

I thank those here mentioned for their contributions made to this work; John Langley and Julie Herniman (mass spectrometry), Joan Street, Neil Wells & Stuart Findlow (NMR) and Shirley Fairhurst and David Lowe (EPR) for their expert help.

I would particularly like to thank Marco for all the work he did on LipA before my arrival, particularly making the plasmid for expression of *S. solfataricus* LipA without which this project would not have been possible. Thanks also for passing on your knowledge, teaching me how everything works in the lab and helping me fix the HPLC when it went wrong.

I would also like to give special thanks to Rob for proof reading this thesis and for all his support and advice throughout this project.

Many thanks also to my parents for their continued encouragement and support, and for putting a roof over my head whilst I wrote this thesis. Thank you also to Paul for all your help and patience and for keeping me smiling.

Finally thanks to all members of the Roach, Neylon and Brown groups who made life on the fifth floor interesting and enjoyable during my three years in Southampton.

Abbreviations

6MT	6-thiooctanoyl
8MT	8-thiooctanoyl
Å	Ångström
ACP	Acyl carrier protein
Ado·	5'-Deoxyadenosyl radical
AdoH	5'-Deoxyadenosine
Arg	Arginine
ARR-AE	Anaerobic ribonucleotide reductase activating enzyme
BioB	Biotin synthase
C	Cysteine
CFL	5(6)-Carboxyfluorescein
CoA	Coenzyme A
Cys	Cysteine
DCC	Dicyclohexylcarbodiimide
DCM	Dichloromethane
Dde	1-(4,4-Dimethyl-2,6-dioxocyclohexylidene) ethyl group
DHL	Dihydrolipoyl
DIC	Diisopropylcarbodiimide
DIPEA	Diisopropylethylamine
DMAP	4-(Dimethylamino) pyridine
DMF	Dimethylformamide
DTB	Dethiobiotin
DTT	Dithiothreitol
E1	Pyruvate decarboxylase
E2	Dihydrolipoate transacetylase
E3	Dihydrolipoyl dehydrogenase
E. coli	*Escherichia coli*
ENDOR	Electron nuclear double resonance
EPR	Electron paramagnetic resonance
FAD	Flavin adenine dinucleotide
FldA	Flavodoxin
FPLC	Fast protein liquid chromatography

Fpr	Favodoxin NADP$^+$ reductase
Fmoc	9-Fluorenylmethyloxycarbonyl
g	Gram
GC-MS	Gas chromatography-mass spectrometry
Glu	Glutamic acid
h	hour
HemN	Coproporphyrinogen III oxidase
HEPES	4-(2-Hydroxyethyl)-1-piperazineethanesulfonic acid
His	Histidine
His$_6$-tag	Hexa-histidine tag
HOBt	Hydroxybenzotriazole
HPLC	High performance liquid chromatography
K	Kelvin
KAM	Lysine 2,3-aminomutase
kDa	Kilo dalton
L	Litre
LC-MS	Liquid chromatography mass spectrometry
Lip	Lipoyl
LipA	Lipoyl synthase
LipB	Octanoyl (lipoyl)-ACP:protein-N-octanoyl(lipoyl)transferase
LplA	Lipoate protein ligase
MALDI-TOF	Matrix-assisted laser desorption/ionization
MiaB	2-Methylthio-N-6-isopentyl adenosine synthase
min	Minutes
MoaA	Molybdenum cofactor biosynthetic protein
mV	Millivolts
NAD$^+$	Nicotinamide adenine dinucleotide phosphate
NADPH	Nicotinamide adenine dinucleotide phosphate, reduced
nm	Nanometer
NMP	N-methylpyrrolidone
NMR	Nuclear magnetic resonance
Oct	Octanoyl
PDH	Pyruvate dehydrogenase
Pfs	(MTA)/S-Adenosylhomocysteine nucleosidase

PFL-AE	Pyruvate formate lyase activating enzyme
PLP	Pyridoxal-5'-phosphate
PyBOP	Benzotriazolyloxy-tris[pyrrolidino]-phosphonium hexafluorophosphate
RNA	Ribonucleic acid
SAM	S-Adenosyl-L-methionine
SDS	Sodium dodecyl sulphate
SDS-PAGE	SDS polyacrylamide gel electrophoresis
TCA	Trichloroacetic acid
TCEP	Tris (2-carboxyethyl) phosphine
TEMED	N,N,N',N'-Tetramethylethylenediamine
TFA	Trifluoroacetic acid
THF	Tetrahydrofolate
ThiH	Tyrosine lyase
TIM	Triosephosphate isomerase
Thr	Threonine
TPP	Thiamine pyrophosphate
UV	ultraviolet

Notations

In this report, gene names are quoted in italics with no capitalization of the first letter, e.g. *lipA*.

Gene products are named in normal type, with first letter capitalized, e.g. LipA.

1

Chapter 1   Introduction

1.1   α-Lipoic acid

α-Lipoic acid (1,2-dithiolane-3-pentanoic acid, thioctic acid) **1** is a biomolecule which is ubiquitous amongst prokaryotic and eukaryotic organisms. The compound was first isolated in 1951 as a pale yellow crystalline solid (*1*) and subsequent characterisation determined that lipoic acid is sulfur containing carboxylic acid (fig. 1.1) (*2*). The molecule has two sulfur atoms which are bound to the C6 and C8 positions of an eight carbon long chain and form a disulfide bond to give a 1,2-dithiolane ring. The molecule has a chiral centre at C6 and naturally occurring lipoic acid exists as the R-enantiomer. Reduction of the disulfide bond generates dihydrolipoic acid **2** (fig. 1.1), an antioxidant that has been identified as a potential treatment for numerous conditions including diabetes insipidus and Alzheimer's disease (*3-5*).
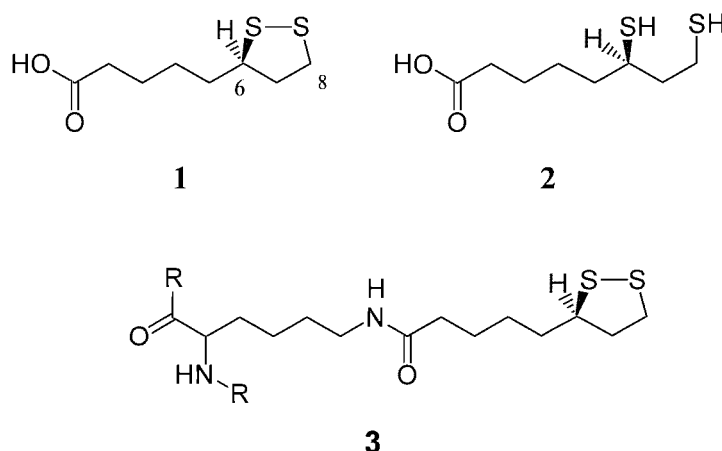
Figure 1.1 Structures of α-lipoic acid **1** and dihydrolipoic acid **2** and protein bound lipoic acid **3**, covalently bound to a lysine residue via an amide bond.

Intracellularly lipoic acid exists primarily as protein bound lipoamide **3** (fig 1.1). The acid forms an amide bond with the ε-amino group of specific lysine residues within certain enzymes for which it serves as a cofactor. In this form the lipoyl group mediates several essential metabolic pathways.

1.2   Biochemical function of lipoic acid

Lipoic acid is required for the catalytic activity of several multienzyme complexes involved in reactions essential for cellular function (fig. 1.2) (*6*). It functions as a cofactor for enzymes that catalyse decarboxylation of 2-oxoacids, for example, pyruvate dehydrogenase (PDH) (*7*), and is also utilised by the glycine cleavage system (*8*). These proteins are large aggregates of different enzymes and the lipoyl cofactor is bound to specific subunits of these complexes.
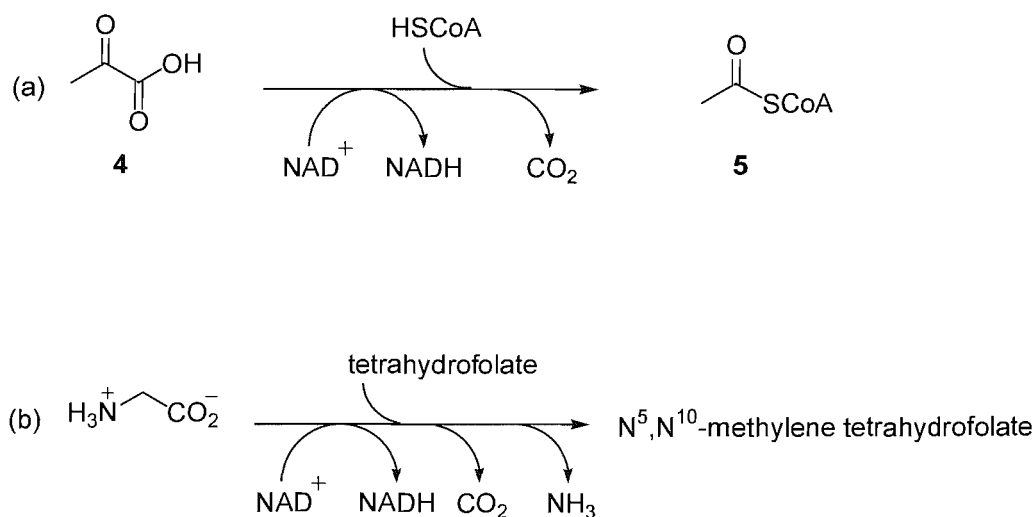
Figure 1.2 Reactions catalysed by enzymes using lipoic acid as a cofactor (a) conversion of pyruvate to acetyl CoA by pyruvate dehydrogenase (b) reaction of glycine with tetrahydrofolate to form N^5,N^{10} methylene THF catalysed by the glycine cleavage system.

1.2.1   Pyruvate dehydrogenase

The role of lipoic acid in 2-oxoacid decarboxylases can be exemplified by the reactions catalysed by the PDH multienzyme complex, which result in the formation of acetyl coenzyme A (acetyl-CoA) **5** (fig. 1.2) from pyruvate **4** (fig. 1.2). PDH is comprised of three subunits; pyruvate decarboxylase (E1), dihydrolipoate transacetylase (E2) and dihydrolipoyl dehydrogenase (E3) (*9*). Multiple copies of subunits E1 and E3 are located at the periphery and have thiamine pyrophosphate (TPP) and flavin adenine dinucleotide (FAD) as cofactors respectively. At the core of the complex are several copies of the E2 subunit, which contains a β-turn that forms

the lipoyl binding site and to which lipoic acid is covalently bound (fig. 1.3) The E2 subunit is responsible for acyl transfer between the subunits of PDH and this is facilitated by the formation of a 1.5 nm long flexible 'swinging arm' upon binding of lipoic acid with the lysine residue **3** (fig 1.1) (*6, 7*).
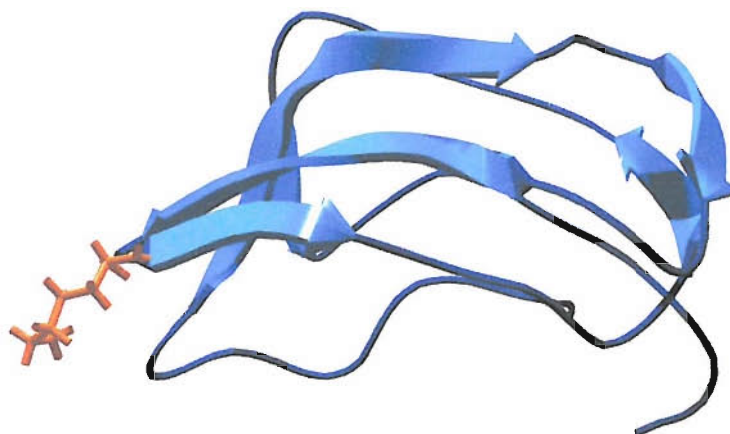
Figure 1.3 NMR structure of the E2 lipoyl domain (residues 1-79 of the E2 polypeptide chain) of *Bacillus stearothermophilus* pyruvate dehydrogenase; coordinates taken from (*10*). The lysine residue involved in lipoyl binding is shown in orange. Coordinates were downloaded from the protein data bank and manipulated in Swiss PDB viewer.

The sequence of reactions catalysed by PDH (fig. 1.4) proceeds as follows: (a) nucleophilic attack of the TPP carbanion from the E1 subunit on the keto carbon of pyruvate is followed by decarboxylation to yield hydroxyethyl-TPP; (b) transfer of the hydroxyethyl group to lipoic acid on E2 then occurs with reduction of the disulfide resulting in formation of acetyl-dihydrolipoamide; (c) the lipoyl-lysyl appendage moves back to E2 where formation of acetyl CoA is catalysed resulting in the formation of dihydrolipoamide; (d) the dihydrolipoamide moiety swings round to E3 where it is reoxidised to lipoamide; (e) oxidation of the reduced E3 domain completes the cycle and the complex is ready for further turnover.
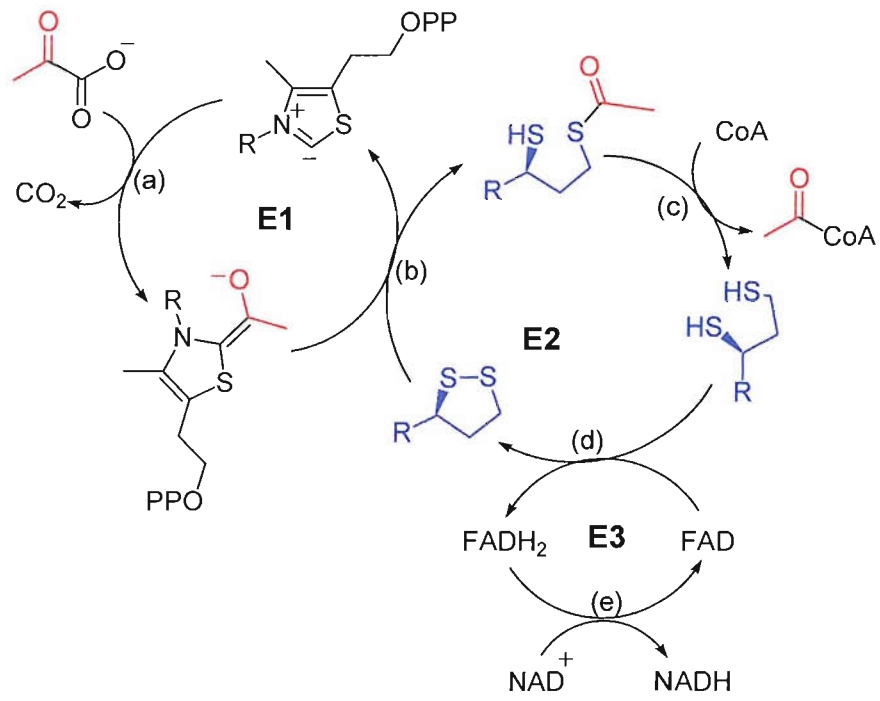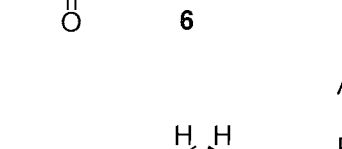
Figure 1.4 Conversion of pyruvate to acetyl CoA by PDH. Lipoic acid is shown in blue.
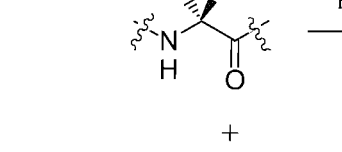
1.2.2 Glycine cleavage system
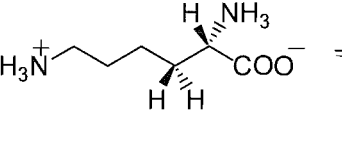
Cleavage of glycine to generate carbon dioxide, ammonia and N^5,N^{10}-methylene tetrahydrofolate is catalysed by the glycine cleavage system. It consists of four enzymes; pyridoxal phosphate (PLP) dependent glycine dehydrogenase (P protein), aminomethyltransferase (T protein), dihydrolipoyl dehydrogenase (L protein) and the H protein to which lipoic is covalently bound (*8, 11*). The function of the lipoyl group in this multienzyme complex is the transfer of a methylene group (fig. 1.5). This is derived from glycine in a reaction catalysed by the P protein and is delivered by the lipoyl-lysyl moiety to the T protein where it is attached to tetrahydrofolate. Reduced lipoamide then moves to the L protein where it is oxidised to restore the disulfide bond.
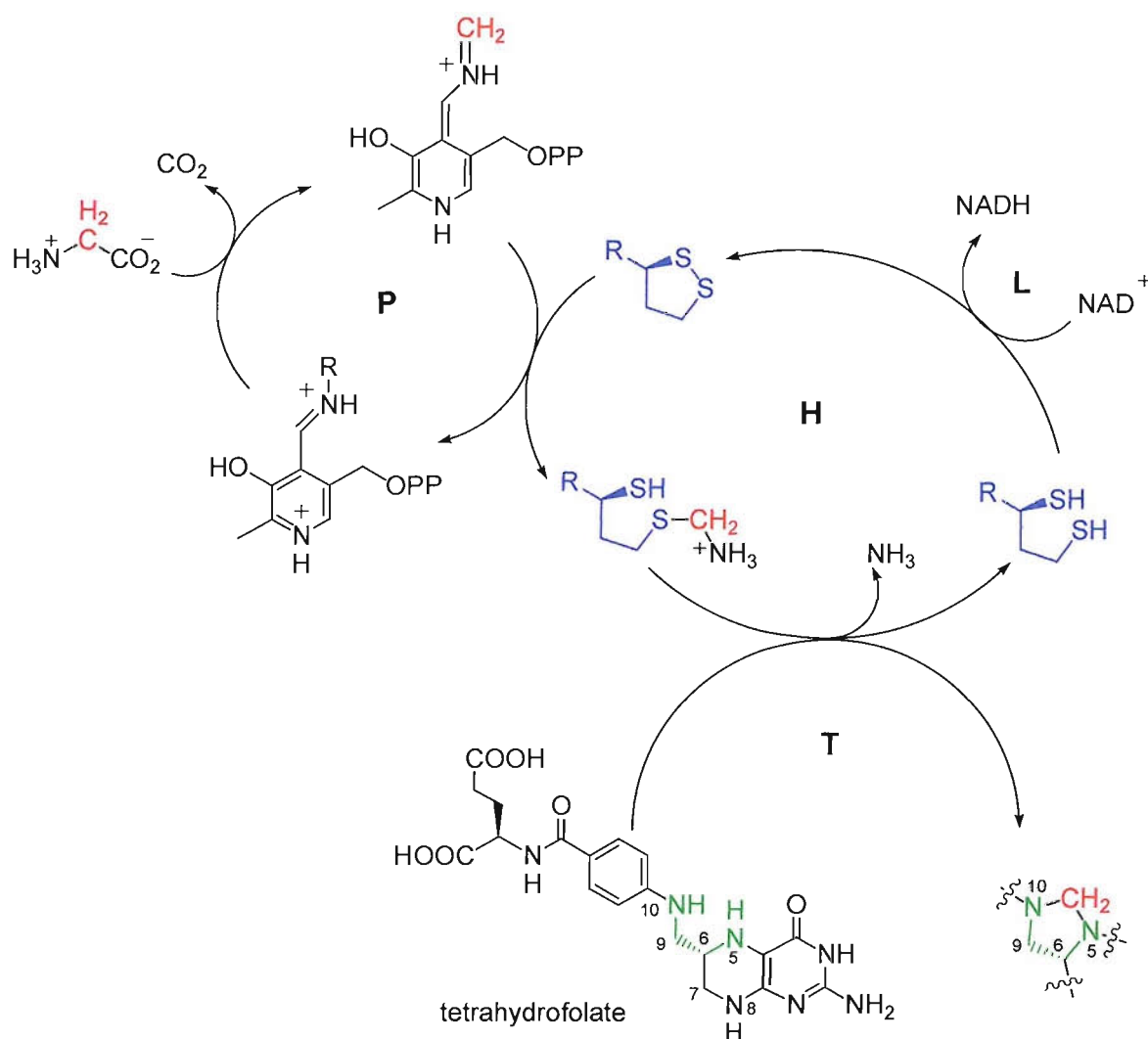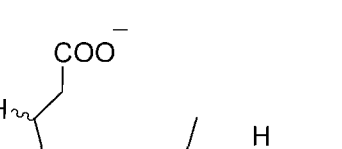
Figure 1.5 Reactions catalysed by the glycine cleavage system. Lipoic acid is shown in blue.

1.3   Lipoic acid biosynthesis and the radical SAM superfamily

De novo biosynthesis of lipoic acid has been identified in prokaryotes (*12, 13*), plants (*14, 15*) and mammals (*16, 17*). Early studies indicated that octanoic acid **6** (fig. 1.6a) is a precursor for lipoyl biosynthesis and that lipoic acid is formed by sulfur insertion into the C6 and C8 positions of this fatty acid (*18*). Insertion of sulfur into octanoic acid is dependent on a single protein, lipoate synthase (LipA) (*19-23*), which been identified as a member of the radical SAM superfamily (*24*).

Figure 1.6 Some reactions which utilise radical SAM proteins: (a) sulfur insertion into octanoic acid by LipA; (b) generation of glycyl radicals at specific residues of anaerobic ribonucleotide reductase and pyruvate formate lyase by their respective activating enzymes ARR-AE and PFL-AE; (c) conversion of the amino acid lysine to β-lysine by lysine 2,3-aminomutase (KAM); (d) oxidative decarboxylation of coproporphyrinogen III to protoporphrinogen by oxygen independent coproporphyrinogen III oxidase (HemN).

The radical SAM superfamily is a group of proteins which was characterised by sequence alignment and consists of at least 600 members which are largely uncharacterised (24). The characteristics which are common to these proteins are the presence of a $[4Fe-4S]^{1+/2+}$ cluster coordinated by three cysteine residues of a conserved CX_3CX_2C motif (table 1.1), (25-29) and that S-adenosyl-L-methionine (SAM) 7 (fig. 1.7) is a required for activity of radical SAM proteins. Members of this family are involved in a diverse range of reactions (fig. 1.6) but are believed to share common mechanistic steps that utilise their iron sulfur cluster to initiate the reductive cleavage of SAM 7 (fig. 1.7) to generate a reactive 5'-deoxadenosyl radical (Ado•) 8 (fig. 1.7) and thus initiate radical chemistry (30, 31).

Protein	Residues	Sequence											
LipA	92-103	A	I	C	T	R	R	C	P	F	C	D	V
BioB	51-62	G	A	C	P	E	D	C	K	Y	C	P	Q
MiaB	155-166	E	G	C	N	K	Y	C	T	Y	C	V	V
ARR-AE	24-35	S	G	C	V	H	E	C	P	G	C	Y	N
PFL-AE	28-39	Q	G	C	L	M	R	C	L	Y	C	H	N
KAM	131-142	N	Q	C	S	M	Y	C	R	Y	C	T	R
HemN	60-71	P	F	C	H	K	L	C	Y	F	C	G	C

Table 1.1 Alignment of amino acid sequences of radical SAM enzymes from E. coli; lipoyl synthase (LipA), biotin synthase (BioB), 2-methylthio-N-6-isopentyl adenosine synthase (MiaB), anaerobic ribonucleotide reductase activating enzyme (ARR-AE), pyruvate formate lyase activating enzyme (PFL-AE), lysine 2,3-aminomutase (KAM) and oxygen independent coproporphyrinogen III oxidase HemN. The CX_3CX_2C motifs that are involved in iron sulfur cluster binding are highlighted.

In addition to $[4Fe-4S]^{1+/2+}$ clusters both $[3Fe-4S]^{1+}$ and $[2Fe-2S]^{1+/2+}$ clusters have been observed in radical SAM proteins (32) which are formed as a result of oxidative degradation. However, it has been shown that only the $[4Fe-4S]^{1+}$ cluster is active (33-35) and this can be restored upon reduction (32, 36-39). Reactions carried out by radical SAM proteins begin with reduction of the inactive $[4Fe-4S]^{2+}$ cluster to the active 1+ state and reducing equivalents can be supplied by a flavodoxin, flavodoxin reductase and NADPH system (40-42), sodium dithionite (23) or by reduced deazaflavin (43). Spectroscopic studies of pyruvate formate lyase activating enzyme

(PFL-AE), and biotin synthase (BioB) have shown that turnover is accompanied by oxidation of the cluster from $[4Fe-4S]^+$ to $[4Fe-4S]^{2+}$ (*34, 44*). This is consistent with the transfer of a single electron from the $[4Fe-4S]^{1+}$ cluster to the sulfonium group of SAM concomitant with the homolytic scission of the C-S bond between the methionine moiety and 5'-deoxyadenosine to yield methionine and a Ado• radical (fig. 1.7). The formation of methionine and 5'-deoxyadenoxine (AdoH) during turnover of radical SAM proteins provide good evidence for this reaction (*44-47*) but the highly reactive Ado• radical has not been observed directly. However, experiments using S-3',4'-anhydroadenosylmethionine **9** (fig 1.8) (an unsaturated analogue of SAM) in a reaction with lysine 2,3-aminomutase (KAM) produced a stabilised allylic radical which was characterised by EPR spectroscopy (*48, 49*). Formation of Ado• by radical SAM proteins has led to comparisons with adenosylcobalamin **10** (fig. 1.8) dependent enzymes which generate this reactive radical by cleavage of a C-Co bond (*50, 51*).
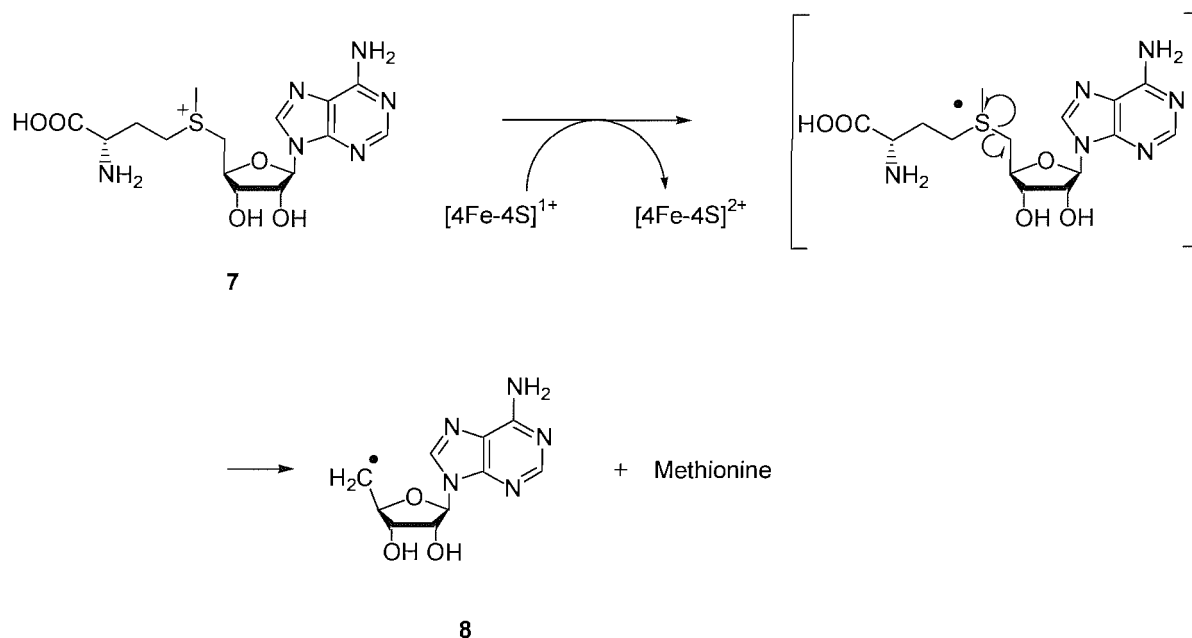
Figure 1.7 Reductive cleavage of of S-adenosylmethionine (SAM) **7** to generate a 5'-deoxyadenosyl radical (Ado•) **8** and methionine. The reaction is initiated by electron transfer from a reduced [4Fe-4S]1+ cluster of a radical SAM protein to the sulfonium of SAM with concomitant cleavage of the C-S bond.
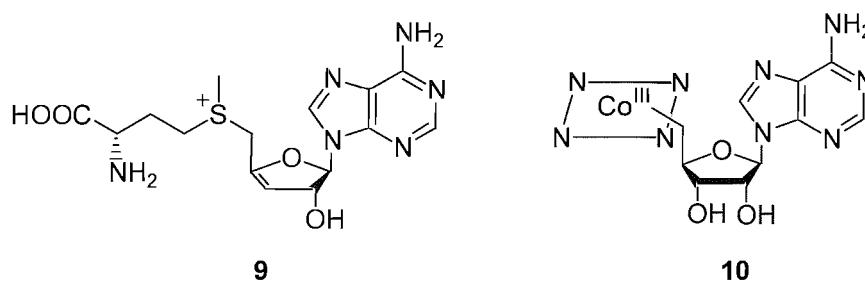
Figure 1.8 Structure of the SAM analogue S-3',4'-anhydroadenosylmethionine **9** and of adenosylcobalamin **10** (the parallelogram with nitrogen ligands to Co(III) is a simplified representation of a corrin ring).

Reductive cleavage of SAM is facilitated by a close interaction with the reduced $[4Fe-4S]^{1+}$ cluster of radical SAM proteins which has been indicated by Mössbauer, electron paramagnetic resonance (EPR) and resonance Raman spectroscopy (*52-55*). Electron nuclear double resonance spectroscopy (ENDOR) has also been used to probe the interaction between SAM and the $[4Fe-4S]^{1+/2+}$ of PFL-AE and KAM showing that it binds as a bidentate ligand via the amino nitrogen and a carboxylate oxygen atom of the methionine moiety (fig. 1.9) (*55-57*).
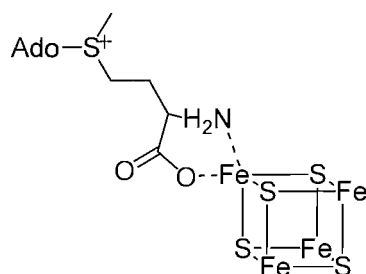
Figure 1.9 Binding of SAM to a unique Fe site of the $[4Fe-4S]^{1+}$ cluster of radical SAM superfamily.

More recently, publication of the crystal structures of BioB (*58*), KAM (*59*), oxygen independent coproporphyrinogen III oxidase (HemN) (*60*) and the molybdenum cofactor biosynthesis protein (MoaA) (*61*) in the presence of SAM has confirmed that three Fe sites of the $[4Fe-4S]^{1+/2+}$ clusters of these proteins are coordinated by the cysteine residues of their CX_3CX_2C motif whilst the final unique Fe site is coordinated by SAM (fig. 1.10). Characterisation of KAM by EPR spectroscopy has shown that SAM is required for reduction of the $[4Fe-4S]^{1+/2+}$ (*35*). Similar

observations have been made for the iron sulfur centre of ThiH which became more susceptible to reduction to the EPR active +1 state in the presence of SAM (62). Electrochemical studies of KAM have subsequently shown that addition of SAM elevates the midpoint potential for the $[4Fe-4S]^{2+/1+}$ transition by 50-86 mV thus facilitating reduction (63). Binding of SAM to the $[4Fe-4S]^{2+}$ cluster is therefore likely to precede reduction.
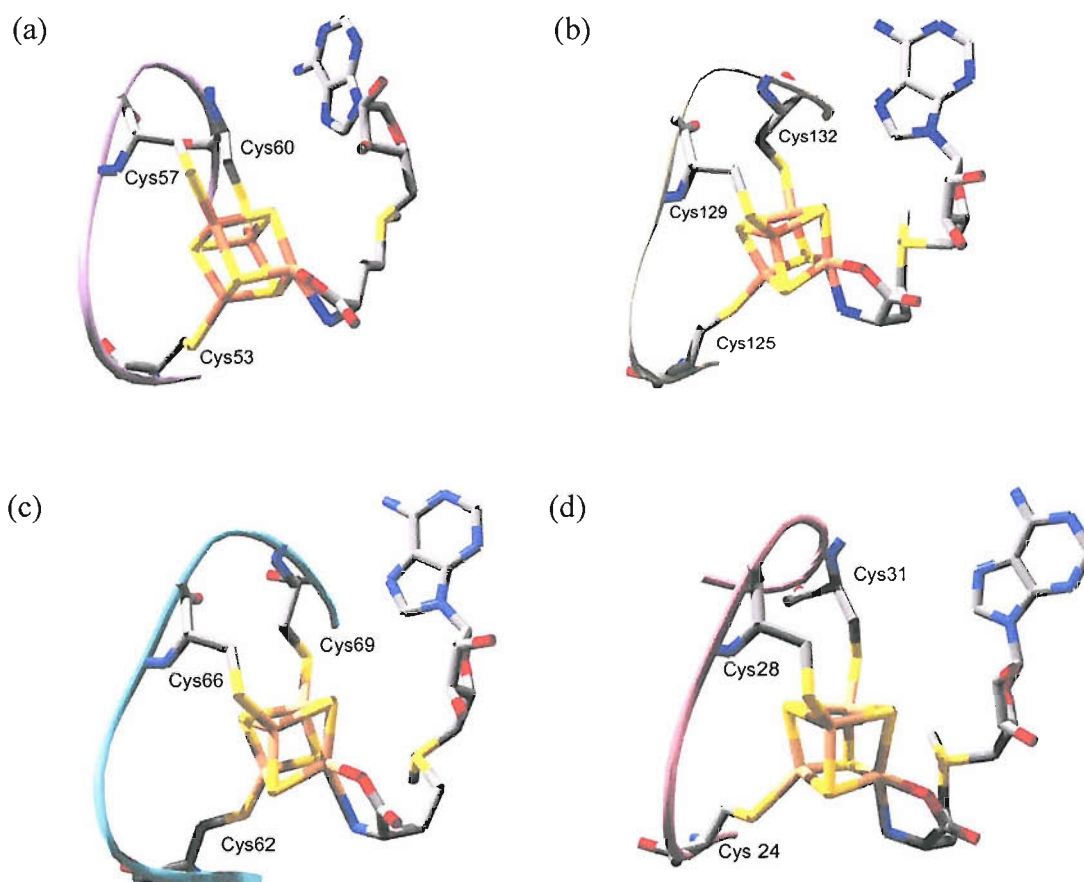
Figure 1.10 Binding of SAM to a unique Fe site of the $[4Fe-4S]^{1+}$ cluster of radical SAM proteins from *E. coli* unless otherwise stated: (a) BioB (58); (b) KAM (*Clostridium subterminale*) (59); (c) HemN (60); (d) MoaA (61). Coordinates were downloaded from the protein data bank and manipulated in Swiss PDB viewer.

Isotope labelling experiments using deuterated substrate analogues of various radical SAM proteins have shown that in each case once an Ado• radical is generated it abstracts a hydrogen atom from the substrate molecule (23, 47, 64-66). In the case of PFL-AE and ARR-AE a hydrogen atom is abstracted from a glycine residue of the substrate protein to generate a glycyl radical which can be observed by EPR (34, 67).

However, for other radical SAM proteins, including LipA, the substrate radicals are transient species and have not been observed experimentally.

A series of mechanistic steps for initiation of reactions involving radical SAM proteins has thus been proposed (fig. 1.11). Reactions commence with binding of SAM to the $[4Fe-4S]^{2+}$ cluster of the protein leading to reduction of the iron sulfur centre to the active +1 state. This followed by electron transfer from the reduced cluster to initiate to the reductive cleavage of SAM. This results in the formation of an Ado• radical which goes on to abstract a hydrogen atom from the substrate. The substrate radical then undergoes further chemistry, which varies between radical SAM proteins, to yield the product of the reaction.
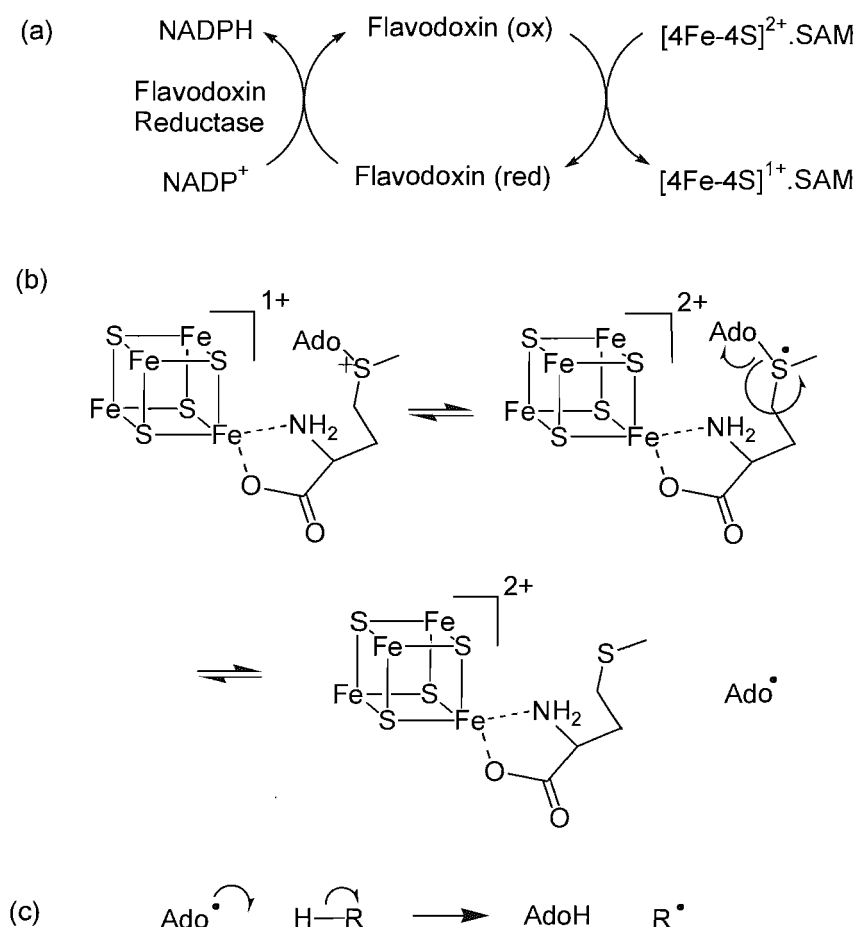
Figure 1.11 General mechanism common to all radical SAM proteins: (a) Reduction of the [4Fe-4S] cluster which is ligated by a CX_3CX_2C motif common to these proteins; (b) electron transfer from the reduced cluster to the sulfonium group of SAM and subsequent homolytic cleavage of the C-S bond to generate an Ado• radical; (c) hydrogen atom abstraction from the substrate by an Ado• radical.

1.4   **Radical SAM and C-S bond formation**

Proteins in the radical SAM family are involved in a broad range of chemistry and one intriguing area is the ability of some members to mediate the insertion of sulfur into unactivated carbon-hydrogen bonds. This may led to the biosynthesis of important metabolites such as lipoic acid and biotin, modification of transfer RNAs and potentially maturation of hydrogenase active site complexes.

Biotin synthase (BioB) is the best characterised of the radical SAM family involved in sulfur insertion reactions and a number of parallels can be drawn between this protein and LipA. A discussion of BioB will therefore serve here as a useful introduction to lipoyl synthase

1.4.1   **Biotin synthase (BioB)**
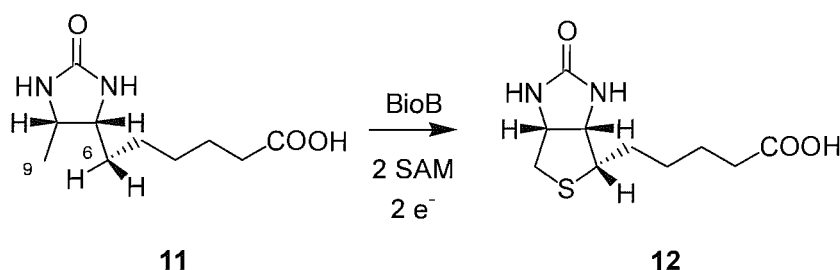
Figure 1.12 Conversion of dethiobiotin to biotin by biotin synthase.

BioB, the product of the *bioB* gene, is responsible for the final step in biotin biosynthesis, conversion of dethiobiotin (DTB) **11** (fig. 1.12) to biotin **12** (fig. 1.12). This reaction requires insertion of a single sulfur atom between the unactivated C6 and C9 positions of DTB (fig. 1.12). Using isotopically labelled DTB it has been found that biotin formation occurs with loss of just two hydrogen atoms, one from each of the C6 and C9 positions (*68, 69*). Sulfur insertion at C6 has been shown to occur with retention of configuration (*70*).

Identification of BioB as the protein required for conversion of DTB to biotin (*71, 72*), led to a number of studies which endeavoured to determine the components required for its activity and all found that SAM was required for activity (*71, 73-75*). A reductant is also essential and flavodoxin, flavodoxin reductase and NADPH are

effective but can be replaced by photoreduced deazaflavin (*43, 76*). These requirements together with the determination that BioB is an FeS protein (*72*) and has a CX_3CX_2C motif led to comparisons with ARR-AE and KAM and subsequent assignment as a member of the radical SAM superfamily.

FeS Cluster Binding in Biotin Synthase

The binding of iron sulfur clusters in BioB has been widely investigated. Mössbauer spectroscopy studies of whole cells overexpressing BioB have found that *in vivo* the protein contains either $[2Fe-2S]^{1+/2+}$ clusters alone (*77*) or $[4Fe-4S]^{1+/2+}$ and $[2Fe-2S]^{1+/2+}$ clusters in a 1:3 ratio (*78*). Aerobic purification of BioB yields protein containing only a $[2Fe-2S]^{1+/2+}$ which exhibits UV absorption at 332 and 452 nm (*72*). This protein is incapable of converting DTB to biotin and loss of the [4Fe-4S] cluster is most likely due to degradation of the cluster upon exposure to oxygen (*79, 80*). When the protein is returned to anaerobic conditions and reduced with dithionite in the presence of 60 % (v/v) glycerol two $[2Fe-2S]^{1+/2+}$ are converted to a single $[4Fe-4S]^{1+}$ cluster (*36, 39*). Reconstitution of BioB with exogenous iron and sulfide under anaerobic and mildly reducing conditions can also facilitate regeneration of an active $[4Fe-4S]^{1+}$ cluster. Reports on the number and types of cluster incorporated vary and appear to depend on conditions used. Upon reconsitution of the apoprotein with exogenous iron and sulfide in the presence of DTT under anaerobic conditions one active $[4Fe-4S]^{2+}$ cluster per polypeptide chain can be generated (*79*). Alternatively reconstitution of as isolated protein can yield BioB containing two different FeS clusters per monomer a $[4Fe-4S]^{1+/2+}$ cluster and a $[2Fe-2S]^{1+/2+}$ (*81*).

Mössbauer spectroscopy has been used to demonstrate that that there are two distinct iron sulfur cluster binding sites in BioB by specifically labelling either the $[4Fe-4S]^{2+}$ or $[2Fe-2S]^{2+}$ with ^{57}Fe (*82*). The $[4Fe-4S]^{1+/2+}$ is typical of those in other radical SAM and has been extensively characterised by UV/vis, resonance Raman, EPR and Mössbauer spectroscopy (*39, 53*). Mutagenesis experiments which removed either Cys-53, Cys-57, Cys-60 of *E. coli* BioB, which form the CX_3CX_2C motif, established that these residues are required for binding of the $[4Fe-4S]^{1+/2+}$ cluster (*25, 26*). Similar studies found that removal of these cysteine residues prevented formation of AdoH and methionine implying that this cluster is involved in reductive cleavage of SAM (*44*). Mutation of the conserved cysteine residues Cys-97, Cys-128

and Cys-188 of *E. coli* BioB yields proteins that can bind an intact [4Fe-4S] but are unable to convert dethiobiotin to biotin, indicating that these residues are involved in binding of the [2Fe-2S] cluster (*26*).

Determination of the crystal structure of *E. coli* BioB has confirmed the nature of binding of the two clusters (*58*). The reconstituted homodimeric protein was co-crystallised with SAM and DTB and the structure solved to 3.4 Å resolution. Each monomer contains one [2Fe-2S] cluster and one [4Fe-4S]. The clusters along with the substrates are shielded from solvent by a $(\alpha/\beta)_8$ barrel (TIM barrel) which forms the main fold of each subunit of the protein (fig. 1.13).
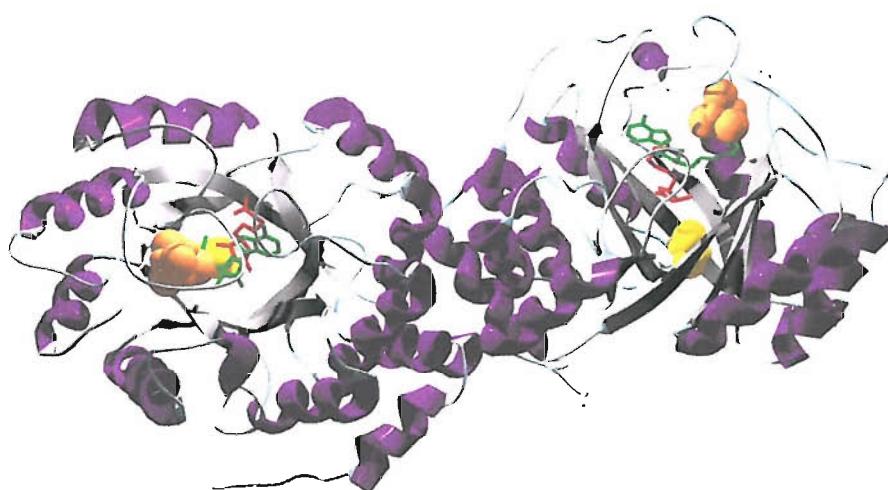
Figure 1.13 Crystal structure of *E. coli* biotin synthase showing $[4Fe-4S]^{2+}$ clusters (orange), $[2Fe-2S]^{2+}$ clusters (yellow), SAM (green) and DTB (red) (*58*).

The [4Fe-4S] cluster is positioned close to the surface of the protein at the C-terminus end of the barrel and is ligated by the cysteine residues of the CX_3CX_2C motif which are found in a 28-residue loop extending from the TIM barrel (fig. 1.14). Proximity of the cluster to the exterior of the protein explains its extreme oxygen sensitivity since it is easily accessible. The fourth iron centre of the cluster is ligated by SAM which binds via both the amino and carboxylate groups of the methionine moiety. Direct ligand binding of SAM to the cluster is consistent with observed spectroscopic changes upon addition of SAM (53, 83).
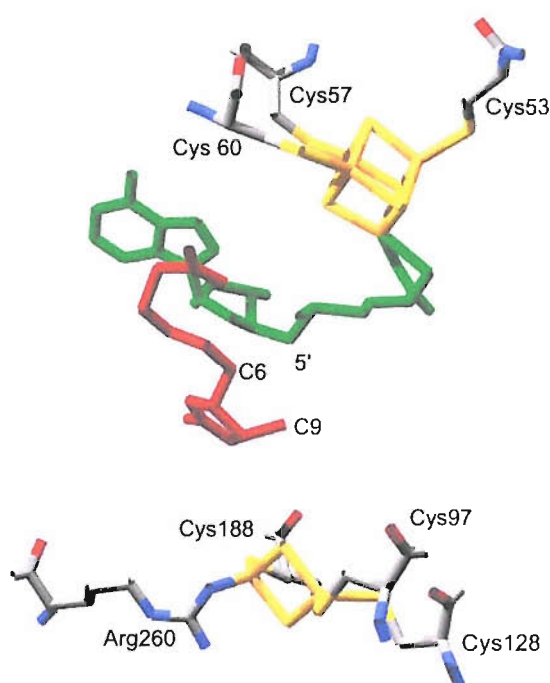
Figure 1.14 Structure of BioB showing iron sulfur cluster and substrate binding. The $[4Fe-4S]^{2+}$ cluster is coordinated by Cys53, Cys57 and C60. The final Fe site of this cluster is coordinated by SAM. The 5' position of SAM lies ~3.9 Å from C9 of DTB. The $[2Fe-2S]^{2+}$ is also found in close proximity to DTB and is coordinated by Cys97, Cys128, Cys188 and Arg260.

The $[2Fe-2S]^{1+/2+}$ cluster of BioB is located deep inside the barrel and lies in close proximity to DTB. This cluster is coordinated by conserved β-strand residues Cys97, Cys128, Cys188 and Arg260. Coordination of a metal by an arginine residue is unprecedented in biology and it was therefore proposed that this unusual ligand might play an essential structural of catalytic role. Recently mutagenesis has been

used to investigate the effect of replacing Arg260 with residues that are more conventional metal ligands (84) This residue was replaced with histidine, cysteine, methionine or alanine mutant to and all four mutants were capable of binding a [2Fe-2S] $^{1+/2+}$ cluster and none of the mutations appeared to have any effect on activity. The presence of arginine at this position does therefore not appear to be essential for activity and this residue may not be involved in cluster binding.

Initiation of a radical reaction by biotin synthase

Binding of SAM to the [4Fe-4S]$^{1+}$ cluster precedes cleavage of the cofactor to generate Ado•. The ensuing mechanistic step is proposed to be abstraction of hydrogen atoms from either the C9 or C6 positions by the reactive primary radical. Labelling of each of these positions with deuterium has provided evidence for this step showing that deuterium was incorporated at the 5' position to form AdoD (66). Analysis of the crystal structure of BioB (58) has shown that the 5' position of SAM lies ~3.9 Å from C9 of DTB and therefore appears to be ideally positioned for hydrogen atom abstraction following cleavage of the C-S bond (fig. 1.14).

Quantification of the products of assays using BioB from both B. sphaericus and E. coli suggested that for each mole of biotin formed approximately 2.9 and 3.1 moles of AdoH and methionine are formed respectively (85, 86) which may be consistent with the use of two 5'-deoxyadenosyl radicals for abstraction of hydrogen from both C6 and C9 of DTB. However, the slight excess of these products with respect to biotin suggests that there may be some cleavage of SAM which does not led to biotin formation.

If the reaction occurs in a stepwise manner then hydrogen atom abstraction would occur from either the C6 or C9 position first leading to the formation of either one of two possible intermediates, 9-mercaptodethiobiotin or 6-mercaptodethiobiotin. An intermediate species has been observed by HPLC analysis of reactions using ^{14}C-labelled DTB but this was not fully characterised (86). It has been found that 9-mercaptodethiobiotin can support growth of bioA minus mutants which are incapable of producing 7,8-diaminopelargonate, the precursor for dethiobiotin biosynthesis (87). Whilst this compound can also be converted to biotin by resting B. sphaericus cells neither 6(R)-mercaptodethiobiotin nor 6(S)-mercaptodethiobiotin could serve as

substrates (*88*). Interpretation of these results has led to formulation of a potential mechanism commencing with hydrogen atom abstraction by Ado• from C9 followed by sulfur insertion leading to the formation of a protein bound 9-mercaptodethiobiotin intermediate. A second hydrogen atom is then abstracted by another Ado• from C6 of this intermediate species then the reaction is completed by cyclisation to form biotin (fig. 1.15).

The source of sulfur during biotin biosynthesis

The source of sulfur in the final step of biotin synthesis has been the subject of much speculation. SAM has been ruled out as the sulfur donor since a ^{35}S label is not transferred from [^{35}S]SAM to biotin (*75, 89*). Sulfur can be transferred from cysteine to biotin in assays which utilise BioB containing whole cell extracts (*74, 89, 90*) but cysteine is unlikely to be the direct source of sulfur since experiments using purified BioB incubated with [^{35}S]cysteine did not result in transfer of the radioactive label to biotin (*75*). Using labelled BioB, which was obtained by growth in the presence of [^{35}S]cysteine and [^{35}S]sulfide, significant transfer of radioactivity to biotin was observed suggesting that the sulfur donor is the protein itself (*91*). A number of studies have implied that one of the FeS clusters is the sulfur source (fig. 1.15). Reconstitution of BioB from both *B. sphaericus* and *E. coli* with $Na_2^{34}S$ resulted in formation of biotin containing approximately 65% of the label as determined by mass spectrometry (*92*). Similar results have also been achieved by reconstitution with Na_2Se which led to formation of selenobiotin (*93*). Degradation of the [2Fe-2S]$^{1+/2+}$ cluster would be expected to accompany turnover if it is the source of sulfur. UV/vis and EPR spectroscopy have been used to monitor the clusters during the reaction and changes characteristic of loss of the [2Fe-2S]$^{1+/2+}$ cluster were observed whilst the [4Fe-4S]$^{1+}$ cluster remained intact (*94*). The crystal structure of BioB has shown that the C9 of DTB lies ~ 4.6 Å from the nearest [2Fe-2S]$^{2+}$ sulfide (fig. 1.14) and is therefore suitably positioned to play a role in sulfur insertion (*58*).
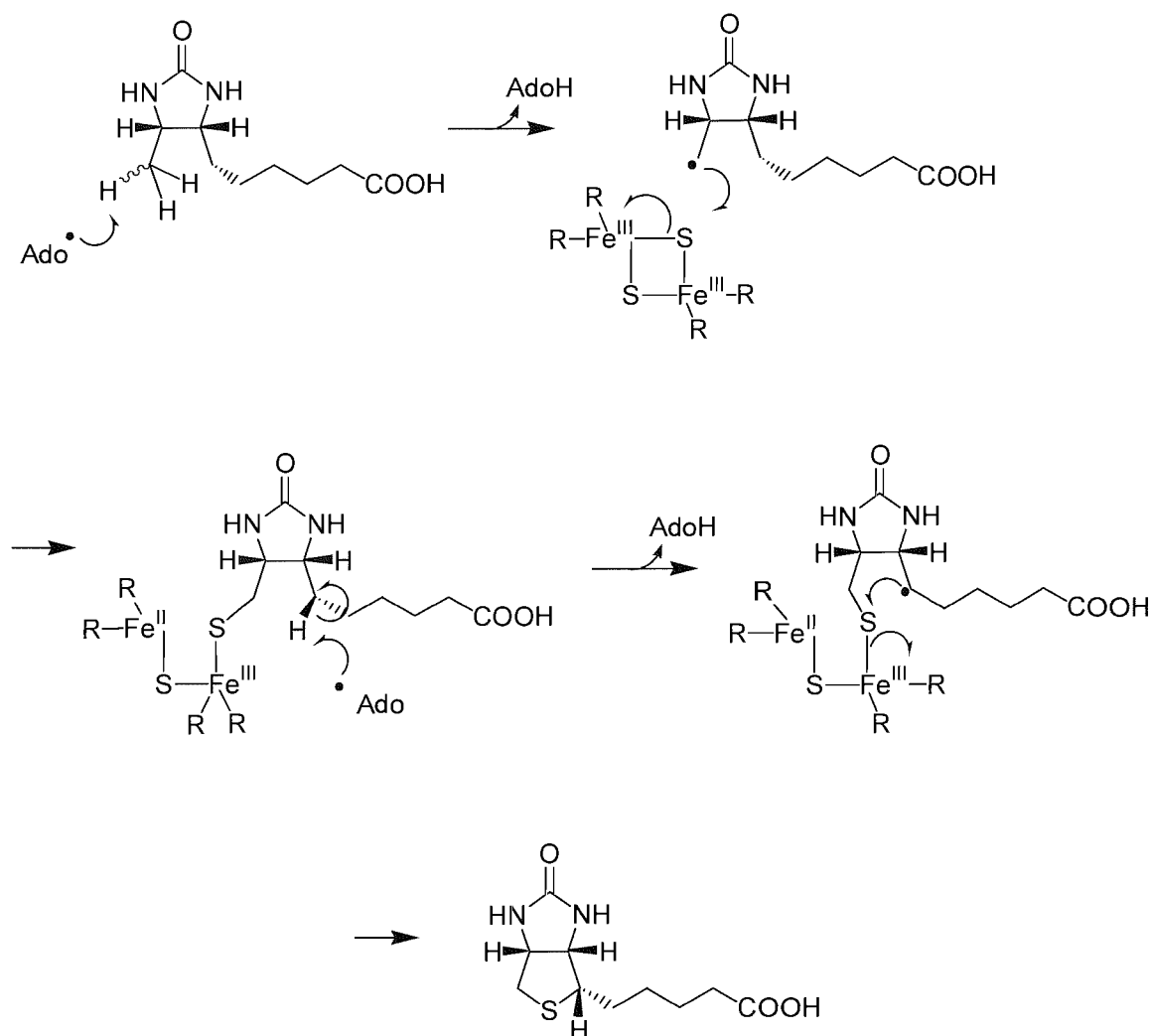
Figure 1.15 Mechanism for conversion of DTB to biotin in which the [2Fe-2S] cluster acts as the source of sulfur.

Selective labelling of the [2Fe-2S]$^{2+}$ cluster with ^{57}Fe allowed degradation of the cluster to be followed by Mössbauer spectroscopy and demonstrated that this occurred at a much faster rate than biotin formation (*95*). It has thus been hypothesised that the cluster degradation product may in fact be the sulfur source. A reaction which involves formation of a persulfide which serves as the sulfur source had previously been suggested as an alternative. Using BioB containing just a [4Fe-4S]$^{1+/2+}$ cluster it was shown that the protein could bind PLP and that alanine was formed upon addition of L-cysteine (*96*). These results were interpreted as consistent with the protein acting as a desulfurase and it is proposed that residues Cys97, and Cys128 and Cys188 serve as a site for persulfide formation and not for binding of a

$[2Fe\text{-}2S]^{2+/1+}$ cluster. However, contradictory reports have suggested that addition of PLP has no effect (97) and the crystal structure of BioB reveals no obvious PLP binding sites (58) and therefore the source of sulfur remains a subject of debate.

Stoichiometry of biotin formation by BioB

Consistently less than 1 mole of biotin is formed per mole of BioB during *in vitro* assays (75, 97, 98). Lack of catalytic activity suggests that the protein might act as a reactant and not a true enzyme under these conditions. If destruction of a $[2Fe\text{-}2S]^{2+}$ cluster accompanies a single turnover (94, 95) this may prevent further activity. However, recent *in vivo* experiments have indicated that BioB is capable of producing 20-60 moles per mole of protein (99) implying that *in vitro* assays are lacking some component required for catalysis.. Attempts to reconstruct the cluster after one turnover by recovering the protein and adding fresh Fe^{2+}, S^{2-} and DTT along with substrates resulted in additional formation of 0.4 mol of biotin per mole of BioB (97). It has been demonstrated that NifS, or Isc type proteins, which have been shown to participate in FeS cluster assembly (100, 101), can facilitate reconstitution *in vitro* leading to incorporation of $[^{35}S]$cysteine into apo BioB (98). Thus, the precise mechanisms for catalytic turnover have not been identified but one hypothesis is that *in vivo* this might be achieved by repair of this cluster by iron sulfur cluster assembly proteins.

Product inhibition may also prevent catalytic behaviour of BioB *in vitro*. Addition of one equivalent of AdoH to assays resulted in a loss of approximately 90% of activity indicating that the SAM cleavage product is an inhibitor (102). AdoH can be removed *in vivo* by the product of the *pfs* gene, 5'-methylthioadenosine (MTA)/S-adenosylhomocysteine nucleosidase (Pfs) which has been shown to cleave the nucleoside to adenine and 5'deoxyribose, (103). Growth of strains of *E. coli* which lack the *pfs* gene was limited in the absence of biotin and supplementation with DTB had no effect (103); however, addition of biotin and lipoic acid resulted in improved growth of these mutants. Thus, removal of AdoH may prevent inhibition and of BioB activity. Inability to generate catalytic activity of BioB *in vitro* limits analysis of this protein but this may be achieved when the factors required are fully identified.

1.4.2 Lipoyl synthase (LipA)

Early mechanistic studies provided evidence that the LipA dependent conversion of octanoic acid to lipoic acid occurs via a radical mechanism. *In vivo* feeding studies with specifically tritiated octanoic acid indicated that insertion of sulfur occurs with abstraction of two hydrogen atoms from the C6 and C8 positions of the substrate (fig. 1.16) (*104*). In addition, it was found that there is no loss of hydrogen from C5 or C7 suggesting that an unsaturated intermediate is unlikely. A pathway involving hydroxylation was ruled out by experiments which established that $[8-^2H_2]-8-$ hydroxyoctanoic acid, $[6(RS)-^2H]-6$-hydroxyoctanoic acid and $[8-^2H_2]-(\pm)-6,8-$ dihydroxyoctanoic are not converted into lipoic acid by *E. coli* (*105*). Sulfur insertion at C6 was shown to occur with inversion of configuration (*106*) (fig. 1.16).
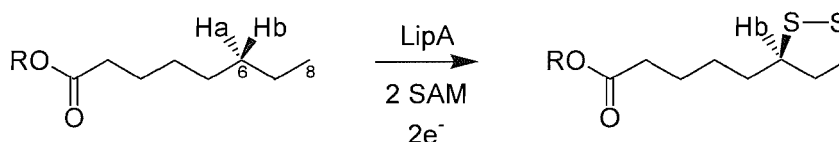
Figure 1.16 Sulfur insertion at C6 of octanoate occurs with inversion of configuration.

Genetic and biochemical studies have led to the discovery that in *E. coli* insertion of both sulfur atoms into octanoic acid is dependent on the product of the *lipA* gene (*19-21*) and mutations in this gene prevent production of lipoic acid (*22*). Isolation of LipA revealed that it is an iron sulfur protein (*107, 108*). Characterisation of the iron sulfur cluster of the as isolated protein by UV/vis, resonance Raman, and EPR spectroscopy was consistent with the presence of a single $[4Fe-4S]^{1+/2+}$ cluster per dimer. Reduction with dithionite or 5'-deazaflavin generates the $[4Fe-4S]^{1+}$ form whilst oxidation results in degradation to a $[2Fe-2S]^{2+}$ cluster (*79*). Under strictly anaerobic conditions reconstitution with iron and sulfide in the presence of DTT can generate one $[4Fe-4S]^{1+/2+}$ cluster per LipA monomer (*79*). More recently, detailed spectroscopic studies have now been used to show that like BioB, two different iron sulfur clusters can be accommodated by LipA (*29*). Two potential cluster binding sites were identified, the CX_3CX_2C motif and a CX_4CX_5C motif found in the N-terminal region. EPR spectroscopy has been used to show that triple variants in which the cysteine residues from either one or the other of these sites were replaced with alanine remained capable of binding an intact $[4Fe-4S]^{1+}$ cluster. The EPR

spectrum of the $[4Fe-4S]^{1+/2+}$ cluster bound by the CX_4CX_5C (g=2.05, 1.91) varies from that bound by the CX_3CX_2C motif (g=2.03, 1.93) which most closely resembles that of other radical SAM proteins. and it seems likely that the latter motif binds the [4Fe-4S] cluster involved in cleavage of SAM. These proteins were expressed in the presence of ^{57}Fe and Mössbauer spectroscopy of the labelled mutants also indicated that they were both capable of binding a $[4Fe-4S]^{2+}$ cluster (29).

Identification of the substrate of LipA

Following initial purification of LipA it became clear that free octanoic acid could not be converted to lipoic acid by the protein (23). *In vitro* activity was first achieved by incubating *E. coli* LipA with octanoylated acyl carrier protein (ACP) and apo-PDH (23). The assay showed for the first time that LipA requires SAM and reduction to generate a $[4Fe-4S]^{1+}$ cluster for activity. It was assumed that octanoyl ACP was the substrate for sulfur insertion and lipoyl formation was assayed by an indirect method which followed activation of apo-PDH by lipoylation, making use of octanoyl (lipoyl)-ACP:protein-N-octanoyl(lipoyl)transferase (LipB) which has been implicated in the transfer of either octanoyl or lipoyl groups from ACP to lipoyl domains (109, 110). Extent of lipoylation of PDH was determined by monitoring reduction of an NAD^+ analogue and formation of lipoyl PDH was also verified using MALDI-TOF spectroscopy. However, lipoyl-ACP was not isolated therefore the true LipA product could not be conclusively identified and since LipB can facilitate transfer of both octanoyl and lipoyl groups, octanoylation of the E2 subunit of PDH might precede sulfur insertion.

Octanoylated derivatives of lipoyl accepting domains have now been shown to be the preferred substrates for LipA (47, 111). Conversion of octanoyl-E2 domains to lipoyl-E2 domains was demonstrated *in vivo* using *E. coli* that lacked LipA activity and were supplemented with d_{15}-octanoic acid in order to accumulate labelled octanoyl-E2 domain (111). LipA activity was then initiated by transduction of the d_{15}-octanoyl labelled cells with phage λ particles containing a *lipA* cosmid. Subsequent analysis of the labelled E2 domains by electrospray mass spectroscopy revealed that they had been lipoylated. The preference for octanoyl-E2 was confirmed using an *in vitro* assay which monitored the formation of methionine and AdoH, showing that the amount of SAM consumed when octanoyl-E2 was the

substrate (1050 pmol) was significantly greater than with octanoyl-ACP (<5 pmol) and no lipoyl products could be detected when the latter substrate was used. These observations led to the proposal of a biosynthetic pathway for lipoyl biosynthesis which proceeds via incorporation of octanoyl groups into lipoyl domains followed by sulfur insertion (fig. 1.17). Two independent systems exist that use either LipB or lipoate protein ligase (LplA) for the octanoylation of the lipoyl domains (*112*). LipB catalyses the transfer of octanoyl groups from ACP which are products of fatty acid biosynthesis. Alternatively free octanoate is attached by LplA in a process that requires ATP.

HO $\sim\sim\sim\sim$ O

ACP-S $\sim\sim\sim\sim$ O

ATP
AMP
LplA
E2-PDH

E2-PDH

LipB

H
E2—Lys-N $\sim\sim\sim\sim$ O

LipA | 2 SAM
2e⁻

H
E2—Lys-N $\sim\sim\sim$ S—S
O
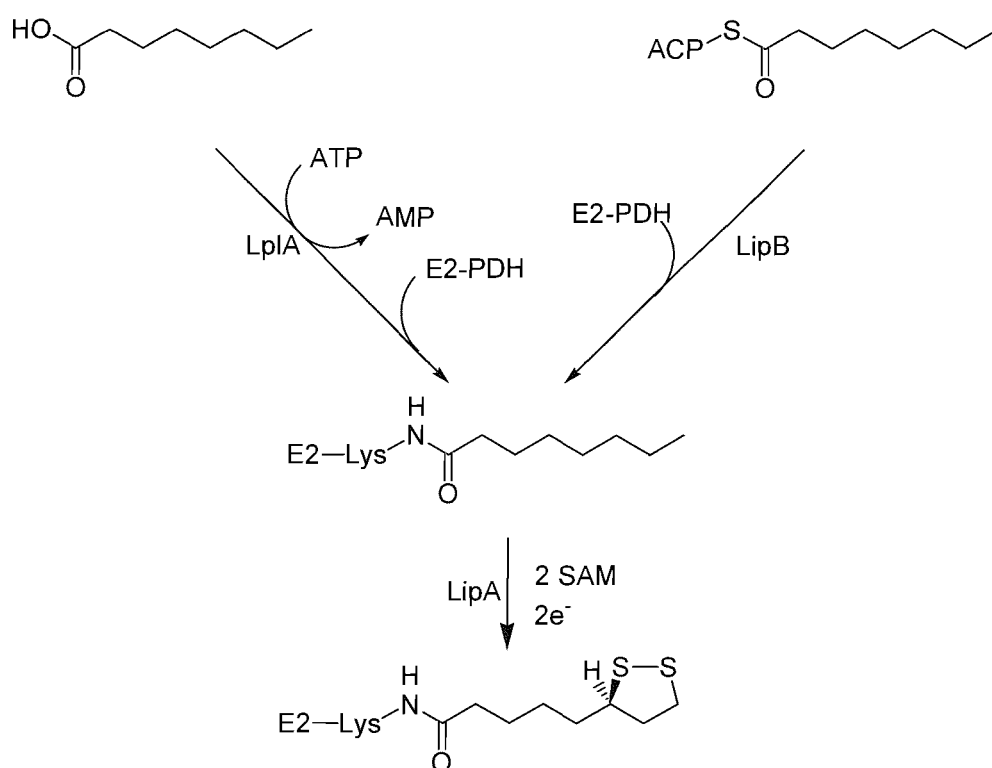
Figure 1.17 Biosynthetic pathway for lipoyl biosynthesis using octanoyl-E2 as substrate.

Further evidence for this biosynthetic pathway has subsequently been provided by *in vitro* experiments which utilised an octanoylated version of the H-protein from the glycine cleavage system as a substrate for LipA (*47*). It was shown that at 37 °C and in the presence of SAM and flavodoxin, flavodoxin reductase and NADPH, purified *E. coli* LipA is able to convert octanoyl H-protein to lipoyl H-protein. Catalytic activity was not observed during these reactions and a substoichiometric amount of lipoyl product was formed (0.36 molar equivalents per LipA monomer) indicating

that *in vitro* activity of LipA resembles that of BioB (*75, 97, 98*). This led to speculation that either 2 equivalents of LipA were required for the formation of 1 equivalent of lipoyl product or that some of the protein was not in an active configuration. Mechanistic studies were subsequently carried out using ^{34}S labelled LipA and indicated that the latter hypothesis is most likely (*113*). These studies made use of GC-MS analysis to quantify the products of reactions in which octanoyl H-protein served as a substrate for an equimolar mixture of [^{34}S] LipA and [^{32}S]LipA in the absence of any other sulfur source. If two equivalents of LipA were required for lipoyl formation, a monothiolated species would dissociate from the protein following the first sulfur insertion reaction then bind to a second LipA monomer and a mixture of ^{32}S/^{32}S, ^{34}S/^{34}S and ^{34}S/^{34}S in a 1:2:1 ratio would be expected. However these reactions yielded an approximately equimolar amount of ^{34}S/^{34}S and ^{32}S/^{32}S lipoyl H-protein showing that both sulfur atoms are derived from the same LipA monomer.

LipA sulfur insertion mechanism

Similarities between BioB and LipA have indicated that they use similar mechanisms that begin with cleavage of SAM to generate Ado• radicals. Formation of AdoH and methionine upon cleavage of SAM by LipA has been demonstrated (*111*). AdoH formation was quantified from assays using octanoyl H-protein as a substrate for LipA showing that two equivalents of SAM are used to synthesise one equivalent of lipoate (*47*). It is hypothesised that these supply two Ado• radicals for abstraction of a hydrogen atom from each of the C6 and C8 positions of octanoyl precursors. Deuterium labelled d_{15}-octanoyl H protein has been used as a substrate in assays of *E. coli* LipA and AdoD was observed as a prodcut of this reaction thus providing evidence for the direct action of Ado• on the substrate (*47*). Lipoyl product was not observed in these reactions, however a monothiolated species was detected indicating that there is a significant deuterium isotope effect for the second hydrogen atom abstraction. During lipoyl formation the role of Ado• is to abstract hydrogen from either C6 or C8 and the resulting carbon radical is quenched by sulfur insertion (fig. 1.18). Generation of a second Ado• is then followed by analogous steps at the second carbon centre to yield lipoate. Feeding studies have shown that [8-^{2}H$_2$]-8-thiooctanoic acid was converted into lipoic acid and [6(RS)-^{2}H]-6-thiooctanoic acid was converted 10-20% as efficiently as the former compound.

Based on this result it was postulated that sulfur insertion occurs at the C8 position first (*105*). However, recent characterisation of an isolated reaction intermediate has shown that in fact a species with sulfur inserted at C6 is formed first (fig. 1.18) (*114*). The source of sulfur in this reaction is unknown although the formation of ^{34}S labelled lipoyl product in assays using [^{34}S]LipA in the absence of any other sulfur source shows that the protein itself is likely to be the sulfur donor (*113*). It seems possible that LipA like BioB might use its second iron sulfur cluster as a source of sulfur (fig. 1.18).
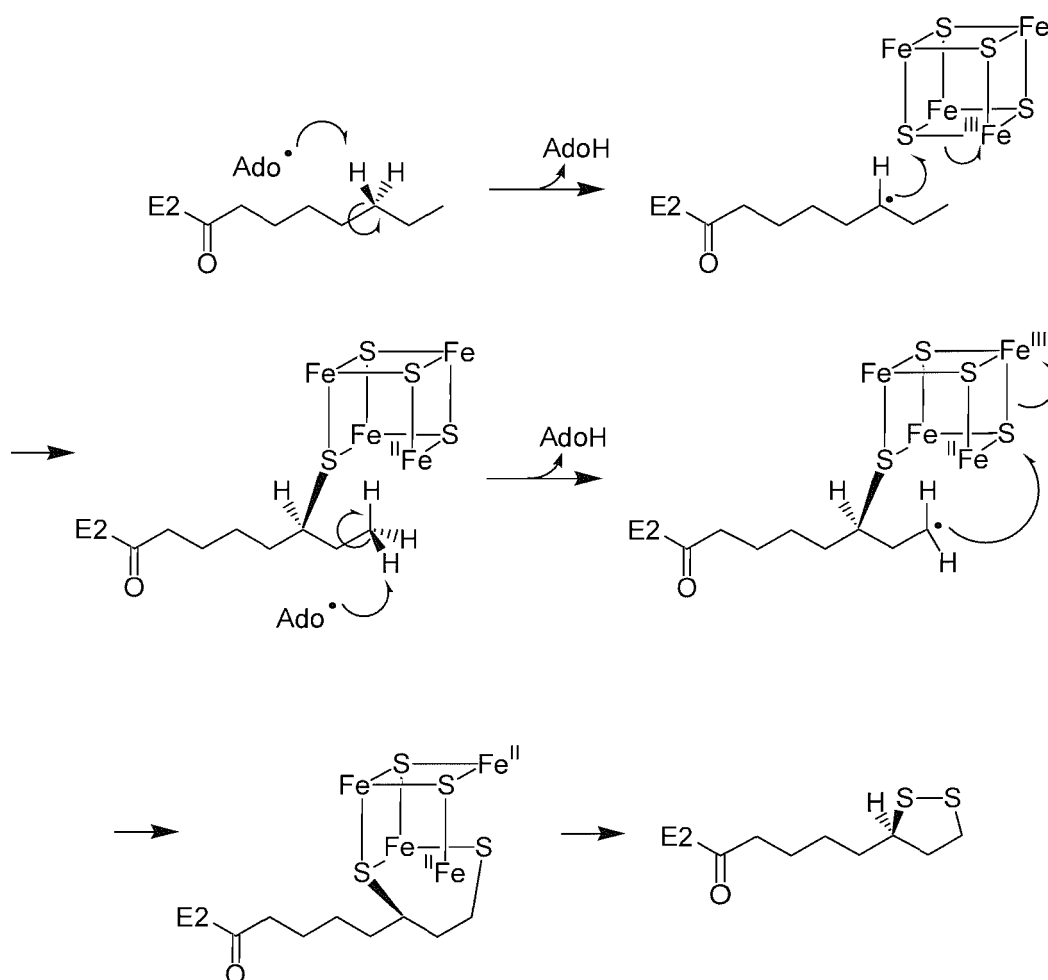
Figure 1.18 Mechanism of sulfur insertion by LipA. A [4Fe-4S] cluster is shown here as the hypothetical source of sulfur but the true sulfur source is yet to be determined.

1.4.3   2-Methylthio-N6-isopentyl Adenosine Synthase (MiaB)
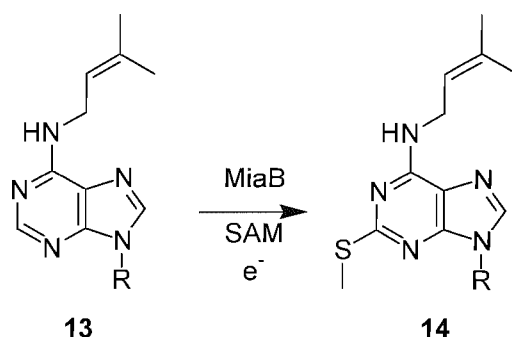
Figure 1.19 Modification of N6-isopentyl adenosine by MiaB.

Transfer RNAs (tRNAs) of all organisms contain modified nucleosides that generate the structural diversity important for activity and are derived from the normal nucleosides adenosine (A), guanosine (G), cytosine (C) and uridine (U) (*115-117*). Numerous enzymes are involved in these modifications which can be simply the addition of a single methyl group, or a sequence of reactions resulting in the formation of hypermodified nucleosides. The MiaB protein is involved in methylthiolation at the C2 position of an isopentyl derivative of adenosine **13** (i^6A) to form 2-methylthio-N6-isopentenyl adenosine **14** (ms^2io^6A) (fig. 1.19) (*118*). Sequence analysis has shown that MiaB has significant sequence similarity with BioB and LipA and bears a CX_3CX_2C motif indicating that it may employ a similar mechanism as these proteins (*118, 119*).

MiaB has been isolated from *E. coli* and *Thermotoga maritima* and is an iron sulfur protein (*120, 121*). Spectroscopic and chemical analyses have shown it contains a $[4Fe-4S]^{1+/2+}$ cluster which is bound by a CX_3CX_2C motif (*121, 122*). The importance of this cluster was elucidated by *in vivo* assays using *miaB-* strains of *E. coli (120)*. Expression of wild type MiaB in these cells could initiate formation of ms^2io^6A but site directed mutants in which the conserved cysteine residues of the CX_3CX_2C triad, expected to be involved in cluster binding, had been replaced with alanine were inactive.

Development of an *in vitro* assay system for MiaB using i⁶A tRNA as a substrate demonstrated that a reductant and SAM are required for activity (*123*). Investigations into the involvement of SAM in this reaction found that it played a dual role (fig. 1.20). Its first function is as a source of Ado•, which was determined by monitoring the formation of AdoH and methionine, confirming that MiaB is a radical SAM protein. The Ado• radical is proposed to abstract hydrogen from the aromatic C2 position of i⁶A leading to sulfur insertion at this position. The second function of SAM is then as a methyl donor for the methylation of the resulting thiol. This was determined by experiments using [³H₃C]SAM which were able to monitor transfer of the radioactive methyl group to the modified nucleoside. Both reductive cleavage of SAM and methylation were dependent on the presence of MiaB and did not require any other protein.
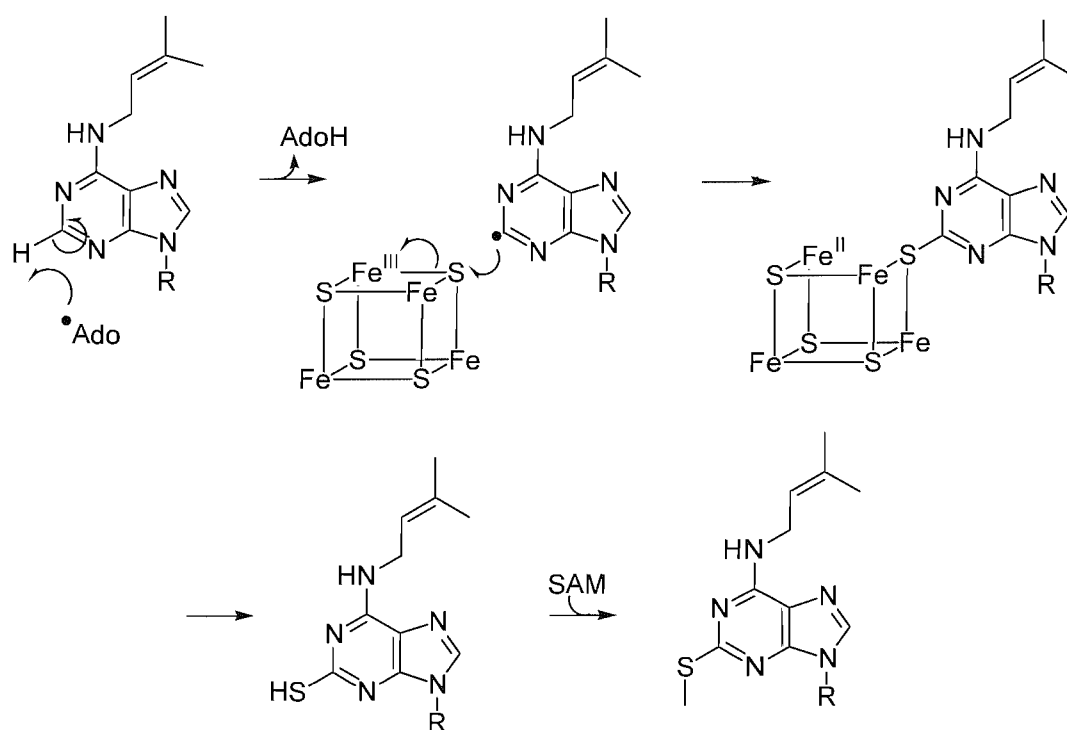
Figure 1.20 Proposed mechanism for methylthiolation by of i⁶A in which both sulfur insertion and methylation are catalysed by MiaB.

Recently it has been shown that MiaB, like LipA and BioB, can bind a second iron sulfur cluster (*122*). A [4Fe-4S]¹⁺/²⁺, is ligated by a CX₃₅CX₃₂C motif at the N-terminus and thus iron sulfur cluster binding in MiaB mirrors that of LipA which also binds two [4Fe-4S]¹⁺/²⁺ (*29*). It seems likely that the second clusters of BioB,

LipA and MiaB play similar mechanistic roles and therefore that the of N-terminal [4Fe-4S]$^{1+/2+}$ may be the source of sulfur during formation of ms^{2}io^{6}A.

1.4.4   Maturation of Fe-only hydrogenase active site complexes

Hydrogenases catalyse the reversible oxidation of molecular hydrogen playing a vital role in anaerobic metabolism in certain microorganisms. Three classes of these enzymes have been identified according to their metal content; Ni-Fe hydrogenases, Fe-only hydrogenases and iron sulfur cluster free hydrogenases. The Fe-only hydrogenases have an active site complex comprised of six Fe centres which has been named the H-cluster (fig. 1.21) (*124, 125*). This complex contains a [4Fe-4S] cluster bridged through a cysteine residue to a Fe-Fe site which has CO and CN$^-$ coordination. Crystallographic and spectroscopic data have revealed that in the H$_2$ uptake enzyme from *D. desufuricans* the two Fe atoms of this unit are ligated by a dithiolate small molecule which is probably di(thiomethyl)amine (*126*).
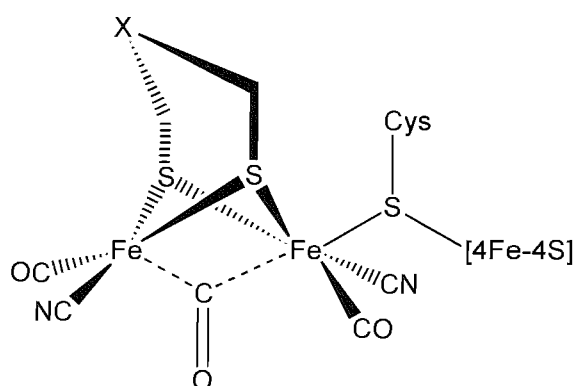
Figure 1.21 Structure of the Fe-only hydrogenase active site complex (H-cluster).

Maturation of hydrogenase active site complexes involves a number of enzymes. In *Chlamydomonas reinhardtii* two genes, *hydEF* and *hydG*, have been identified that encode three proteins, HydE, HydF and HydG, which are required for the maturation process (*127*). Both HydE and HydG contain highly conserved motifs characteristic of members of the radical SAM family and characterisation of homologues from *T. maritima* has confirmed that they are iron sulfur proteins which are capable of initiating reductive cleavage of SAM (*128*). It is hypothesised that one (or both) of these proteins may be required in the formation of a C-S bond during the assembly of the di(thiomethyl)amine (or dithiopropane) ligand. Interestingly the HydE protein

binds two [4Fe-4S] iron sulfur clusters (*128*), reminiscent of the two distinct iron sulfur clusters found in BioB and LipA. Thus, this protein might speculatively be assigned to a newly emerging sub-group of radical SAM proteins that use a second cluster as a sulfur donor for the formation of C-S bonds at unactivated carbon centres.

1.5 Aims of this thesis

The aim of this project was to develop methods for the investigation of LipA activity in vitro and to use these techniques to study the mechanism of lipoyl biosynthesis.

1.6   References

(1)   Reed, L. J., De, B. B., Gunsalus, I. C., and Hornberger, C. S., Jr. (1951) Crystalline alpha-lipoic acid; a catalytic agent associated with pyruvate dehydrogenase. *Science 114*, 93-4.

(2)   Reed, L. J., Gunsalus, I. C., Schnakenberg, G. H. F., Soper, Q. F., Boaz, H. E., Kern, S. F., and V., P. T. (1953) Isolation, characterization and structure of α-lipoic acid. *J. Am. Chem. Soc. 75*, 1267-1270.

(3)   Packer, L., Kraemer, K., and Rimbach, G. (2001) Molecular aspects of lipoic acid in the prevention of diabetes complications. *Nutrition 17*, 888-95.

(4)   Smith, A. R., Shenvi, S. V., Widlansky, M., Suh, J. H., and Hagen, T. M. (2004) Lipoic acid as a potential therapy for chronic diseases associated with oxidative stress. *Curr. Med. Chem. 11*, 1135-46.

(5)   Holmquist, L., Stuchbury, G., Berbaum, K., Muscat, S., Young, S., Hager, K., Engel, J., and Munch, G. (2007) Lipoic acid as a novel treatment for Alzheimer's disease and related dementias. *Pharmacol. Ther. 113*, 154-64.

(6)   Perham, R. N. (2000) Swinging arms and swinging domains in multifunctional enzymes: catalytic machines for multistep reactions. *Annu. Rev. Biochem. 69*, 961-1004.

(7)   Perham, R. N. (1991) Domains, motifs, and linkers in 2-oxo acid dehydrogenase multienzyme complexes: a paradigm in the design of a multifunctional protein. *Biochemistry 30*, 8501-12.

(8)   Fujiwara, K., Okamura-Ikeda, K., and Motokawa, Y. (1992) Expression of mature bovine H-protein of the glycine cleavage system in *Escherichia coli* and in vitro lipoylation of the apoform. *J. Biol. Chem. 267*, 20011-6.

(9)   Reed, L. J., and Hackert, M. L. (1990) Structure-function relationships in dihydrolipoamide acyltransferases. *J. Biol. Chem. 265*, 8971-4.

(10)   Dardel, F., Davis, A. L., Laue, E. D., and Perham, R. N. (1993) Three-dimensional structure of the lipoyl domain from *Bacillus stearothermophilus* pyruvate dehydrogenase multienzyme complex. *J. Mol. Biol. 229*, 1037-48.

(11)   Douce, R., Bourguignon, J., Macherel, D., and Neuburger, M. (1994) The glycine decarboxylase system in higher plant mitochondria: structure, function and biogenesis. *Biochem. Soc. Trans. 22*, 184-8.

(12)   Herbert, A. A., and Guest, J. R. (1968) Biochemical and genetic studies with lysine & methionine mutants of *Escherichia coli*: lipoic acid and α-ketoglutarate dehydrogenase-less mutants. *J. Gen. Microbiol. 53*, 363-81.

(13)   Herbert, A. A., and Guest, J. R. (1975) Lipoic acid content of *Escherichia coli* and other microorganisms. *Arch. Microbiol. 106*, 259-66.

(14)   Gueguen, V., Macherel, D., Jaquinod, M., Douce, R., and Bourguignon, J. (2000) Fatty acid and lipoic acid biosynthesis in higher plant mitochondria. *J. Biol. Chem. 275*, 5016-5025.

(15)   Thomsen-Zieger, N., Schachtner, J., and Seeber, F. (2003) Apicomplexan parasites contain a single lipoic acid synthase located in the plastid. *FEBS Lett. 547*, 80-86.

(16)   Morikawa, T., Yasuno, R., and Wada, H. (2001) Do mammalian cells synthesize lipoic acid? Identification of a mouse cDNA encoding a lipoic acid synthase located in mitochondria. *FEBS Lett. 498*, 16-21.

(17)   Yi, X., and Maeda, N. (2005) Endogenous production of lipoic acid is essential for mouse development. *Mol. Cell. Biol. 25*, 8387-8392.

(18)   Reed, L. J. (1966) in *Comprehensive Biochemistry* (Florkin, M., and Stotz, E. M., Eds.) pp 99-126, Elsevier, Amsterdam.

(19)   Vanden Boom, T. J., Reed, K. E., and Cronan, J. E. (1991) Lipoic acid metabolism in *Escherichia coli*: isolation of null mutants defective in lipoic acid biosynthesis, molecular cloning and characterization of the *E. coli lip* locus, and identification of the lipoylated protein of the glycine cleavage system. *J. Bacteriol. 173*, 6411-6420.

(20)   Hayden, M. A., Huang, I., Bussiere, D. E., and Ashley, G. W. (1992) The biosynthesis of lipoic acid. Cloning of *lip*, a lipoate biosynthetic locus of *Escherichia coli. J. Biol. Chem. 267*, 9512-5.

(21)   Hayden, M. A., Huang, I. Y., Iliopoulos, G., Orozco, M., and Ashley, G. W. (1993) Biosynthesis of lipoic acid: characterization of the lipoic acid auxotrophs *Escherichia coli* W1485-lip2 and JRG33-lip9. *Biochemistry 32*, 3778-82.

(22)   Reed, K. E., and Cronan, J. E. (1993) Lipoic acid metabolism in *Escherichia coli*: sequencing and functional characterization of the *lipA* and *lipB* genes. *J. Bacteriol. 175*, 1325-1336.

(23)   Miller, J. R., Busby, R. W., Jordan, S. W., Cheek, J., Henshaw, T. F., Ashley, G. W., Broderick, J. B., Cronan, J. E., Jr., and Marletta, M. A. (2000) *Escherichia coli* LipA is a lipoyl synthase: *in vitro* biosynthesis of lipoylated pyruvate dehydrogenase complex from octanoyl-acyl carrier protein. *Biochemistry 39*, 15166-78.

(24)   Sofia, H. J., Chen, G., Hetzler, B. G., Reyes-Spindola, J. F., and Miller, N. E. (2001) Radical SAM, a novel protein superfamily linking unresolved steps in familiar biosynthetic pathways with radical mechanisms: functional characterization using new analysis and information visualization methods. *Nucleic Acids Res. 29*, 1097-106.

(25)   Hewitson, K. S., Baldwin, J. E., Shaw, N. M., and Roach, P. L. (2000) Mutagenesis of the proposed iron-sulfur cluster binding ligands in *Escherichia coli* biotin synthase. *FEBS Letters 466*, 372-376.

(26)   Hewitson, K. S., Ollagnier-de Choudens, S., Sanakis, Y., Shaw, N. M., Baldwin, J. E., Munck, E., Roach, P. L., and Fontecave, M. (2002) The iron-sulfur center of biotin synthase: site-directed mutants. *J. Biol. Inorg. Chem. 7*, 83-93.

(27)   Layer, G., Verfurth, K., Mahlitz, E., and Jahn, D. (2002) Oxygen-independent coproporphyrinogen-III oxidase HemN from *Escherichia coli*. *J. Biol. Chem. 277*, 34136-42.

(28)   Tamarit, J., Gerez, C., Meier, C., Mulliez, E., Trautwein, A., and Fontecave, M. (2000) The activating component of the anaerobic ribonucleotide reductase from *Escherichia coli*. An iron-sulfur center with only three cysteines. *J. Biol. Chem. 275*, 15669-75.

(29)   Cicchillo, R. M., Lee, K. H., Baleanu-Gogonea, C., Nesbitt, N. M., Krebs, C., and Booker, S. J. (2004) *Escherichia coli* lipoyl synthase binds two distinct [4Fe-4S] clusters per polypeptide. *Biochemistry 43*, 11770-81.

(30)   Fontecave, M., Mulliez, E., and Ollagnier-de-Choudens, S. (2001) Adenosylmethionine as a source of 5'-deoxyadenosyl radicals. *Curr. Opin. Chem. Biol. 5*, 506-511.

(31)   Jarrett, J. T. (2003) The generation of 5'-deoxyadenosyl radicals by adenosylmethionine-dependent radical enzymes. *Curr. Opin. Chem. Biol. 7*, 174-82.

(32)   Krebs, C., Henshaw, T. F., Cheek, J., Huynh, B. H., and Broderick, J. B. (2000) Conversion of 3Fe-4S to 4Fe-4S clusters in native pyruvate formate-lyase activating enzyme: Mössbauer characterization and implications for mechanism. *J. Am. Chem. Soc. 122*, 12497-12506.

(33)   Padovani, D., Thomas, F., Trautwein, A. X., Mulliez, E., and Fontecave, M. (2001) Activation of class III ribonucleotide reductase from *E. coli*. The electron transfer from the iron-sulfur center to S-adenosylmethionine. *Biochemistry 40*, 6713-9.

(34)   Henshaw, T. F., Cheek, J., and Broderick, J. B. (2000) The [4Fe-4S](1+) cluster of pyruvate formate-lyase activating enzyme generates the glycyl radical on pyruvate formate-lyase: EPR-detected single turnover. *J. Am. Chem. Soc. 122*, 8331-8332.

(35)   Lieder, K. W., Booker, S., Ruzicka, F. J., Beinert, H., Reed, G. H., and Frey, P. A. (1998) S-Adenosylmethionine-dependent reduction of lysine 2,3-aminomutase and observation of the catalytically functional iron-sulfur centers by electron paramagnetic resonance. *Biochemistry 37*, 2578-85.

(36)   Ugulava, N. B., Gibney, B. R., and Jarrett, J. T. (2000) Iron-sulfur cluster interconversions in biotin synthase: dissociation and reassociation of iron during conversion of [2Fe-2S] to [4Fe-4S] clusters. *Biochemistry 39*, 5206-14.

(37)   Broderick, J. B., Henshaw, T. F., Cheek, J., Wojtuszewski, K., Smith, S. R., Trojan, M. R., McGhan, R. M., Kopf, A., Kibbey, M., and Broderick, W. E. (2000) Pyruvate formate-lyase-activating enzyme: strictly anaerobic isolation yields active enzyme containing a [3Fe-4S]$^+$ cluster. *Biochem. Biophys. Res. Commun. 269*, 451-6.

(38)   Imlay, J. A. (2006) Iron-sulphur clusters and the problem with oxygen. *Mol Microbiol 59*, 1073-82.

(39)   Duin, E. C., Lafferty, M. E., Crouse, B. R., Allen, R. M., Sanyal, I., Flint, D. H., and Johnson, M. K. (1997) [2Fe-2S] to [4Fe-4S] cluster conversion in *Escherichia coli* biotin synthase. *Biochemistry 36*, 11811-20.

(40)   Mulliez, E., Padovani, D., Atta, M., Alcouffe, C., and Fontecave, M. (2001) Activation of class III ribonucleotide reductase by flavodoxin: a protein radical-driven electron transfer to the iron-sulfur center. *Biochemistry 40*, 3730-6.

(41)   Ifuku, O., Koga, N., Haze, S., Kishimoto, J., and Wachi, Y. (1994) Flavodoxin is required for conversion of dethiobiotin to biotin in *Escherichia coli*. *Eur. J. Biochem. 224*, 173-8.

(42)   Bianchi, V., Eliasson, R., Fontecave, M., Mulliez, E., Hoover, D. M., Matthews, R. G., and Reichard, P. (1993) Flavodoxin is required for the activation of the anaerobic ribonucleotide reductase. *Biochem. Biophys. Res. Commun. 197*, 792-7.

(43)   Mejean, A., Tse Sum Bui, B., Florentin, D., Ploux, O., Izumi, Y., and Marquet, A. (1995) Highly purified biotin synthase can transform dethiobiotin into biotin in the absence of any other protein, in the presence of photoreduced deazaflavin. *Biochem. Biophys. Res. Commun. 217*, 1231-7.

(44)   Ollagnier-de Choudens, S., Sanakis, Y., Hewitson, K. S., Roach, P., Munck, E., and Fontecave, M. (2002) Reductive cleavage of S-adenosylmethionine by biotin synthase from *Escherichia coli. J. Biol. Chem. 277*, 13449-13454.

(45)   Moss, M. L., and Frey, P. A. (1990) Activation of lysine 2,3-aminomutase by S-adenosylmethionine. *J. Biol. Chem. 265*, 18112-5.

(46)   Ollagnier, S., Mulliez, E., Schmidt, P. P., Eliasson, R., Gaillard, J., Deronzier, C., Bergman, T., Graslund, A., Reichard, P., and Fontecave, M. (1997) Activation of the anaerobic ribonucleotide reductase from *Escherichia coli*. The essential role of the iron-sulfur center for S-adenosylmethionine reduction. *J. Biol. Chem. 272*, 24216-23.

(47)   Cicchillo, R. M., Iwig, D. F., Jones, A. D., Nesbitt, N. M., Baleanu-Gogonea, C., Souder, M. G., Tu, L., and Booker, S. J. (2004) Lipoyl synthase requires two equivalents of S-adenosyl-L-methionine to synthesize one equivalent of lipoic acid. *Biochemistry 43*, 6378-86.

(48)   Magnusson, O. T., Reed, G. H., and Frey, P. A. (1999) Spectroscopic evidence for the participation of an allylic analogue of the 5'-deoxyadenosyl radical in the reaction of lysine 2,3-aminomutase. *J. Am. Chem. Soc. 121*, 9764-9765.

(49)   Magnusson, O. T., Reed, G. H., and Frey, P. A. (2001) Characterization of an allylic analogue of the 5'-deoxyadenosyl radical: an intermediate in the reaction of lysine 2,3-aminomutase. *Biochemistry 40*, 7773-82.

(50) Frey, P. A., and Reed, G. H. (2000) Radical mechanisms in adenosylmethionine- and adenosylcobalamin-dependent enzymatic reactions. *Arch. Biochem. Biophys. 382*, 6-14.

(51) Frey, P. A. (2001) Radical mechanisms of enzymatic catalysis. *Annu. Rev. Biochem. 70*, 121-48.

(52) Liu, A., and Graslund, A. (2000) Electron paramagnetic resonance evidence for a novel interconversion of $[3Fe-4S]^+$ and $[4Fe-4S]^+$ clusters with endogenous iron and sulfide in anaerobic ribonucleotide reductase activase *in vitro. J. Biol. Chem. 275*, 12367-73.

(53) Cosper, M. M., Jameson, G. N., Davydov, R., Eidsness, M. K., Hoffman, B. M., Huynh, B. H., and Johnson, M. K. (2002) The $[4Fe-4S]^{2+}$ cluster in reconstituted biotin synthase binds S-adenosyl-L-methionine. *J. Am. Chem. Soc. 124*, 14006-7.

(54) Krebs, C., Broderick, W. E., Henshaw, T. F., Broderick, J. B., and Huynh, B. H. (2002) Coordination of adenosylmethionine to a unique iron site of the [4Fe-4S] of pyruvate formate-lyase activating enzyme: a Mössbauer spectroscopic study. *J. Am. Chem. Soc. 124*, 912-913.

(55) Walsby, C. J., Hong, W., Broderick, W. E., Cheek, J., Ortillo, D., Broderick, J. B., and Hoffman, B. M. (2002) Electron-nuclear double resonance spectroscopic evidence that S-adenosylmethionine binds in contact with the catalytically active $[4Fe-4S]^+$ cluster of pyruvate formate-lyase activating enzyme. *J. Am. Chem. Soc. 124*, 3143-3151.

(56) Walsby, C. J., Ortillo, D., Broderick, W. E., Broderick, J. B., and Hoffman, B. M. (2002) An anchoring role for FeS clusters: chelation of the amino acid moiety of S-adenosylmethionine to the unique iron site of the [4Fe-4S] cluster of pyruvate formate-lyase activating enzyme. *J. Am. Chem. Soc. 124*, 11270-11271.

(57) Chen, D., Walsby, C., Hoffman, B. M., and Frey, P. A. (2003) Coordination and mechanism of reversible cleavage of S-adenosylmethionine by the [4Fe-4S] center in lysine 2,3-aminomutase. *J. Am. Chem. Soc. 125*, 11788-9.

(58) Berkovitch, F., Nicolet, Y., Wan, J. T., Jarrett, J. T., and Drennan, C. L. (2004) Crystal structure of biotin synthase, an S-adenosylmethionine-dependent radical enzyme. *Science 303*, 76-9.

(59) Lepore, B. W., Ruzicka, F. J., Frey, P. A., and Ringe, D. (2005) The X-ray crystal structure of lysine-2,3-aminomutase from *Clostridium subterminale*. *Proc. Natl. Acad. Sci. U. S.A. 102*, 13819-24.

(60) Layer, G., Moser, J., Heinz, D. W., Jahn, D., and Schubert, W. D. (2003) Crystal structure of coproporphyrinogen III oxidase reveals cofactor geometry of radical SAM enzymes. *EMBO J. 22*, 6214-24.

(61) Hanzelmann, P., and Schindelin, H. (2006) Binding of 5'-GTP to the C-terminal FeS cluster of the radical S-adenosylmethionine enzyme MoaA provides insights into its mechanism. *Proc. Natl. Acad. Sci. U. S.A. 103*, 6829-34.

(62) Kriek, M., Martins, F., Leonardi, R., Fairhurst, S. A., Lowe, D. J., and Roach, P. L. (2007) Thiazole synthase from Escherichia coli: an investigation of the substrates and purified proteins required for activity in vitro. *J. Biol. Chem. 282*, 17413-23.

(63) Hinckley, G. T., and Frey, P. A. (2006) Cofactor dependence of reduction potentials for $[4Fe-4S]^{2+/1+}$ in lysine 2,3-aminomutase. *Biochemistry 45*, 3219-25.

(64) Moss, M., and Frey, P. A. (1987) The role of S-adenosylmethionine in the lysine 2,3-aminomutase reaction. *J. Biol. Chem. 262*, 14859-62.

(65) Frey, M., Rothe, M., Wagner, A. F., and Knappe, J. (1994) Adenosylmethionine-dependent synthesis of the glycyl radical in pyruvate formate-lyase by abstraction of the glycine C-2 pro-S hydrogen atom. Studies of [2H]glycine-substituted enzyme and peptides homologous to the glycine 734 site. *J. Biol. Chem. 269*, 12432-7.

(66) Escalettes, F., Florentin, D., Bui, B. T. S., Lesage, D., and Marquet, A. (1999) Biotin synthase mechanism: Evidence for hydrogen transfer from the substrate into deoxyadenosine. *J. Am. Chem. Soc. 121*, 3571-3578.

(67) Knappe, J., and Wagner, A. F. (2001) Stable glycyl radical from pyruvate formate-lyase and ribonucleotide reductase (III). *Adv. Protein Chem. 58*, 277-315.

(68) Guillerm, G., Frappier, F., Gaudry, M., and Marquet, A. (1977) On the mechanism of conversion of dethiobiotin to biotin in *Escherichia coli*. *Biochimie 59*, 119-21.

(69)   Parry, R. J., and Kunitani, M. G. (1976) Letter: Biotin biosynthesis. 1. The incorporation of specifically tritiated dethiobiotin into biotin. *J. Am. Chem. Soc. 98*, 4024-6.

(70)   Trainor, D. A., Parry, R. J., and Gitterman, A. (1980) Biotin Biosynthesis .2. stereochemistry of sulfur introduction at C-4 of dethiobiotin. *J. Am. Chem. Soc. 102*, 1467-1468.

(71)   Ifuku, O., Kishimoto, J., Haze, S., Yanagi, M., and Fukushima, S. (1992) Conversion of dethiobiotin to biotin in cell-free extracts of *Escherichia coli*. *Biosci. Biotechnol. Biochem. 56*, 1780-5.

(72)   Sanyal, I., Cohen, G., and Flint, D. H. (1994) Biotin synthase: purification, characterization as a [2Fe-2S] cluster protein, and *in vitro* activity of the *Escherichia coli bioB* gene product. *Biochemistry 33*, 3625-31.

(73)   Ohshiro, T., Yamamoto, M., Izumi, Y., Bui, B. T., Florentin, D., and Marquet, A. (1994) Enzymatic conversion of dethiobiotin to biotin in cell-free extracts of a *Bacillus sphaericus bioB* transformant. *Biosci. Biotechnol. Biochem. 58*, 1738-41.

(74)   Birch, O. M., Fuhrmann, M., and Shaw, N. M. (1995) Biotin Synthase From Escherichia-Coli, an Investigation of the Low- Molecular-Weight and Protein-Components Required For Activity in- Vitro. *J. Biol. Chem. 270*, 19158-19165.

(75)   Sanyal, I., Gibson, K. J., and Flint, D. H. (1996) Escherichia coli biotin synthase: an investigation into the factors required for its activity and its sulfur donor. *Arch. Biochem. Biophys. 326*, 48-56.

(76)   Ohshiro, T., Kishimoto, T., Arase, M., and Izumi, Y. (1998) Characterization of the biotin synthase reaction from *Bacillus sphaericus* using the photoreduced deazaflavin system. *J. Ferment. Bioeng. 86*, 446-450.

(77)   Cosper, M. M., Jameson, G. N., Eidsness, M. K., Huynh, B. H., and Johnson, M. K. (2002) Recombinant *Escherichia coli* biotin synthase is a $[2Fe-2S]^{2+}$ protein in whole cells. *FEBS Lett. 529*, 332-6.

(78)   Benda, R., Tse Sum Bui, B., Schunemann, V., Florentin, D., Marquet, A., and Trautwein, A. X. (2002) Iron-sulfur clusters of biotin synthase in vivo: a Mössbauer study. *Biochemistry 41*, 15000-6.

(79) Ollagnier-De Choudens, S., Sanakis, Y., Hewitson, K. S., Roach, P., Baldwin, J. E., Munck, E., and Fontecave, M. (2000) Iron-sulfur center of biotin synthase and lipoate synthase. *Biochemistry 39*, 4165-73.

(80) Tse Sum Bui, B., Florentin, D., Marquet, A., Benda, R., and Trautwein, A. X. (1999) Mössbauer studies of *Escherichia coli* biotin synthase: evidence for reversible interconversion between $[2Fe-2S]^{2+}$ and $[4Fe-4S]^{2+}$ clusters. *FEBS Lett. 459*, 411-4.

(81) Ugulava, N. B., Gibney, B. R., and Jarrett, J. T. (2001) Biotin synthase contains two distinct iron-sulfur cluster binding sites: chemical and spectroelectrochemical analysis of iron-sulfur cluster interconversions. *Biochemistry 40*, 8343-51.

(82) Ugulava, N. B., Surerus, K. K., and Jarrett, J. T. (2002) Evidence from Mössbauer spectroscopy for distinct $[2Fe-2S]^{2+}$ and $[4Fe-4S]^{2+}$ cluster binding sites in biotin synthase from *Escherichia coli. J. Am. Chem. Soc. 124*, 9050-1.

(83) Ugulava, N. B., Frederick, K. K., and Jarrett, J. T. (2003) Control of adenosylmethionine-dependent radical generation in biotin synthase: a kinetic and thermodynamic analysis of substrate binding to active and inactive forms of BioB. *Biochemistry 42*, 2708-2719.

(84) Broach, R. B., and Jarrett, J. T. (2006) Role of the $[2Fe-2S]^{2+}$ cluster in biotin synthase: mutagenesis of the atypical metal ligand arginine 260. *Biochemistry 45*, 14166-14174.

(85) Guianvarc'h, D., Florentin, D., Tse Sum Bui, B., Nunzi, F., and Marquet, A. (1997) Biotin synthase, a new member of the family of enzymes which uses S-adenosylmethionine as a source of deoxyadenosyl radical. *Biochem. Biophys. Res. Commun. 236*, 402-6.

(86) Shaw, N. M., Birch, O. M., Tinschert, A., Venetz, V., Dietrich, R., and Savoy, L. A. (1998) Biotin synthase from *Escherichia coli*: isolation of an enzyme-generated intermediate and stoichiometry of S-adenosylmethionine use. *Biochem. J. 330*, 1079-1085.

(87) Baxter, R. L., Camp, D. J., Coutts, A., and Shaw, N. (1992) Synthesis and biological activity of 9-mercaptodethiobiotin - a putative Biotin precursor in *Escherichia coli. J. Chem. Soc., Perkin Trans. 1*, 255-258.

(88)   Marquet, A., Frappier, F., Guillerm, G., Azoulay, M., Florentin, D., and Tabet, J. C. (1993) Biotin biosynthesis - synthesis and biological evaluation of the putative intermediate thiols. *J. Am. Chem. Soc. 115*, 2139-2145.

(89)   Florentin, D., Bui, B. T., Marquet, A., Ohshiro, T., and Izumi, Y. (1994) On the mechanism of biotin synthase of *Bacillus sphaericus*. *C. R. Acad. Sci. III 317*, 485-8.

(90)   DeMoll, E., and Shive, W. (1983) The origin of sulfur in biotin. *Biochem. Biophys. Res. Commun. 110*, 243-249.

(91)   Gibson, K. J., Pelletier, D. A., and Turner, I. M., Sr. (1999) Transfer of sulfur to biotin from biotin synthase (BioB protein). *Biochem. Biophys. Res. Commun. 254*, 632-5.

(92)   Tse Sum Bui, B., Florentin, D., Fournier, F., Ploux, O., Mejean, A., and Marquet, A. (1998) Biotin synthase mechanism: on the origin of sulphur. *FEBS Lett. 440*, 226-30.

(93)   Tse Sum Bui, B., Mattioli, T. A., Florentin, D., Bolbach, G., and Marquet, A. (2006) *Escherichia coli* biotin synthase produces selenobiotin. Further evidence of the involvement of the $[2Fe-2S]^{2+}$ cluster in the sulfur insertion step. *Biochemistry 45*, 3824-34.

(94)   Ugulava, N. B., Sacanell, C. J., and Jarrett, J. T. (2001) Spectroscopic changes during a single turnover of biotin synthase: destruction of a [2Fe-2S] cluster accompanies sulfur insertion. *Biochemistry 40*, 8352-8.

(95)   Jameson, G. N., Cosper, M. M., Hernandez, H. L., Johnson, M. K., and Huynh, B. H. (2004) Role of the [2Fe-2S] cluster in recombinant *Escherichia coli* biotin synthase. *Biochemistry 43*, 2022-31.

(96)   Ollagnier-de-Choudens, S., Mulliez, E., Hewitson, K. S., and Fontecave, M. (2002) Biotin synthase is a pyridoxal phosphate-dependent cysteine desulfurase. *Biochemistry 41*, 9145-9152.

(97)   Tse Sum Bui, B., Lotierzo, M., Escalettes, F., Florentin, D., and Marquet, A. (2004) Further investigation on the turnover of *Escherichia coli* biotin synthase with dethiobiotin and 9-mercaptodethiobiotin as substrates. *Biochemistry 43*, 16432-41.

(98)   Tse Sum Bui, B., Escalettes, F., Chottard, G., Florentin, D., and Marquet, A. (2000) Enzyme-mediated sulfide production for the reconstitution of [2Fe-2S]

clusters into apo-biotin synthase of *Escherichia coli*. Sulfide transfer from cysteine to biotin. *Eur. J. Biochem. 267*, 2688-94.

(99) Choi-Rhee, E., and Cronan, J. E. (2005) Biotin synthase is catalytic *in vivo*, but catalysis engenders destruction of the protein. *Chem Biol 12*, 461-8.

(100) Zheng, L., White, R. H., Cash, V. L., and Dean, D. R. (1994) Mechanism for the desulfurization of L-cysteine catalyzed by the *nifS* gene product. *Biochemistry 33*, 4714-20.

(101) Zheng, L. M., Cash, V. L., Flint, D. H., and Dean, D. R. (1998) Assembly of iron-sulfur clusters - Identification of an *iscSUA- hscBA-fdx* gene cluster from *Azotobacter vinelandii*. *J. Biol. Chem.273*, 13264-13272.

(102) Ollagnier-de-Choudens, S., Mulliez, E., and Fontecave, M. (2002) The PLP-dependent biotin synthase from *Escherichia coli*: mechanistic studies. *FEBS Lett. 532*, 465-468.

(103) Choi-Rhee, E., and Cronan, J. E. (2005) A nucleosidase required for *in vivo* function of the S-adenosyl-L-methionine radical enzyme, biotin synthase. *Chem. Biol. 12*, 589-593.

(104) Parry, R. J. (1977) Biosynthesis of lipoic acid. 1. Incorporation of specifically tritiated octanoic acid into lipoic acid. *J. Am. Chem. Soc. 99*, 6464-6.

(105) White, R. H. (1980) Biosynthesis of lipoic acid - extent of incorporation of deuterated hydroxyoctanoic and thiooctanoic acids into lipoic acid. *J. Am. Chem. Soc. 102*, 6605-6607.

(106) Parry, R. J., and Trainor, D. A. (1978) Biosynthesis of lipoic acid. 2. Stereochemistry of sulfur introduction at C-6 of octanoic acid. *J. Am. Chem. Soc. 100*, 5243-4.

(107) Busby, R. W., Schelvis, J. P. M., Yu, D. S., Babcock, G. T., and Marletta, M. A. (1999) Lipoic acid biosynthesis: LipA is an iron-sulfur protein. *J. Am. Chem. Soc. 121*, 4706-4707.

(108) Ollagnier-de Choudens, S., and Fontecave, M. (1999) The lipoate synthase from *Escherichia coli* is an iron-sulfur protein. *FEBS Lett. 453*, 25-8.

(109) Jordan, S. W., and Cronan, J. E., Jr. (1997) A new metabolic link. The acyl carrier protein of lipid synthesis donates lipoic acid to the pyruvate dehydrogenase complex in *Escherichia coli* and mitochondria. *J. Biol. Chem. 272*, 17903-6.

(110)   Jordan, S. W., and Cronan, J. E., Jr. (2003) The *Escherichia coli lipB* gene encodes lipoyl (octanoyl)-acyl carrier protein:protein transferase. *J. Bacteriol. 185*, 1582-9.

(111)   Zhao, X., Miller, J. R., Jiang, Y., Marletta, M. A., and Cronan, J. E. (2003) Assembly of the covalent linkage between lipoic acid and its cognate enzymes. *Chem. Biol. 10*, 1293-302.

(112)   Cronan, J. E., Zhao, X., and Jiang, Y. (2005) Function, attachment and synthesis of lipoic acid in *Escherichia coli*. *Adv Microb Physiol 50*, 103-46.

(113)   Cicchillo, R. M., and Booker, S. J. (2005) Mechanistic investigations of lipoic acid biosynthesis in *Escherichia coli*: both sulfur atoms in lipoic acid are contributed by the same lipoyl synthase polypeptide. *J. Am. Chem. Soc. 127*, 2860-1.

(114)   Douglas, P., Kriek, M., Bryant, P., and Roach, P. L. (2006) Lipoyl synthase inserts sulfur atoms into an octanoyl substrate in a stepwise manner. *Angew. Chem. Int. Ed. Engl. 45*, 5197-9.

(115)   Bjork, G. R., Ericson, J. U., Gustafsson, C. E., Hagervall, T. G., Jonsson, Y. H., and Wikstrom, P. M. (1987) Transfer RNA modification. *Annu. Rev. Biochem. 56*, 263-87.

(116)   Crain, P. F., and McCloskey, J. A. (1997) The RNA modification database. *Nucleic Acids Res. 25*, 126-7.

(117)   Dunin-Horkawicz, S., Czerwoniec, A., Gajda, M. J., Feder, M., Grosjean, H., and Bujnicki, J. M. (2006) MODOMICS: a database of RNA modification pathways. *Nucleic Acids Res. 34*, 145-9.

(118)   Esberg, B., Leung, H. C., Tsui, H. C., Bjork, G. R., and Winkler, M. E. (1999) Identification of the *miaB* gene, involved in methylthiolation of isopentenylated A37 derivatives in the tRNA of Salmonella typhimurium and Escherichia coli. *J. Bacteriol. 181*, 7256-65.

(119)   Anantharaman, V., Koonin, E. V., and Aravind, L. (2001) TRAM, a predicted RNA-binding domain, common to tRNA uracil methylation and adenine thiolation enzymes. *FEMS Microbiol. Lett. 197*, 215-221.

(120)   Pierrel, F., Bjork, G. R., Fontecave, M., and Atta, M. (2002) Enzymatic modification of tRNAs - MiaB is an iron-sulfur protein. *J. Biol. Chem. 277*, 13367-13370.

(121) Pierrel, F., Hernandez, H. L., Johnson, M. K., Fontecave, M., and Atta, M. (2003) MiaB protein from *Thermotoga maritima*. Characterization of an extremely thermophilic tRNA-methylthiotransferase. *J. Biol. Chem. 278*, 29515-24.

(122) Hernandez, H. L., Pierrel, F., Elleingand, E., Garcia-Serres, R., Huynh, B. H., Johnson, M. K., Fontecave, M., and Atta, M. (2007) MiaB, a bifunctional radical-S-adenosylmethionine enzyme involved in the thiolation and methylation of tRNA, contains two essential [4Fe-4S] clusters. *Biochemistry*.

(123) Pierrel, F., Douki, T., Fontecave, M., and Atta, M. (2004) MiaB protein is a bifunctional radical-S-adenosylmethionine enzyme involved in thiolation and methylation of tRNA. *J. Biol. Chem. 279*, 47555-63.

(124) Nicolet, Y., Piras, C., Legrand, P., Hatchikian, C. E., and Fontecilla-Camps, J. C. (1999) *Desulfovibrio desulfuricans* iron hydrogenase: the structure shows unusual coordination to an active site Fe binuclear center. *Structure 7*, 13-23.

(125) Peters, J. W., Lanzilotta, W. N., Lemon, B. J., and Seefeldt, L. C. (1998) X-ray crystal structure of the Fe-only hydrogenase (CpI) from *Clostridium pasteurianum* to 1.8 angstrom resolution. *Science 282*, 1853-8.

(126) Nicolet, Y., de Lacey, A. L., Vernede, X., Fernandez, V. M., Hatchikian, E. C., and Fontecilla-Camps, J. C. (2001) Crystallographic and FTIR spectroscopic evidence of changes in Fe coordination upon reduction of the active site of the Fe-only hydrogenase from *Desulfovibrio desulfuricans*. *J. Am. Chem. Soc. 123*, 1596-601.

(127) Posewitz, M. C., King, P. W., Smolinski, S. L., Zhang, L., Seibert, M., and Ghirardi, M. L. (2004) Discovery of two novel radical S-adenosylmethionine proteins required for the assembly of an active [Fe] hydrogenase. *J. Biol. Chem. 279*, 25711-20.

(128) Rubach, J. K., Brazzolotto, X., Gaillard, J., and Fontecave, M. (2005) Biochemical characterization of the HydE and HydG iron-only hydrogenase maturation enzymes from *Thermatoga maritima*. *FEBS Lett. 579*, 5055-60.

Chapter 2. Development of Novel Assay for LipA Activity

2.1   Introduction

Investigation into the biosynthesis of lipoyl groups was limited for some time by the lack of a sensitive and reliable *in vitro* assay. Recently, activity has been achieved *in vitro* using octanoylated versions of lipoyl domains as substrates for LipA from *Escherichia coli (1, 2)*. However, measuring the insertion of sulfur into octanoyl protein domains by LipA is technically challenging given the difficulty of isolating nonlipoylated subunits and the extreme oxygen sensitivity of *E. coli* LipA. This chapter describes the development of a novel assay which overcomes these difficulties by utilising simple peptides **15**, **20** and **25** (fig. 2.1) with an octanoyl group covalently attached to the side chain of a lysine residue as substrates for a putative LipA from the archaeon *Sulfolobus solfataricus* P2 (*3*).

The amino acid sequences of octanoyl peptides **15**, **20** and **25** (fig. 2.1) correspond to the lipoylation site of the E2 component of the putative 2-oxoacid dehydrogenase complex of *S. solfataricus* P2 (ORF no. SSO1529), which was identified by BLAST sequence analysis on the basis of close similarity with the sequence of the lipoylation site of the *E. coli* PDH E2 domain and other predicted lipoylation domains (table 2.1). The octanoyl group attached to the lysine residues of each of these peptides **15**, **20** and **25** (fig. 2.1) serves as a site for sulfur insertion by LipA. A further helpful modification is the fluorescent tagging of the N-terminus of peptide **15** in order to allow analysis by HPLC using fluorescence detection. Product analogues **16**, **21** and **26** (fig. 2.1) that have lipoic acid covalently attached to the lysine side chain were also prepared and these served as standards for comparison with assay products.

Organism	Residues	Sequence														
E. coli	238-252	L	I	T	V	E	G	D	K	A	S	M	E	V	P	A
S. solfataricus	36-50	L	V	I	I	E	T	E	K	I	T	T	T	V	K	S
T. volcanium	35-49	L	V	E	V	M	T	D	K	V	T	V	K	I	P	S
S. cerevisiae	68-82	I	A	E	I	E	T	D	K	A	Q	M	D	F	E	F
H. sapiens	252-266	L	A	E	I	E	T	D	K	A	T	I	G	F	E	V

Table 2.1 Aligned sequences of E2 components of 2-oxoacid dehydrogenase complexes of certain organisms. Conserved lysine residues involved in lipoyl binding are highlighted.
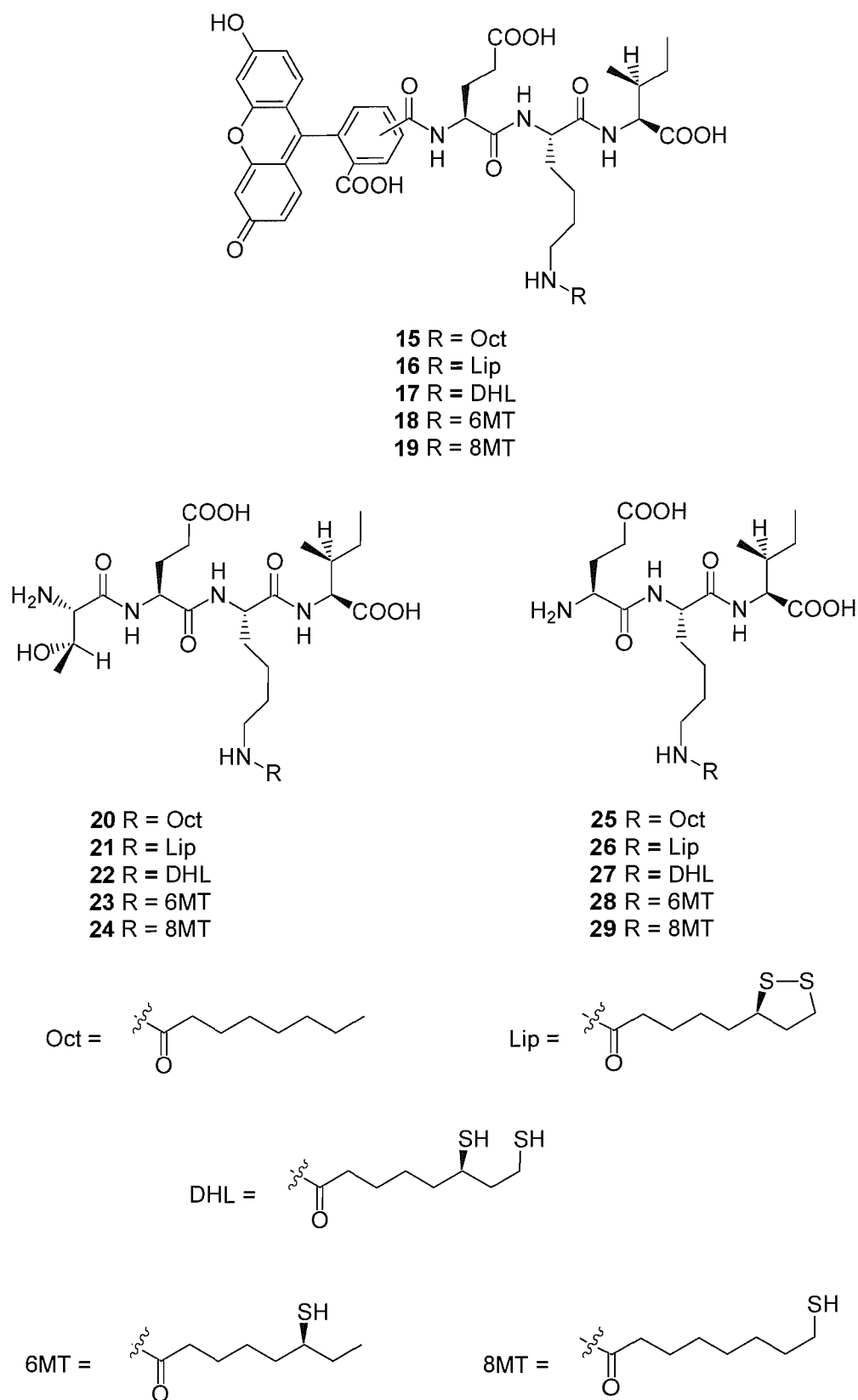
Figure 2.1 Structures of octanoyl (oct) substrate analogue peptides and products which might be from these during sulfur insertion reactions using LipA: lip = lipoyl group; DHL = dihydrolipoyl group; 6MT = 6-thiooctanoyl group; 8MT = 8-thiooctanoyl group.

It had been noted by Dr. M Kriek that *E. coli* LipA is unstable *in vitro* and has a tendency to precipitate (unpublished observations). A number of characterised proteins from hyperthermophilic organisms have been shown to have greater stability than eukaryotic and bacterial proteins (*4-7*). *S. solfataricus* is a hyperthermophilic archaeon which grows optimally at 80-85 °C and pH 2-4 and has been isolated from volcanic springs (*8-10*). The potential of a putative lipoyl synthase from *S. solfataricus* to initiate sulfur insertion into octanoyl substrates has thus been investigated. The putative *lipA* gene of *S. solfataricus* was identified by BLAST sequence analysis (table 2.2). The product of this gene is a 33 kDa protein, which contains both CX_3CX_2C and CX_4CX_5C iron sulfur cluster binding motifs and has a high degree of sequence similarity to *E. coli* LipA (*11*). *In vitro* assays using the *S. solfataricus lipA* gene product and octanoyl peptides **15, 20** and **25** (fig. 2.1) have subsequently been used to investigate the potential of both the protein and substrate analogues in the study of lipoyl biosynthesis.

Organism	Residue	Sequence
S. solfataricus	21-42	I A T V C E E A L C P N I M E C W G S G
E. coli	58-75	L H S V C E E A S C P N L A E C F N H G
S. solfataricus	52-67	M M G S I C T R G C R F C Y V L K G
E. coli	89-109	M L G A I C T R R C P F C D V A H G

Table 2.2 Aligned sequences of LipA from *S. solfataricus* (ORF no. SSO3158) and *E. coli*. The cysteine residues of the CX_3CX_2C motif are highlighted in blue and those of the CX_4CX_5C motif highlighted in red.

The coexpression of *E. coli* LipA with proteins that are the product of the *isc* operon (*12*) (fig. 2.2), has been shown to yield a greater proportion of soluble protein containing more equivalents of iron and sulfide (*13*). Genes of the *isc* operon from *E. coli* encode for proteins that are involved in the assembly and repair of FeS clusters (*14*). The product of the *iscS* gene is a cysteine desulfurase that is involved in the mobilisation of sulfur from L-cysteine (*15*). IscA, the product of the *iscA* gene, is an iron-binding protein that is believed to provide iron for the iron-sulfur cluster assembly (*16, 17*). The *iscU* gene encodes a protein (IscU) that serves as a scaffold for the construction of FeS clusters (*18*). Molecular chaperones that participate in the

incorporation of the FeS clusters into apoproteins are encoded by the *hscA* and *hscB* genes *(19)*. The final gene in the operon, *fdx*, encodes a ferrodoxin which is thought to maintain electron balance during the formation of FeS clusters *(20)*. The putative LipA from *S. solfataricus* has also been co-expressed the *E. coli isc* operon.
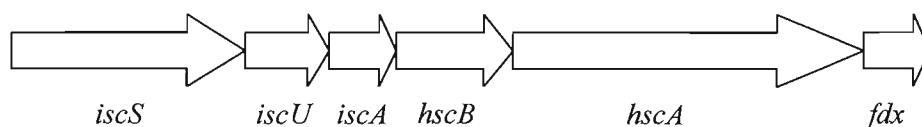
Figure 2.2 The gene structure of the *isc* operon from *E. coli*.

The plasmid pMK024 (fig. 2.3) was used for the co-expression of *S. solfataricus* LipA and proteins encoded by the *E. coli isc* operon. This was constructed by Dr. M. Kriek and carries the *S. solfataricus lipA* gene and the *E. coli isc* operon.
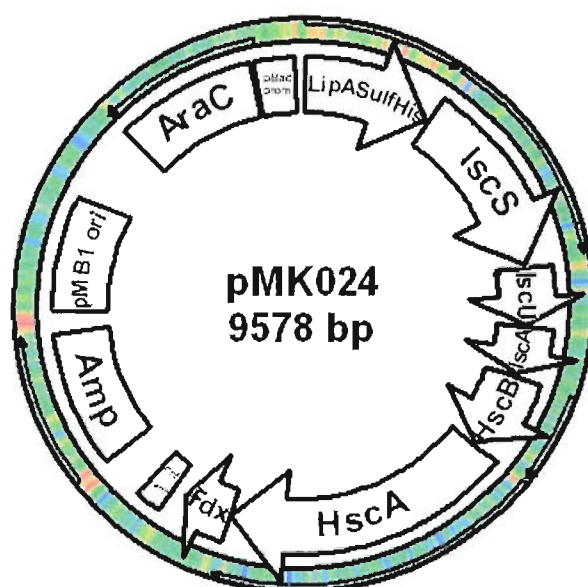
Figure 2.3 pMK024, constructed by Dr. M .Kriek for the co-expression of *S. solfataricus* LipA and proteins encoded by the *E. coli isc* operon

2.2 ` Expression and purification of *S. solfataricus* LipA

For expression of *S. solfataricus* LipA, BL21(DE3) or LMG194 cells were transformed with pMK024. N-terminal His$_6$-tagged *S. solfataricus* LipA obtained from these cells was then purified by Ni affinity chromatography followed by size exclusion chromatography (fig. 2.4) using a method developed by Dr. Kriek which is analogous to that described previously for *E. coli* LipA (*13*).
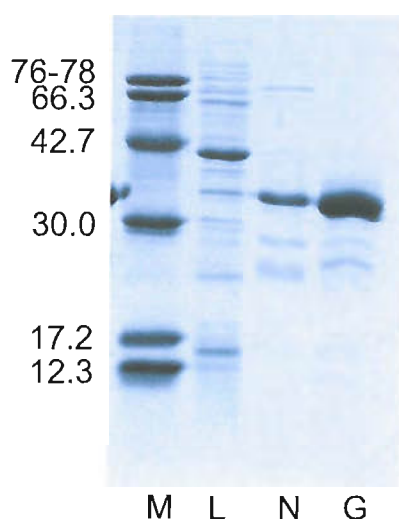
Figure 2.4 SDS–PAGE (15%) of LipA purification. Lanes indicate the following samples: M, molecular weight markers (kDa); L, cleared cell lysate; N, eluate from nickel affinity chromatography; G, eluate from gel filtration chromatography (monomeric LipA).

The UV absorption trace of the eluate of the gel filtration column exhibited three different peaks (fig. 2.5). The first corresponded to grey coloured fractions which contained no protein as judged by Bradford assay and therefore may contain iron sulfide derived from the partial degradation of the iron sulfur cluster. The second and third peaks contained dimeric and monomeric LipA respectively. Fractions corresponding to each protein peak were analysed by SDS-PAGE and all appeared as 33 kDa LipA monomers (fig. 2.6).
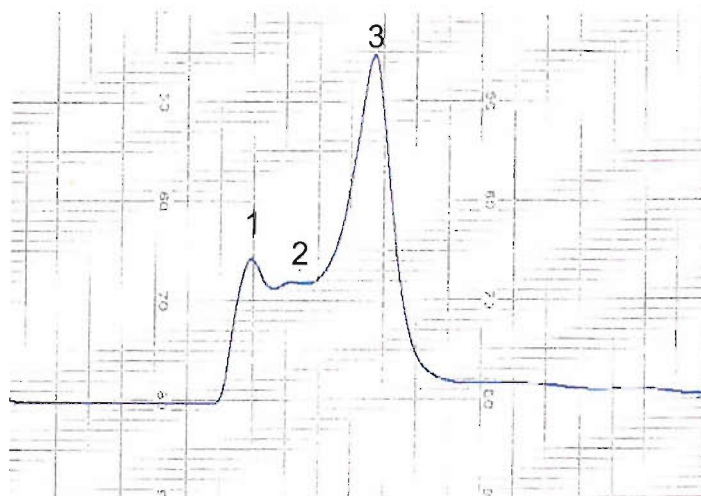
Figure 2.5 UV absorption trace for gel filtration of LipA: (1) grey coloured fractions which contained no protein and therefore maybe iron sulfide; (2) dimeric LipA; (3) monomeric LipA.
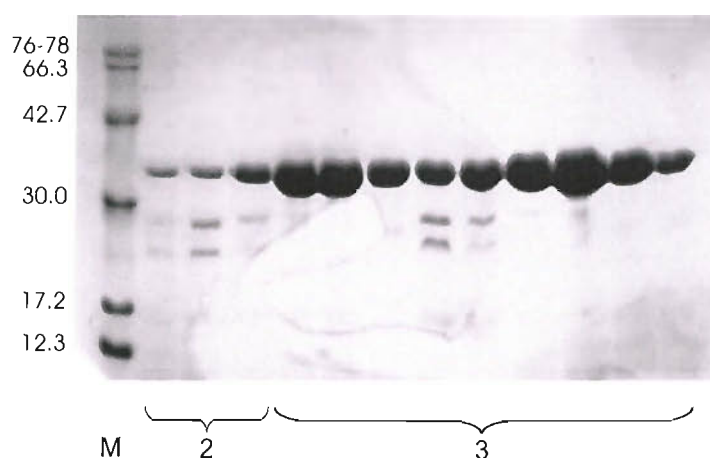
Figure 2.6 SDS–PAGE (15%) of fractions taken from gel filtration column. Lanes indicate the following samples: M, molecular weight markers (kDa); (2) LipA eluted from gel filtration column in dimeric form; (3) LipA eluted from gel filtration in monomeric form.

Purified dimeric LipA was isolated with typical yields of 10 to 20 mg whilst yields of purified monomeric LipA were typically 80 to 100 mg from 30 g of cells. This protein contained 3.6 ± 0.3 mol Fe and 3.0 ± 0.2 mol S^{2-} per mole of protein as determined by the methods of Fish (21) and Beinert (22) respectively.

2.3   Peptide synthesis

Substrate and product analogue peptides were prepared manually according to standard solid-phase protocols, using a sintered glass bubbler device (scheme 2.1) (23). Peptides were synthesised on Wang resin with 9-fluorenylmethyloxycarbonyl (Fmoc) protected amino acids using diisopropylcarbodiimide (DIC), hydroxybenzotriazole (HOBt) coupling chemistry.
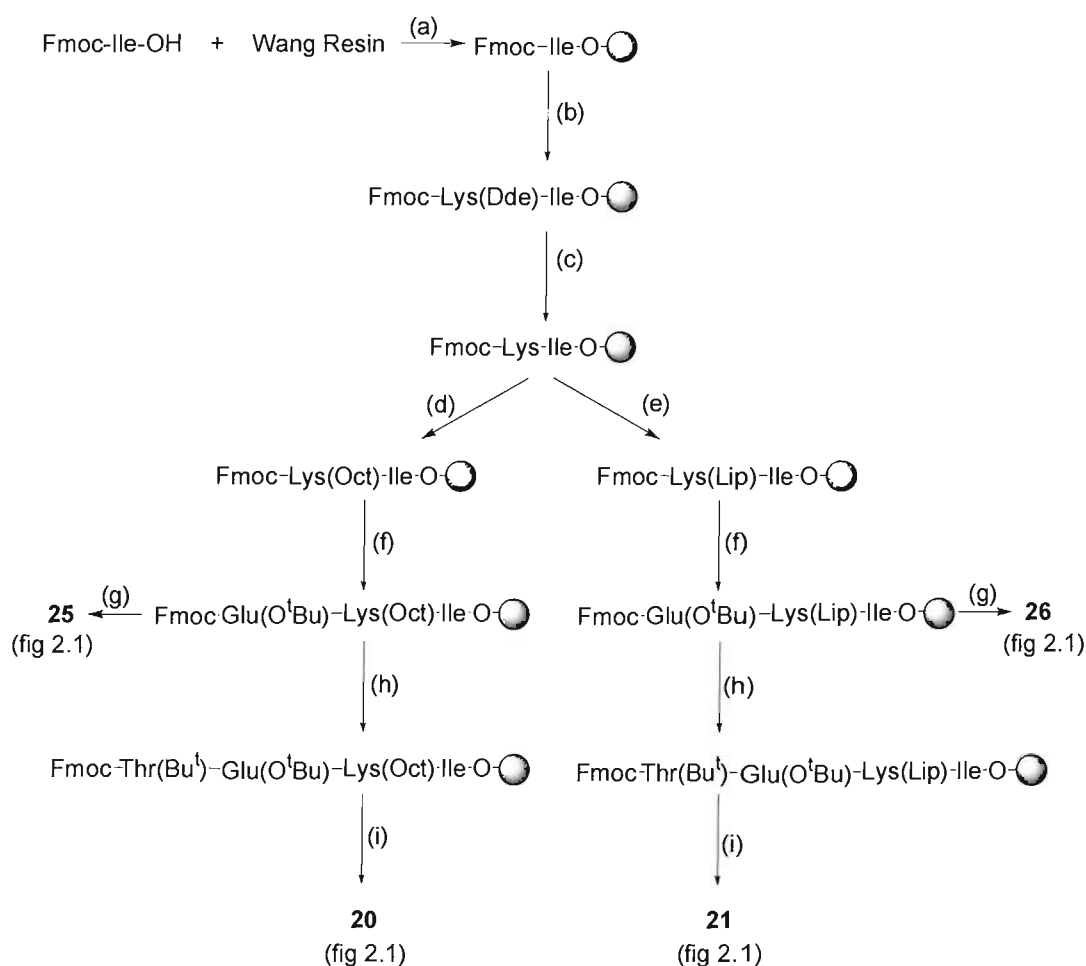
Scheme 2.1 Preparation of substrate and product analogues for *S. solfataricus* LipA assays. Reagents and conditions: (a) DIC, DMAP, DMF, 3 h; (b) 20% (v/v) piperidine, DMF, 30 min then Fmoc-Lys(Dde)-OH, DIC/HOBt, DMF, 1h; (c) NH₂OH.HCl, imidazole, NMP, 3 h; (d) octanoic acid, PyBOP, DIPEA, 1 h; (e) lipoic acid, PyBOP, DIPEA, 1 h; (f) 20% (v/v) piperidine, DMF, 30 min then Fmoc-Glu(O^{t}Bu)-OH, DIC, HOBt, DMF, 1 h; (g) TFA, anisole, H₂O, 2 h, (h) 20% (v/v) piperidine, DMF, 30 min then Fmoc-Thr(^{t}Bu)-OH, DIC, HOBt, DMF, 1 h; (i) TFA, anisole, H₂O, 2 h.

Orthogonality was introduced at the ε-amino group on the lysine side chain using the Dde protecting group (scheme 2.1) which is stable under Fmoc deprotection conditions (20% piperidine in DMF). Selective removal of Dde was achieved using a mixture of $NH_2OH.HCl$ and imidazole in N-methylpyrrolidone (NMP) since the Fmoc group is completely stable under these conditions (*24*). For coupling of octanoic acid or lipoic acid to the deprotected lysine $N^ε$ amine, use of benzotriazole-1-yl-oxy-tris-pyrrolidino-phosphonium hexafluorophosphate (PyBOP) in the presence of N,N-diisopropylethylamine (DIPEA) was found to be the most efficient method.

5(6)-Carboxyfluorescein (5(6)-CFL) was used for preparation of fluorescently labelled tripeptides and was introduced following Fmoc deprotection of the glutamic acid residue (scheme 2.2). Coupling of 5(6)-CFL could not be achieved using HOBt/DIC and therefore this was replaced with PyBOP. This resulted in formation of labelled peptide but coupling remained inefficient and the reaction needed to be repeated several times. Use of an isomeric mixture of 5- and 6-CFL for fluorescent labelling led to formation of a mixture of the two possible geometric isomers of the peptide in a 4:3 ratio as judged by ^1H NMR. However, these isomers co-eluted under the HPLC conditions used for analysis and were therefore used as a mixture in assays of LipA.

Fmoc-Glu(O^tBu)—Lys(Oct)-Ile-O-◯   OR   Fmoc-Glu(O^tBu)—Lys(Lip)-Ile-O-◯

(a)

CFL-Glu(O^tBu)-Lys(Oct)-Ile-O-◯   OR   CFL-Glu(O^tBu)-Lys(Lip)-Ile-O-◯

(b)

13   OR   **16**
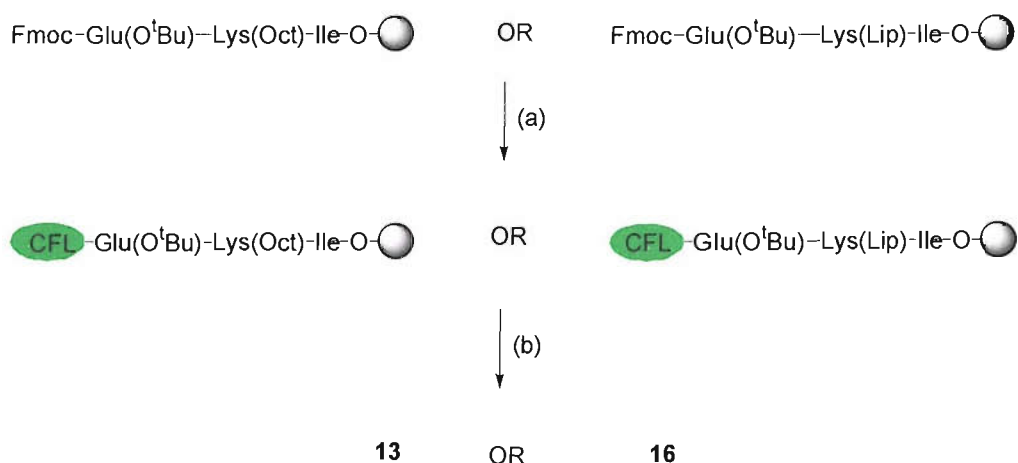
Scheme 2.2 Fluorescent labelling of peptides with 5(6)-CFL. Reagents and conditions: (a) 5(6)-CFL, PyBOP, DIPEA, DMF, 1 h; (b) TFA, anisole, H_2O, 2 h.

Peptides were cleaved from the resin using a mixture of TFA, anisole and water and the typical yields of crude peptides were 90-95%. Preparative HPLC was required for purification of fluorescent peptides as some unlabelled products were present due to the inefficiency of 5(6)-CFL labelling. Typical yields of purified fluorescent peptides using this method were 12-30%. Preparative HPLC was also used initially for purification of unlabelled peptides but since this resulted in relatively poor yields (<30%) the potential of low pressure chromatography on pre-packed reverse phase columns was investigated. This method significantly improved the yield of pure peptides to 65-71% for octanoyl peptides and 50-58% for lipoyl peptides and was therefore subsequently used for purification.

All of the peptides that were prepared had limited solubility in aqueous solution and were insoluble in organic solvents. Tetrapeptides **20** and **21** (fig. 2.1) exhibited the greatest solubility and aqueous solutions at concentrations of up to 10 mg/mL (16 mM octanoyl peptide **20**, 15 mM lipoyl peptide **21**) could be prepared. The shorter octanoyl tripeptide **25** was less soluble and the maximum concentration of aqueous solutions of this compound was 5 mg/mL (9 mM). The lipoyl tripeptide **26** had very poor solubility and aqueous solutions of this peptide could not exceed 2 mg/mL (3.5 mM). Fluorescent peptides **15** and **16** exhibited similar solubility to the corresponding octanoyl and lipoyl tripeptides. As solubility was lost upon shortening of the peptide backbone the tripeptide was deemed to be the minimum length for octanoyl peptides which could be practically used in assays. It has subsequently been found by M. Challand that N6-octanoyl lysine is very insoluble in water (less than 0.5 mg/mL).

2.4   LipA activity assay using fluorescent tripeptide substrate analogue

Initial experiments were carried out with fluorescent octanoyl peptide **15** (fig. 2.1) and *S. solfataricus* LipA under anaerobic conditions. Assays with as-isolated LipA showed no activity, but activity was restored by chemical reconstitution of the iron–sulfur clusters with exogenous iron and sulfur. Reconstitution was achieved using a method similar to that described previously for reconstitution of apo-BioB (*25*) and involved incubation of as isolated LipA which had been reduced with DTT with 5 molar equivalents of Fe^{2+} (with respect to protein concentration) and 10 molar equivalents of S^{2-}.

Assay mixtures which made use of the fluorescent substrate **15** (fig. 2.1) contained one molar equivalent of reconstituted LipA with respect to peptide concentration. These sulfur insertion reactions also required SAM for activity and an electron-donating system consisting of *E. coli* flavodoxin (FldA), flavodoxin reductase (Fpr), and NADPH was employed to reduce the [4Fe–4S] cluster. Assay mixtures containing SAM, FldA/Fpr/NADPH, octanoyl peptide **15** (fig. 2.1) and reconstituted LipA were incubated at 37 °C for 4 h then LipA and other protein components were precipitated by acidification. Analysis of the assay supernatants by HPLC with fluorescence detection revealed a new peak in the chromatogram at 19.8 ± 0.3 min (fig. 2.7) that coeluted with the synthetic fluorescent lipoyl tripeptide standard **16** (fig. 2.1). A second product peak was also observed by HPLC with a retention time of 20.2 ± 0.3 min (fig. 2.8) and the addition of the reducing agent tris (2-carboxyethyl) phosphine (TCEP, 1 mM) to reaction mixtures enhanced this peak and decreased the peak corresponding to the lipoyl peptide. The peak also coeluted with a TCEP-treated sample of the synthetic lipoyl product. On this basis, the peak at 20.2 min was tentatively assigned to the dihydrolipoyl (DHL) peptide **17** (fig. 2.1), formed upon reduction of the disulfide bond in lipoic acid.
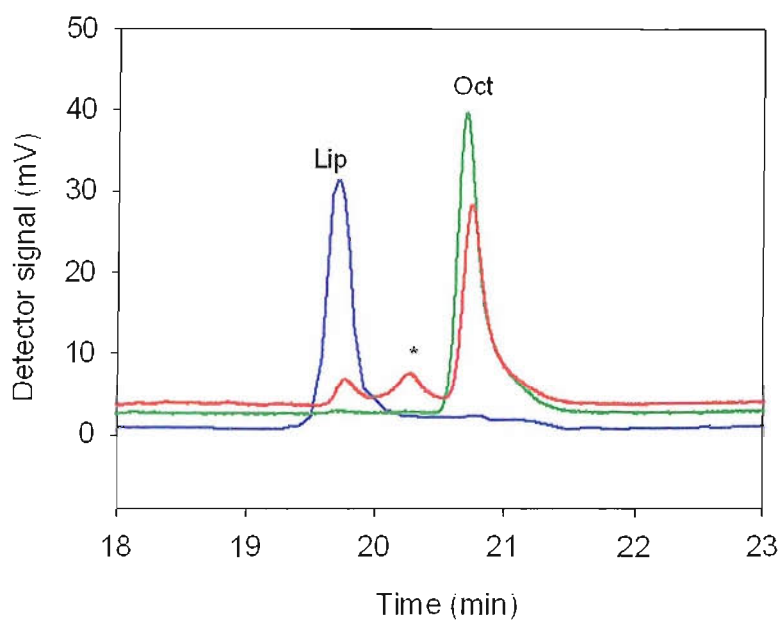
Figure 2.7 HPLC analysis with fluorescence detection of *S. solfataricus* LipA assay at 37 °C using fluorescent octanoyl peptide **15** (fig. 2.1) as substrate: (—) LipA assay; (—) octanoyl peptide 15 standard; (—) lipoyl peptide **16** (fig. 2.1) standard.
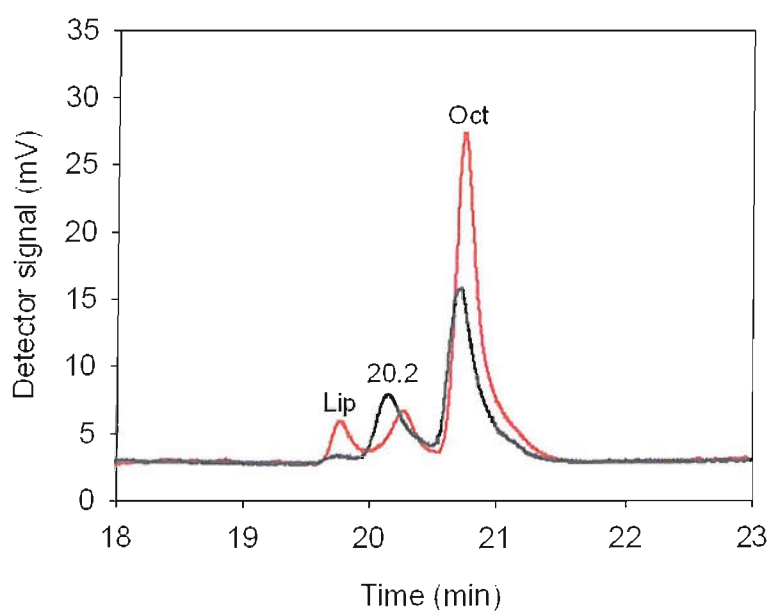
Figure 2.8 HPLC analysis with fluorescence detection of *S. solfataricus* lipoyl synthase assay at 37 °C using fluorescent octanoyl peptide **15** as substrate: (—) without TCEP; (—) following treatment with TCEP

The extent of turnover was estimated to be just 5% by comparing the relative peak areas of the octanoyl starting material and the products of the reaction. An equimolar amount of LipA with respect to substrate concentration had been used and it was thought that this may have limited activity since catalytic activity of LipA has not been achieved *in vitro (2, 26)*. Assays using an octanoyl protein domain as substrate have been found to yield less than 0.4 molar equivalents with respect to LipA and 1.0 molar equivalents of AdoH leading to the proposal that only 40% of the *E. coli* LipA used in these assays was in an active configuration (*2*). It was therefore thought that an increase in concentration of *S. solfataricus* LipA might improve turnover as there may have also been some of this protein present in an in-active form. However, addition of a two-fold excess of *S. solfataricus* LipA to reactions with respect to the concentration of fluorescent octanoyl peptide **15** (fig. 2.1) had no effect on the extent of turnover.

Analysis of the time dependent formation of lipoyl peptide showed that an increase in reaction time led to no significant change in the amount of turnover. After 2 h incubation at 37 °C HPLC analysis revealed that both lipoyl peptide **16** (fig. 2.1) and the putative DHL peptide **17** (fig. 2.1) had formed (fig. 2.9) and comparison of the peak areas of these species indicated that the DHL peptide was present in greater amount. Analysis of assays which were stopped at later time points showed that the amount of the putative DHL peptide decreased with a concomitant increase in the amount of lipoyl peptide (fig. 2.9). After 21 hours the peak assigned to the putative DHL peptide was barely detectable whilst that corresponding to the lipoyl peptide remained visible. However, the combined area of these peaks did not increase significantly over time and therefore turnover was not improved by longer incubation.
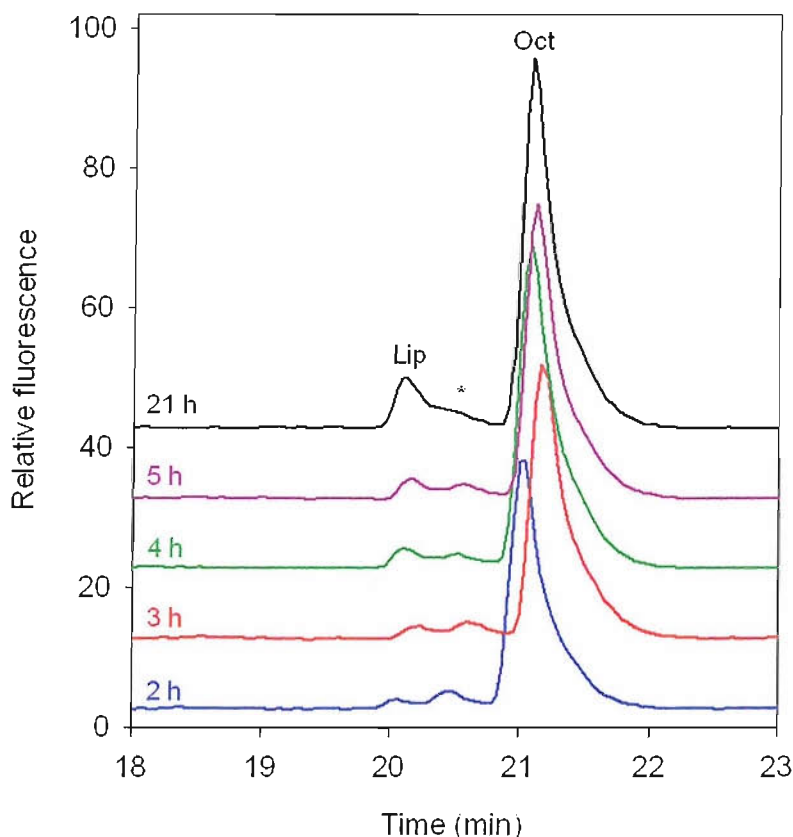
Figure 2.9 HPLC analysis with fluorescence detection of *S. solfataricus* lipoyl synthase assay using fluorescent octanoyl peptide **15** (fig. 2.1) as substrate following incubation at 37 °C for 2 hours, 3 hours, 4 hours, 5 hours and 21 hours: (Lip) lipoyl peptide **16** (fig. 2.1); (*) may be DHL peptide **17** (fig. 2.1) or 6MT peptide 18 (fig. 3.1); (Oct) octanoyl peptide **15** (fig. 2.1).

The gradual loss of the peak at 20.5 min might be due to oxidation of DHL peptide to yield a lipoyl species but this seems unlikely since the reaction is carried out under strongly reducing conditions. LC-MS analysis of reactions that used octanoyl protein domains as a substrate has identified a product that has a mass corresponding to a monothiolated species (*2*). The second product formed during reactions using *S. solfataricus* LipA and octanoyl peptide **15** (fig. 2.1) could therefore be a monothiolated product **18** or **19** (fig. 2.1) generated by insertion of a single sulfur atom at C6 of C8 of the octanoyl group respectively. The insertion of a second sulfur atom into these species to yield lipoyl peptide **16** (fig. 2.1) would explain the disappearance of the peak at 20.5 min and increase of the peak corresponding to lipoyl peptide over time.

As a member of the radical SAM superfamily, LipA is expected to require a reduced $[4Fe-4S]^{1+}$ for activity and poor turnover may have resulted from inefficient electron transfer by the *E. coli* derived FldA/ Fpr/ NADPH electron donating system. Sodium dithionite was thus investigated as an alternative as this has been used to reduce the $[4Fe-4S]^{2+}$ clusters of BioB (*27*) and *E. coli* LipA (*26*). Assays utilising dithionite were analysed by HPLC (fig. 2.10) and comparison of the peak areas corresponding to the lipoyl and octanoyl peptides indicated that amount of turnover was apparently enhanced upon replacement of the reductant (approximately 76% conversion from the octanoyl substrate) however, results were inconclusive since the fluorescence of the peptides had been decreased significantly in the presence of dithionite. This made analysis by HPLC with fluorescence detection difficult as the peak intensity for the peptides was significantly diminished (fig. 2.10). Thus, since the advantages of using a fluorescent substrate were lost this was substituted with unlabelled peptides **20** and **25** (fig. 2.1) to determine the potential for dithionite as reductant as these could be more easily prepared and characterised.
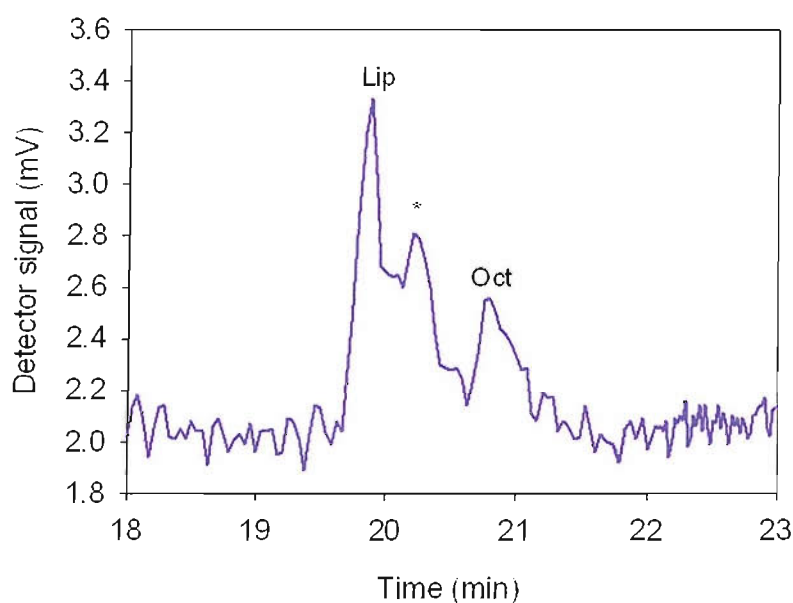
Figure 2.10 HPLC analysis with fluorescence detection of *S. solfataricus* lipoyl synthase assay using sodium dithionite to generate the reduced $[4Fe-4S]^{1+}$ cluster and fluorescent octanoyl peptide **15** as substrate following incubation at 37 °C for 4 h.

2.5   LipA activity assays using unlabelled substrate analogues

Initial experiments using unlabelled substrates were carried out using tetrapeptide substrate **21** (fig. 2.1) as this was more soluble than tripeptide **25** (fig. 2.1). However, some later experiments utilised tripeptide **25** (fig. 2.1) since this could be more easily characterised by ^{1}H NMR and would facilitate characterisation of small amounts of peptides isolated from assay mixtures to enable mechanistic studies (*28*).

2.5.1   HPLC analysis of LipA activity assay

In vitro assays of reconstituted LipA activity were carried out with octanoyl peptide substrates and sodium dithionite to maintain the reduced $[4Fe-4S]^{1+}$ cluster. Reaction mixtures also contained SAM which was essential for activity. Assays using non-fluorescent peptides contained greater concentrations of substrate those using fluorescent peptide **15** (fig. 2.1) to facilitate analysis by HPLC with UV detection. Sulfur insertion reactions using these unlabelled substrates contained two molar equivalents of reconstituted LipA with respect to octanoyl substrate concentration. Assay mixtures were incubated at 37 °C for 3 h then LipA was precipitated by acidification and this led to dilution of the peptide concentration to 125 µM (from an initial concentration of 150 µM). A product peak was present in the HPLC trace of assay supernatants at 17.2 ± 0.5 min (fig. 2.11) that coeluted with the synthetic lipoyl tetrapeptide **21** (fig. 2.1) standard. Similarly to assays which made use of fluorescent octanoyl tripeptide **15** (fig. 2.1), a second product peak was observed for assays using octanoyl tetrapeptide **20** (fig. 2.1) which eluted at 18.0 ± 0.5 min (fig. 2.11). This peak may contain either DHL peptide **22** (fig. 2.1) and/or a monothiolated peptide **23** or **24** (fig. 2.1) as indicated by experiments using fluorescent octanoyl tripeptide **15** (fig. 2.1).
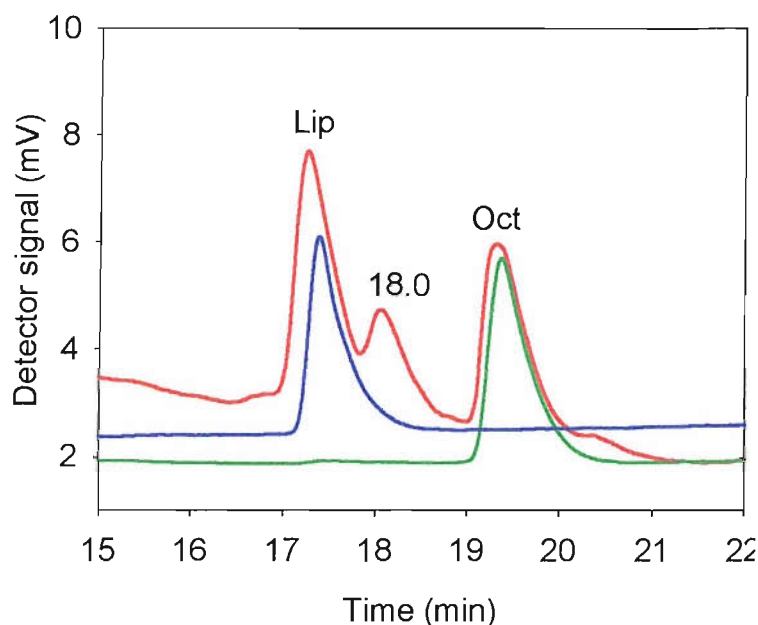
Figure 2.11 HPLC analysis with UV detection (230 nm) of *S. solfataricus* lipoyl synthase assay at 37 °C using tetrapeptide **20** (fig. 2.1). For clarity, the detector signals for lipoyl (Lip, —) and octanoyl (Oct, —) standards are normalized to the signal from the lipoyl synthase assay (—).

Lipoyl formation was quantified using a calibration curve (fig. 2.12) constructed from standard solutions of synthetic lipoyl peptide **21** (fig. 2.1). This revealed that there was significant turnover; 68.8 ± 6.0 μM of lipoyl tetrapeptide **21** (fig. 2.1) were formed from 125 μM of octanoyl tetrapeptide (55% conversion). For comparison an assay was carried out using the FldA/ Fpr/ NADPH reducing system with octanoyl tetrapeptide **20** (fig. 2.1) as substrate (fig. 2.13). This gave a poor yield of lipoyl peptide (4.9 μM from 125 μM of peptide) showing that electron transfer from sodium dithionite to the $[4Fe-4S]^{2+}$ cluster of *S. solfataricus* LipA is more efficient than from the *E. coli* derived flavodoxin reducing system. All subsequent experiments therefore utilised dithionite as reductant.
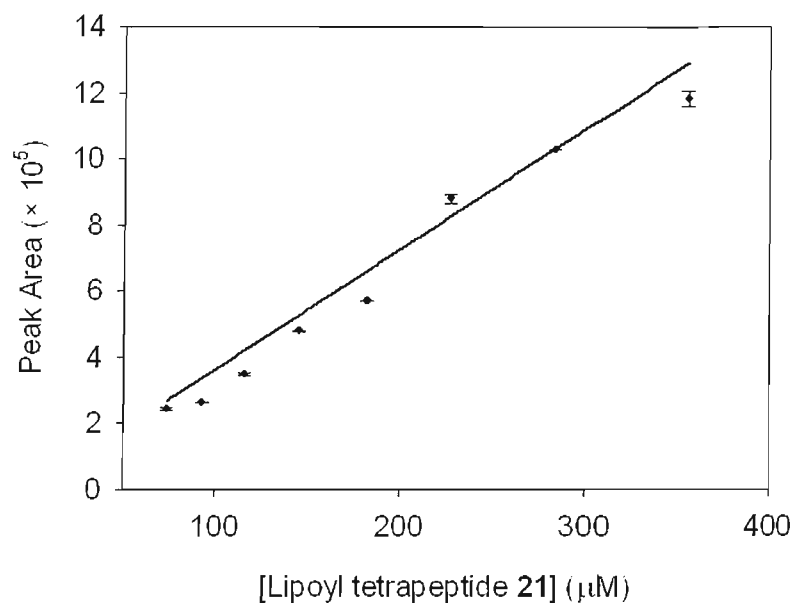
Figure 2.12 Standard curve for lipoyl tetrapeptide **21** (fig. 2.1) concentration: 100 μL of standard solutions applied to HPLC column; UV detection at 230 nm; y = 3463x; $R_2 = 0.9593$.
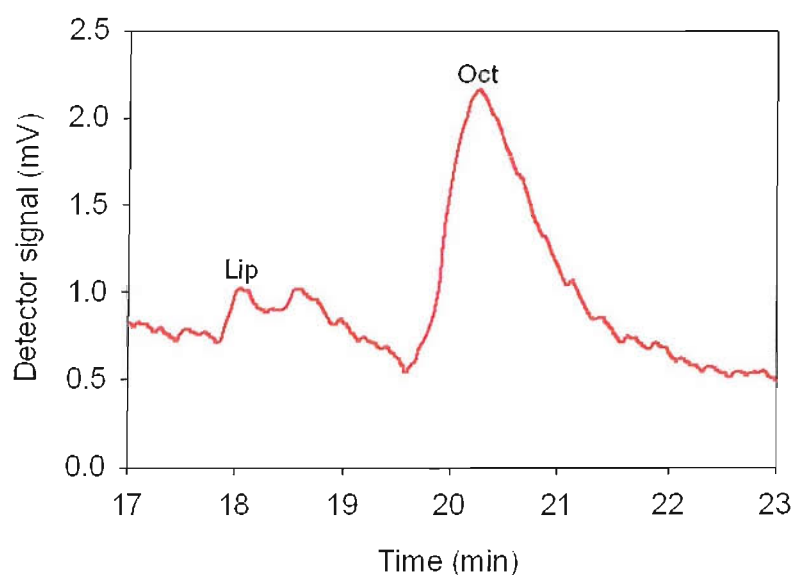
Figure 2.13 HPLC analysis with UV detection (230 nm) of *S. solfataricus* lipoyl synthase assay at 37 °C using tetrapeptide **20** (fig. 2.1) and FldA/ Fpr/ NADPH reducing system.

HPLC analysis of LipA activity assays using octanoyl tetrapeptide **20** (fig. 2.1) also revealed that AdoH is a product of sulfur insertion reactions (fig. 2.14). This observation supports the proposal of a radical mechanism for lipoyl formation by

S. solfataricus LipA that begins with cleavage of SAM to yield Ado• which subsequently abstract hydrogen atoms from the octanoyl substrate to generate AdoH. Quantification was carried out using a calibration curve constructed from standard solutions (fig. 2.15) and showed that 183 ± 13 μM of AdoH was formed after incubation of assays at 37 °C for 3 hours. This equates to 2.7 molar equivalents of AdoH with respect to lipoyl peptide formed and is consistent, within experimental error, with cleavage of 2 equivalents of SAM per lipoyl group formed as indicated previously by experiments using *E. coli* LipA and octanoyl protein domains as substrate (*2*).
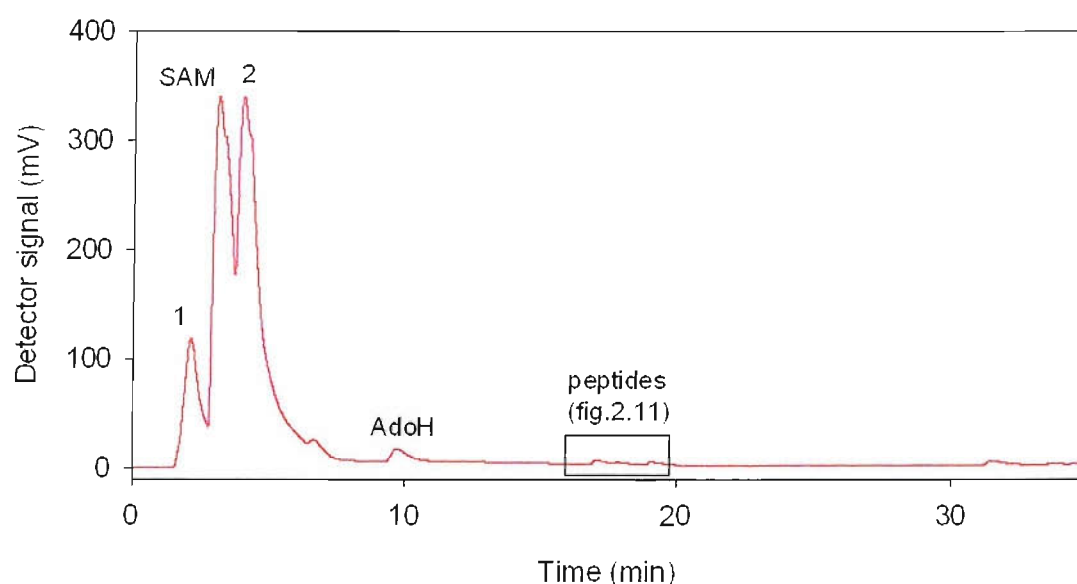
Figure 2.14 HPLC analysis with UV detection (230 nm) of *S. solfataricus* lipoyl synthase assay at 37 °C using tetrapeptide **20** (fig. 2.1): (1) HEPES; (2) DTT.
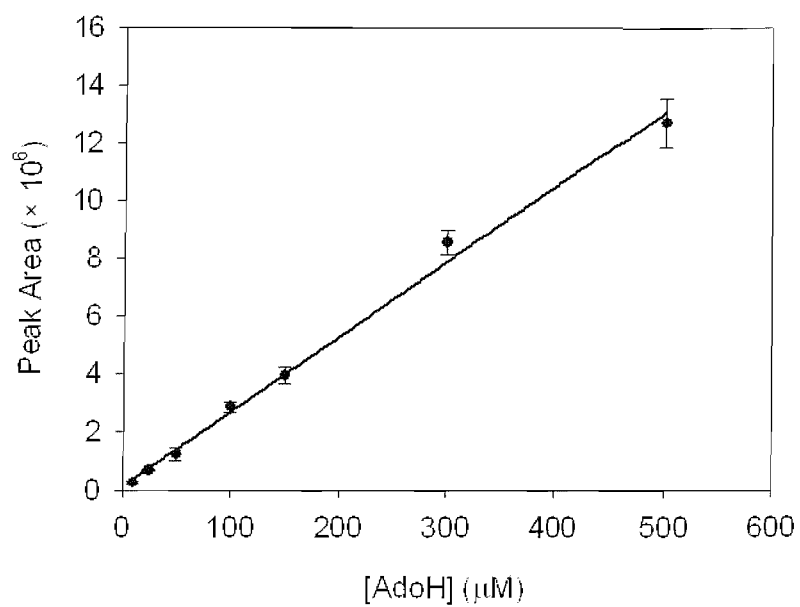
Figure 2.15 Standard curve for AdoH concentration: 100 µL of standard solutions applied to HPLC column; UV detection at 230 nm; y = 25970x; R_2 = 0.9987.

2.5.2 LC-MS Analysis of LipA Activity Assays

To further characterise the products of the LipA reaction assay mixtures were analysed by LC-MS which revealed that four peptide species were present (fig. 2.13). Some unreacted octanoyl substrate **18** (fig. 2.1) remained and eluted at 22.5 min. Lipoyl formation was confirmed by the presence of two new species at 20.9 min and 21.5 min corresponding to lipoyl peptide **19** (fig. 2.1) (m/z = 678.8) and dihydrolipoyl peptide **20** (fig. 2.1) (m/z = 680.3) respectively. The LC-MS spectrum suggested a greater proportion of DHL product but this could be representative of their different ionisation properties. The final product co-elutes with the dihydrolipoyl peptide and has a m/z of 648.8 corresponding to a monothiolated species.
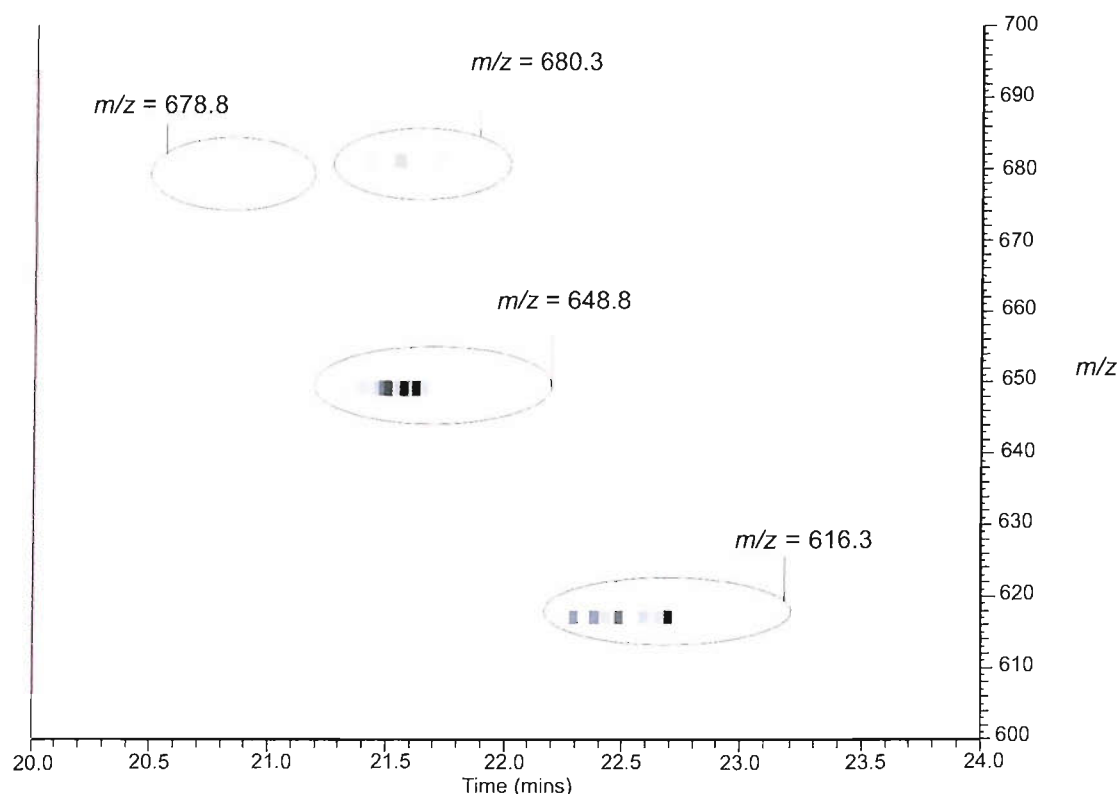
Figure 2.16 LC-MS analysis of assay mixtures; m/z = 616.3, octanoyl peptide **20** (fig. 2.1); m/z =678.8, lipoyl peptide **21** (fig. 2.1); m/z =680.3, dihydrolipoyl peptide **22** (fig. 2.1); m/z = 648.8, monothiolated species **23** or **24** (fig. 2.1).

The monothiolated peptide species represents a potential intermediate formed upon insertion of a single sulfur atom into the octanoyl precursor to form either **23** or **24** (fig. 2.1). It is expected that a second sulfur insertion into this species would occur leading to lipoyl formation. Use of this assay method with octanoyl tripeptide **25** (fig. 2.1) has subsequently allowed P. Douglas to isolate the monothiolated species (*28*) and characterise it as the 6-thiooctanoyl (6MT) peptide **28** (fig. 2.1). Lipoyl formation has thus been shown to occur in a stepwise manner with sulfur insertion first at C6 of the octanoyl group followed by at C8.

LC-MS analysis of assays has also confirmed the formation of AdoH which coeluted with SAM under the chromatography conditions used (fig. 2.17). A large peak was also seen in the chromatogram which corresponded to a species with m/z = 239.2 and corresponds to the protonated mass of HEPES which was used as a buffer (fig. 2.17).
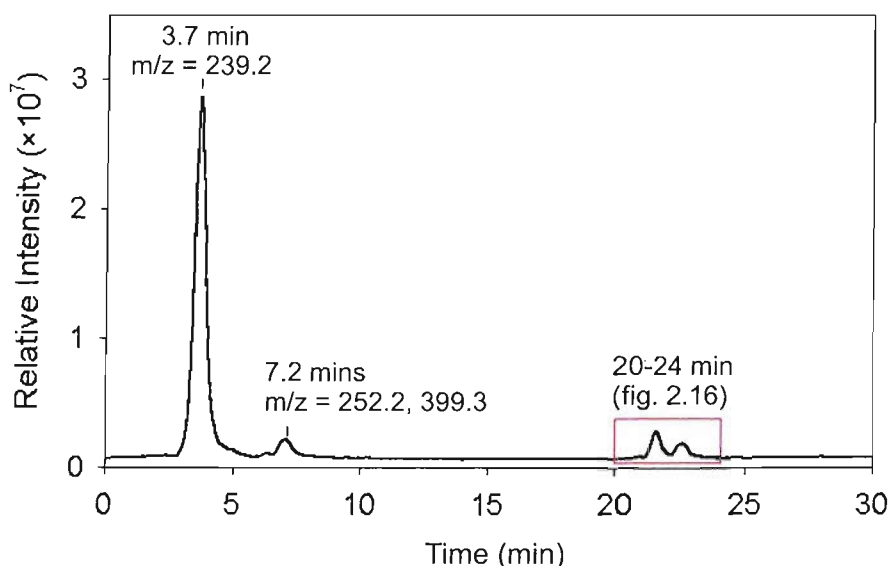
Figure 2.17 LC-MS analysis of *S. solfataricus* LipA assay at 37 °C using tetrapeptide **20** as substrate: HEPES m/z = 239.2 $(M+H)^+$, eluted at 3.7 min; SAM m/z =399.3 $(M+H)^+$ and AdoH m/z = 252.2 $(M+H)^+$, co-eluted at 7.2 min; peptides eluted between 20-24 min and a more detailed analysis of these can be seen in fig. 2.11.

2.5.3 Effect of changes in concentration of LipA

Assays of *E. coli* LipA using an octanoyl protein domain as substrate have indicated that lipoyl formation may be limited by the presence of LipA monomers which are not in an active configuration. (*2, 29*). Thus, it was predicted that optimum turnover of octanoyl peptides by *S. solfataricus* LipA might be achieved if 2 molar equivalents of protein with respect to peptide concentration were present. The effect of changes in LipA concentration was investigated and assays incubated at 37°C which contained two molar equivalents of LipA with respect to substrate concentration produced greater yields of lipoyl product (68.8 ± μM, 55% conversion from octanoyl substrate) than those with an equimolar mixture of protein and substrate (38.1 ± μM, 30% conversion from octanoyl substrate) or with 0.5 molar equivalents of LipA (19.8 ± 2.5 μM, 16% conversion from octanoyl substrate) (fig. 2.18).
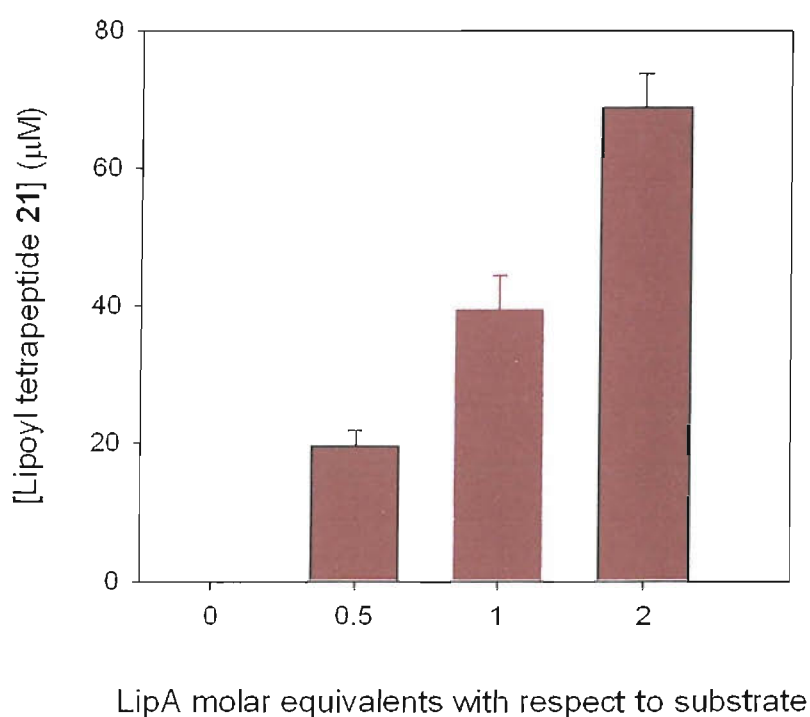
Figure 2.18 Effect of varying LipA concentration on amount of lipoyl peptide formed.

The low levels of turnover at lower concentrations of LipA that activity was not catalytic under the conditions used in these assays. This is consistent with observations from reactions using *E. coli* LipA and octanoyl protein domains as

substrates (*2*). Increase in activity with increasing LipA concentration might result from a requirement for 2 molar equivalents of LipA with respect to octanoyl concentration to generate 2 Ado• radicals needed for hydrogen atom abstraction from C6 and C8 of the octanoyl group. However, mechanistic studies using labelled LipA have shown that both sulfur atoms are derived from the same LipA monomer and therefore this is unlikely (*29*). It is possible that reconstitution was not efficient and therefore some LipA polypeptides did not bind complete $[4Fe-4S]^{1+/2+}$ cluster(s) (*11*). These protein molecules would be inactive and could not initiate sulfur insertion reactions.

The activity of dimeric LipA was compared with monomeric LipA which had been used in all assays described above. No significant difference was observed and 65 μM of lipoyl peptide (52% conversion of octanoyl peptide) was formed in an assay using dimeric LipA. Analysis by SDS-PAGE has shown that under denaturing conditions dimeric LipA behaves as the monomer (fig. 2.6). Treatment of dimeric LipA with DTT during reconstitution may therefore result in the conversion to monomeric LipA.
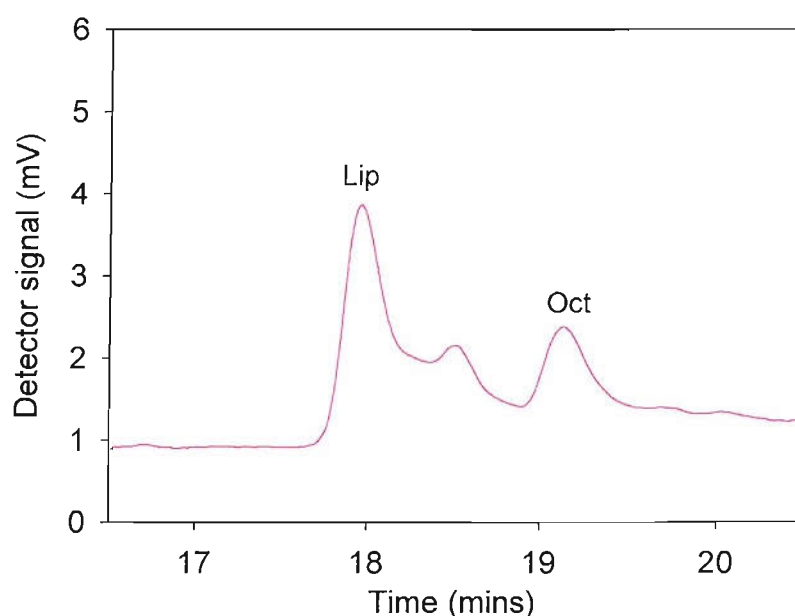
2.19 HPLC analysis with UV detection (230 nm) of *S. solfataricus* lipoyl synthase assay at 37 °C using dimeric LipA and tetrapeptide **20** (fig. 2.1).

2.5.4 Effect of changes in Fe^{2+} and S^{2-} concentration.

Since reconstitution of the iron sulfur cluster(s) of *S. solfataricus* LipA is essential for activity the effect of varying concentrations of Fe^{2+} and S^{2-} was investigated. LipA was reduced with DTT (final concentration 5 mM) then $FeCl_2$ was added followed by Na_2S. Components had to be added in this order since addition of Na_2S prior to the addition of $FeCl_2$ led to precipitation of LipA. The maximum amount of Fe^{2+} which could be added without precipitation of LipA was 5 molar equivalents with respect to protein concentration. When no Fe^{2+} was added no lipoyl formation was observed at low S^{2-} concentrations (fig. 2.20). However, as greater amounts of S^{2-} were added lipoyl formation was observed and there was a general trend for increased lipoyl formation with increased sulfide concentration. Optimum turnover was achieved upon addition of 5 molar equivalents of Fe^{2+} and 10 molar equivalents of S^{2-} with respect to protein concentration (fig. 2.20). These quantities had been used in previous assays and were continued to be used for all subsequent reconstitutions.
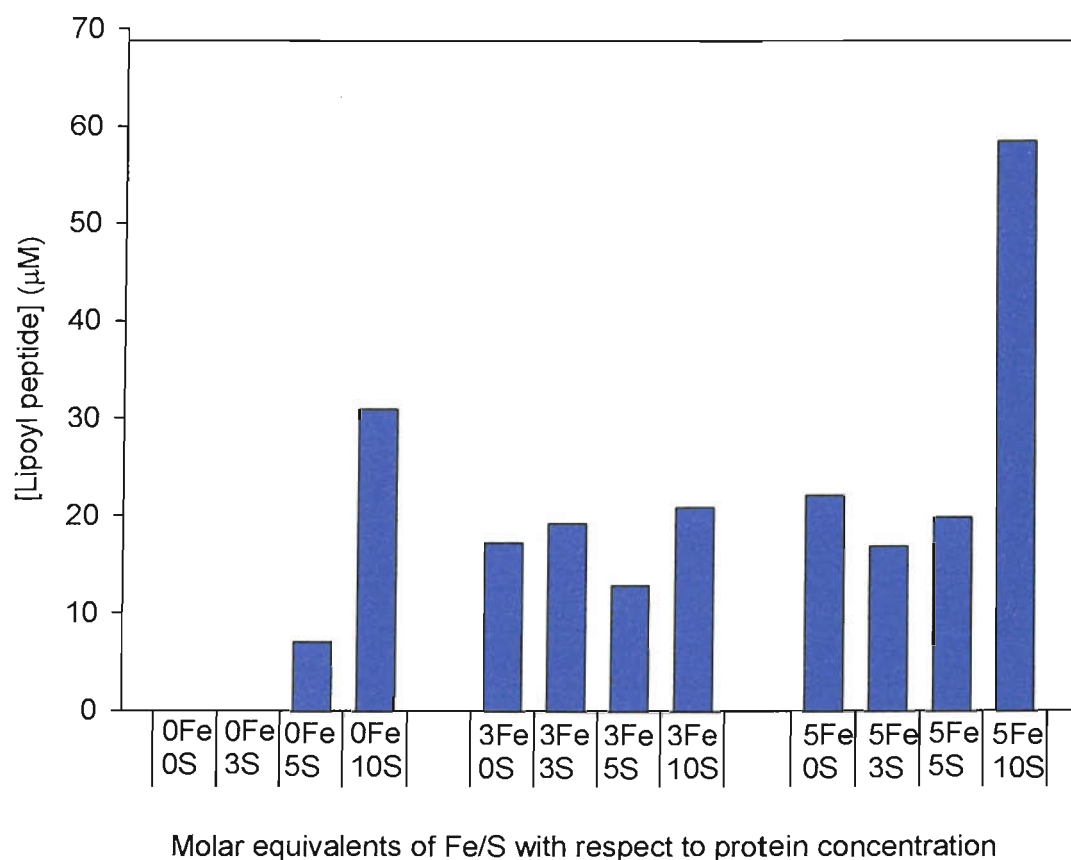
Figure 2.20 Effect of changes in concentration of Fe^{2+} and S^{2-} on lipoyl formation.

2.5.5 Optimum temperature for sulfur insertion by *S. solfataricus* LipA

The activity of *S. solfataricus* LipA was investigated over the temperature range of 8 to 70 °C, measuring the yield of lipoyl peptide after 30 min. Precipitation of LipA was observed in assays maintained at 70°C, and these yielded less lipoyl product than expected. HPLC analysis of assays using either octanoyl tetrapeptide **20** (fig. 2.1) or tripeptide **25** (fig. 2.1) indicated that turnover increased at higher temperatures and was maximal at 60 °C (fig. 2.21) (*3*). After 30 min incubation at 60 °C the peaks corresponding to octanoyl peptide were not detected whilst that corresponding to lipoyl peptide had increased significantly.

A   **B**
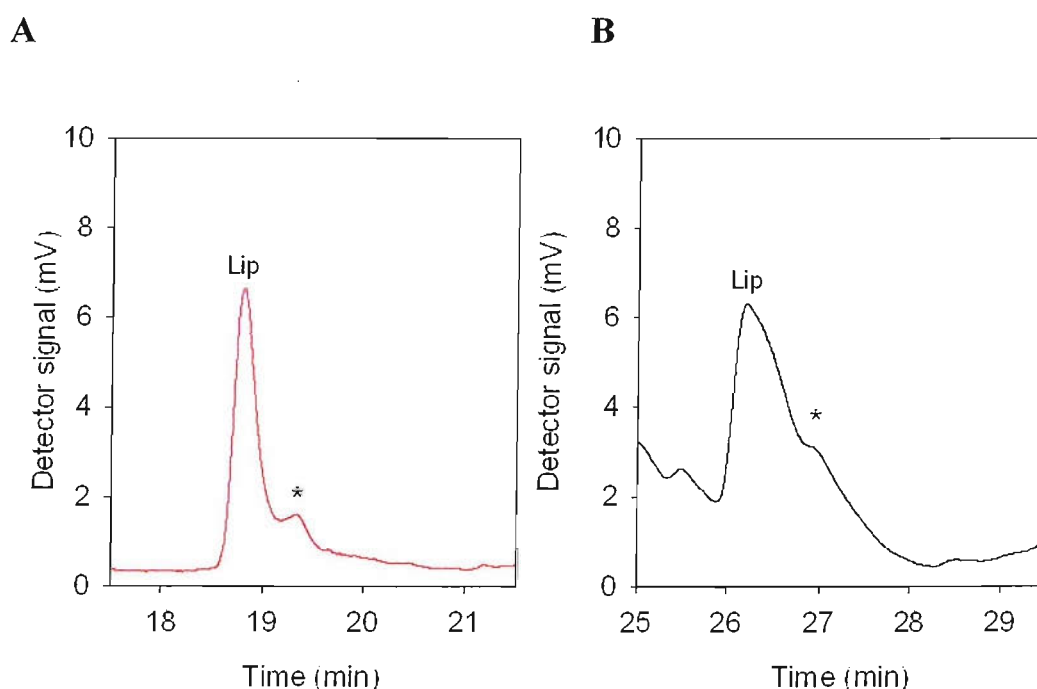
Figure 2.21 HPLC analysis of *S. solfataricus* lipoyl synthase assays at 60 °C after 30 min incubation: (A) using octanoyl tetrapeptide **20** (fig. 2.1) as substrate; (B) using octanoyl tripeptide **25** (fig. 2.1) as substrate.

Quantification of lipoyl peptide revealed that, after 30 min incubation, product formation increased exponentially with increase in temperature (fig. 2.22). After 30 min incubation at 60 °C there was almost complete conversion with formation of 113.0 ±1.0 µM of lipoyl tetrapeptide **21** (90% conversion from octanoyl substrate) (fig. 2.1) and 102.6 ± 3.2 µM lipoyl tripeptide **26** (87% conversion from octanoyl

substrate) (fig. 2.1). It is somewhat surprising that the optimum temperature for activity is not higher since *S. solfataricus* thrives at 80 °C. It may be that LipA is further stabilized by interactions with other proteins in an intracellular environment and that this allows it to function at higher temperatures. However, the stability of *S. solfataricus* LipA up to 60 °C *in vitro* has allowed activity to be assayed over a wide range of temperatures leading to approximation of activation energies for lipoyl formation. These experiments will be described in more detail in chapter 3.
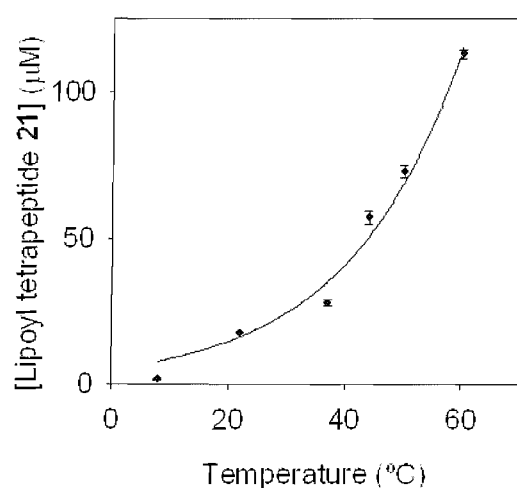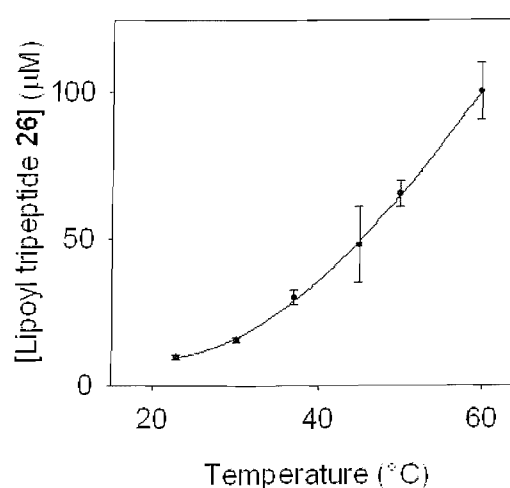
Figure 2.22 Lipoyl formation after incubation over a range of temperatures for and 30 min: (A) lipoyl tetrapeptide **21** (fig. 2.1); (B) lipoyl tripeptide **26** (fig. 2.1).

2.6   Assays using *E. coli* LipA

To demonstrate the generality of this LipA assay the activity of *E. coli* LipA with a tripeptide substrate **30** (fig. 2.23) corresponding in sequence to the E2 domains found within *E. coli* pyruvate dehydrogenase (accession code P06959) was investigated.

30 R = Oct
31 R = Lip
32 R = DHL
33 R = 6MT

Oct =

Lip =

DHL =

6MT =
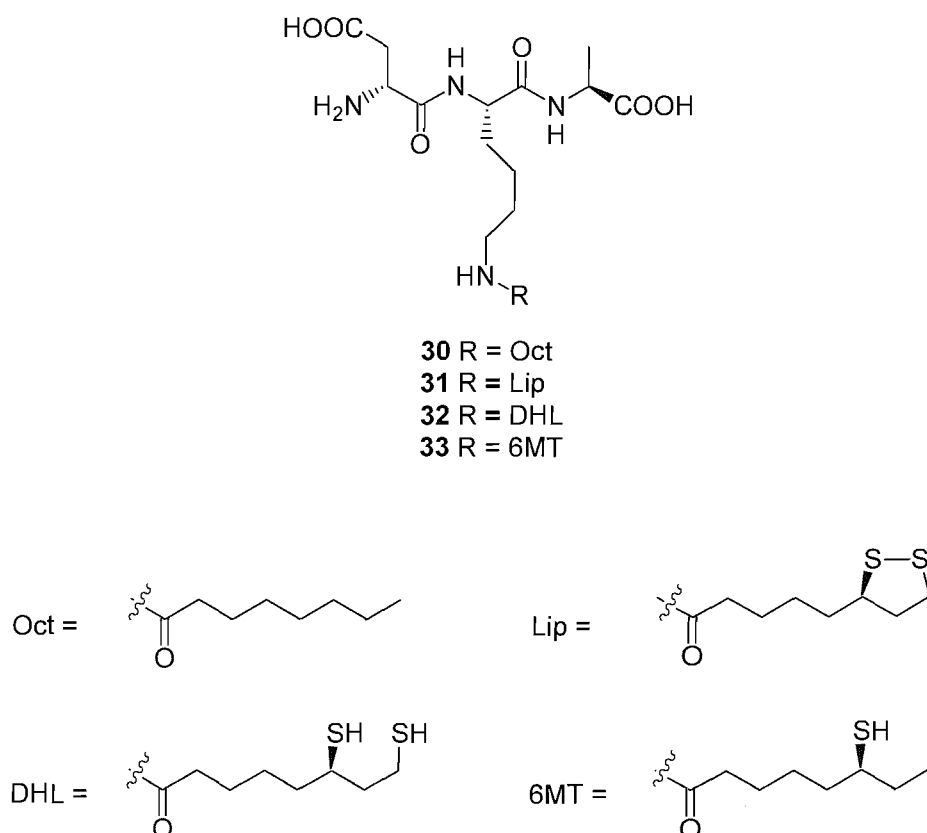
Figure 2.23 Structures of octanoyl substrate for use in *in vitro* assays of *E. coli* LipA. Structures of potential products of these reactions are also shown; lip = lipoyl group; DHL = dihydrolipoyl group; 6MT = 6-thiooctanoyl group.

Substrate analogue **30** (fig. 2.23) was prepared following a similar synthetic rout methodology to that described for preparation of peptides that corresponded to the lipoyl binding domain of the putative 2-oxoacid dehydrogenase complex of *S. solfataricus* P2 (scheme 2.3). The peptides was purified using preparative HPLC and the yield was 50% for octanoyl peptide **30** (fig. 2.23).

Fmoc-Ala-OH   +   Wang Resin

| (a)

Fmoc-Ala-O-◯

| (b)

Fmoc-Lys(Dde)-Ala-O-◯

| (c)

Fmoc-Lys-Ala-O-◯

| (d)

Fmoc-Lys(Oct)-Ala-O-◯

| (e)

Fmoc-Asp(O^{t}Bu)-Lys(Oct)-Ile-O-◯

| (f)

30
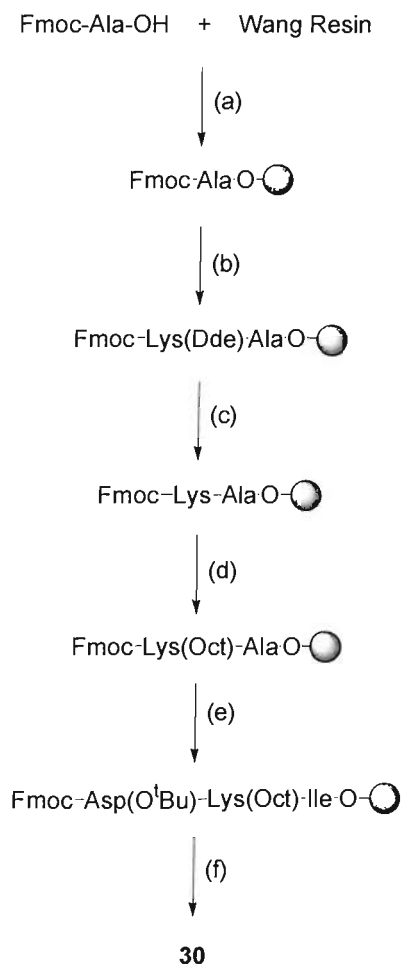
Scheme 2.3 Preparation of octanoyl substrate analogue for use in assays of *E. coli* LipA. Reagents and conditions: (a) DIC, DMAP, DMF, 3 h; (b) 20% (v/v) piperidine, DMF, 30 min then Fmoc-Lys(Dde)-OH, DIC/HOBt, DMF, 1 h; (c) NH$_2$OH.HCl, imidazole, NMP, 3 h; (d) octanoic acid, PyBOP, DIPEA, 1 h; (e) 20% (v/v) piperidine, DMF, 30 min then Fmoc-Asp(O^{t}Bu)-OH, DIC, HOBt, DMF, 1 h; (f) TFA, anisole, H$_2$O, 2 h.

Assay mixtures containing *E. coli* LipA, substrate **30**, SAM and dithionite, were incubated at 37 °C for 30 min and at this point the protein was observed to precipitate. This demonstrated that under these assay conditions *E. coli* LipA is less stable than the *S. solfataricus* protein. Reactions using *E. coli* LipA were acidified after 30 min the precipitated protein removed by centrifugation. The resulting supernatants were analysed by LC-MS which revealed that three new peptide species were formed a lipoyl product **31** (fig. 2.23), a DHL product **32** (fig. 2.23, m/z = 523.1) and a monothiolated species (m/z = 491.1), which coeluted (fig. 2.24 and fig. 2.25). However, a significant amount of octanoyl starting material remained (82 μM,

66% of initial concentration) showing that turnover was significantly less than was observed in assays using S. *solfataricus* LipA under the same conditions.
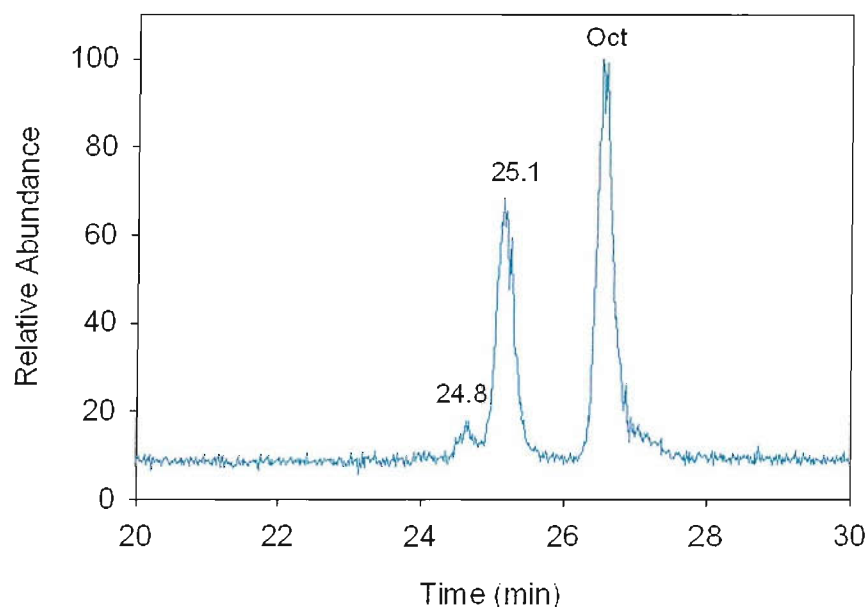
Figure 2.24 TIC chromatogram obtained by LC-MS analysis of *E.coli* lipoyl synthase assay at 37 °C which used octanoyl peptide **30** (fig. 2.23) as substrate; peak at 24.8 min corresponds lipoyl peptide **31** (fig. 3.23), m/z = 521.2; peak at 25.1 min contains DHL peptide **32** (fig. 3.23) and 6MT peptide **33** (fig. 3.23), m/z = 523.1 and 491.1 respectively.
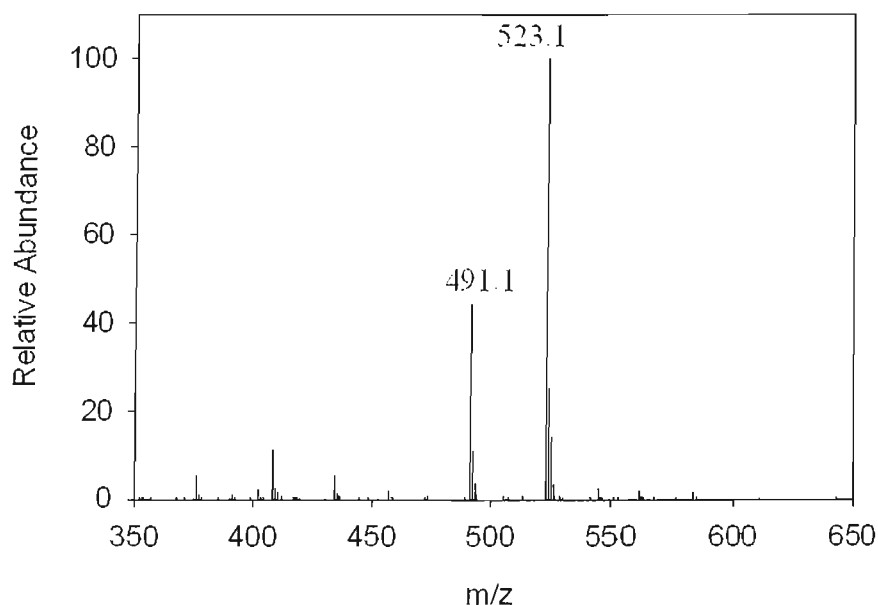
Figure 2.25 Spectrum of the peak eluting at 25.1 min during LC-MS analysis of *E.coli* lipoyl synthase assay at 37 °C which used octanoyl peptide **30** (fig. 2.23) as substrate: m/z = 523.1, DHL peptide **32** (fig. 3.23); m/z = 491.1 and 6MT peptide **33** (fig. 3.23).

2.7 Conclusions

Simple octanoyl peptides can replace octanoyl protein domains as substrates for LipA *in vitro*. The use of an octanoyl tetrapeptide substrate has enabled the quantification of lipoyl group formation and provides a straightforward generic protocol for measuring the activity of putative lipoyl synthases. The *S. solfataricus lipA* gene product has been shown to be a lipoyl synthase using this assay method and lipoyl formation requires SAM and a reducing agent indicating that this protein, like *E. coli* LipA, is a member of the radical SAM superfamily.

Optimum conditions for turnover have been investigated. Lipoyl formation was found to increase with higher concentrations of LipA and catalytic activity was not observed. The addition of Fe^{2+} and high concentrations of S^{2-} also increased activity. LipA from the hyperthermophilic organism *S. solfataricus* has also been shown to have maximum activity at relatively high temperatures (60 °).

It has also been demonstrated that this method can be extended to lipoyl synthases from other organisms. LipA from *E. coli* was shown to initiate sulfur insertion into an octanoyl tripeptide substrate. However, the *E. coli* protein is unstable and therefore assays which make use of *S. solfataricus* LipA are more practical.

2.8   References

(1)   Zhao, X., Miller, J. R., Jiang, Y., Marletta, M. A., and Cronan, J. E. (2003) Assembly of the covalent linkage between lipoic acid and its cognate enzymes. *Chem. Biol.10*, 1293-302.

(2)   Cicchillo, R. M., Iwig, D. F., Jones, A. D., Nesbitt, N. M., Baleanu-Gogonea, C., Souder, M. G., Tu, L., and Booker, S. J. (2004) Lipoyl synthase requires two equivalents of S-adenosyl-L-methionine to synthesize one equivalent of lipoic acid. *Biochemistry 43*, 6378-86.

(3)   Bryant, P., Kriek, M., Wood, R. J., and Roach, P. L. (2006) The activity of a thermostable lipoyl synthase from *Sulfolobus solfataricus* with a synthetic octanoyl substrate. *Anal. Biochem. 351*, 44-9.

(4)   Witzmann, S., and Bisswanger, H. (1998) The pyruvate dehydrogenase complex from thermophilic organisms: thermal stability and re-association from the enzyme components. *Biochim. Biophys. Acta 1385*, 341-52.

(5)   Cacciapuoti, G., Forte, S., Moretti, M. A., Brio, A., Zappia, V., and Porcelli, M. (2005) A novel hyperthermostable 5'-deoxy-5'-methylthioadenosine phosphorylase from the archaeon *Sulfolobus solfataricus*. *FEBS J. 272*, 1886-99.

(6)   Huang, Y., Krauss, G., Cottaz, S., Driguez, H., and Lipps, G. (2005) A highly acid-stable and thermostable endo-beta-glucanase from the thermoacidophilic archaeon *Sulfolobus solfataricus*. *Biochem. J. 385*, 581-8.

(7)   Zhang, Y., Porcelli, M., Cacciapuoti, G., and Ealick, S. E. (2006) The crystal structure of 5'-deoxy-5'-methylthioadenosine phosphorylase II from *Sulfolobus solfataricus*, a thermophilic enzyme stabilized by intramolecular disulfide bonds. *J. Mol. Biol. 357*, 252-62.

(8)   Kates, M. (1993) *The biochemistry of archaea (archaebacteria)* Vol. 26, Elsevier, Amsterdam.

(9)   Madigan, M. T. (1997) *Brock biology of microorganisms* 8th ed., Prentice Hall, Upper Saddle River.

(10)   Brock, T. D., Brock, K. M., Belly, R. T., and Weiss, R. L. (1972) *Sulfolobus*: a new genus of sulfur-oxidizing bacteria living at low pH and high temperature. *Arch. Microbiol. 84*, 54-68.

(11)   Cicchillo, R. M., Lee, K. H., Baleanu-Gogonea, C., Nesbitt, N. M., Krebs, C., and Booker, S. J. (2004) *Escherichia coli* lipoyl synthase binds two distinct [4Fe-4S] clusters per polypeptide. *Biochemistry 43*, 11770-81.

(12)   Zheng, L. M., Cash, V. L., Flint, D. H., and Dean, D. R. (1998) Assembly of iron-sulfur clusters - Identification of an *iscSUA- hscBA-fdx* gene cluster from *Azotobacter vinelandii*. *J. Biol. Chem. 273*, 13264-13272.

(13)   Kriek, M., Peters, L., Takahashi, Y., and Roach, P. L. (2003) Effect of iron-sulfur cluster assembly proteins on the expression of *E. coli* lipoic acid synthase. *Protein Expression Purif. 28*, 241-245.

(14)   Kessler, D. (2006) Enzymatic activation of sulfur for incorporation into biomolecules in prokaryotes. *FEMS Microbiol. Rev. 30*, 825-40.

(15)   Schwartz, C. J., Djaman, O., Imlay, J. A., and Kiley, P. J. (2000) The cysteine desulfurase, IscS, has a major role in *in vivo* Fe- S cluster formation in *Escherichia coli*. *Proc. Natl. Acad. Sci. U. S. A. 97*, 9009-9014.

(16)   Ding, H., Clark, R. J., and Ding, B. J. (2004) IscA mediates iron delivery for assembly of iron-sulfur clusters in IscU under the limited accessible free iron conditions. *J. Biol. Chem. 279*, 37499-37504.

(17)   Ding, H., Harrison, K., and Lu, J. (2005) Thioredoxin reductase system mediates iron binding in IscA and iron delivery for the iron-sulfur cluster assembly in IscU. *J. Biol. Chem. 280*, 30432-7.

(18)   Adinolfi, S., Rizzo, F., Masino, L., Nair, M., Martin, S. R., Pastore, A., and Temussi, P. A. (2004) Bacterial IscU is a well folded and functional single domain protein. *Eur. J. Biochem. 271*, 2093-2100.

(19)   Vickery, L. E., Silberg, J. J., and Ta, D. T. (1997) Hsc66 and Hsc20, a new heat shock cognate molecular chaperone system from *Escherichia coli*. *Protein Sci. 6*, 1047-56.

(20)   Kakuta, Y., Horio, T., Takahashi, Y., and Fukuyama, K. (2001) Crystal structure of Escherichia coli Fdx, an adrenodoxin-type ferredoxin involved in the assembly of iron-sulfur clusters. *Biochemistry 40*, 11007-12.

(21)   Fish, W. W. (1988) Rapid colorimetric micromethod for the quantitation of complexed iron in biological samples. *Methods Enzymol. 158*, 357-64.

(22)   Beinert, H. (1983) Semi-micro methods for analysis of labile sulfide and of labile sulfide plus sulfane sulfur in unusually stable iron sulfur proteins. *Anal. Biochem. 131*, 373-378.

(23)   Atherton, E., Sheppard, R. C. (1989) *Solid phase peptide synthesis a practicle approach*, IRL Press at Oxford University Press.

(24)   Diaz-Mochon, J. J., Bialy, L., and Bradley, M. (2004) Full orthogonality between Dde and Fmoc: the direct synthesis of PNA--peptide conjugates. *Org Lett 6*, 1127-9.

(25)   Tse Sum Bui, B., Florentin, D., Fournier, F., Ploux, O., Mejean, A., and Marquet, A. (1998) Biotin synthase mechanism: on the origin of sulphur. *FEBS Lett. 440*, 226-30.

(26)   Miller, J. R., Busby, R. W., Jordan, S. W., Cheek, J., Henshaw, T. F., Ashley, G. W., Broderick, J. B., Cronan, J. E., Jr., and Marletta, M. A. (2000) *Escherichia coli* LipA is a lipoyl synthase: *in vitro* biosynthesis of lipoylated pyruvate dehydrogenase complex from octanoyl-acyl carrier protein. *Biochemistry 39*, 15166-78.

(27)   Ugulava, N. B., Gibney, B. R., and Jarrett, J. T. (2001) Biotin synthase contains two distinct iron-sulfur cluster binding sites: chemical and spectroelectrochemical analysis of iron-sulfur cluster interconversions. *Biochemistry 40*, 8343-51.

(28)   Douglas, P., Kriek, M., Bryant, P., and Roach, P. L. (2006) Lipoyl synthase inserts sulfur atoms into an octanoyl substrate in a stepwise manner. *Angew. Chem. Int. Ed. Engl. 45*, 5197-9.

(29)   Cicchillo, R. M., and Booker, S. J. (2005) Mechanistic investigations of lipoic acid biosynthesis in *Escherichia coli*: both sulfur atoms in lipoic acid are contributed by the same lipoyl synthase polypeptide. *J. Am. Chem. Soc. 127*, 2860-1.

Chapter 3   Kinetic Analysis of Sulfur Insertion by *S. solfataricus* LipA

3.1   Introduction

A number of radical SAM proteins have now been characterised (*1*) but only lysine 2,3-aminomutase (*2, 3*) and spore photoproduct lyase (*4*) have been found to be catalytic *in vitro* and are able to reversibly cleave SAM. None of the radical SAM proteins involved in sulfur insertion have shown catalytic activity *in vitro* and both LipA and BioB require one equivalent of SAM for each hydrogen atom abstracted during formation of their respective products (*5-7*). It has also been proposed that the $[2Fe-2S]^{2+}$ cluster of BioB is the source of sulfur during biotin biosynthesis (*8*), hence both the protein and SAM appear to be substrates in the reaction and this may also be the case for LipA (*9*). This makes kinetic analysis of sulfur insertion by LipA challenging since yields of products are low. However development of a novel assay using octanoyl peptides as substrate for LipA facilitates the quantification of both substrate and products (*10*). This assay method has been applied to the kinetic analysis of *S. solfataricus* LipA activity.

Use of thermally stable LipA from a hypothermophilic organism has allowed kinetic data to be recorded over a wide range of temperatures. Rate constants are usually found to vary with temperature according to the Arrhenius equation (eqn. 3.1) where k is the rate constant, A is the pre-exponential factor, E_a is the activation energy, R is the gas constant and T is the temperature (*11*).

$$k = Ae^{\left(-E_a/RT\right)}$$ (equation 3.1)

Determination of rate constants at varying temperature can thus enable calculation of the activation energy for a reaction by using this equation. The enhanced thermal stability of enzymes from hypothermophilic organisms has facilitated the calculation of their activation energies (*12, 13*). The thermal stability of *S. solfataricus* LipA has now permitted the activation of a radical SAM protein to be determined for the first time. Moreover, analysis of reactions using *S. solfataricus* LipA has allowed the activation energies for sulfur insertion at C6 and C8 to be independently determined.

Methods used for timecourse analysis of LipA activity are described in this chapter. This is followed by a discussion of kinetic analysis carried out to determine rate constants for the overall rate of lipoyl formation (k_{obs}) and for sulfur insertion at C6 (k_{obs1}) and at C8 (k_{obs2}) of the octanoyl precursor by analysis of changes in substrate and product concentration over time (scheme 3.1).
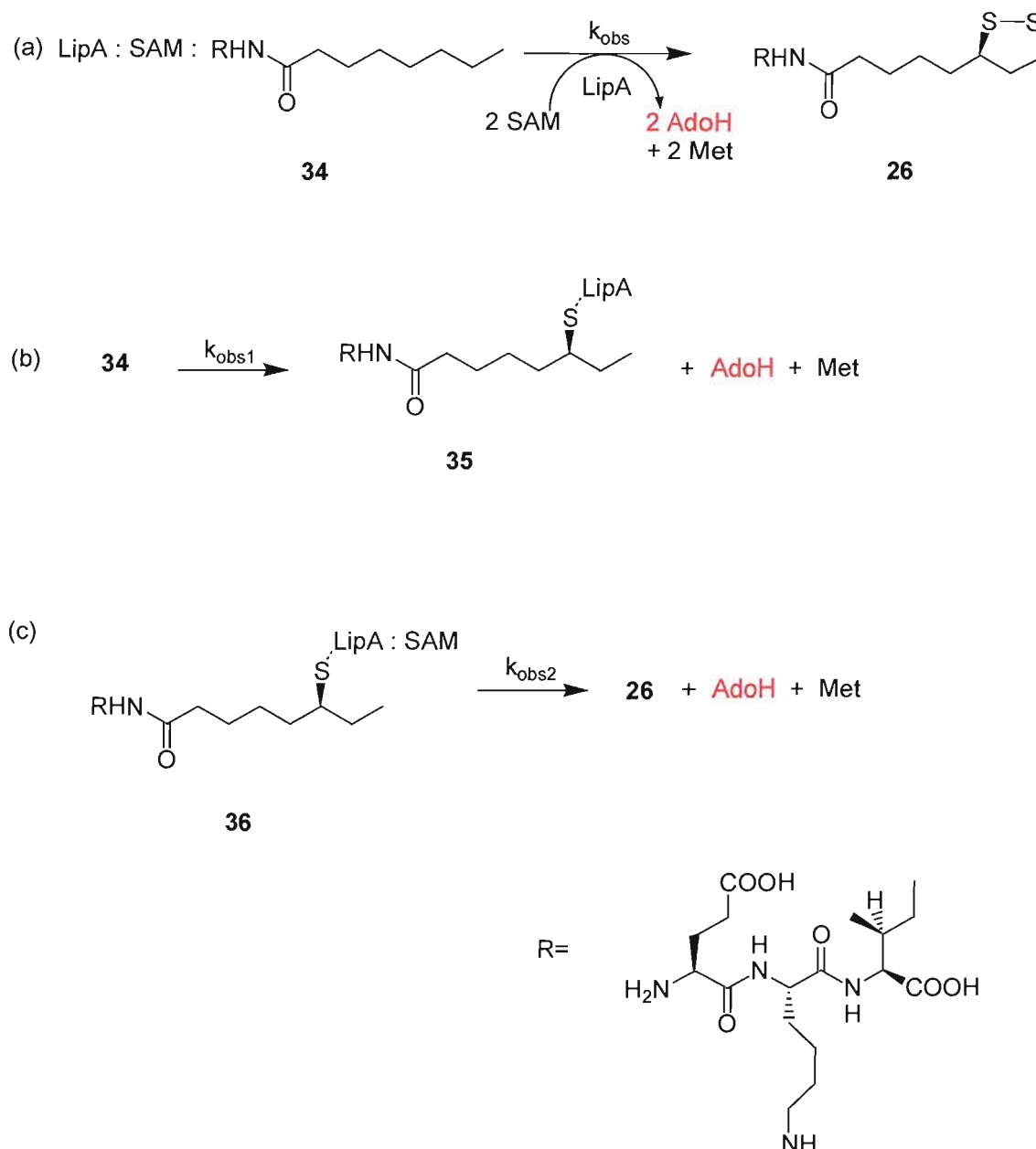
Scheme 3.1 (a) The overall lipoyl forming reaction with rate constant k_{obs}. (b) Sulfur insertion at C6 of a LipA bound octanoyl precursor **34** with rate constant k_{obs1}. (c) Sulfur insertion at C8 of a LipA bound 6MT (**35**) with rate constant k_{obs2}. AdoH formation (shown in red) occurs via two processes, hydrogen atom abstraction from C6 and C8 with rate constants k_{obs1} and k_{obs2} respectively.

3.2   Timecourse sulfur insertion reactions
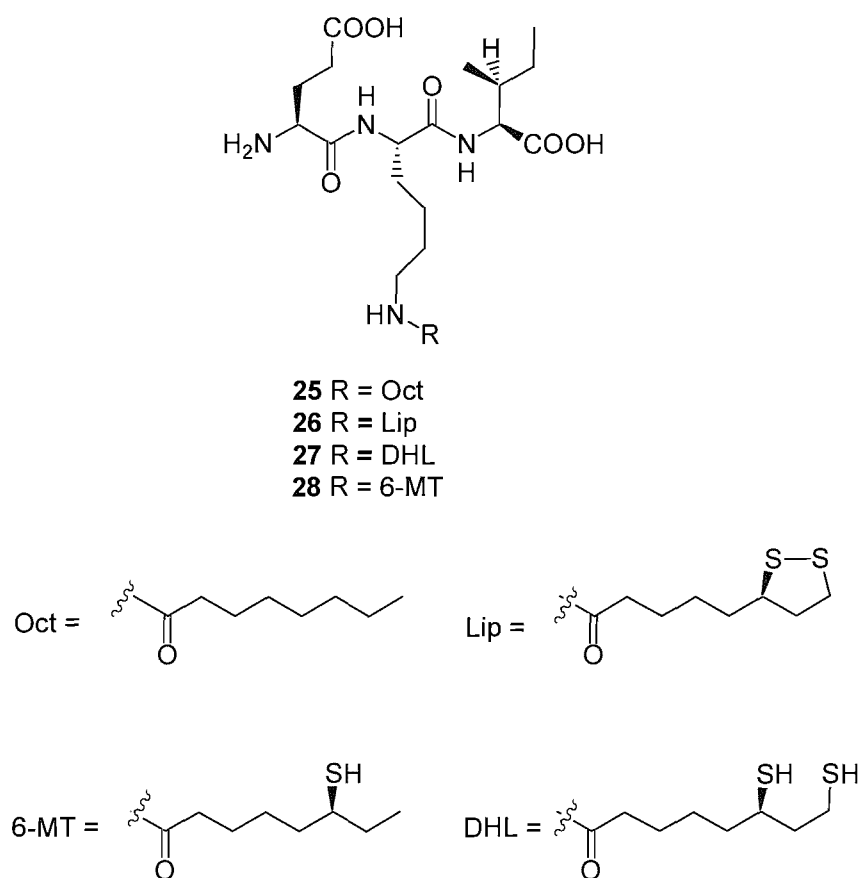
Figure 3.1 Structures of substrate analogue and product peptides observed during kinetic analysis of lipoyl biosynthesis.

To enable kinetic analysis of sulfur insertion reactions using *S. solfataricus* LipA timecourse reactions were carried out which made use of octanoyl tripeptide **25** (fig. 3.1) as substrate. Series of sulfur insertion reactions were prepared by incubating reconstituted LipA with excess dithionite and SAM for 5 min before addition of the octanoyl substrate to ensure the generation of reduced $[4Fe-4S]^+$ clusters bound to SAM. Following addition of octanoyl tripeptide **25** (fig. 3.1), reactions were incubated at several temperatures over the range 23-60 °C and then stopped at different time intervals by acidification. Substrate and product concentrations at each time point for experiments at different temperatures were subsequently quantified to generate data for kinetic analysis.

3.2.1 HPLC analysis of timecourse assays

HPLC analysis of timecourse assays has allowed the simultaneous measurement of octanoyl substrate, lipoyl product and AdoH. Assays were analysed by reverse phase HPLC with UV detection at 230 nm for quantification of octanoyl tripeptide **25** (fig. 3.1) and lipoyl tripeptide **26** (fig. 3.1) which eluted at 29.5 ± 0.7 min and 27.4 ± 0.7 min respectively under the conditions used for analysis of timecourse assays (fig. 3.2).
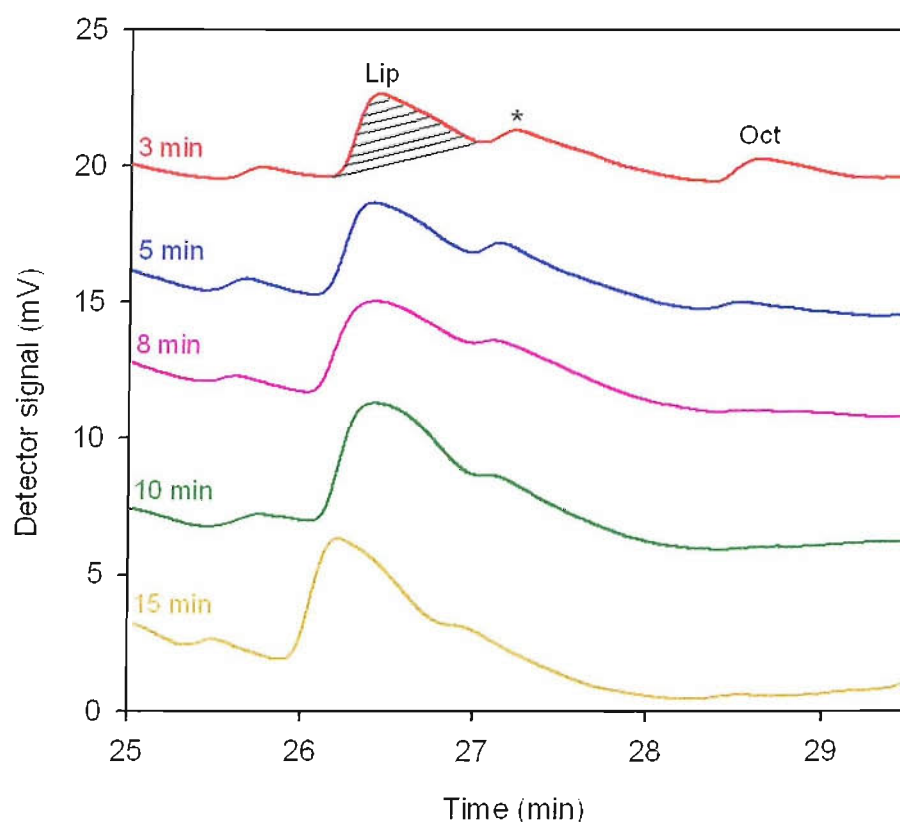
Figure 3.2 HPLC analysis with UV detection at 230 nm of timecourse assays carried out at 60 °C. For clarity traces for 3, 5, 8 and 10 min incubation are offset by 7, 12, 16 and 20 mV respectively: (Lip) lipoyl tripeptide **26** (26.4 min); (*) DHL peptide **27** and/or 6MT peptide **28** (27.3 min); (Oct) octanoyl peptide **25** (28.5 min). The filled area underneath the lipoyl peak at 3 min represents the area integrated for quantification of lipoyl formation.

The amount of lipoyl tripeptide **26** (fig. 3.1) formed was quantified from HPLC data by comparison of peak areas with a calibration curve plotted by analysis of standard solutions (fig. 3.3). The loss of octanoyl peptide **25** (fig. 3.1) was quantified similarly by comparison with a standard curve for this species (fig. 3.4).
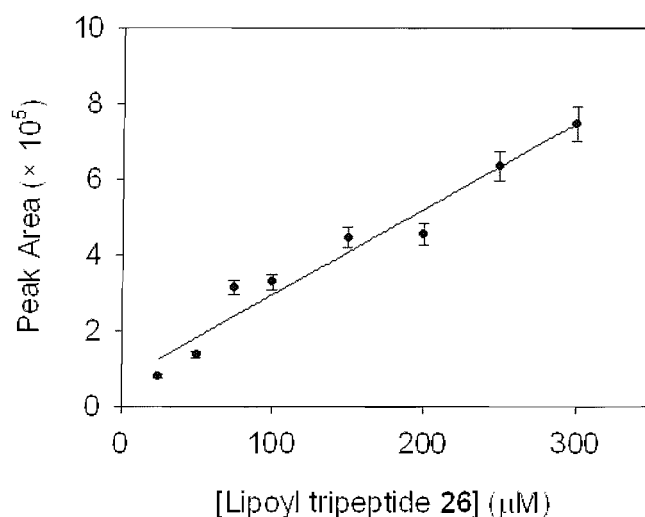
Figure 3.3 Standard curve for concentration of lipoyl tripeptide **26**: 100 μL of standard solutions applied to HPLC column; UV detection at 230 nm; detector sensitivity 0.01; $y = 2603x$; $R_2 = 0.9222$.
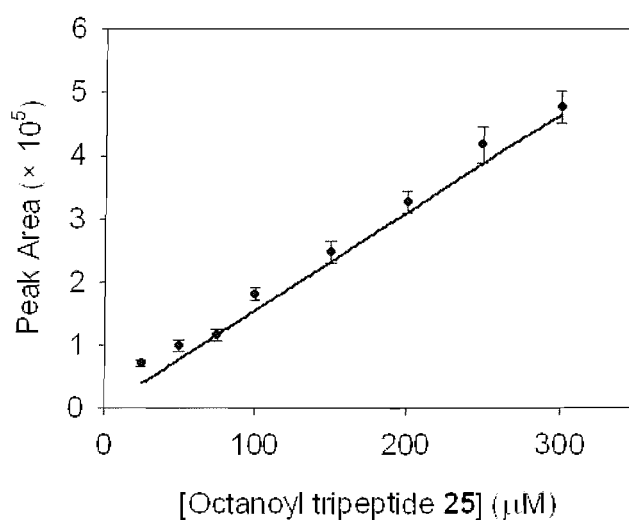
Figure 3.4 Standard curve for concentration of octanoyl tripeptide **25**: 100 μL of standard solutions applied to HPLC column; UV detection at 230 nm; detector sensitivity 0.01; $y = 2345x$; $R_2 = 0.9942$.

The analysis of the timecourses of LipA reactions by HPLC revealed that the peak corresponding to the lipoylated product increased with time. This increase was accompanied by a rapid decrease in the concentration of octanoyl peptide **25** (fig. 3.1) from an initial concentration of 125 µM.
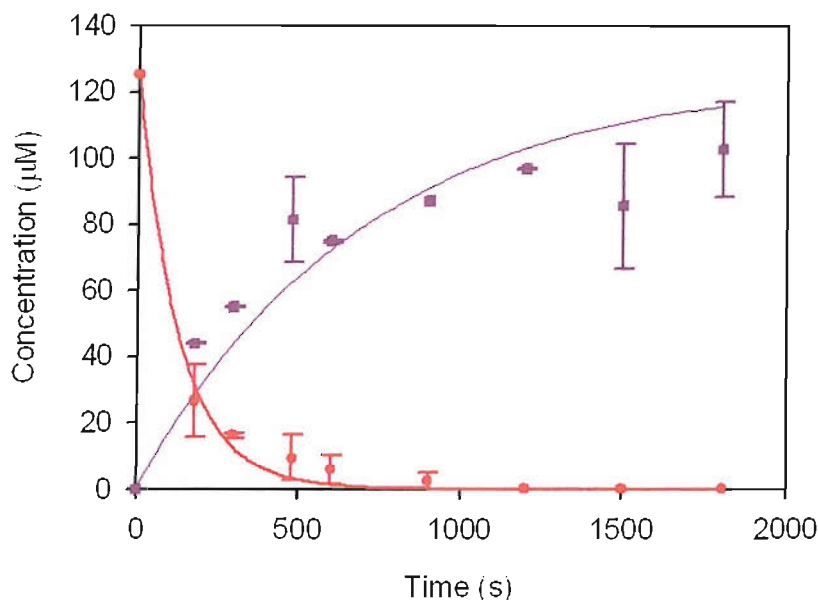
Figure 3.5 Time dependent changes in the concentrations of octanoyl tripeptide **25** (fig. 3.1) (——●) and lipoyl tripeptide **26** (fig. 3.1) (——■). The initial peptide concentration was 125 µM. Data were fitted to a single exponential step by using Sigma Plot. Error bars are derived from standard deviations of two data sets.

There are a number of potential inaccuracies in the quantification of lipoyl formation using this method. It was assumed that the major product of double sulfur insertion observed under conditions used for HPLC analysis was lipoyl tripeptide and not DHL peptide, but LC-MS analysis had shown that the latter might also be present (*14*). Furthermore, the lipoyl peptide peak is not completely resolved from that corresponding to 6MT and/or DHL peptides and this made accurate integration of the peak area very difficult.

To aid the quantification and identification of AdoH during HPLC analysis, UV detection was simultaneously carried out at 259 nm since at this wavelength SAM and AdoH have a strong absorption whilst peptide species are not observed. An initial long isocratic phase (10 min) of 95% aqueous buffer (10 mM ammonium bicarbonate) was applied during HPLC analysis to enhance the separation of AdoH from other hydrophilic components of the assay. The chromatogram for analysis at 259 nm exhibits main peaks (fig. 3.5) at 5.3 min which corresponds to SAM and at 12.1 min with the same retention time as a standard of AdoH.
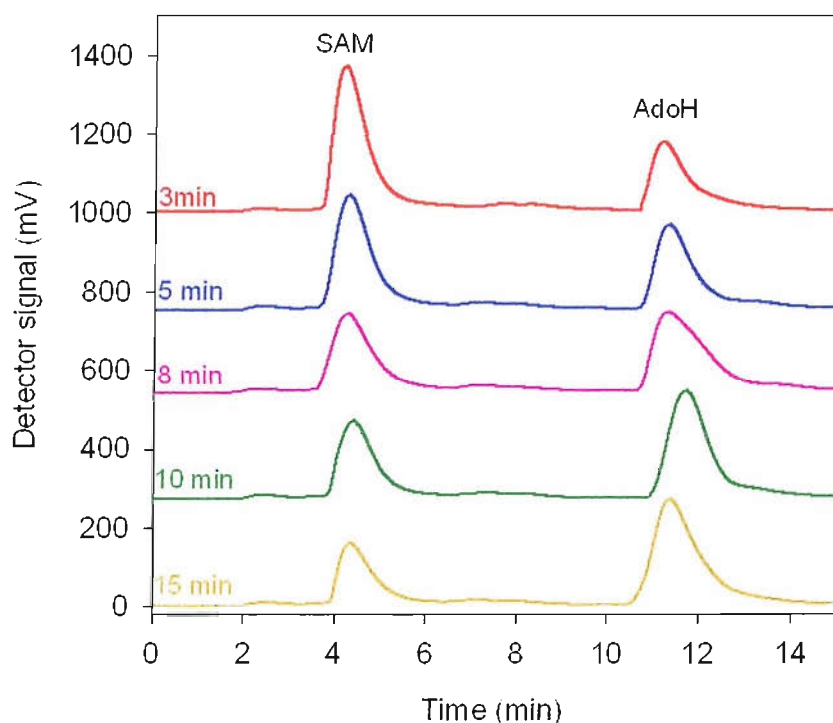
Figure 3.6 HPLC analysis with UV detection at 259 nm of timecourse assays carried out at 60 °C. For clarity traces for 3, 5, 8 and 10 min incubation are offset by 250, 500, 750 and 1000 mV respectively.

Formation of AdoH was quantified from HPLC data by comparison of peak areas with a calibration curve plotted by analysis of standard solutions (fig. 3.7). This showed that there is a rapid increase in AdoH formation which accompanies loss of the octanoyl substrate (fig. 3.8). The rate of AdoH formation also appears to exceed the rate of lipoyl formation (fig. 3.8).
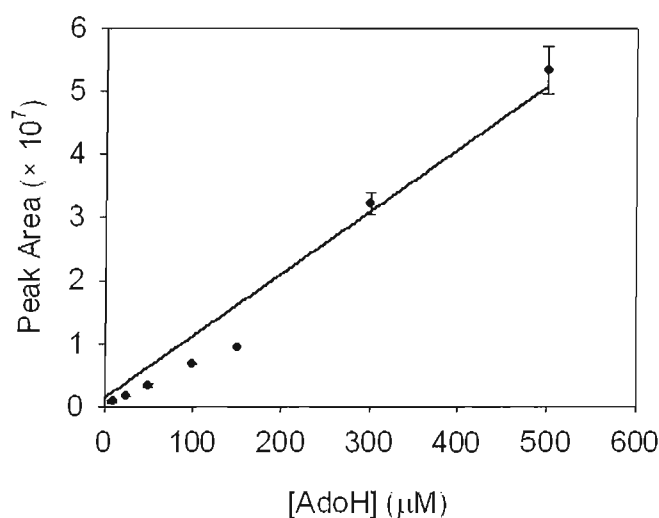
Figure 3.7 Standard curve for AdoH: 100 μL of standard solutions applied to HPLC column; UV detection at 259 nm; detector sensitivity 0.01; y = 102803x; R_2 = 0.9751
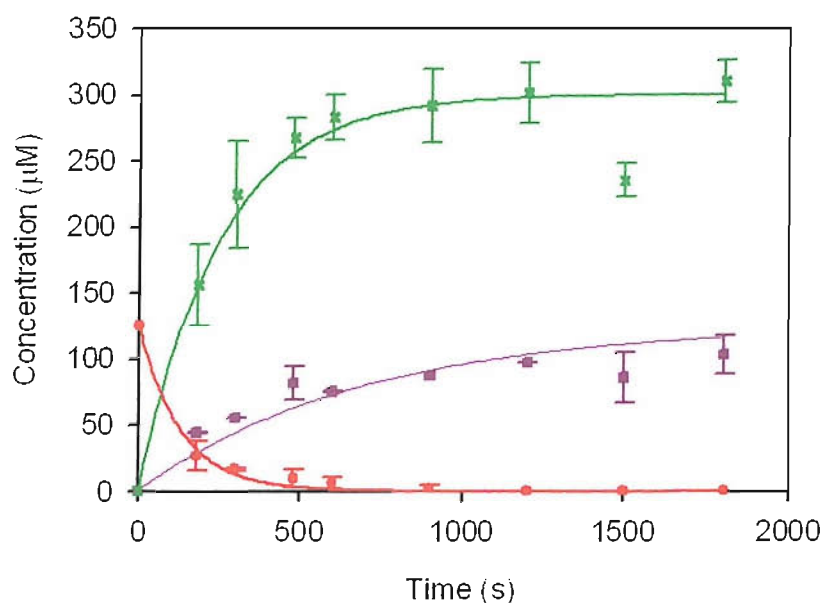
Figure 3.8 Time dependent changes in the concentrations of octanoyl tripeptide **25** (fig.3.1) (——●) and lipoyl tripeptide **26** (fig. 3.1) (——■) and AdoH (——×). Curves shown here are exponential decay and growth curves and do not relate to rates of reaction. Error bars are derived from standard deviations of two data sets.

The maximal expected concentration of AdoH was 250 µM, assuming that two molar equivalents were generated per mole of octanoyl substrate. However, at higher temperatures (above 45 °C) the amount of AdoH formed exceeded this expected value and reached a maximum of 309 µM suggesting there may be some cleavage of SAM which does not lead to hydrogen abstraction from the octanoyl substrate. Similar observations have been made in assays of BioB during which for each mole of biotin formed approximately 2.9 moles of AdoH were generated (6).

T (°C)	Time (min)	[AdoH] (µM)	[lipoyl tripeptide 26] (µM)	[AdoH] /[lipoyl]
23	5	27.5	5.7	4.8
	30	123.9	17.1	7.2
30	5	67.7	8.9	7.6
	30	173.4	19.7	8.8
37	5	67.4	9.5	7.1
	30	227.0	41.4	5.4
45	5	125.7	20.5	6.1
	30	268.9	59.4	4.5
50	5	156.9	53.4	2.9
	30	295.9	89.9	3.3
60	5	155.6	54.5	2.9
	30	309.8	102.2	3.0

Table 3.1 Ratio AdoH to lipoyl tripeptide **26** (fig. 3.1) at varying temperature after 5 min and 30 min incubation.

Simultaneous quantification of products from timecourse assays of *S. solfataricus* LipA showed that the ratio of AdoH to lipoyl product was typically greater than two molar equivalents throughout the reaction (table 3.1). At lower temperatures (23-45) the ratio was up to 8.8 equivalents of AdoH with respect to lipoyl tripeptide. These observations differ from results of timecourse assays using *E. coli* and with octanoyl protein domains as substrate at 37 °C which showed that 2.5 ± 0.1 molar equivalents of AdoH were present with respect to lipoyl formation throughout the reaction (5). However, at higher temperatures (50-60 °C) the ratio of AdoH to lipoyl product in

S. solfataricus assays was more consistent with these results and an average of 3.0 ± 0.6 molar equivalents of AdoH with respect to lipoyl product were formed. The large excess of AdoH at lower temperatures may reflect a difference in rates for sulfur insertion at C6 and C8 of the octanoyl substrate. If the rate for the first sulfur insertion at C6 were the faster step, an excess of AdoH would accumulate along with a protein bound 6MT species **33** (scheme 3.1) prior to sulfur insertion at C8 to form the lipoyl product. At temperatures where LipA activity is optimal (60 °C for *S. solfataricus* LipA and 37 °C for *E. coli* LipA) the rates for both processes would be increased and the reaction has been shown to approach an endpoint at which the amount of lipoyl formation is maximal and therefore this effect is less noticeable.

3.2.2 LC-MS & HPLC analysis of timecourse assays following derivatisation with iodoacetamide

The method described above for analysis of timecourse assays allowed quantification of AdoH and octanoyl substrate but lipoyl formation could not be monitored accurately due to poor separation of peaks and the presence of DHL peptide 27 (fig. 3.1). A method has therefore been developed which would allow quantification of both lipoyl and DHL products. Reduction of assay mixtures with TCEP was used to convert lipoyl tripeptide 26 (fig. 3.1) into the DHL tripeptide 27 (fig. 3.1) and subsequent derivatisation with iodoacetamide yields functionalised 6-carbamoylmethylsulfanyl-octanoyl and 6,8-dicarbamoylmethylsulfanyl-octanoyl peptides 37 and 38 respectively (scheme 3.2). The formation of these derivatives allowed better separation of DHL and 6MT species during HPLC or LC-MS analysis of assays (14). This allowed all double sulfur insertion products to be quantified simultaneously.
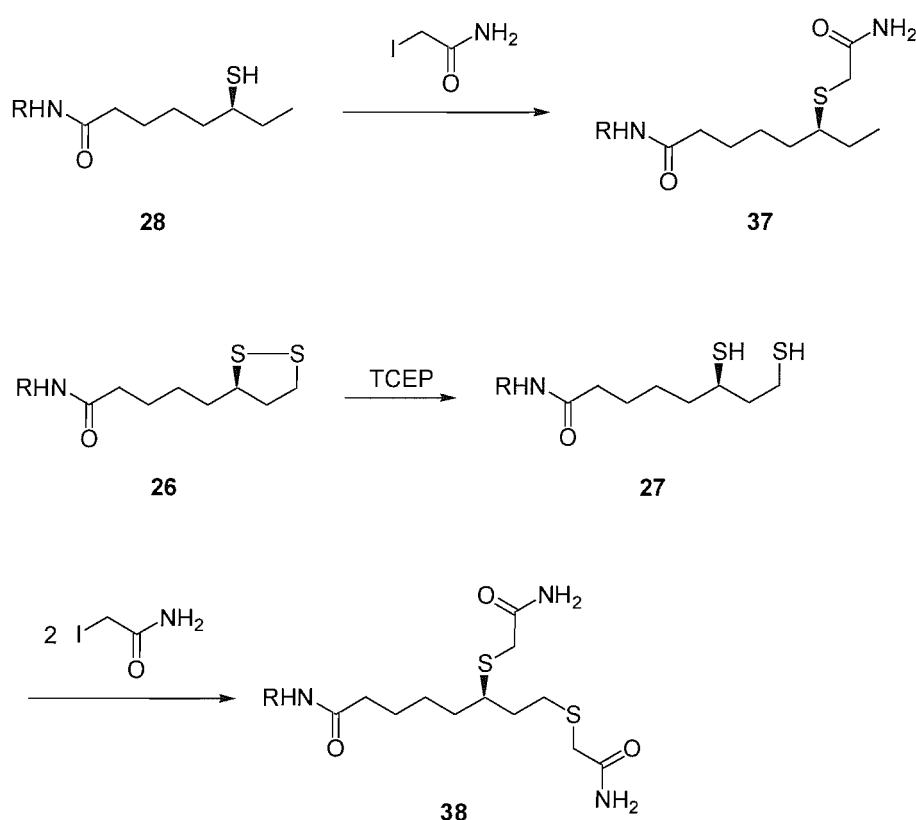
Scheme 3.2 Derivatisation with iodoacetamide of 6MT tripeptide 28 (fig. 3.1) and lipoyl tripeptide 26 (fig. 3.1) formed as products of *S. solfataricus* LipA reactions.

A series of timecourse assays which made use of octanoyl tripeptide **26** (fig. 3.1) as a substrate for *S. solfataricus* LipA were carried out at 50 °C to determine the potential of derivatisation with iodoacetamide for quantification of lipoyl and DHL peptides. Alkylation of the sulfur containing products of timecourse reactions with iodoacetamide required basic conditions. To this end, assays were carried out in ammonium bicarbonate buffer and quenched by addition of TFA since both are lyophilizable and could therefore be removed before redissolving the assay residue in a basic buffer (pH 11.0). Reactions were incubated at 50 °C then stopped by acidification at various time points. Since octanoyl peptide had been observed to be depleted rapidly at higher temperatures (fig. 3.2), assays were stopped at several early time points during the first 10 min of the reaction.

The method which has been described previously for derivatisation with iodoacetamide (*14*) involved initial reduction of disulfides, under anaerobic conditions, with a 5 fold excess of TCEP with respect to initial octanoyl peptide concentration. This was followed by addition of a 10 fold excess of iodoacetamide. However, when these conditions were used for derivatisation of timecourse reactions at 50 °C, which contained substantial quantities of lipoyl product, alkylation was incomplete and underivatised 6MT, DHL and lipoyl peptides were observed by LC-MS analysis (fig. 3.9). An increase in the amount of iodoacetamide added (20 equiv) resulted in complete functionalisation of the monothiolated and DHL species but some unreduced lipoyl product remained. This was overcome by increasing both the amount of TCEP added and increasing the length of reduction time (fig. 3.9). A black precipitate was observed upon addition of TCEP to the assays which might potentially be residual protein. This might have also been alkylated and might explain the requirement for large excesses of reductant and iodoacetamide.
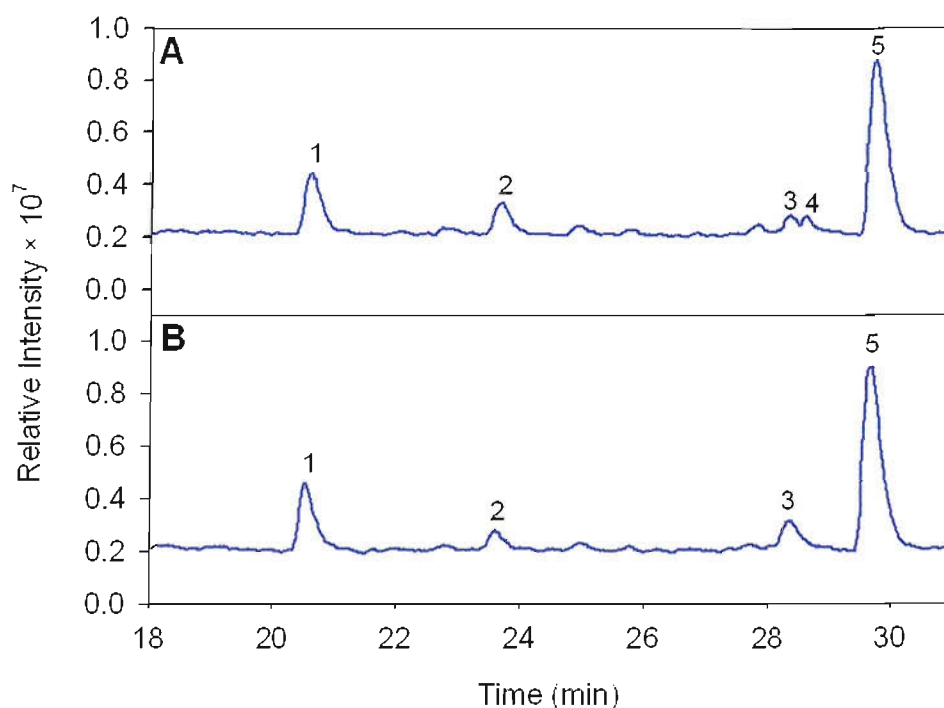
Figure 3.9 TIC of *S. solfataricus* LipA reactions incubated at 50 °C for 6 min followed by derivatisation with iodoacetamide: **A** 5 equiv TCEP, 10 equiv iodoacetamide; **B** 5 equiv TCEP, 20 equiv iodoacetamide(1) 20.5 min, m/z = 693.4, $(M + H)^+$, derivatised DHL tripeptide **38** (scheme 3.2); (2) 23.6 min, m/z = 604.4, $(M + H)^+$, derivatised 6MT tripeptide **37** (scheme 3.2); (3) 28.2 min, m/z = 577.3, $(M + H)^+$, lipoyl tripeptide **26** (fig. 3.1); (4) 28.7 min, m/z = 579.3, $(M + H)^+$, DLH tripeptide **27** (fig. 3.1) & m/z = 548.3, $(M + H)^+$, 6MT tripeptide **28** (fig. 3.1); (5) 29.7 min, m/z = 515.4, $(M + H)^+$, octanoyl tripeptide **25** (fig. 3.1).

Following derivatisation, sulfur insertion reactions were analysed by LC-MS (fig. 3.10) coupled with UV detection (fig. 3.11) or by HPLC using the same method but with the mass spectrometer uncoupled. This showed that octanoyl, 6MT and DHL/lipoyl species had been well resolved by derivatisation of assay mixtures with iodoacetamide.
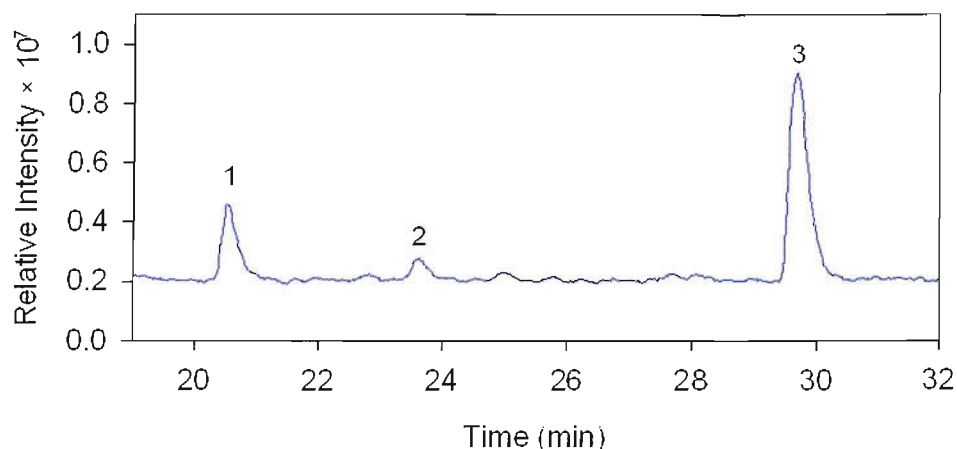
Figure 3.10 TIC of *S. solfataricus* LipA sulfur insertion reaction incubated at 50 °C for 6 min followed by derivatisation of iodoacetamide: (1) 20.5 min, m/z = 693.4, (M + H)$^+$, derivatised DHL tripeptide **38** (scheme 3.2); (2) 23.6 min, m/z = 604.4, (M + H)$^+$, derivatised 6MT tripeptide **37** (scheme 3.2); (3) 29.7 min, m/z = 515.4, (M + H)$^+$, octanoyl tripeptide **26** (fig. 3.1).
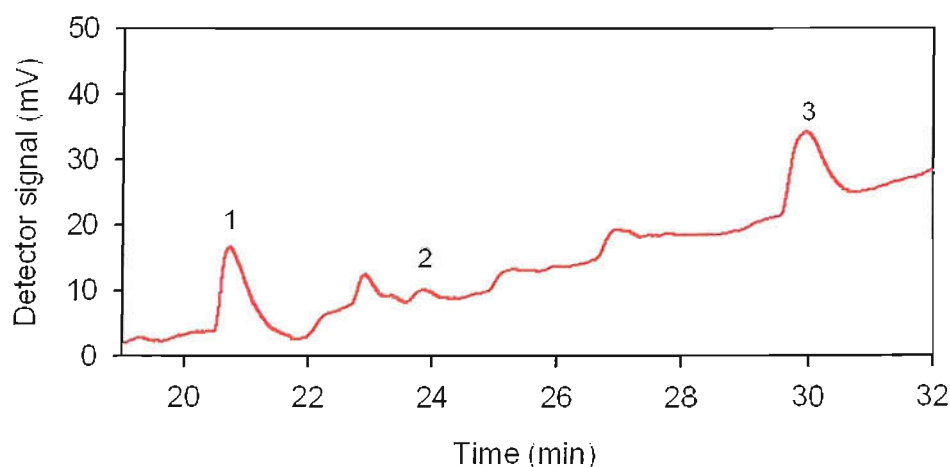
Figure 3.11 UV trace for LC-MS analysis of *S. solfataricus* LipA sulfur insertion reaction incubated at 50 °C for 6 min followed by derivatisation of iodoacetamide: (1) 20.5 min, derivatised DHL tripeptide **38** (scheme 3.2); (2) 23.6 min, derivatised 6MT tripeptide **37** (scheme 3.2); (3) 29.7 min, octanoyl tripeptide **26** (fig. 3.1).

Substrate and product peptides were quantified by integration of peaks observed in the UV chromatogram. Comparison of peak areas with calibration curves constructed from standards of octanoyl peptide (fig. 3.12) allowed the amounts of substrate remaining to be determined. A similar calibration curve (fig. 3.13) was constructed from a synthetic standard of derivatised lipoyl peptide **38** (scheme 3.2) which was prepared by reduction of lipoyl peptide **26** (fig. 3.1) with TCEP followed by

functionalisation with iodoacetamide. A synthetic standard of derivatised 6MT tripeptide **37** (scheme 3.2) was not available and therefore although this species could be detected it could not be quantified accurately. AdoH co-eluted with SAM under the conditions used for LC-MS analysis and therefore could not be quantified from these timecourse reactions.

[Octanoyl tripeptide 26] (μM)
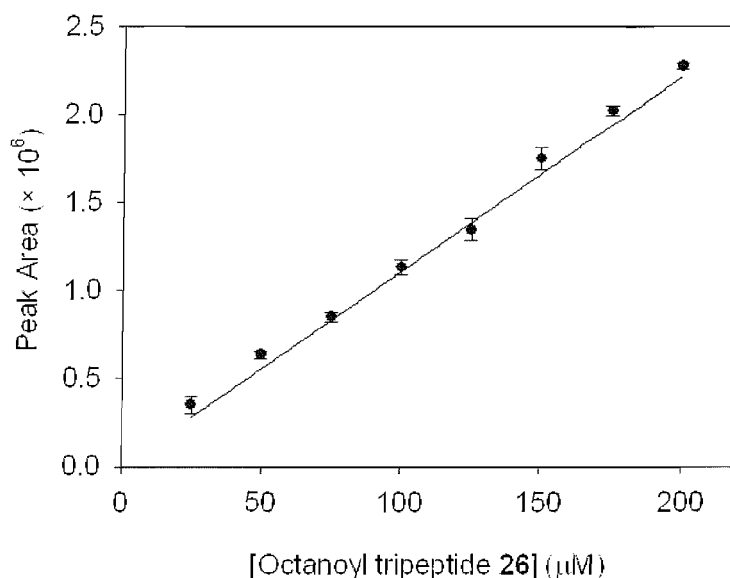
Figure 3.12 Standard curve for octanoyl peptide **25** (fig. 3.1): 100 μL of standard solutions applied to HPLC column; UV detection at 230 nm; detector sensitivity 0.002; y = 11570x; $R_2 = 0.9981$.

[Derivatised lipoyl peptide 36] (μM)
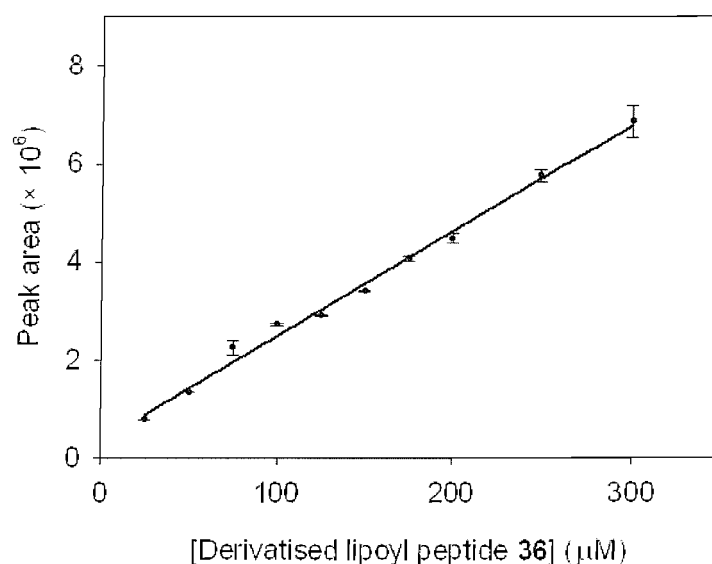
Figure 3.13 Standard curve for derivatised lipoyl tripeptide **38** (scheme 3.2): 100 μL of standard solution applied to HPLC column; UV detection at 230 nm; detector sensitivity 0.002; y = 25281x; $R_2 = 0.9836$.

The derivatisation process resulted in dilution of the total peptide concentration to 120 μM (from 150 μM in assays) and quantification of peptide species revealed that the amount of octanoyl substrate detected decreased from this amount with longer incubation times (fig. 3.14). Integration of the peak corresponding to derivatised 6MT peptide **37** (scheme 3.2) indicated that the decrease in substrate concentration was accompanied by an initial rapid increase in the monothiolated species (fig. 3.15). After a short time (4 min) the amount of this monothiolated peptide began to decline whilst derivatised lipoyl peptide **36** (scheme 3.2) increased after an initial lag period (fig. 3.16).
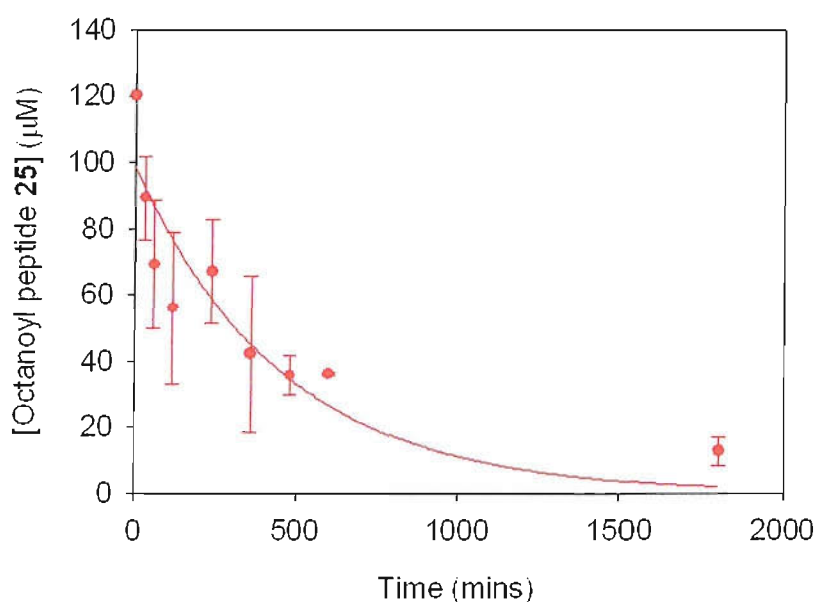
Figure 3.14 Changes with time in concentration of octanoyl peptide **25** (fig. 3.1) for LipA assays at 50 °C which were derivatised with iodoacetamide (peptide concentration 120 μM). Data has been fitted to a first order process and error bars are derived from standard deviations from two data sets.
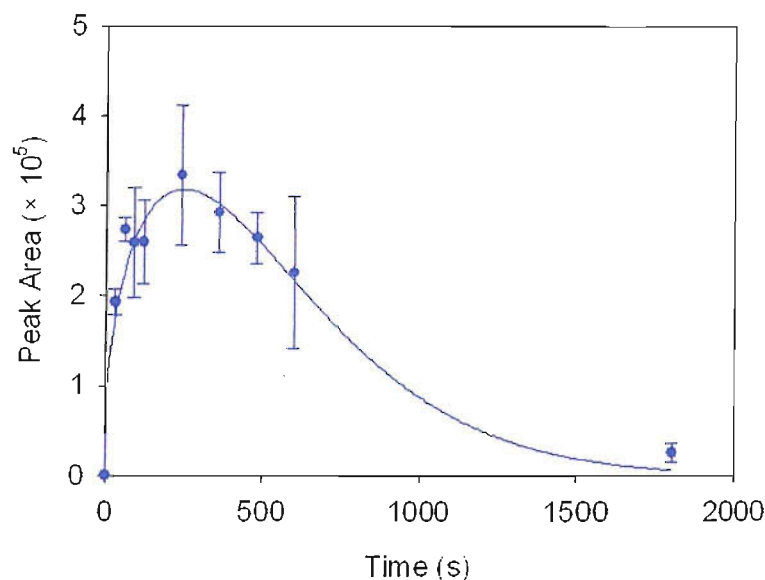
Figure 3.15 Peak areas corresponding to functionalised 6MT peptide **37** (scheme 3.2) plotted against time for LipA assays at 50 °C which were derivatised with iodoacetamide. Error bars are derived from standard deviations from two data sets.
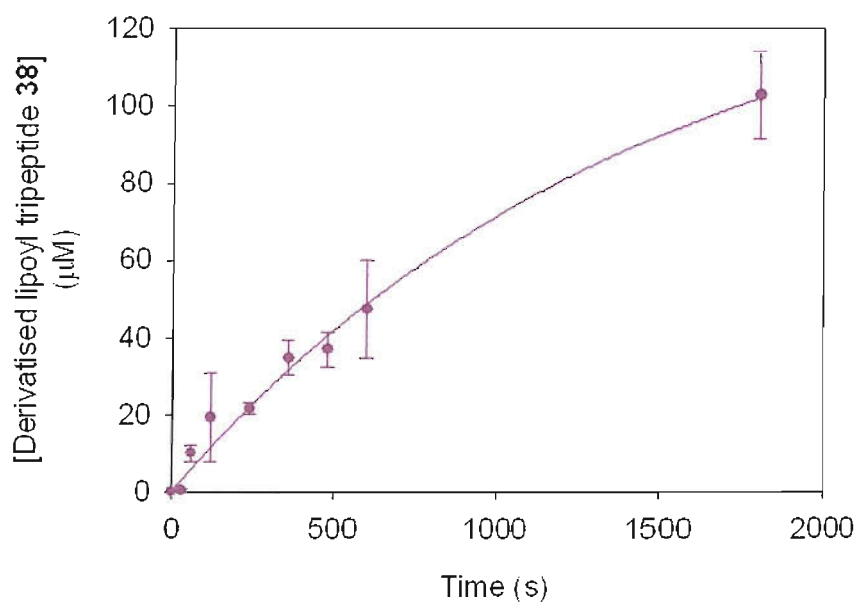
Figure 3.16 Changes in concentration of functionalised DHL peptide **38** (scheme 3.2) with time for assays of LipA at 50 °C which were derivatised with iodoacetamide. Data has been fitted to a first order process and error bars are derived from standard deviations from two data sets.

Analysis of average values from two sets of timecourse assays at 50 °C has shown that large errors were incurred in quantification of all peptide species using this method. There are a number of possible reasons for experimental error. The detection

sensitivity for peptide species is low which may have led to errors in integration. Recovery of peptides following sulfur insertion reactions and derivatisation with iodoacetamide may also have been incomplete. It has been shown that under non-denaturing conditions the 6MT peptide **28** (fig. 3.1) remains bound to LipA (*14*). This may involve interaction between the thiol of this species with iron centres of the protein. The thiol groups of DHL may also remain associated with free iron following reduction of assays with TCEP and therefore addition of EDTA to chelate any residual iron might improve recovery of sulfur containing peptides. A further reason for errors in quantification might be inefficient dissolution of peptide species following freeze drying of assays prior to derivatisation. Use of the more soluble octanoyl tetrapeptide substrate **20** (fig. 2.1) may resolve this problem.

Timecourse assays were repeated over a range of temperatures (23-60 °C) and were derivatised with iodoacetamide as described above for reactions at 50 °C. In the case of assays at 60 °C, although all 6MT and DHL products were successfully derivatised, some underivatised lipoyl peptide **26** remained. The amount of this underivatised product was estimated by comparison with the standard curve for octanoyl tripeptide (fig. 3.12) and the value determined was added to the quantified amount of derivatised lipoyl peptide **38** to calculate the total amount of lipoyl product. Amounts of lipoyl product detected in all these assays could then be compared with underivatised assays showing that after 30 min incubation the amount of lipoyl product detected was greater in the former samples (table 3.2). This shows that both lipoyl and DHL products may be detected using this method allowing better quantification of these products of double sulfur insertion by LipA. This has allowed kinetic analysis of the lipoylation reaction to be carried out.

T (°C)	Amount of lipoyl/DHL product detected after 30 min (µM)	
	Underivatised assays	Iodoacetamide derivatised assays
23	17.1	36.0
30	19.7	47.5
50	89.9	102.6
60	102.2	107.1

Table 3.2 Comparison of amounts of double sulfur insertion product detected after 30 min incubation from underivatised and iodoacetamide derivatised assays.

3.3   Kinetic analysis of lipoyl formation

Quantification lipoyl products from timecourse assays using the methods described above has allowed kinetic analysis of the overall rate of lipoyl formation. Data from both underivatised and iodoacetamide derivatised timecourse assays was analysed to determine rate constants for the overall lipoylation reaction. The changes in lipoyl tripeptide **26** (fig. 3.1) concentration measured from underivatised timecourse reactions were plotted against time for series of assays conducted at each temperature (fig. 3.17). Similar plots were obtained for the concentration of iodoacetamide functionalised DHL peptide **38** (scheme 3.2) after derivatisation of assays (fig. 3.18).
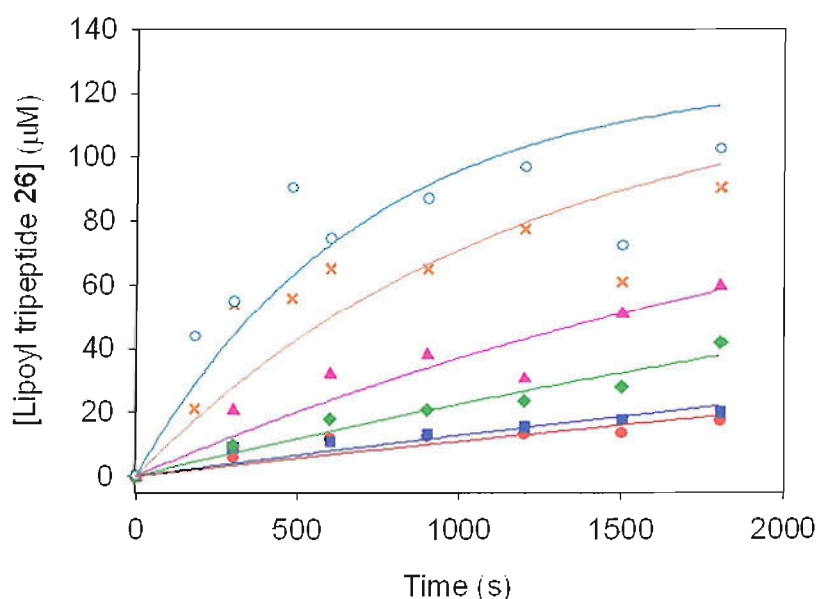
Figure 3.17 Time dependent formation of lipoyl tripeptide at varying temperatures determined by analysis of underivatised assays. Plots were derived by averaging two data sets: (——•) 23 °C; (——■) 30 °C; (——♦) 37 °C; (——▲)45 °C; (——×) 50 °C; (——○) 60 °C. Curves were fitted by approximation of data to a pseudo-first order process using the program DYNAFIT.
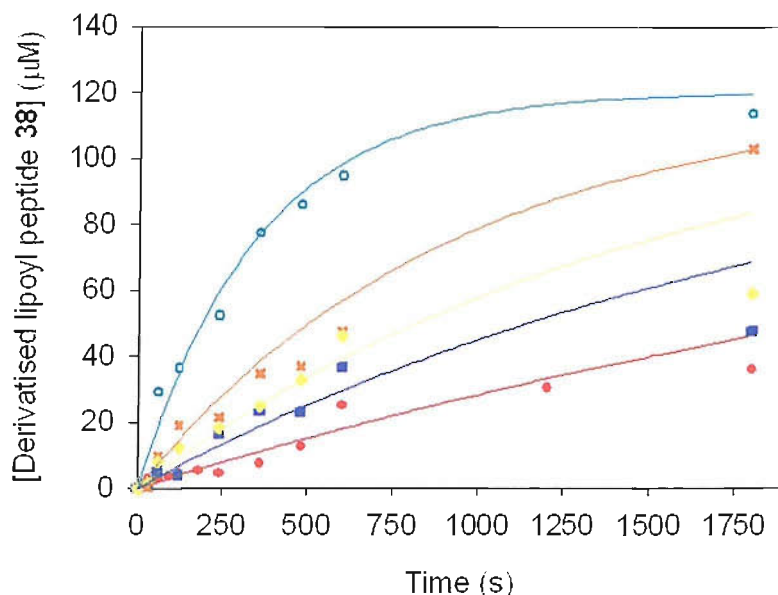
Figure 3.18 Time dependent formation at of lipoyl tripeptide **26** (fig. 3.1) which was quantified following derivatisation with iodoacetamide to yield **38** (scheme 3.2): (——●) 23 °C; (——■) 30 °C; (●) 40 °C; (——×) 50 °C; (——○) 60 °C. Curves were fitted by approximation of data to a pseudo-first order process using the program DYNAFIT.

When fitting timecourse data for lipoyl formation to kinetic equations it has been assumed that both SAM and the octanoyl peptide **25** (fig. 3.1) bind to LipA via a rapid equilibrium to form a protein substrate complex **34** (scheme 3.3). Kinetic analysis of substrate binding to BioB has shown that SAM binds with a K_d of 900 μM (*15*). Furthermore, the binding of dethiobiotin to BioB was shown to occur at a moderate rate which has been modelled to a second order rate constant $k = 10^4$ $M^{-1}s^{-1}$ (*15*). However, the rate of sulfur insertion to form biotin occurs more slowly and a first order rate constant $k = 1.2 \times 10^{-3}$ s^{-1} has been reported for this reaction (*8*). It has been assumed that in the case of lipoyl formation by *S. solfataricus* LipA, the contribution to the observed rate from dissociation constants (K_{d1} and K_{d2}) for the binding of substrates is negligible. Time dependent lipoyl formation during assays of *S. solfataricus* LipA at each temperature has therefore been approximated to a pseudo-first order process (*11*) for the formation of the lipoyl product from the protein substrate complex **34** (scheme 3.3). Rate constants (k_{obs}) for the conversion of a LipA bound octanoyl group to a lipoyl group (scheme 3.3) were derived from each timecourse using the program DYNAFIT (*16*) by fitting to a first order equation (*11*) (eqn. 3.2) and are shown in table 3.3.

$$\text{LipA} + \text{SAM} \underset{}{\overset{K_{d1}}{\rightleftharpoons}} \text{LipA : SAM}$$

$$\text{LipA : SAM} + \text{RHN}\!\!\!\overset{\displaystyle\frown\frown\frown}{\underset{O}{\bigg|\bigg|}}\!\!\! \underset{}{\overset{K_{d2}}{\rightleftharpoons}} \text{LipA : SAM : RHN}\!\!\!\overset{\displaystyle\frown\frown\frown}{\underset{O}{\bigg|\bigg|}}$$

25   **34**

$$\mathbf{34} \xrightarrow{\ k_{obs}\ } \text{RHN}\!\!\!\overset{\displaystyle\frown\frown}{\underset{O}{\bigg|\bigg|}}\!\!\!\overset{S-S}{\diagdown} + \ 2\text{AdoH} + 2\text{Met}$$

26
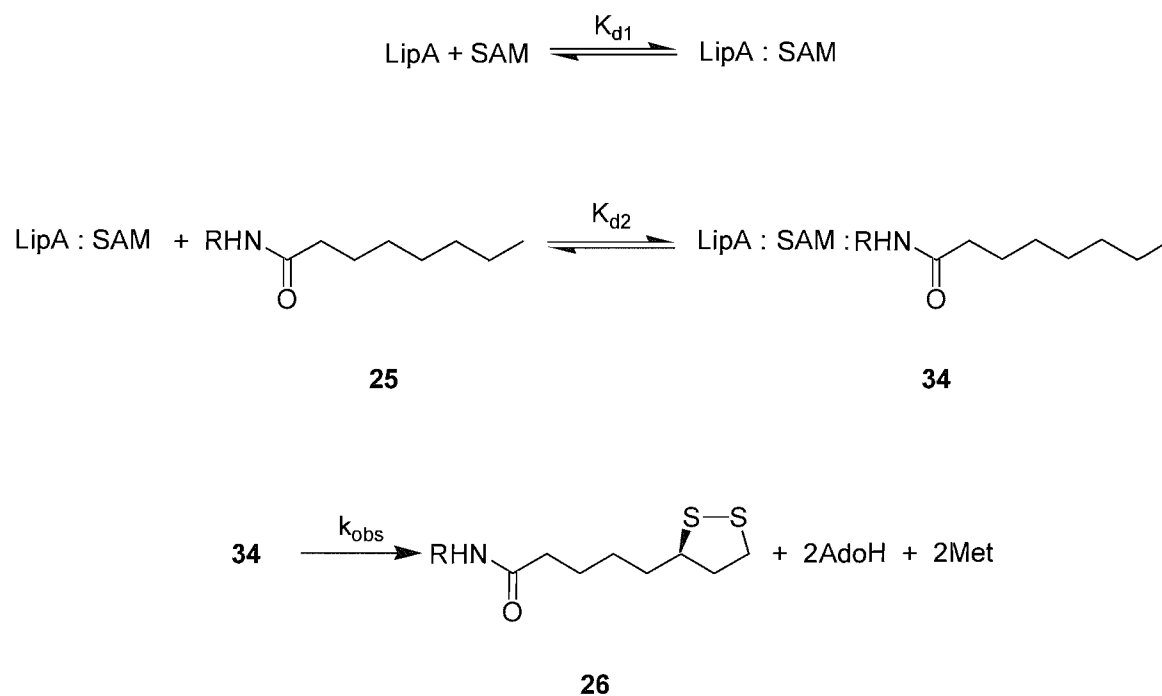
Scheme 3.3 Binding of SAM and octanoyl peptide **25** (fig. 3.1) to LipA to generate a protein substrate complex **34**. This is proposed to react to form a lipoyl product **26** with rate constant k_{obs}.

$$\frac{d[26]}{dt} = k_{obs}[34]_0 \qquad\qquad\qquad \text{(equation 3.2)}$$

T (°C)	$k_{obs} \times 10^{-4}$ (s^{-1}) from analysis of underivatised timecourse assays	$k_{obs} \times 10^{-4}$ (s^{-1}) from analysis of derivatised timecourse assays
23	0.9 ± 0.1 [b]	2.7 ± 0.2 [b]
30	1.1 ± 0.1 [a]	4.7 ± 0.9 [b]
37	2.0 ± 0.1 [a]	-
40	-	6.6 ± 0.4 [b]
45	3.5 ± 0.5 [a]	-
50	8.4 ± 1.3 [a]	10.7 ± 0.5 [a]
60	14.5 ± 0.3 [a]	28.6 ± 2.3 [b]

Table 3.3 Rate constants (k_{obs}) calculated for lipoyl formation over temperature range 23-60 °C. *a* values derived from average values taken from two data sets; *b* values derived from single data set.

The rate constants approximated from derivatised assays were greater than those approximated from underivatised reactions. This reflects the errors in quantification of lipoyl product from underivatised assays which were described above. Since derivatisation with iodoacetamide results has allowed measurement of both the products of double sulfur insertion by LipA, rate constants for overall lipoyl formation derived from derivatised assays are likely to be more accurate and therefore this data was used for all further kinetic and thermodynamic analysis of changes in lipoyl concentration.

The observed rate constant for the reaction of *S. solfataricus* LipA with octanoyl tripeptide **25** (fig. 3.1) at 37 °C is substantially lower than the rate constant observed for the *E. coli* protein using an octanoyl protein domain as a substrate (*5*). This slower reaction of *S. solfataricus* LipA might result from the weaker association of LipA with the octanoyl tripeptide relative to the natural substrate protein domain. However, it has been shown that the optimum temperature for activity of *S. solfataricus* LipA is 60 °C (*10*) whilst the optimum temperature for activity of *E. coli* LipA is likely to be 37 °C and this could account for the difference in rate

constants at equivalent temperatures. The rate constant for the reaction of *S. solfataricus* LipA with octanoyl tripeptide at 60 °C determined from iodoacetamide derivatised assays (28.6 × 10^{-4} s^{-1}) is very close to that observed for the *E. coli* protein at 37 °C (29.0 × 10^{-4} s^{-1}) (*5*). These values are also both similar to the rate constant calculated for biotin biosynthesis (12.0 × 10^{-4} s^{-1}) by BioB (*8*) which may reflect the similar mechanisms employed by these proteins.

3.3.1 Calculation of activation energy for lipoyl formation

The activation energy for lipoyl biosynthesis by *S. solfataricus* LipA has been estimated from an Arrhenius plot (*11*) which was obtained by plotting $\ln(k_{obs})$ derived from iodoacetamide derivatised assays against the reciprocal temperature (fig. 3.19). The data could be fitted to a linear plot and the activation energy (E_a) was then calculated from the gradient of this plot according to eqn. 3.1. This gave a value of 47.2 ± 5.4 kJ/mol for the activation energy of lipoyl formation.

$$E_a = 47.2 \pm 5.4 \text{ kJ/mol}$$
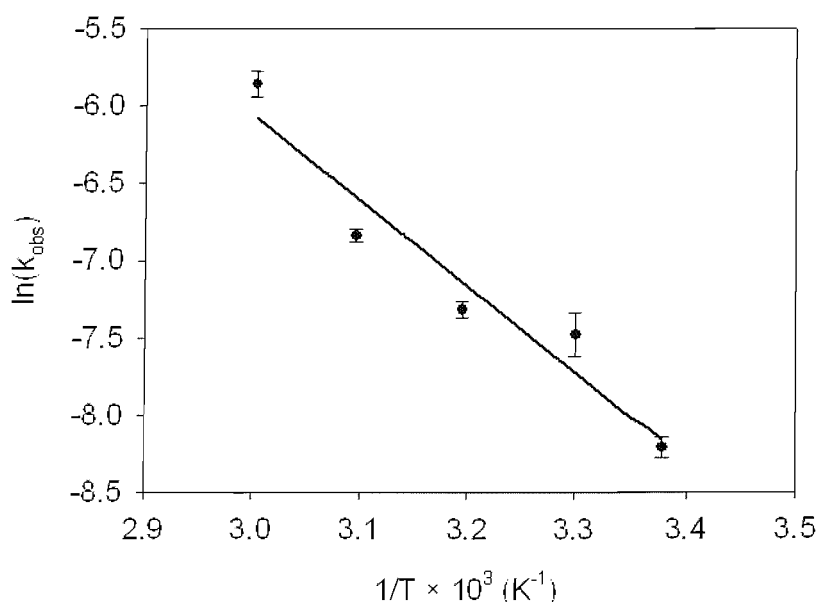
Figure 3.19 Arrhenius plot for lipoyl formation derived from rate constants (k_{obs}) obtained from derivatised assays: y = -5680x + 11.1; R_2 = 0.9618

The bond dissociation energy for homolytic cleavage of a carbon-sulfur bond of SAM to generate AdoH in the absence of a radical SAM protein is estimated to be

greater than 250 kJ/mol (17). The activation energy calculated for lipoyl formation by *S. solfataricus* LipA is considerably less than this showing that LipA significantly lowers the activation energy barrier for this process. Lowering of the energy barrier for homolytic cleavage is likely to be facilitated by a close interaction between SAM and the reduced $[4Fe-4S]^{1+}$ cluster of LipA similar to that which has been shown to exist in other radical SAM proteins (18, 19).

Enzymes which utilise adenosylcobalamin as a source of Ado• radicals share some similar mechanistic steps to radical SAM proteins: generation of an Ado• radical followed by hydrogen atom abstraction by this species from a substrate radical. Stopped flow UV/vis spectroscopy analysis of assays of an adenosylcobalamin dependent enzyme, methylmalonyl-CoA mutase, has yielded an overall activation energy barrier of 54.8 ± 2.5 kJ/mol for these steps (20). Meanwhile, experiments which studied the thermodynamic properties of ribonucleotide reductase have indicated that this adenosylcobalamin dependent enzyme generates an activation energy of 65.7 ± 0.4 kJ/mol for formation of Ado• followed by hydrogen atom abstraction (21). These values are similar to that calculated for the activation energy barrier for lipoyl formation despite the disparity between bond dissociation energies for cleavage of the C-Co bond of adenosylcobalamin (125 kJ/mol (22)) and that for cleavage of the C-S bond of SAM (>250 kJ/mol). The activation energy barriers for these proteins and LipA are similar to that for abstraction of hydrogen atom from methane by a methyl radical (50 kJ/mol) (23). Thus, upon lowering of the energy barrier for generation of Ado•, hydrogen abstraction from the substrate by this radical may be the rate determining step.

The overall rate of lipoyl formation has been approximated to a single first order process and this has allowed calculation of an activation energy barrier for this process. However, these values do not reflect the actual mechanism for lipoyl formation which proceeds via two sulfur insertion steps (14). The activation energies for sulfur insertion at C6 and C8 may differ from each other and the value calculated for the overall rate of lipoyl formation would then approximate the rate determining step.

3.4   Analysis of the observed rate of the first sulfur insertion step

To approximate rate constants for the first sulfur insertion step during lipoyl formation, the rates of loss of octanoyl peptide have been analysed. It has been assumed that a protein substrate complex 34 (scheme 3.4) is formed prior to this sulfur insertion reaction and that the contribution to the observed rate constant from the dissociation constants (K_{d1} and K_{d2}) for the binding of SAM and octanoyl substrate is negligible. It has then been assumed that loss of the octanoyl substrate occurs via the irreversible formation of a C-S bond at C6 to generate a protein bound 6MT peptide 35 (fig. 3.1). The observed rate of loss of octanoyl peptide has therefore been expected to equal the rate of formation of the 6MT species. Based on these assumptions rate constants (k_{obs1}) have been approximated for sulfur insertion at C6 by analysis of octanoyl peptide concentrations from both underivatised and iodoacetamide derivatised *S. solfataricus* LipA timecourse assays.
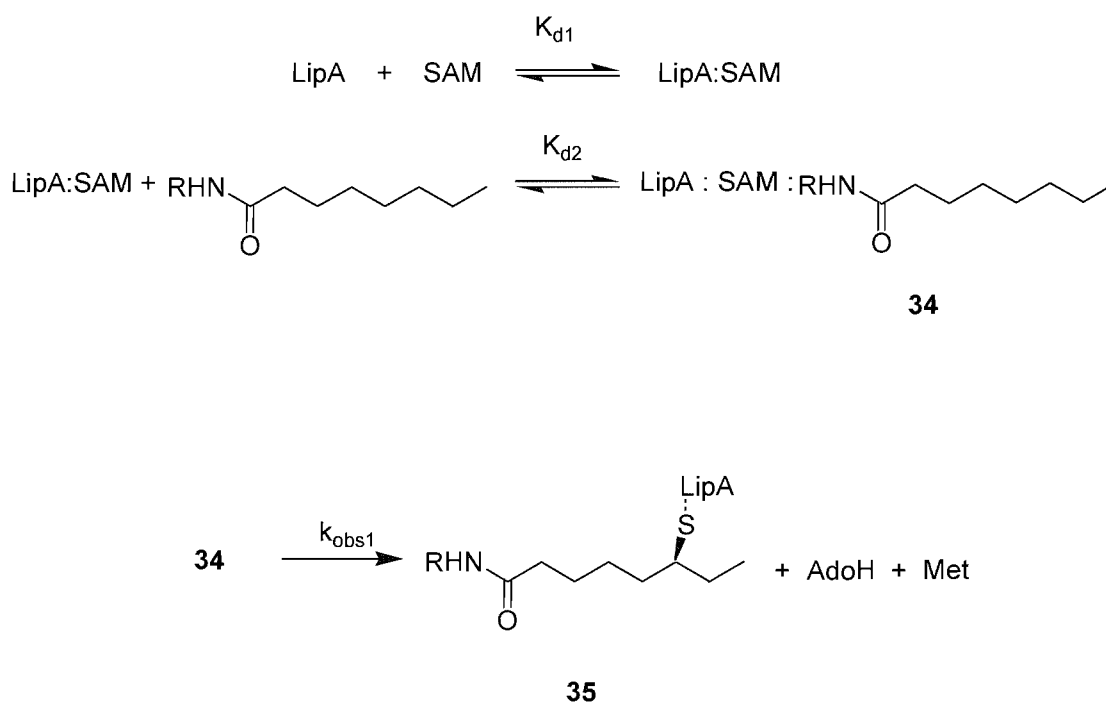
Scheme 3.4 Conversion of LipA bound octanoyl peptide 34 (fig. 3.1) to a protein bound 6MT species 35 with rate constant k_{obs1}.

The concentration of octanoyl peptide **25** (fig. 3.1) was plotted against time for each timecourse. The time dependent decrease in the amount of starting material at each temperature was then approximated to a pseudo-first order process (*11*) using the program DYNAFIT (*16*). Data from underivatised assays fitted well to curves derived from approximation first order rate constant (fig. 3.20) however, the values derived from derivatised assays fit less well (fig. 3.21). The rate plots for data from derivatised assays fit reasonably well during the early stages of the reaction (0-10 min) but the final amount of octanoyl substrate after 30 min is underestimated at all temperatures. This discrepancy might result from binding of some octanoyl peptide to inactive LipA which has not been fully reconstituted to bind two [4Fe-4S]$^{1+/2+}$. It is likely that two complete [4Fe-4S]$^{1+/2+}$ clusters are required for LipA activity (*24*). If some LipA monomers were not in this active form then this might explain the unexpected change in rate.
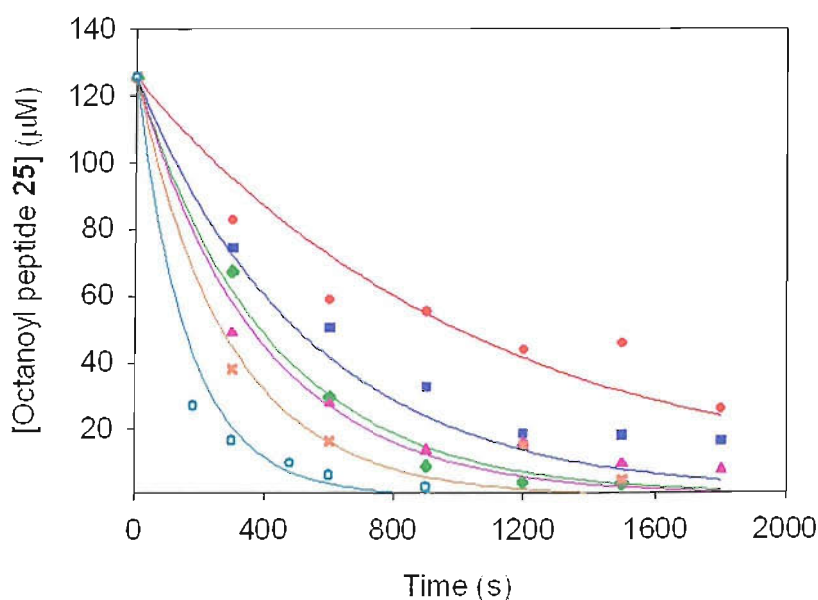
Figure 3.20 Time dependent decrease in concentration of octanoyl tripeptide **25** (fig. 3.1) which was quantified underivatised assays: (—●) 23 °C; (—■) 30 °C; (—◆)37 °C; (—▲)45 °C; (—×) 50 °C; (—○) 60 °C. Curves were fitted by approximation of data to a pseudo-first order process using the program DYNAFIT.
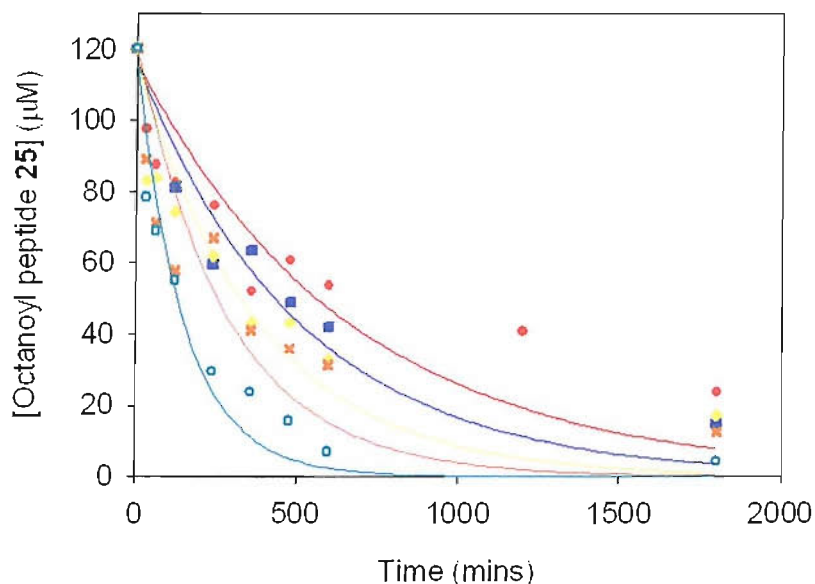
Figure 3.21 Time dependent decrease in concentration of octanoyl tripeptide **25** (fig. 3.1) which was quantified following derivatisation of assays with iodoacetamide: (——●) 23 °C; (——■) 30 °C; (——) 40 °C; (——×) 50 °C; (——○) 60 °C. Curves were fitted by approximation of data to a pseudo-first order process using the program DYNAFIT.

Rate constants (k_{obs1}) for the insertion of sulfur at C6 of the octanoyl substrate (scheme 3.4) derived from each timecourse by fitting to a first order equation (*11*) (eqn. 3.3) are shown in table 3.4. The rate constants derived from derivatised assays lie within experimental error of those predicted from underivatised assays indicating that these values represent a reasonable estimate. The rate constants approximated for the first sulfur insertion reaction at C6 of the octanoyl substrate are greater than determined for the overall rate of lipoyl formation. This suggests the second sulfur insertion reaction is slower and is consistent with the observation of large excesses of AdoH with respect to lipoyl concentration in underivatised timecourse assays.

$$\frac{d[34]}{dt} = -k_{obs1}[35]_0$$

(equation 3.3)

T	$k_{obs1} \times 10^{-4}$	$k_{obs1} \times 10^{-4}$	$k_{obs} \times 10^{-4}$
(°C)	(s^{-1})	(s^{-1})	(s^{-1})
	from analysis of underivatised timecourse assays	from analysis of derivatised timecourse assays	from analysis of derivatised timecourse assays
23	9.3 ± 0.9 [b]	10.1 ± 2.7 [b]	2.7 ± 0.2 [b]
30	15.8 ± 3.0 [a]	19.5 ± 1.9 [b]	4.7 ± 0.9 [b]
37	24.0 ± 2.6 [a]	-	-
40	-	27.7 ± 4.5 [b]	8.7 ± 1.0 [b]
45	25.8 ± 3.0 [a]	-	-
50	42.5 ± 7.1 [a]	34.5 ± 9.4 [a]	12.0 ± 1.3 [a]
60	60.2 ± 3.6 [a]	66.3 ± 9.7 [b]	28.6 ± 2.3 [b]

Table 3.4 Rate constants (k_{obs1}) calculated for loss of octanoyl peptide **25** (fig. 3.1) over temperature range 23-60 °C: *a* values derived from average values taken from two data sets; *b* values derived from a single data set. Rate constants (k_{obs}) calculated for the overall rate of lipoyl formation are also listed for comparison.

3.4.1 Estimation of activation energy for the first sulfur insertion

The activation energy for sulfur insertion at C6 of an octanoyl moiety by *S. solfataricus* LipA has been estimated from an Arrhenius plots (*11*) which were obtained by plotting $\ln(k_{obs1})$ derived from underivatised (fig. 3.22) and derivatised assays (fig. 3.22) against the reciprocal temperature. The data from both sets of timecourse reactions could be fitted to a linear plot and the activation energy (E_{a1}) was then calculated from the gradient of each of these plots according to eqn. 3.1 which gave values of 40.9 ± 2.3 kJ/mol and 39.1 ± 5.7 kJ/mol for data obtained from underivatised and derivatised assays respectively. These values are in good agreement with each other and show that the activation energy barrier for sulfur insertion at C6 is in the range 33.4-43.2 kJ/mol.

$$E_{a1} = 40.9 \pm kJ/mol$$
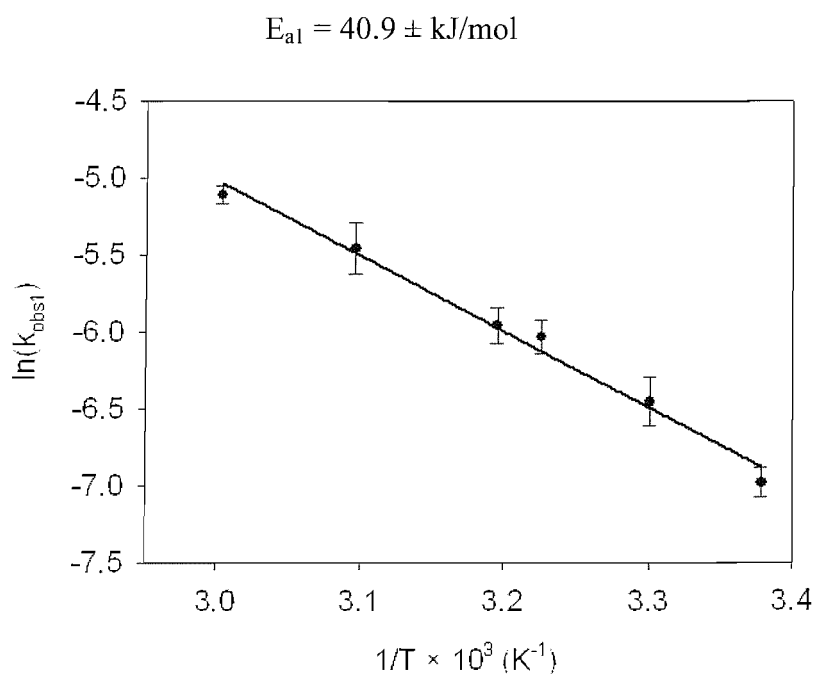
Figure 3.22 Arrhenius plot for sulfur insertion at C6 of octanoyl peptide **25** (fig. 3.1) derived from rate constants (k_{obs1}) calculated from underivatised assays of *S. solfataricus* LipA activity: $y = -4907x + 9.7$; $R_2 = 0.9872$

$$E_{a1} = 39.1 \pm 5.7 \ kJ/mol$$
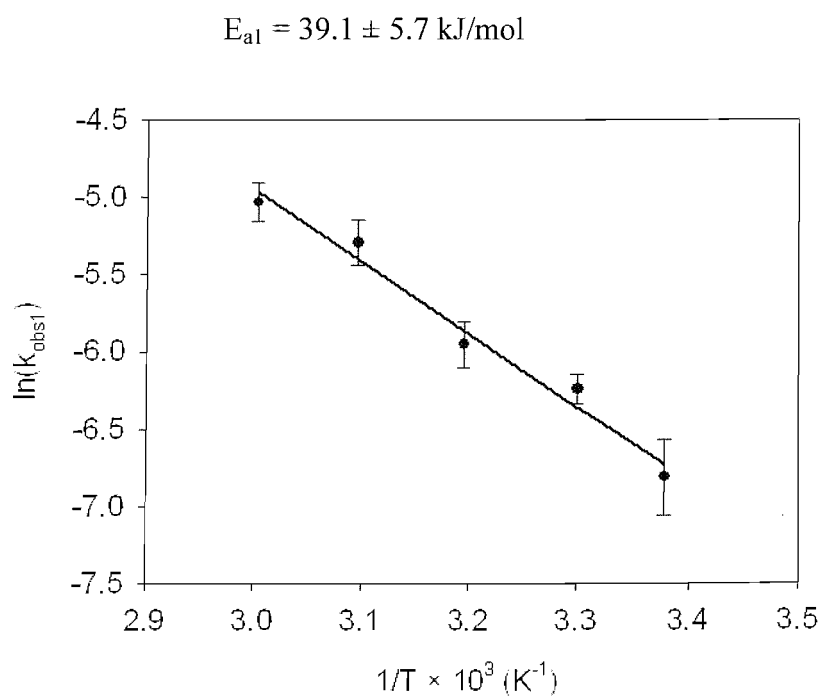
Figure 3.23 Arrhenius plot for sulfur insertion at C6 of octanoyl peptide **25** (fig. 3.1) derived from rate constants (k_{obs1}) calculated from derivatised assays of *S. solfataricus* LipA activity: $y = -4709x + 9.2$; $R_2 = 0.9784$

The activation energy barrier estimated for sulfur insertion at C6 of octanoyl tripeptide **25** (fig. 3.1) is lower than that observed for the overall formation of lipoyl tripeptide **26** (fig. 3.1). Thus, the activation energy for the second sulfur insertion step is likely to be greater making sulfur insertion at C8 the rate determining step during lipoyl biosynthesis. Further kinetic analysis has therefore been carried out to determine the activation energy barrier for this second sulfur insertion step.

3.5   Analysis of the observed rate of the second sulfur insertion step

3.5.1   Approximation of lipoyl formation to a two step process

To determine rate constants for the second sulfur insertion step during lipoyl formation, changes in concentration of derivatised lipoyl peptide **33** (scheme 3.2) were approximated to two processes (scheme 3.5); sulfur insertion at C6 (rate constant, k_{obs1}) then sulfur insertion at C8 (rate constant k_{obs2}). In order to approximate data to this mechanism it has been assumed that following the first sulfur insertion at C6, binding of SAM occurs to generate a second reactive protein substrate complex **34** (scheme 3.5). It has further been assumed that the contribution to the observed rate constant from the dissociation constant (K_{d3}) for binding of a second molecule of SAM is negligible. Lipoyl peptide **26** (fig. 3.1) is then expected to be formed via the irreversible formation of a C-S bond at C8 of the protein bound 6MT species.
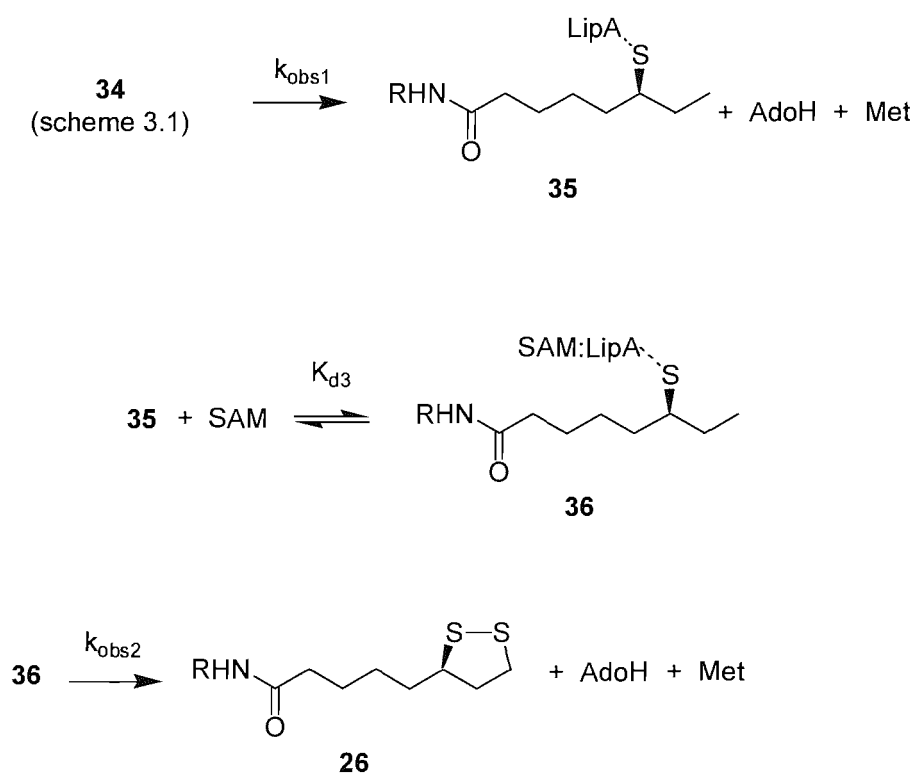
Scheme 3.5 Stepwise formation of lipoyl product by *S. solfataricus* LipA from a protein bound octanoyl peptide substrate **32**. Sulfur insertion occurs first at C6 (rate constant k_{obs1}) to generate a protein bound 6MT intermediate **33**. Subsequent binding of SAM is followed by sulfur insertion at C8 to generate the lipoyl product **26** with rate constant k_{obs2}.

Based on the assumptions made for lipoyl formation via a two step process, changes in derivatised lipoyl peptide **38** (scheme 3.2) concentrations determined from iodoacetamide derivatised assays were fitted to this mechanism using the program DYNAFIT (*16*) by setting values for k_{obs1} at those determined by analysis of substrate concentration (table 3.4) and then varying values for k_{obs2} (table 3.5) to fit data to equation 3.4 for the formation of lipoyl product.

$$\frac{d[26]}{dt} = k_{obs1}[36]$$ (equation 3.4)

T (°C)	$k_{obs2} \times 10^{-4}$ (s^{-1})	$k_{obs1} \times 10^{-4}$ (s^{-1}) from analysis of derivatised timecourse assays
23	4.8 ± 1.0 [b]	10.1 ± 2.7 [b]
30	9.1 ± 4.8 [b]	19.5 ± 1.9 [b]
40	19.8 ± 6.3 [b]	27.7 ± 4.5 [b]
50	24.8 ± 3.8 [a]	50.9 ± 9.4 [a]
60	61.5 ± 6.0 [b]	66.3 ± 9.7 [b]

Table 3.5 Rate constants (k_{obs2}) calculated for sulfur insertion at C8 of 6MT peptide **28** (fig. 3.1) by approximation of lipoyl formation to two first order processes: *a* values derived from average values taken from two data sets. Rate constants (k_{obs1}) for sulfur insertion at C6 are listed for comparison; *b* values derived from a single data set.

Curves derived from approximation of lipoyl formation to two first order rate constants do not fit well to the experimental data and the final amount of octanoyl substrate after 30 min is overestimated at all temperatures (fig. 3.24). This might reflect inaccuracies in quantification of peptides and collection of more data may minimise these errors. Furthermore, overestimation of lipoyl formation may be due to binding of the octanoyl substrate to inactive LipA which does not bind two $[4Fe-4S]^{1+/2+}$ cluster and therefore does not initiate sulfur insertion. Approximated rate constants for the second sulfur insertion reaction at C8 of the 6MT species are

lower than those determined for sulfur insertion at C6 of the octanoyl starting material (table 3.5). This is consistent with the formation of large excesses of AdoH observed in timecourse assays at lower temperatures and the accumulation of a 6MT species.
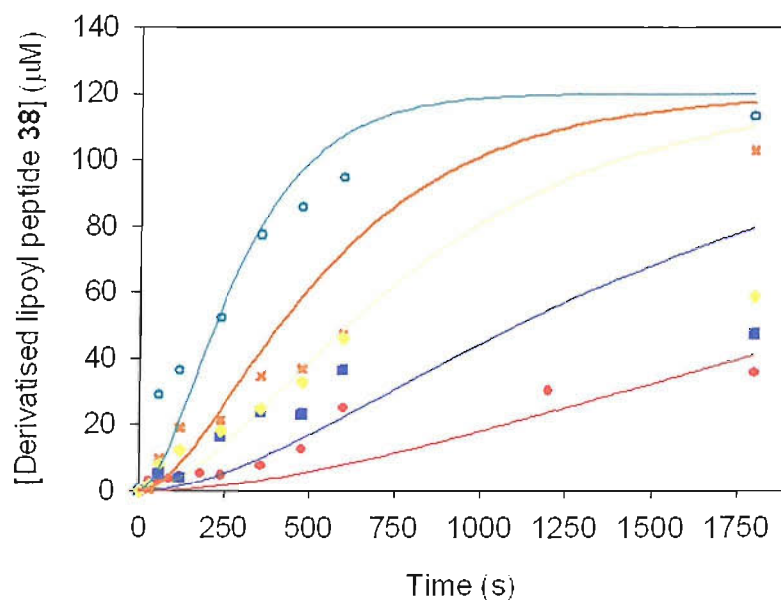
Figure 3.24 Time dependent change in concentration of lipoyl tripeptide **26** (fig. 3.1) which was quantified following derivatisation with iodoacetamide to yield **33** (scheme 3.2): (—●) 23 °C; (—■) 30 °C; (◆) 40 °C; (—×) 50 °C; (—○) 60 °C. Curves were fitted using the program DYNAFIT by approximation of data to two pseudo-first order processes, sulfur insertion at C6 (k_{obs1}) and sulfur insertion at C8 (k_{obs2}).

3.5.2 Approximation of AdoH formation to a two step process

Rate constants (k_{obs2}) for sulfur insertion at C8 have also been determined by analysis of AdoH formation using a similar methodology to that used for analysis of lipoyl formation. AdoH is formed via two processes; hydrogen atom abstraction at C6 and C8 of a protein bound octanoyl complex **34** (scheme 3.1). To fit changes in AdoH concentration to these two processes it has been assumed that one molar equivalent of AdoH is formed irreversibly per mole of protein bound octanoyl peptide **34** (scheme 3.1) converted to a protein bound 6MT species **35** (scheme 3.1). Based on this assumption it is expected that the observed rate of formation of AdoH from this reaction is equal to the rate of loss of the octanoyl substrate and can be approximated by values of k_{obs1} determined by analysis of loss of octanoyl peptide. However, a second molar equivalent of AdoH is then expected to be formed irreversibly for each mole of lipoyl product formed. The observed rate of formation of AdoH via this process is expected to equal the rate of formation of lipoyl product from the 6MT intermediate with a rate constant k_{obs2}.
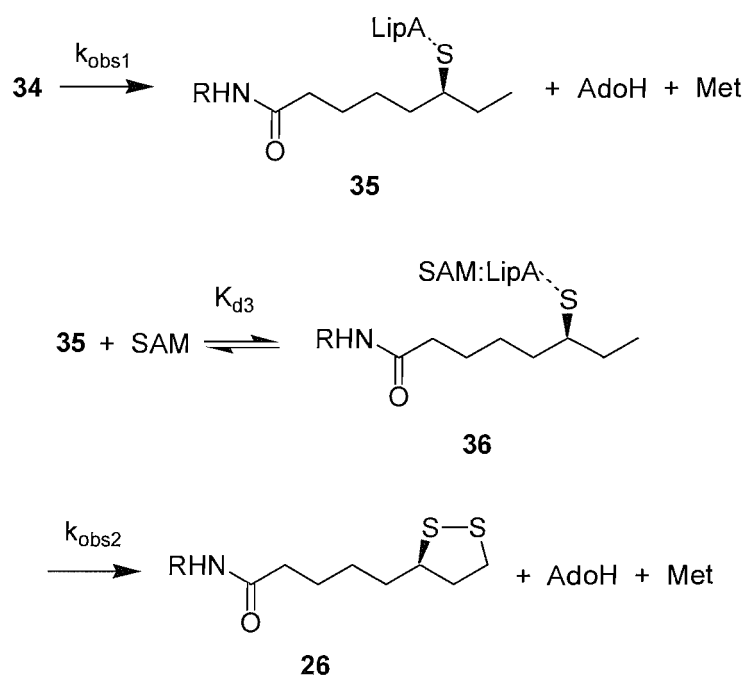
Scheme 3.6 Formation of AdoH by *S. solfataricus* LipA. AdoH is formed irreversibly from the protein substrate complex **34** during sulfur C6 of the octanoyl moiety. Following binding of SAM to the resulting intermediate species **35** to form a reactive protein substrate complex **36**, a further equivalent of AdoH is irreversibly formed during sulfur insertion at C8 of the protein bound 6MT intermediate

Based on the assumptions made for the observed rate of AdoH formation, data was approximated to two first order processes (scheme 3.6) using the program DYNAFIT (16) by setting values for k_{obs1} at those determined by analysis of substrate concentration (table 3.6) and then varying values for rate constants (k_{obs2}) for sulfur insertion at C8 (table 3.5).
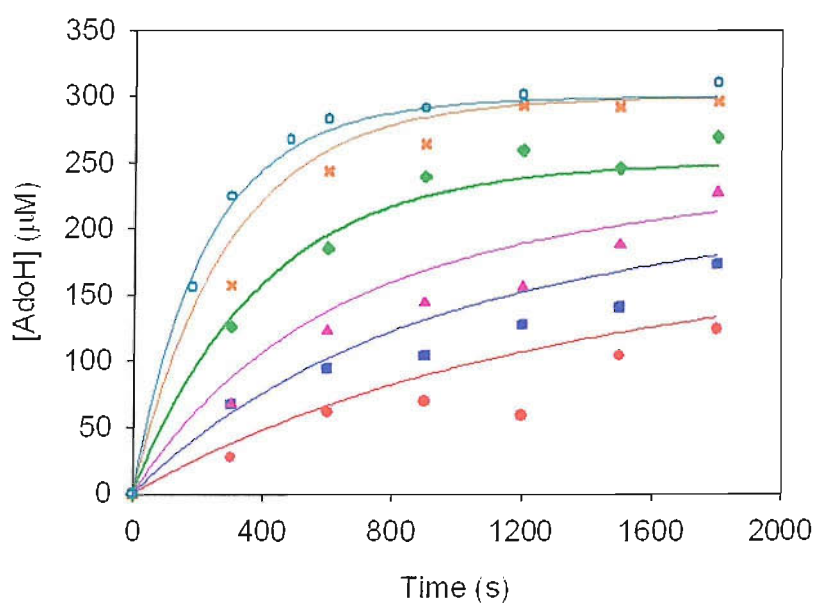
Figure 3.25 Time dependent change in concentration of AdoH: (——●) 23 °C; (——■) 30 °C; (——♦) 37 °C; (——▲)45 °C; (——×) 50 °C; (——○) 60 °C. Curves were fitted using the program DYNAFIT by approximation of data to two pseudo-first order processes, sulfur insertion at C6 (k_{obs1}) and sulfur insertion at C8 (k_{obs2}).

T (°C)	$k_{obs2} \times 10^{-4}$ (s^{-1}) from analysis of AdoH formation	$k_{obs2} \times 10^{-4}$ (s^{-1}) from analysis of lipoyl formation
23	2.5 ± 1.3 [b]	4.8 ± 1.0 [b]
30	3.8 ± 0.8 [a]	9.1 ± 4.8 [b]
37	7.9 ± 1.4 [a]	-
45	24.8 ± 6.0 [a]	-
50	27.7 ± 2.3 [a]	24.8 ± 3.8 [a]
60	34.0 ± 6.3 [a]	61.5 ± 6.0 [b]

Table 3.6 Rate constants (k_{obs2}) calculated for sulfur insertion at C8 of 6MT peptide **28** (fig. 3.1) by approximation of AdoH formation to two first order processes: a values derived from average values taken from two data sets. Rate constants (k_{obs1}) for sulfur insertion at C6 are listed for comparison; b values derived from a single data set.

Rate constants for the second sulfur insertion reaction at C8 of the 6MT species derived from analysis of AdoH formation are lower than those determined for sulfur insertion at C6 of the octanoyl starting material (table 3.5). This observation provides further evidence that sulfur insertion at C8 is the rate determining step during lipoyl formation. However, rate constants predicted for sulfur insertion at C8 based on analysis of AdoH formation are lower than those predicted by analysis of lipoyl formation. This is unexpected due to the observed uncoupled cleavage of SAM to generate more than two equivalents of AdoH with respect to the initial substrate concentration. Due to this excess, initial concentrations of octanoyl peptide were set at a higher value (150 µM) than were actually present in assays (125 µM) when approximating AdoH formation to a two step process. Therefore the values determined for k_{obs2} by analysis of AdoH formation are unlikely to be a valid approximation and highlight the limitations of this method.

3.5.3 Estimation of activation energy for the second sulfur insertion step

The activation energy for sulfur insertion at C8 of 6MT peptide **28** (fig. 3.1) by *S. solfataricus* LipA has been estimated from Arrhenius plots (*11*) which were obtained by plotting values for $\ln(k_{obs2})$ which were approximated by analysis of changes in lipoyl concentration (fig. 3.26) or from changes in AdoH concentration (fig. 3.27) against the reciprocal temperature. Each data set was fitted to a linear plot and the activation energy (E_{a2}) was then calculated from the gradient of these plots according to eqn. 3.1 to gave values of 46.9 ± 5.7 kJ/mol and 62.6 ± 6.5 kJ/mol for data obtained from analysis of lipoyl formation and AdoH formation derivatised assays respectively. The difference in these values is likely to reflect the inaccuracies in kinetic analysis based on AdoH formation due to uncoupled turnover. The value calculated for E_{a2} based on lipoyl formation is therefore likely to be more accurate and therefore the activation energy barrier for sulfur insertion at C8 is likely to be in the range 41.2-52.6 kJ/mol.

$$E_{a2} = 46.9 \pm 5.7 \text{ kJ/mol}$$
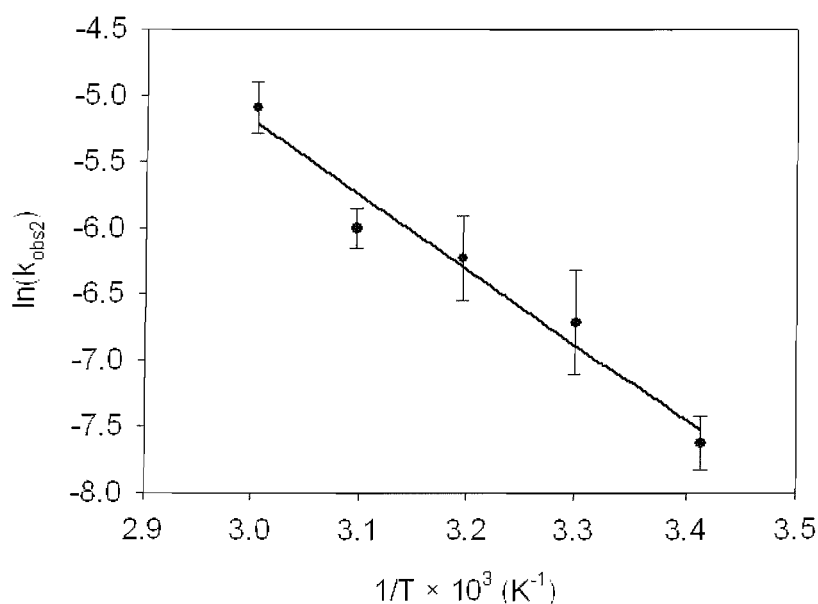
Figure 3.26 Arrhenius plot for sulfur insertion at C8 derived from analysis of lipoyl formation: y = -5642x +11.7; R_2 = 0.9264.

$$E_{a2} = 62.6 \pm 5.6 \text{ kJ/mol}$$
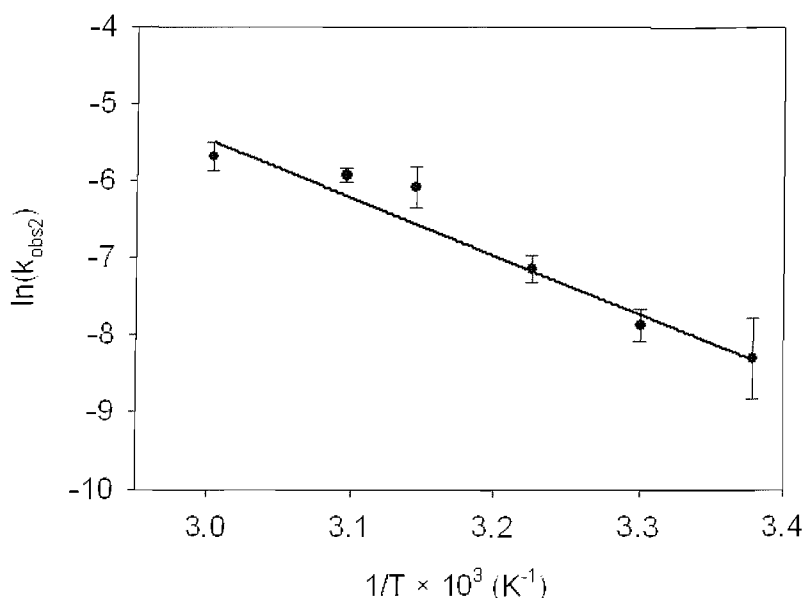
Figure 3.27 Arrhenius plot for sulfur insertion at C8 derived from analysis of AdoH formation: y=-7530x +17.11; R_2 = 0.9468

The activation energy barrier for sulfur insertion at C8 is similar to that calculated for the overall formation of lipoyl product (47.2 ± 5.4 kJ/mol) and both these values are less than that determined for the first sulfur insertion reaction at C6 of the octanoyl substrate (33.4-43.2 kJ/mol). These results thus indicate that following sulfur insertion at C6, lipoyl formation proceeds through a higher activation energy barrier for sulfur insertion at C8 which forms the rate determining step (fig. 3.28). This might be expected since this reaction involves formation of a primary carbon centred radical whereas sulfur insertion at C6 proceeds via formation of a more stable secondary radical (*23*). However, there are significant errors in the calculation of these values and more accurate data is required to confirm these observations.
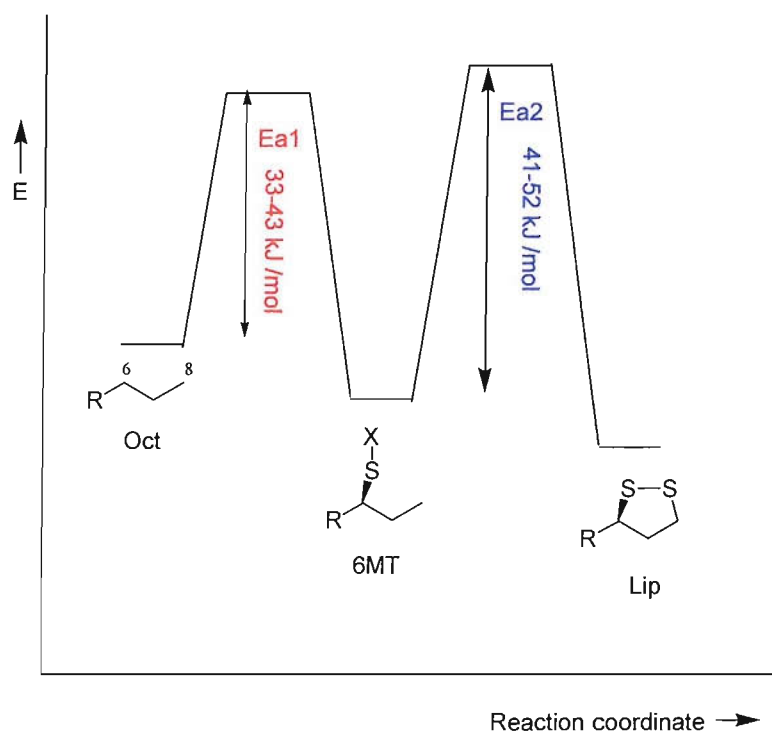
Figure 3.28 Reaction profile for lipoyl formation based on activation energies estimated for stepwise sulfur insertion reactions from kinetic analysis of timecourse reactions using *S. solfataricus* LipA.

3.4 Conclusions

Rate constants for reactions utilising *S. solfataricus* LipA can be derived by analysis of timecourse reactions which make use of an octanoyl peptide **25** (fig. 3.1) as substrate. The overall rate of lipoyl formation can be estimated by HPLC analysis of assays showing that the rate constant for this reaction by *S. solfataricus* LipA at its optimal temperature (60 °C) is similar to those derived for *E. coli* LipA and also for biotin formation in reactions using BioB. However, quantification of lipoyl peptide using this method is hampered by the presence of DHL peptide which co-elutes with a 6MT peptide and also by poor separation of these species. These problems could be overcome by reduction of the lipoyl product with TCEP followed by derivatisation with iodoacetamide but conditions need to be improved to maximise recovery of peptides following this process.

Analysis of the loss of octanoyl peptide can be used to estimate the rate of the first sulfur insertion reaction at C6 of the substrate. This allows estimation of the rate of the second sulfur insertion reaction by fitting lipoyl formation to two processes, the first (sulfur insertion at C6) with a rate constant derived from analysis of changes in octanoyl peptide concentration. This indicates that the rate of the first sulfur insertion is greater but more accurate analysis is required to confirm this observation.

Activation energies for the overall reaction involving LipA and also for stepwise sulfur insertion steps could be estimated from the kinetic data accumulated from analysis of timecourse assays. The activation energy barrier for the first sulfur insertion step was approximated to be 33-43 kJ/mol and this value was lower than those calculated for the overall rate of lipoyl and AdoH formation indicating that the second sulfur insertion is the rate determining step. Comparison of the overall activation energy for AdoH formation and lipoyl formation with that estimated for the rate of the second sulfur step suggests that the activation energy for sulfur insertion at C8 of 6-thiooctanoyl lies within the range 41-52 kJ/mol. This assumes that the observed overall rate should equal that of the rate determining step.

The formation of lipoyl species by LipA is a complex process involving several steps. These experiments have provided initial estimates of the kinetic and thermodynamic

properties of some to the processes involved. However, more data is required for more detailed analysis of each of the steps involved in lipoyl biosynthesis.

3.5   References

(1)   Wang, S. C., and Frey, P. A. (2007) S-adenosylmethionine as an oxidant: the radical SAM superfamily. *Trends in biochemical sciences 32*, 101-10.

(2)   Moss, M., and Frey, P. A. (1987) The role of S-adenosylmethionine in the lysine 2,3-aminomutase reaction. *J. Biol. Chem. 262*, 14859-62.

(3)   Moss, M. L., and Frey, P. A. (1990) Activation of lysine 2,3-aminomutase by S-adenosylmethionine. *J. Biol. Chem. 265*, 18112-5.

(4)   Buis, J. M., Cheek, J., Kalliri, E., and Broderick, J. B. (2006) Characterization of an active spore photoproduct lyase, a DNA repair enzyme in the radical S-adenosylmethionine superfamily. *The Journal of biological chemistry 281*, 25994-6003.

(5)   Cicchillo, R. M., Iwig, D. F., Jones, A. D., Nesbitt, N. M., Baleanu-Gogonea, C., Souder, M. G., Tu, L., and Booker, S. J. (2004) Lipoyl synthase requires two equivalents of S-adenosyl-L-methionine to synthesize one equivalent of lipoic acid. *Biochemistry 43*, 6378-86.

(6)   Guianvarc'h, D., Florentin, D., Tse Sum Bui, B., Nunzi, F., and Marquet, A. (1997) Biotin synthase, a new member of the family of enzymes which uses S-adenosylmethionine as a source of deoxyadenosyl radical. *Biochem. Biophys. Res. Commun. 236*, 402-6.

(7)   Shaw, N. M., Birch, O. M., Tinschert, A., Venetz, V., Dietrich, R., and Savoy, L. A. (1998) Biotin synthase from *Escherichia coli*: isolation of an enzyme-generated intermediate and stoichiometry of S-adenosylmethionine use. *Biochem. J. 330*, 1079-1085.

(8)   Ugulava, N. B., Sacanell, C. J., and Jarrett, J. T. (2001) Spectroscopic changes during a single turnover of biotin synthase: destruction of a [2Fe-2S] cluster accompanies sulfur insertion. *Biochemistry 40*, 8352-8.

(9)   Cicchillo, R. M., and Booker, S. J. (2005) Mechanistic investigations of lipoic acid biosynthesis in *Escherichia coli*: both sulfur atoms in lipoic acid are contributed by the same lipoyl synthase polypeptide. *J. Am. Chem. Soc. 127*, 2860-1.

(10)   Bryant, P., Kriek, M., Wood, R. J., and Roach, P. L. (2006) The activity of a thermostable lipoyl synthase from Sulfolobus solfataricus with a synthetic octanoyl substrate. *Analytical biochemistry 351*, 44-9.

(11)   Atkins, P. W. (1994) Physical Chemistry, in *Physical Chemistry* pp 861-897, OUP, Oxford.

(12)   Russo, A. D., Rullo, R., Masullo, M., Ianniciello, G., Arcari, P., and Bocchini, V.   (1995)   Glyceraldehyde-3-phosphate   dehydrogenase   in   the hyperthermophilic archaeon *Sulfolobus solfataricus*: characterization and significance in glucose metabolism. *Biochem Mol Biol Int 36*, 123-35.

(13)   Cacciapuoti, G., Forte, S., Moretti, M. A., Brio, A., Zappia, V., and Porcelli, M. (2005) A novel hyperthermostable 5'-deoxy-5'-methylthioadenosine phosphorylase from the archaeon *Sulfolobus solfataricus*. *FEBS J. 272*, 1886-99.

(14)   Douglas, P., Kriek, M., Bryant, P., and Roach, P. L. (2006) Lipoyl synthase inserts sulfur atoms into an octanoyl substrate in a stepwise manner. *Angew Chem Int Ed Engl 45*, 5197-9.

(15)   Ugulava, N. B., Frederick, K. K., and Jarrett, J. T. (2003) Control of adenosylmethionine-dependent radical generation in biotin synthase: a kinetic and thermodynamic analysis of substrate binding to active and inactive forms of BioB. *Biochemistry 42*, 2708-2719.

(16)   Kuzmic, P. (1996) Program DYNAFIT for the analysis of enzyme kinetic data: application to HIV proteinase. *Anal. Biochem. 237*, 260-73.

(17)   Frey, P. A. (1993) Lysine 2,3-aminomutase: is adenosylmethionine a poor man's adenosylcobalamin? *FASEB J. 7*, 662-70.

(18)   Berkovitch, F., Nicolet, Y., Wan, J. T., Jarrett, J. T., and Drennan, C. L. (2004) Crystal structure of biotin synthase, an S-adenosylmethionine-dependent radical enzyme. *Science 303*, 76-9.

(19)   Walsby, C. J., Ortillo, D., Yang, J., Nnyepi, M. R., Broderick, W. E., Hoffman, B. M., and Broderick, J. B. (2005) Spectroscopic approaches to elucidating novel iron-sulfur chemistry in the "radical-Sam" protein superfamily. *Inorg. Chem. 44*, 727-41.

(20)   Chowdhury, S., and Banerjee, R. (2000) Thermodynamic and kinetic characterization of Co-C bond homolysis catalyzed by coenzyme B(12)-dependent methylmalonyl-CoA mutase. *Biochemistry 39*, 7998-8006.

(21)   Licht, S. S., Lawrence, C. C., and Stubbe, J. (1999) Thermodynamic and kinetic studies on carbon-cobalt bond homolysis by ribonucleoside triphosphate reductase: the importance of entropy in catalysis. *Biochemistry 38*, 1234-42.

(22)   Hay, B. P., and Finke, R. G. (1988) Thermolysis of the Co-C Bond in Adenosylcobalamin (Coenzyme B-12) .4. Products, Kinetics and Co-C Bond-Dissociation Energy Studies in Ethylene-Glycol. *Polyhedron 7*, 1469-1481.

(23)   Perkins, M. J. (2000) *Radical Chemistry: The Fundamentals*, OUP, Oxford.

(24)   Cicchillo, R. M., Lee, K. H., Baleanu-Gogonea, C., Nesbitt, N. M., Krebs, C., and Booker, S. J. (2004) *Escherichia coli* lipoyl synthase binds two distinct [4Fe-4S] clusters per polypeptide. *Biochemistry 43*, 11770-81.

Chapter 4. Mechanistic Roles of the FeS Clusters of *S. solfataricus* LipA

4.1 Introduction
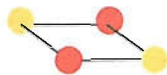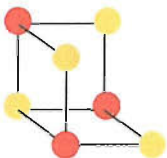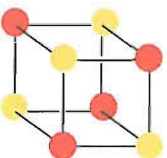
The presence of a $[4\text{Fe-4S}]^{1+/2+}$ cluster is a defining characteristic of proteins belonging to the radical SAM superfamily (*1, 2*). The cluster plays a central role in the initiation of a radical mechanism, supplying the single electron required for the reductive cleavage of SAM (*3*). In addition to the CX_3CX_2C iron sulfur cluster binding motif common to all radical SAM proteins, *E. coli* LipA contains a unique CX_4CX_5C motif which binds a second $[4\text{Fe-4S}]^{1+/2}$ cluster (*4*). An analogous binding site has been identified in the amino acid sequence of *S. solfataricus* LipA (*5*) (table 4.1) and it therefore seems likely that this protein may also bind two $[4\text{Fe-4S}]^{1+/2}$ clusters. Using UV/vis spectroscopy, electron paramagnetic resonance spectroscopy (EPR) spectroscopy and biochemical techniques the properties and roles of the iron sulfur clusters of *S. solfataricus* LipA have been investigated.

Organism	Residues	Sequence
S. solfataricus	23-38	T V **C** E E A L **C** P N I M E **C** W G
E. coli	60-75	S V **C** E E A S **C** P N L A E **C** F N

Table 4.1 The CX_4CX_5C motifs of *S.solfataricus* and *E. coli* LipA

Fe-S clusters are widespread throughout nature and several different types exist. (*6, 7*) (table 4.2). In addition to $[4\text{Fe-4S}]^{1+/2+}$ clusters, $[4\text{Fe-4S}]^{3+}$, $[3\text{Fe-4S}]^{1+}$ (*8, 9*) and $[2\text{Fe-2S}]^{1+/2+}$ (*10-12*) clusters have been observed in radical SAM proteins. Each different Fe-S cluster exhibits distinctive UV/vis absorptions and therefore the presence of a cluster and its type can be determined by recording the UV/vis spectrum of a protein (*13*). EPR is a spectroscopic technique that detects chemical species that have unpaired electrons and has been widely used to analyse transition metal centres in biological systems(*14*). Paramagnetic iron sulfur cluster with a non integer spin state can be detected by EPR (table 4.2) and generate EPR spectra with distinctive properties allowing their characterisation (*15*).

Cluster type	Overall oxidation states	Spin state	EPR g values (ferredoxin)[a]	λ_{max} (nm), ε ($\times 10^{-3}$, per Fe) (ferredoxin[a]
[2Fe-2S]	2+	$S = 0$	-	325 (6.4), 420 (4.8), 465 (4.9)
	1+	$S = 1/2$	1.89, 1.95, 2.05 (<100K)[a]	-
[3Fe-4S]	1+	$S = 1/2$	1.97, 2.00, 2.02 (<20K)[a]	305 (7.7), 415 (5.2), 455 (4.4)
[4Fe-4S]	3+	$S = \frac{1}{2}$	2.04, 2.04, 2.12 (<100K)[a]	325 (8.1), 385 (5.0), 450 (4.6)
	2+	$S = 0$	-	305 (4.9), 390 (3.8)
	1+	$S = 1/2$	1.88, 1.92, 2.06 (<20K)	Unfeatured; absorbance declines upon reduction

Table 4.2 Structures, core oxidation states, and spin states of [2Fe-2S], [3Fe-4S] & [4Fe-4S] clusters which have been observed in radical SAM proteins. Iron is shown in red, and sulfur is shown in yellow. *a* Typical features of EPR and UV spectra of iron sulfur clusters of ferredoxins taken from (*16*)

A number of radical SAM proteins have now been shown to bind two iron sulfur clusters. These include BioB, MiaB and HydE which are also involved in sulfur insertion reactions and MoaA which is not. The second cluster of MoaA has been shown to tightly bind its substrate 5'-GTP and therefore it has been proposed that it serves to anchor 5'-GTP in a suitable position for hydrogen abstraction from its C8

position by Ado radicals (*17*). However, Raman and EPR spectroscopy have suggested that the substrate of MiaB does not bind to its second iron sulfur cluster(*18*). Furthermore spectroscopic and biochemical studies have suggested that the $[2\text{Fe-}2\text{S}]^{2+}$ cluster of BioB serves as the source of sulfur during biotin biosynthesis (*12, 19*). Reconstitution of BioB with $\text{Na}_2[^{34}\text{S}]$ (*19*) or Na_2Se (*20*) resulted in insertion of ^{34}S and selenium respectively into dethiobiotin.

Expression of LipA in minimal medium supplemented with ^{34}S to yield fully labelled LipA has shown that both sulfur atoms came from the same polypeptide but did not reveal the sulfur source (*21*). It is possible that the second $[4\text{Fe-}4\text{S}]^{1+/2+}$ cluster of LipA plays a similar role to the $[2\text{Fe-}2\text{S}]^{2+}$ of BioB and serves as the source of sulfur. To determine whether or not this is the case LipA has been reconstituted with $\text{Na}_2[^{34}\text{S}]$ in a similar fashion to BioB and then assayed using octanoyl peptide substrates (fig. 4.1).
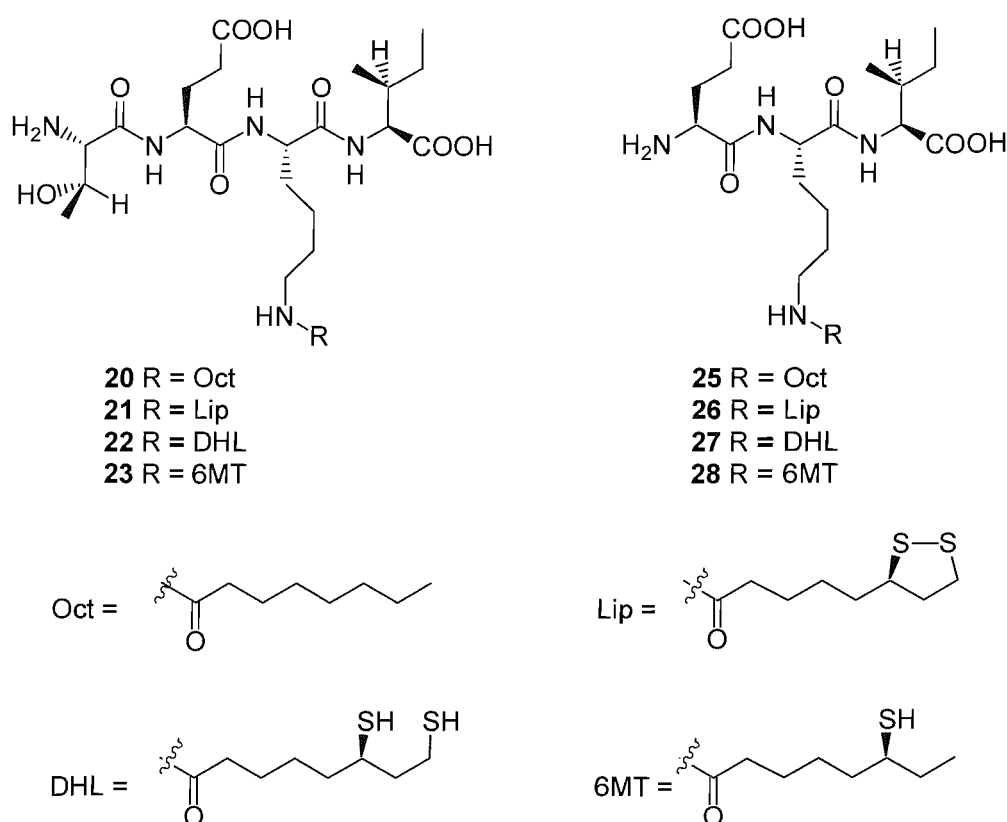
Figure 4.1 Structures of octanoyl (oct) substrate analogue peptides used in investigation of the roles of the [4Fe-4S] clusters of *S. solfataricus* LipA. Products of sulfur insertion reactions are also shown.

4.2   UV spectroscopy of *S. solfataricus* LipA

UV/vis spectra of *S. solfataricus* LipA were recorded under anaerobic conditions. The spectrum of as isolated LipA exhibited a broad band centred at 400 nm which is typical of $[4Fe-4S]^{2+}$ clusters of radical SAM proteins (*18, 22-24*) (fig. 4.2). A peak at 280 nm corresponded to absorption by the protein backbone and the ratio A_{400}/A_{280} was 0.35 ± 0.08. The molar extinction coefficient at 400 nm (ε_{400}) was 16 ± 4 mM^{-1} cm^{-1} which suggested the presence of a single $[4Fe-4S]^{2+}$ cluster since these typically have ε_{400} = 15-17 mM^{-1} cm^{-1} on a per cluster basis in biological systems (*18*). This is consistent with analysis of the iron content of the protein which showed that the protein contained 3.9 ± 0.4 mole Fe per mole of protein.
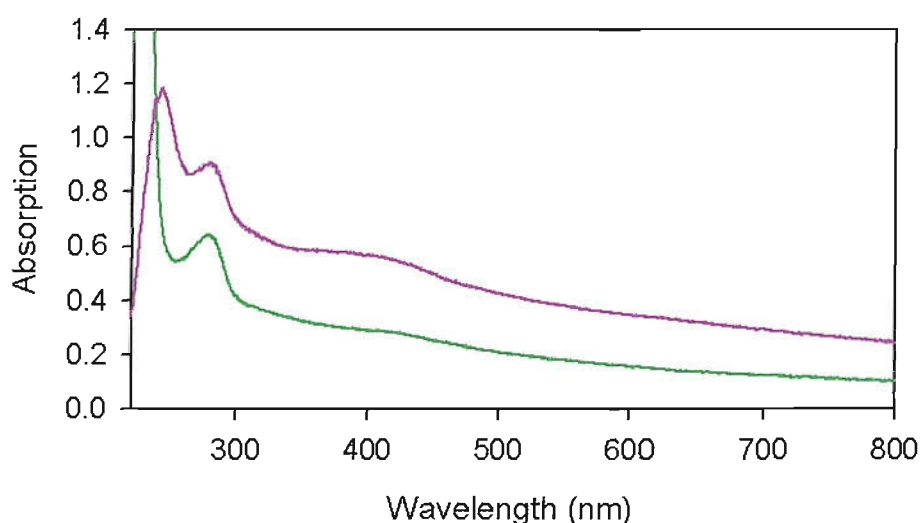
Figure 4.2 UV-visible absorption *S. solfataricus* LipA: (——) as isolated LipA; (——) reconstituted LipA.

Following reconstitution of the protein the UV/vis spectrum which remained consistent with the presence of a $[4Fe-4S]^{2+}$ cluster. The ratio A_{400}/A_{280} ratio was 0.67 ± 0.08 and suggested that there was an increase in the number of clusters per LipA monomer consistent with an increase in iron content with was found to be 8.8 ± 0.7. However, the A_{400}/A_{280} ratio may not be an accurate representation of the cluster content of the protein as there is an overall increase in background signal. This also meant that approximations of ε_{400} were unreliable. The change in background signal

may be due to adventitiously bound sulfide; however, gel filtration of the protein following reconstitution had no effect on the spectrum.

When SAM was added to reconstituted *S. solfataricus* LipA the UV/visible spectrum remained typical of a $[4Fe-4S]^{2+}$ cluster and retained a broad band at 400 nm (fig. 4.3). There was also a strong peak at 312 nm which resulted from absorbance by SAM. To investigate any changes in the UV/visible spectrum during turnover SAM and octanoyl tetrapeptide **20** (fig. 4.1) were added to reconstituted LipA then following reduction with sodium dithionite spectra were recorded at various time points. No significant spectral changes were observed in the time period 0-60 mins (fig. 4.3). This result indicated that this method is not sensitive enough to detect changes in iron sulfur clusters of LipA during turnover.
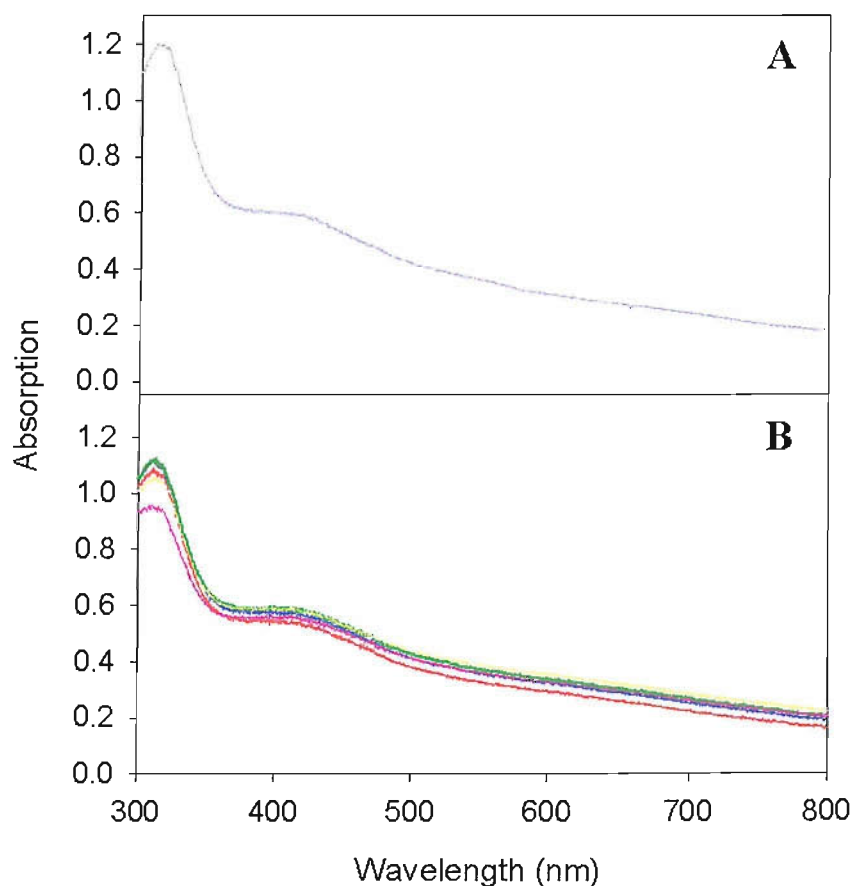
Figure 4.3 UV/visible spectra of LipA in the presence of SAM: (A) LipA (15 μM) following addition of an excess of SAM (100 μM); (B) LipA (15 μM) containing SAM (100 μM), octanoyl tetrapeptide **20** (fig. 4.1) (30 μM) following incubation with sodium dithionite (100 μM) for 2 mins (—), 4 mins (—), 10 mins (—), 30 mins (   ), 60 mins (—).

4.3 EPR spectroscopy of *S. solfataricus* LipA

EPR spectra were recorded in collaboration with Prof. D. J. Lowe and Dr. S. A. Fairhurst (John Innes Centre, Norwich).

4.3.1 The iron sulfur cluster(s) of reconstituted *S. solfataricus* LipA

The iron sulfur centres of *S. solfataricus* LipA were investigated using EPR spectroscopy. Samples of reconstituted LipA prepared under anaerobic conditions were EPR silent containing no paramagnetic species. Reduction of the reconstituted protein with sodium dithionite generated an EPR spectrum with characteristics that are consistent with the presence of S = $\frac{1}{2}$, $[4Fe-4S]^{1+}$ clusters. An axial signal ($g_\parallel$ = 2.05, $g_\perp$ = 1.93) is observed at 10 K (fig. 4.4) which closely resembles that reported for *E. coli* LipA (*4, 23, 25, 26*). The temperature dependence of the signal, which was almost undetectable at 30 K and completely lost at 60 K (fig. 4.4), also indicated the presence of $[4Fe-4S]^+$ as this is a typical property of this cluster type (*15*).
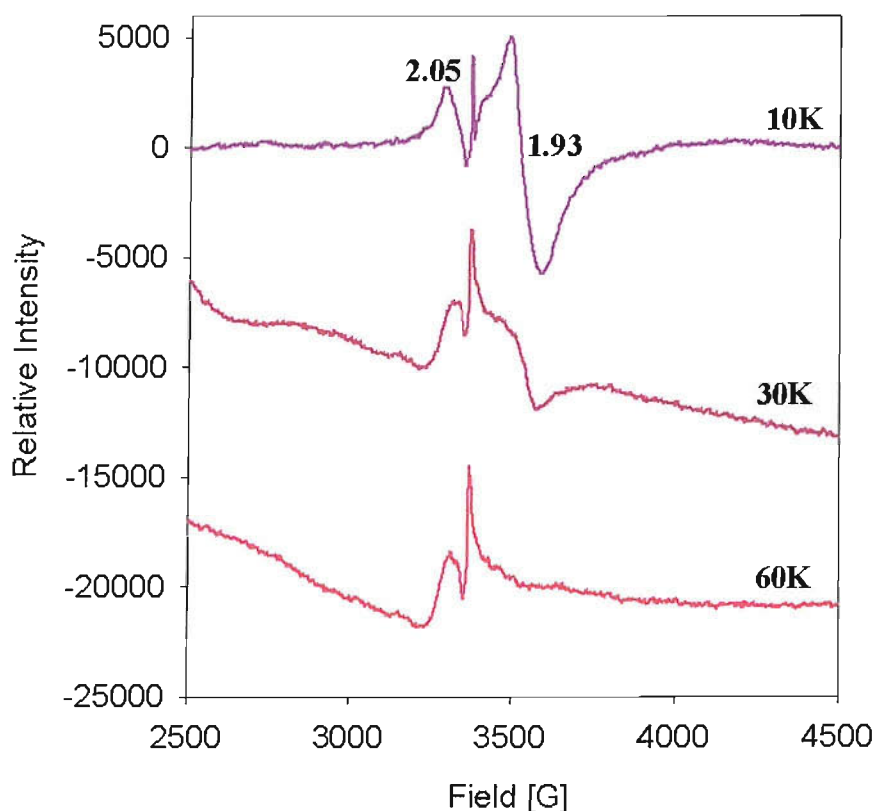
Figure 4.4 X-band EPR spectra of reconstituted LipA (206 μM) reduced with dithionite, after subtraction of a background buffer spectrum. The sharp signal at 3371 G is an artefact of the background subtraction. The spectra were recorded under the following conditions: temperature, 10 K, 30K and 60K; microwave frequency, 9.44 GHz; microwave power, 2.00 mW; modulation amplitude, 0.4 mT.

Spin quantitation was carried out using a Cu-EDTA standard. The peak observed at 10 K integrated to 157 μM which equates to 0.76 equivalents of spin per LipA monomer. This is significantly greater than has been observed by EPR spectroscopy of *E. coli* LipA (0.3 equivalents of spin per polypeptide (*23*)) and this may reflect the enhanced stability of *S. solfataricus* LipA. However, less than one iron sulfur clusters were observed per *S. solfataricus* LipA monomer by spin quantification under these conditions. This is likely to be due to inefficient reduction of the clusters by sodium dithionite in the absence of substrates.

4.3.2 Changes in the EPR spectrum of LipA upon addition of substrates

Addition of octanoyl peptide **20** (fig. 4.1) to reconstituted LipA prior to reduction with dithionite had no effect on the EPR signal. However, addition of an excess of SAM had significant effects on the spectrum (fig. 4.4). Spin quantitation revealed that the proportion of paramagnetic species had increased indicating that the FeS clusters of LipA are more effectively reduced in the presence of SAM. The peak integrated to 263 μM which equates to 1.52 equivalents of spin per LipA monomer providing evidence for the presence of more than one FeS cluster per *S. solfataricus* LipA polypeptide. No EPR signal was observed at 30 K for LipA samples containing SAM suggesting that the spectrum results from $[4Fe-4S]^{1+}$ clusters. This was consistent with UV/vis spectroscopy of LipA in the presence of SAM which showed characteristics typical of a $[4Fe-4S]^{2+}$ cluster and not of a $[2Fe-2S]^{2+}$ (fig. 4.5). The enhancement of the EPR signal of the $[4Fe-4S]^{1+}$ of LipA in the presence of SAM is consistent with observations made for the radical SAM proteins KAM and ThiH (*27, 28*). These results show that binding of SAM to the $[4Fe-4S]^{2+}$ cluster enhances reduction to the +1 state and this is therefore likely to precede reduction (scheme 4.1).

There was also a significant change in the spectrum shape and an almost rhombic signal was observed with major features at g = 2.03 and g = 1.87 (fig. 4.5). This change in signal shape reflects a perturbation of the 3D electronic structure of a [4Fe-4S]$^+$ centre (*14*) and thus indicates a close interaction with SAM and the cluster. The EPR spectra of radical SAM proteins BioB (*29*), ARR-AE (*30*) and PFL-AE (*31*) have been shown to be similarly affected by the presence of SAM and covalent binding of SAM to the $[4Fe-4S]^{1+}$ clusters of PFL-AE and BioB has been confirmed

by ENDOR studies (*31*) and crystallographic evidence(*32*) respectively. Similarities between the EPR spectra of these proteins and that of *S. solfataricus* LipA imply that SAM is also bound at a unique iron site of a $[4Fe-4S]^{1+}$ cluster of LipA.
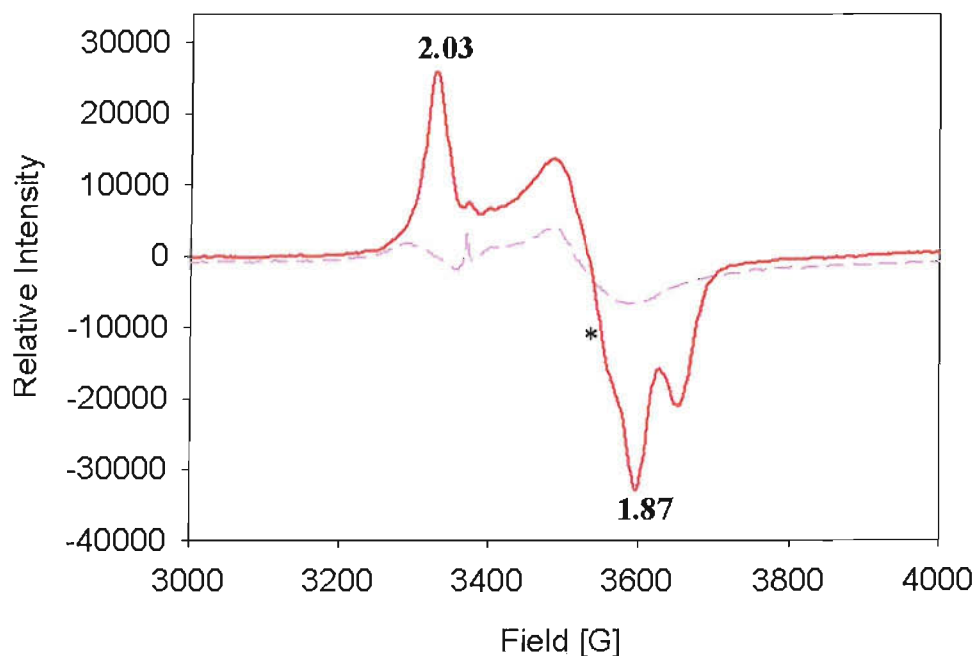
Figure 4.5 X-band EPR spectrum of reconstituted LipA (206 μM) reduced with dithionite in the absence of SAM (- - -) and after addition of SAM (412 μM) (—). A shoulder at g = 1.91 is marked by *. The spectra were recorded under the following conditions: temperature, 10 K; microwave frequency, 9.44 GHz; microwave power, 2.00 mW; modulation amplitude, 0.4 mT.

$$[4Fe-4S]^{2+} + SAM \rightleftharpoons [4Fe-4S]^{2+}:SAM \xrightarrow{e^-} [4Fe-4S]^{1+}:SAM$$
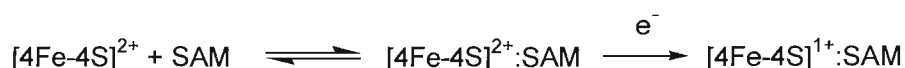
Scheme 4.1 Binding of SAM to a $[4Fe-4S]^{2+}$ cluster of S. solfataricus LipA followed by reduction of the cluster.

The EPR spectrum of LipA in the presence of SAM is not simple however, with a shoulder clearly visible on the high field part of the spectrum (g = 1.91). Spin quantitation revealed that more than one S = ½ cluster is present per LipA poly peptide and hence this feature may result from the presence of two different clusters with different anisotropy that generate different signals which overlap. Since the change in signal shape appears to be associated with SAM binding, different signals

could be generated either because there is insufficient SAM added to saturate all the clusters or because one cluster binds SAM whilst the second does not. To investigate whether the former possibility is the case the effect of adding increasing amounts of SAM on the EPR signal was investigated. When less than one molar equivalent of SAM was added with respect to protein concentration, no rhombic features were observed and the spectrum resembled that of reconstituted LipA to which no substrates had been added (fig. 4.6). Features at g = 1.86 & 1.84, which are associated with SAM binding, became visible when 1 molar equivalent was added and remained with increasing SAM concentrations (fig. 4.6). However the shoulder at g = 1.91 was visible when up to 10 molar equivalents of SAM were added indicating that the different signals do not result from unavailability of SAM to bind to all the clusters. Hence it seems likely that the different signals result from two different [4Fe-4S]$^{1+}$ clusters and that one of these binds SAM and therefore has a different anisotropy to the other.
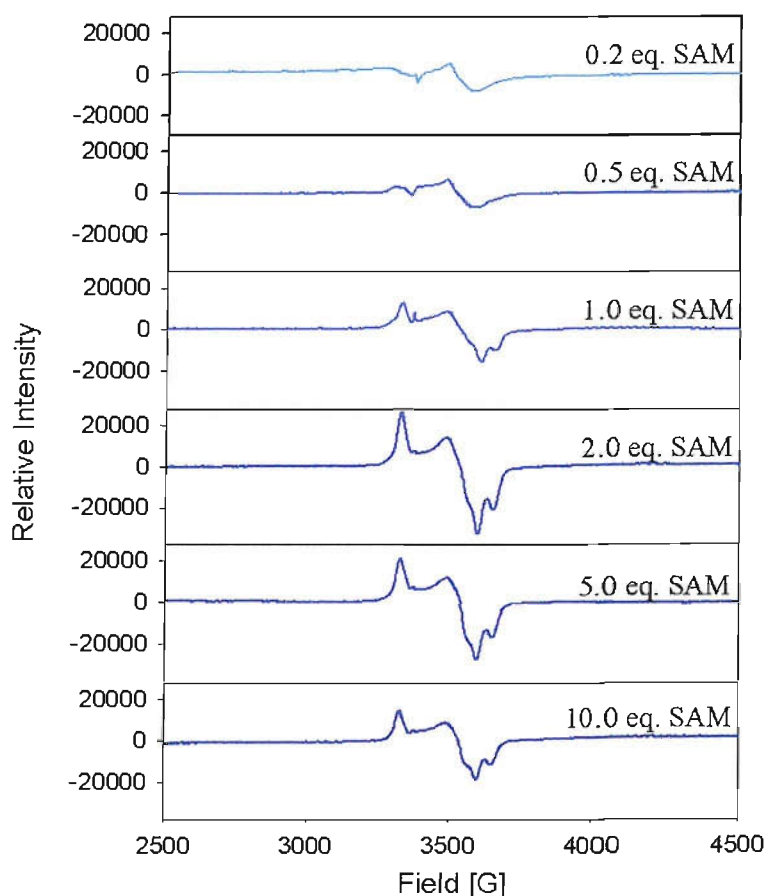
Figure 4.6 EPR spectra of LipA which had been incubated with varying amounts of SAM and reduced with sodium dithionite. The spectra were recorded under the following conditions: temperature, 10 K; microwave frequency, 9.44 GHz; microwave power, 2.00 mW; modulation amplitude, 0.4 mT.

These results imply that like *E. coli* LipA, *S. solfataricus* LipA contains $[4Fe-4S]^{1+}$ clusters which serve different roles. Comparisons can be drawn with BioB which also binds two iron sulfur clusters, a $[4Fe-4S]^{1+/2+}$ which is involved in SAM cleavage and a $[2F2-2S]^{1+/2+}$ cluster which has been proposed to act as a source of sulfur (*12, 19*). The EPR data obtained for *S. solfataricus* LipA suggests a role for one cluster, which interacts closely with SAM, in the generation of Ado• radicals. A second cluster does not appear to bind SAM and may play a similar role to the $[2Fe-2S]^{1+}$ cluster of BioB, perhaps serving as a sulfur donor during lipoyl formation.

4.3.3 Changes in the EPR signal of *S. solfataricus* LipA during turnover

Changes in the EPR signal of LipA during turnover were investigated using octanoyl tetrapeptide **20** (fig. 4.1) as a substrate for sulfur insertion. Addition of the substrate **20** (fig. 4.1) to samples of LipA, which had been reduced with sodium dithionite and contained SAM, resulted in a rapid decline of the EPR signal intensity. Integration of peaks revealed that the spin concentration had decreased by 57 % in the first 5 minutes to 112 μM (0.65 equivalents with respect to protein concentration) (fig. 4.7). This was followed by a more gradual decrease in intensity up to 20 minutes and the final spin concentration after this time was 65 μM (0.38 equivalents with respect to protein concentration). Thus, during the course of the reaction some of the iron sulfur clusters of LipA were converted to EPR silent forms.
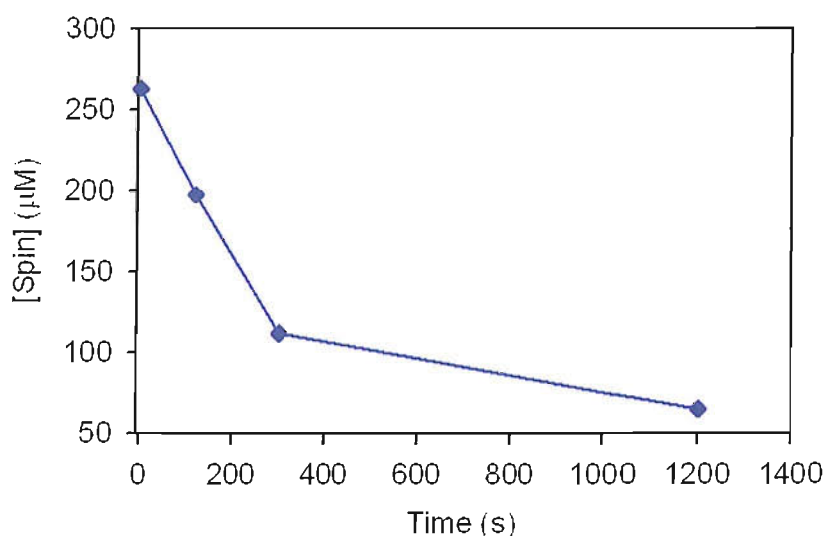
Figure 4.7 Changes in spin concentration of *S. solfataricus* LipA during turnover as determined by spin quantitation of EPR spectra by comparison with a Cu-EDTA standard.

The loss in intensity of the EPR signal during turnover coincided with a change in the spectrum shape and after 2 mins incubation there is a noticeable broadening of the feature centred at g = 1.96 (fig. 4.8). Features at g = 1.86 & 1.84, which were associated with the interaction of a $[4Fe-4S]^{1+}$ cluster with SAM, had become less prominent after 2 mins and by 20 minutes the feature at g = 1.84 could not be distinguished. This suggests that the decrease in signal intensity is partly due to reductive cleavage of SAM leading to oxidation of the cluster (with which SAM interacts) to the EPR silent $[4Fe-4S]^{2+}$ form. The loss of more than one cluster per

LipA monomer after 20 minutes might be due to oxidation of both clusters in this manner; however this seems unlikely since features associated with SAM binding are no longer clearly visible (fig 4.8). Degradation of a $[4Fe-4S]^{1+}$ cluster which acts as a source of sulfur may therefore result in part of the decrease in EPR signal intensity during turnover.
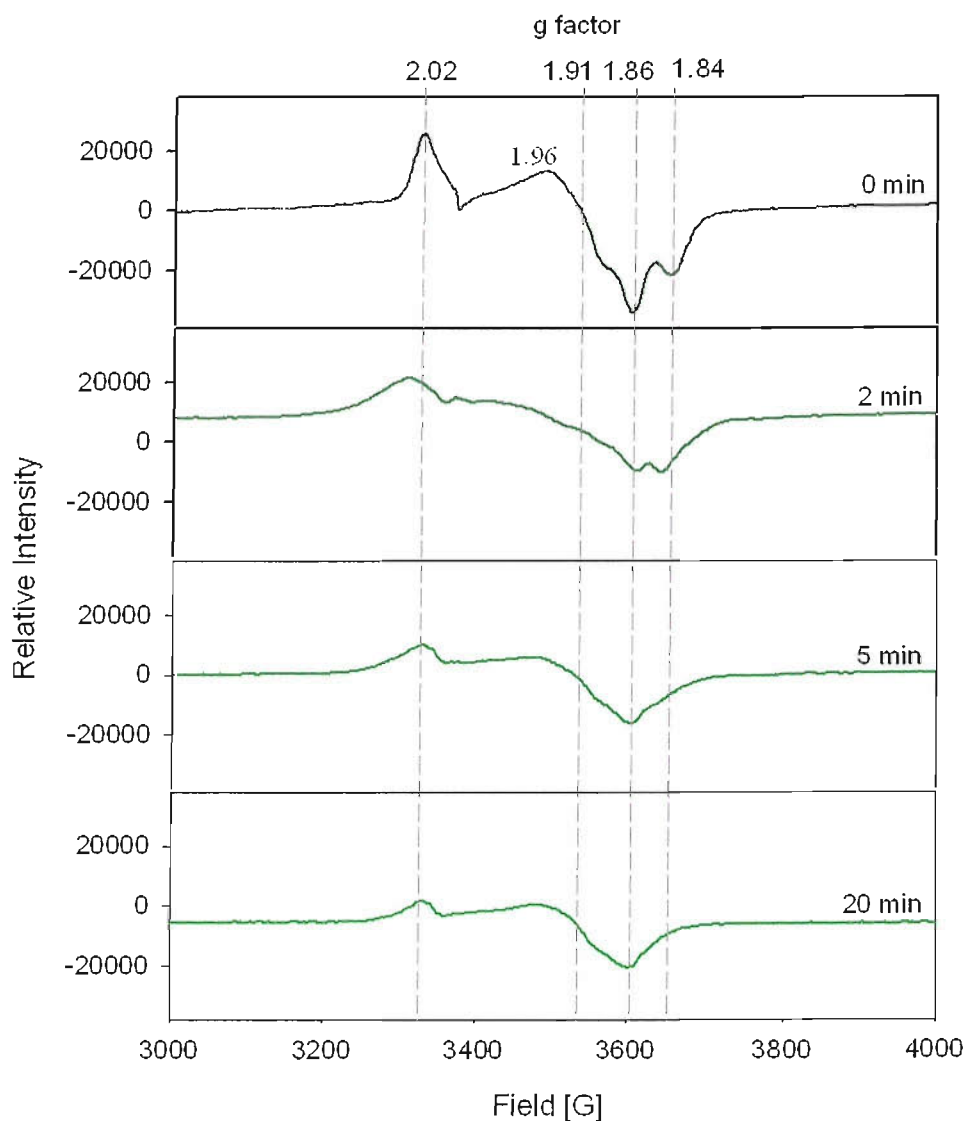
Figure 4.8 EPR spectra of LipA in the presence SAM and octanoyl tetrapeptide **20** (fig. 4.1) following reduction with sodium dithionite for 0-20 min. The spectra were recorded under the following conditions: temperature, 10 K; microwave frequency, 9.44 GHz; microwave power, 2.00 mW; modulation amplitude, 0.4 mT.

4.4 ^{34}S labelling of the FeS clusters of LipA

To investigate whether one of the iron sulfur clusters of LipA is the source of sulfur in the biosynthesis of lipoic acid the clusters were labelled with ^{34}S. This was achieved by removing the iron sulfur clusters from the as isolated protein by treatment with excess dithionite in the presence of EDTA according to the method described in (*19*) for the preparation of apo biotin synthase. After incubation under these conditions for two hours the protein was then applied to a small gel filtration column in an effort to remove any free sulfide. The apoprotein was then reconstituted by the addition of iron chloride and $Na_2[^{34}S]$ in the presence of DTT as described previously. The removal and re-formation of the $[4Fe-4S]^{1+/2+}$ clusters confirmed by monitoring the absorption at 410 nm (fig 4.9).
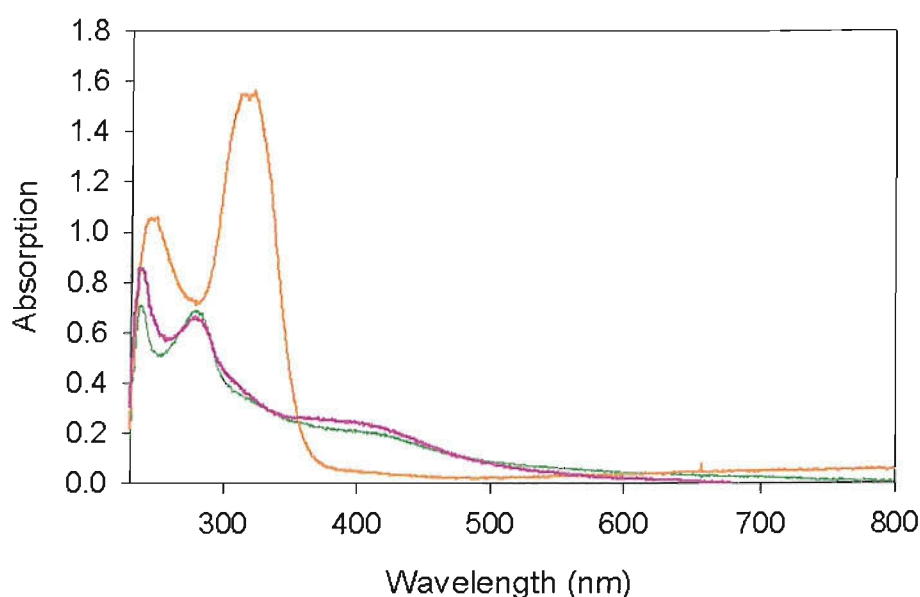
Figure 4.9 UV/vis spectrum of different preparations of LipA: as isolated S. LipA (—); apo-protein prepared by treatment with dithionite and EDTA (—); after reconsitution with FeCl$_3$, and $Na_2[^{34}S]$ in the presence of DTT (—).

Assays were then carried out with the ^{34}S reconstituted LipA using octanoyl tripeptide **20** (fig. 4.1) as the substrate for sulfur insertion. Insertion of either ^{32}S or ^{34}S during the reaction could result in the potential formation of six different species **39-44** (fig. 4.10).

Monothiolated species
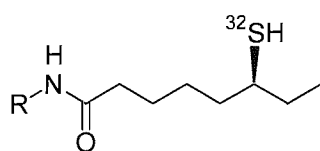
39
MW = 546.3
(M+H)$^+$ = 547.3
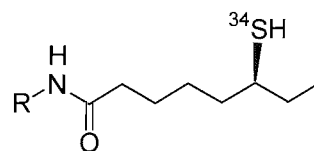
40
MW = 548.3
(M+H)$^+$ = 549.3

Lipoyl species
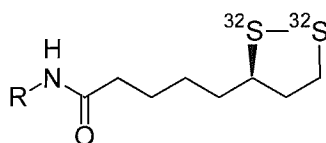
41
MW = 576.3
(M+H)$^+$ = 577.3
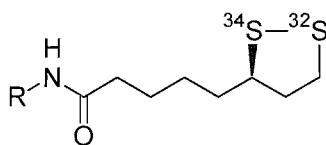
42
MW = 578.3
(M+H)$^+$ = 579.3
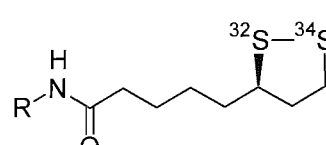
43
MW = 578.3
(M+H)$^+$ = 579.3

44
MW = 580.3
(M+H)+ =581.3

R =
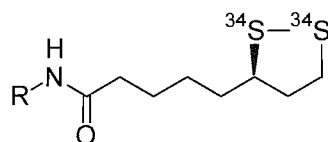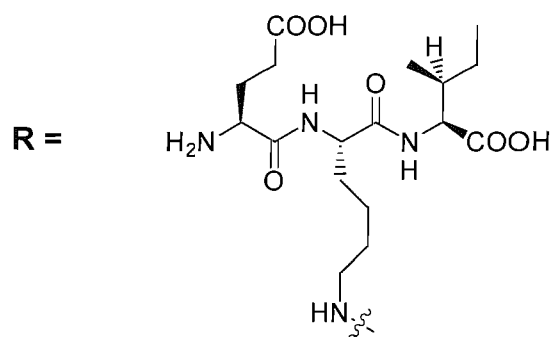
Figure 4.10 Structures of species that could be formed in the reaction of ^{34}S labelled LipA with octanoyl substrate **20** (fig. 4.1).

Reactions were analysed by LC-MS which confirmed that ^{34}S was incorporated during the reaction. A species which elutes at 23.5 mins corresponds to the expected protonated mass of a monothiolated species **40** containing a single ^{34}S atom (fig. 4.11). However, this co-elutes with a second monothiolated species **39** containing a single ^{32}S atom. The ratio of the relative intensities of the ^{34}S species and ^{32}S species peaks was 0.94: 1 which represents a significant incorporation of the label ($\sim$ 47%). Lipoylated species were also formed which co-eluted at 22.8 mins and contained either two ^{32}S atoms **41**, a ^{32}S atom and ^{34}S atom **42/43** or two ^{34}S atoms **44** (fig. 4.12).
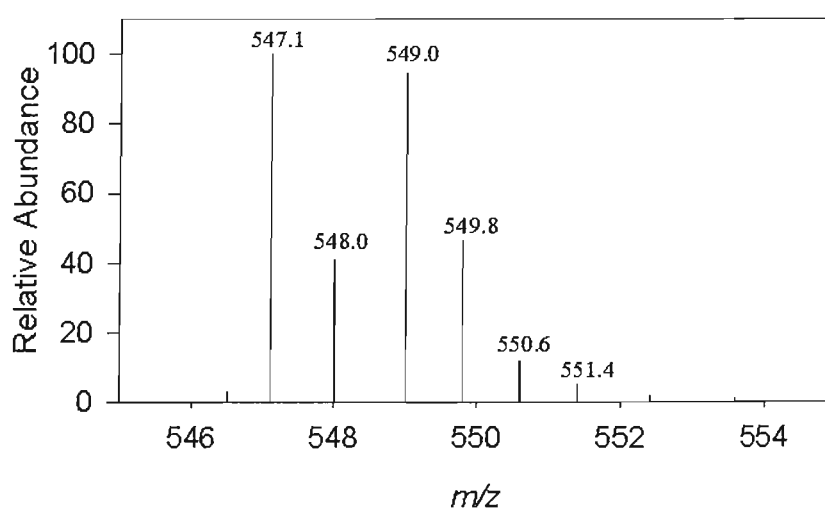
Figure 4.11 Mass spectrum of species which eluted at 23.5 mins; m/z = 547.1, monothiolated species **39** (fig. 4.10); m/z = 549.0, monothiolated species **40** (fig. 4.10).
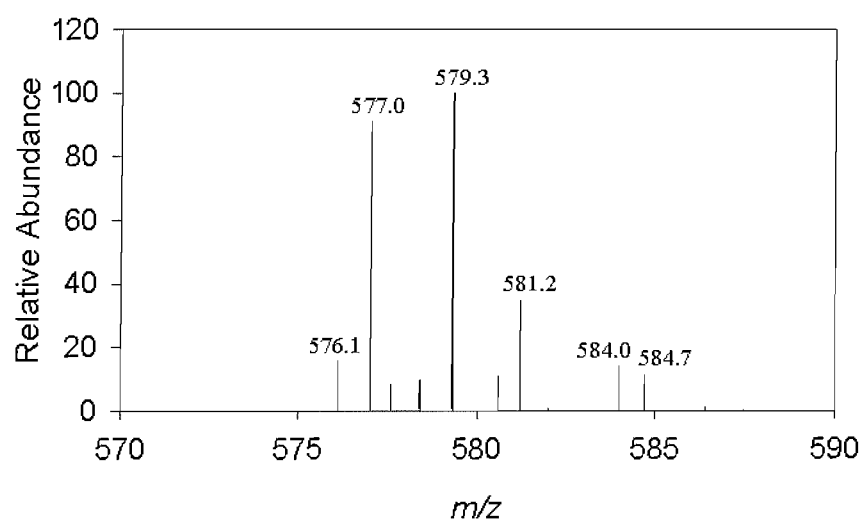
Figure 4.12 Mass spectrum of species which eluted at 22.8 mins; m/z = 577.0, lipoyl species **41** (fig. 4.10); m/z = 579.3, lipoyl species **42** &/or **43** (fig. 4.10); m/z = 581.2, lipoyl species **44** (fig. 4.10).

These results show that LipA reconstituted with ^{34}S can produce a labelled monothiolated and lipoyl species suggesting that a [4Fe-4S] cluster may be the source of sulfur although extent of labelling was rather poor. Similar experiments using biotin synthase also resulted in incomplete incorporation of ^{34}S into dethiobiotin to yield 62-67 % [^{34}S]biotin which was attributed to residual ^{32}S which might have remained in the apoprotein (*19*). The application of apo-LipA to a small desalting column may have been insufficient to remove all ^{32}S sulfide and residual amounts of this may also have led to incomplete labelling with ^{34}S. However, the possibility of a different sulfur donor can not be completely excluded by these results.

4.5 Conclusions

Spectroscopic analysis of *S. solfataricus* LipA has confirmed that the protein binds $[4Fe-4S]^{1+/2+}$ clusters. Furthermore integration of EPR spectra and iron analysis of protein samples suggests that the *S. solfataricus* protein, like *E. coli* LipA (*4*), binds not one but two $[4Fe-4S]^{1+/2+}$ clusters. LipA from both organisms thus exhibits similarities to BioB, MiaB (*10, 18*) and HydE (*33*) which are radical SAM proteins involved in sulfur insertion reactions that bind a second iron sulfur cluster in addition to that bound by the CX_3CX_2.

EPR spectroscopy has also provided evidence for binding of SAM to one of the iron sulfur clusters of LipA. It has been shown previously that LipA can reductively cleave SAM (*34*) and these results indicate that this is facilitated by the close interaction between the cofactor and a $[4Fe-4S]^{1+/2+}$ cluster. It seems likely that the $[4Fe-4S]^{1+/2+}$ cluster of LipA binds SAM via the through its carboxylate and α-amino groups in the same manner as the clusters of PFL-AE (*31*), BioB (*32*), and LAM (*35*). The mechanism for SAM cleavage by LipA might therefore proceed via inner sphere electron transfer from the cluster to the sulfonium followed by homolytic cleavage of the C5'-S bond as has been proposed for these proteins (*31, 32, 35*).

Reconstitution of LipA with $Na_2[^{34}S]$ has indicated that the second $[4Fe-4S]^{1+/2+}$ cluster may be the source of sulfur. Although the results can not rule out another sulfur source the extent of ^{34}S incorporation seems to support this hypothesis since free sulfide is very unlikely to quench a radical reaction.

4.6   References

(1)   Layer, G., Heinz, D. W., Jahn, D., and Schubert, W. D. (2004) Structure and function of radical SAM enzymes. *Curr. Opin. Chem. Biol. 8*, 468-76.

(2)   Cheek, J., and Broderick, J. B. (2001) Adenosylmethionine-dependent iron-sulfur enzymes: versatile clusters in a radical new role. *J. Biol. Inorg. Chem. 6*, 209-26.

(3)   Fontecave, M., Mulliez, E., and Ollagnier-de-Choudens, S. (2001) Adenosylmethionine as a source of 5'-deoxyadenosyl radicals. *Curr. Opin. Chem. Biol. 5*, 506-511.

(4)   Cicchillo, R. M., Lee, K. H., Baleanu-Gogonea, C., Nesbitt, N. M., Krebs, C., and Booker, S. J. (2004) *Escherichia coli* lipoyl synthase binds two distinct [4Fe-4S] clusters per polypeptide. *Biochemistry 43*, 11770-81.

(5)   She, Q., Singh, R. K., Confalonieri, F., Zivanovic, Y., Allard, G., Awayez, M. J., Chan-Weiher, C. C. Y., Clausen, I. G., Curtis, B. A., De Moors, A., Erauso, G., Fletcher, C., Gordon, P. M. K., Heikamp-de Jong, I., Jeffries, A. C., Kozera, C. J., Medina, N., Peng, X., Thi-Ngoc, H. P., Redder, P., Schenk, M. E., Theriault, C., Tolstrup, N., Charlebois, R. L., Doolittle, W. F., Duguet, M., Gaasterland, T., Garrett, R. A., Ragan, M. A., Sensen, C. W., and Van der Oost, J. (2001) The complete genome of the crenarchaeon Sulfolobus solfataricus P2. *Proc. Natl. Acad. Sci. U. S. A. 98*, 7835-7840.

(6)   Johnson, D. C., Dean, D. R., Smith, A. D., and Johnson, M. K. (2005) Structure, function, and formation of biological iron-sulfur clusters. *Annu. Rev. Biochem. 74*, 247-81.

(7)   Beinert, H., Holm, R. H., and Munck, E. (1997) Iron-sulfur clusters: nature's modular, multipurpose structures. *Science 277*, 653-9.

(8)   Krebs, C., Henshaw, T. F., Cheek, J., Huynh, B. H., and Broderick, J. B. (2000) Conversion of 3Fe-4S to 4Fe-4S clusters in native pyruvate formate-lyase activating enzyme: Mössbauer characterization and implications for mechanism. *J. Am. Chem. Soc. 122*, 12497-12506.

(9)   Broderick, J. B., Henshaw, T. F., Cheek, J., Wojtuszewski, K., Smith, S. R., Trojan, M. R., McGhan, R. M., Kopf, A., Kibbey, M., and Broderick, W. E. (2000) Pyruvate formate-lyase-activating enzyme: strictly anaerobic isolation

yields active enzyme containing a $[3Fe-4S]^+$ cluster. *Biochem. Biophys. Res. Commun. 269*, 451-6.

(10) Pierrel, F., Bjork, G. R., Fontecave, M., and Atta, M. (2002) Enzymatic modification of tRNAs - MiaB is an iron-sulfur protein. *J. Biol. Chem. 277*, 13367-13370.

(11) Ugulava, N. B., Gibney, B. R., and Jarrett, J. T. (2001) Biotin synthase contains two distinct iron-sulfur cluster binding sites: chemical and spectroelectrochemical analysis of iron-sulfur cluster interconversions. *Biochemistry 40*, 8343-51.

(12) Ugulava, N. B., Sacanell, C. J., and Jarrett, J. T. (2001) Spectroscopic changes during a single turnover of biotin synthase: destruction of a [2Fe-2S] cluster accompanies sulfur insertion. *Biochemistry 40*, 8352-8.

(13) Johnson, M. K. (1994) Encyclopedia of Inorganic Chemistry, (King, R. C., Ed.) pp 1896-1915, Wiley, Chichester, UK.

(14) Hagen, W. R. (2006) EPR spectroscopy as a probe of metal centres in biological systems. *Dalton. Trans*, 4415-34.

(15) Guigliarelli, B., and Bertrand, P. (1999) Application of EPR spectroscopy to the structural and functional study of iron-sulfur proteins, in *Advances in Inorganic Chemistry, Vol 47* pp 421-497.

(16) Lippard, S. J., and Berg, J. M. (1994) Principles of Bioinorganic Chemistry, in *Principles of Bioinorganic Chemistry* pp 115-125, University Science Books, Mill Valley, CA.

(17) Hanzelmann, P., and Schindelin, H. (2006) Binding of 5'-GTP to the C-terminal FeS cluster of the radical S-adenosylmethionine enzyme MoaA provides insights into its mechanism. *Proc. Natl. Acad. Sci. U. S. A. 103*, 6829-34.

(18) Hernandez, H. L., Pierrel, F., Elleingand, E., Garcia-Serres, R., Huynh, B. H., Johnson, M. K., Fontecave, M., and Atta, M. (2007) MiaB, a bifunctional radical-S-adenosylmethionine enzyme involved in the thiolation and methylation of tRNA, contains two essential [4Fe-4S] clusters. *Biochemistry*.

(19) Tse Sum Bui, B., Florentin, D., Fournier, F., Ploux, O., Mejean, A., and Marquet, A. (1998) Biotin synthase mechanism: on the origin of sulphur. *FEBS Lett. 440*, 226-30.

(20)   Tse Sum Bui, B., Mattioli, T. A., Florentin, D., Bolbach, G., and Marquet, A. (2006) *Escherichia coli* biotin synthase produces selenobiotin. Further evidence of the involvement of the $[2Fe-2S]^{2+}$ cluster in the sulfur insertion step. *Biochemistry 45*, 3824-34.

(21)   Cicchillo, R. M., and Booker, S. J. (2005) Mechanistic investigations of lipoic acid biosynthesis in *Escherichia coli*: both sulfur atoms in lipoic acid are contributed by the same lipoyl synthase polypeptide. *J. Am. Chem. Soc. 127*, 2860-1.

(22)   Ollagnier, S., Mulliez, E., Schmidt, P. P., Eliasson, R., Gaillard, J., Deronzier, C., Bergman, T., Graslund, A., Reichard, P., and Fontecave, M. (1997) Activation of the anaerobic ribonucleotide reductase from *Escherichia coli*. The essential role of the iron-sulfur center for S-adenosylmethionine reduction. *J. Biol. Chem. 272*, 24216-23.

(23)   Ollagnier-De Choudens, S., Sanakis, Y., Hewitson, K. S., Roach, P., Baldwin, J. E., Munck, E., and Fontecave, M. (2000) Iron-sulfur center of biotin synthase and lipoate synthase. *Biochemistry 39*, 4165-73.

(24)   Leonardi, R., Fairhurst, S. A., Kriek, M., Lowe, D. J., and Roach, P. L. (2003) Thiamine biosynthesis in Escherichia coli: isolation and initial characterisation of the ThiGH complex. *FEBS Lett. 539*, 95-99.

(25)   Ollagnier-de Choudens, S., and Fontecave, M. (1999) The lipoate synthase from *Escherichia coli* is an iron-sulfur protein. *FEBS Lett. 453*, 25-8.

(26)   Miller, J. R., Busby, R. W., Jordan, S. W., Cheek, J., Henshaw, T. F., Ashley, G. W., Broderick, J. B., Cronan, J. E., Jr., and Marletta, M. A. (2000) *Escherichia coli* LipA is a lipoyl synthase: *in vitro* biosynthesis of lipoylated pyruvate dehydrogenase complex from octanoyl-acyl carrier protein. *Biochemistry 39*, 15166-78.

(27)   Lieder, K. W., Booker, S., Ruzicka, F. J., Beinert, H., Reed, G. H., and Frey, P. A. (1998) S-Adenosylmethionine-dependent reduction of lysine 2,3-aminomutase and observation of the catalytically functional iron-sulfur centers by electron paramagnetic resonance. *Biochemistry 37*, 2578-85.

(28)   Kriek, M., Martins, F., Leonardi, R., Fairhurst, S. A., Lowe, D. J., and Roach, P. L. (2007) Thiazole synthase from Escherichia coli: an investigation of the substrates and purified proteins required for activity in vitro. *J. Biol. Chem. 282*, 17413-23.

(29)   Cosper, M. M., Jameson, G. N., Davydov, R., Eidsness, M. K., Hoffman, B. M., Huynh, B. H., and Johnson, M. K. (2002) The [4Fe-4S]$^{2+}$ cluster in reconstituted biotin synthase binds S-adenosyl-L-methionine. *J. Am. Chem. Soc. 124*, 14006-7.

(30)   Liu, A., and Graslund, A. (2000) Electron paramagnetic resonance evidence for a novel interconversion of [3Fe-4S]$^{+}$ and [4Fe-4S]$^{+}$ clusters with endogenous iron and sulfide in anaerobic ribonucleotide reductase activase *in vitro. J. Biol. Chem. 275*, 12367-73.

(31)   Walsby, C. J., Hong, W., Broderick, W. E., Cheek, J., Ortillo, D., Broderick, J. B., and Hoffman, B. M. (2002) Electron-nuclear double resonance spectroscopic evidence that S-adenosylmethionine binds in contact with the catalytically active [4Fe-4S]$^{+}$ cluster of pyruvate formate-lyase activating enzyme. *J. Am. Chem. Soc. 124*, 3143-3151.

(32)   Berkovitch, F., Nicolet, Y., Wan, J. T., Jarrett, J. T., and Drennan, C. L. (2004) Crystal structure of biotin synthase, an S-adenosylmethionine-dependent radical enzyme. *Science 303*, 76-9.

(33)   Rubach, J. K., Brazzolotto, X., Gaillard, J., and Fontecave, M. (2005) Biochemical characterization of the HydE and HydG iron-only hydrogenase maturation enzymes from *Thermatoga maritima. FEBS Lett. 579*, 5055-60.

(34)   Cicchillo, R. M., Iwig, D. F., Jones, A. D., Nesbitt, N. M., Baleanu-Gogonea, C., Souder, M. G., Tu, L., and Booker, S. J. (2004) Lipoyl synthase requires two equivalents of S-adenosyl-L-methionine to synthesize one equivalent of lipoic acid. *Biochemistry 43*, 6378-86.

(35)   Chen, D., Walsby, C., Hoffman, B. M., and Frey, P. A. (2003) Coordination and mechanism of reversible cleavage of S-adenosylmethionine by the [4Fe-4S] center in lysine 2,3-aminomutase. *J. Am. Chem. Soc. 125*, 11788-9.

Chapter 5. Experimental

5.1 Materials

Yeast extract and tryptone were purchased from Oxoid (Basingstoke, UK).

Fluorenylmethoxycarbonyl (Fmoc) amino acids, coupling reagents (diisopropylcarbodiimide [DIC], benzotriazolyloxy-tris[pyrrolidino]-phosphonium hexafluorophosphate [PyBOP], and hydroxybenzotriazole [HOBt]), and Wang resin were purchased from Novabiochem (Nottingham, UK). (DL)-Lipoic acid was purchased from Sigma–Aldrich (Poole, UK). N,N-Dimethylformamide (DMF) and N-methylpyrrolidone (NMP) were purchased from Rathburn Chemicals (Walkerburn, UK). HEPES and dithiothreitol (DTT) were purchased from Melford Laboratories (Ipswich, UK). Elemental 34-S (purity 96%) and deuterium oxide were purchased from Goss Scientific Instruments (Great Baddow, Essex). Iodoacetamide, TCEP, and 5'-deoxyadenosine (AdoH) were purchased from Sigma-Aldrich (Poole, UK). Octanoic acid, HPLC-grade acetonitrile, and all other reagents were purchased from Fisher Scientific (Loughborough, UK).

S-Adenosylmethionine tosylate salt was a generous gift from H. Schroeder (BASF, Ludwigshafen, Germany).

NAP-10 columns were purchased from Amersham Biosciences (Buckinghamshire, UK). Supelclean ™ LC-18 solid phase extraction columns from Supelco were purchased through Sigma-Aldrich (Poole, UK).

5.2 Instrumentation

Anaerobic Glovebox

All experiments using LipA were carried out in an anaerobic glovebox (Belle Technology, Portesham, UK) maintained under nitrogen at less than 0.2 ppm O_2.

Freeze drying

Samples were freeze dried using a Heto PowerDry LL3000.

NMR

^{1}H NMR and ^{13}C NMR spectra were recorded using either a Bruker AC300 FT-NMR spectrometer (^{1}H, 300 MHz), a Bruker DPX 400 spectrometer (^{1}H, 400 MHz)or a Varian Innova 600 spectrometer (^{1}H, 600 MHz). COSY spectra were used for assignment of peptide ^{1}H NMR and HMQC spectra were used for assignment of ^{13}C NMR.

Mass spectroscopy

Electrospray mass spectra were recorded on a Waters ZMD single quadrupole mass spectrometer. High resolution electrospray mass spectra were recorded on a Bruker Apex IIIFT-ICR mass spectrometer.

HPLC

Reversed-phase HPLC analysis was carried out on a Gilson 321 workcenter equipped with a dual wavelength UV-visible detector and a Shimadzu RF-10Axl fluorescence detector. For analytical HPLC methods; chromatograms were collected and analyzed using the Gilson Unipoint software (Gilson).

LC-MS

Reversed-phase HPLC analysis was carried out on a Gilson system workcenter and LCMS experiments coupled this HPLC via a 1:4 split into a ThermoFinnigan Surveyor MSQ electrospray mass spectrometer. The data were collectedand processed using the XCalibur software system.

Fermentation

Fermentation was carried out in an Incubator Shaker Innova^{TM}4400 (New Brunswick Scientific).

UV spectroscopy

UV-visible spectra of *S. solfataricus* LipA (1 mg/ml) were recorded with an Ocean Optics (Duiven, The Netherlands) USB2000 spectrophotometer using a light source Mini-D2-GS connected by optical fibres P-400-2-UV/SR to a cuvette holder inside the glove box.

EPR spectroscopy

EPR spectra were recorded by Prof. D. J. Lowe and Dr. S. A. Fairhurst (John Innes Centre, Norwich). Spectra were recorded at X-band on a Bruker ELEXYS 500 spectrometer with an ER094X microwave bridge using an ER4122SHQ cavity. Low temperature experiments were performed using an ESR 900 liquid helium flow cryostat and ITC3 temperature controller (Oxford Instruments). Double integration of spectra was done by comparison with a 1 mM sample of Cu(EDTA).

5.3 General experimental methods

5.3.1 Expression and purification of *S. solfataricus* LipA

Buffers

Buffer A

25 mM HEPES pH 7.5

imidazole	50 mM
NaCl	500 mM
glycerol	10% (w/v)

Buffer B

25 mM HEPES pH 7.5

imidazole	250 mM
NaCl	500 mM
glycerol	10% (w/v)

Buffer C

25 mM HEPES pH 7.5

| NaCl | 100 mM |
| glycerol | 10% (w/v) |

Media

2YT (1L)

Yeast extract	10 g
Bacto-tryptone	16 g
NaCl	5 g
Dilute with H_2O to	1 L

Sterilise by autoclaving.

SOC (100 mL)

To sterile (autoclaved) 2YT (100 mL) was added the following:

1mL filter sterilised $MgSO_4$ (1 M)

1mL filter sterilised $MgCl_2$ (1M)

1mL filter sterilised glucose (2M).

Plasmids

pMK024 – pBADHis(lipAHis, iscSUA, hscBA, fdx)

This plasmid was constructed by Dr Marco Kriek. It is a pBADHis derived vector which encodes the His tagged *lipA* gene from *Sulfolobus solfotaricus* (ORF no. SSO3158) and also *isc, hsc* and *fdx* genes. The plasmid possesses an ampicillin resistance marker.

Transformations

Expression plasmid pMK024 was used to transform *E. coli* BL21(DE3) or LMG194 cells. The plasmid and cells were incubated on ice for 10 min then plasmid mixtures (1.0 μL) were added to cells (50 μL). The resulting mixtures were incubated on ice for a further 30 min then heat shocked for 30 seconds at 42 °C. Mixtures were returned to ice for 3 min before addition of SOC medium (250 μL), then incubated at 37 °C for 1 hour. Cells (100μL aliquots) were spread onto agar plates containing ampicillin (100 mg/L.), which were then incubated at 37 °C overnight.

Cell growth and protein expression

2YT medium (10 mL) containing ampicillin (100 mg/L) was inoculated with single colonies from a plate or cells from a glycerol stock, which were grown overnight at 37 °C and 190 rpm. The overnight culture was used to inoculate fresh 2YT medium (5L) containing ampicillin (100 mg/L). Bacterial cultures were incubated at 37 °C and 190 rpm until OD_{600} reached 0.6-0.8, at which point expression was induced by addition of filter sterilised arabinose solution (20% w/v, 10 mL/L). Growth then continued at 27 °C. 190 rpm for 4 hours. Cells were harvested by centrifugation (Beckman JLA 10,500 rotor; 6000 rpm; 4 °C; 15 minutes) and cell pellets were stored at −80 °C until required.

Anaerobic purification of LipA

Purification was carried out in anaerobic glovebox and all buffers were degassed in glovebox for 24 hours. Cell paste (30-40 g) was resuspended in anaerobic buffer A (3 mL/g of cells). Lysozyme (10 mg) and benzonase (4 µL, 25 U/µL) were added and the suspension stirred for 1 hour. Cells were lysed by sonication (10 mins, 1 s pulse) and then the lysate was centrifuged (Beckmann JA-14 rotor, 12000 rpm, 4 °C, 30 mins). The supernatant was applied to a nickel-charged affinity column (Chelating Sepharose FF) previously equilibrated in buffer A. The column was washed with buffer A (5 column volumes) then the protein eluted with buffer B. The LipA containing fractions were pooled and concentrated to 10 mL (~20 mg/mL) then applied to a S-75 gel filtration column (33 × 750 mm) equilibrated with anaerobic buffer C. The protein was eluted with buffer C and the purest fractions, as judged by SDS-PAGE, were concentrated (18 mg/mL) and stored at −80°C (1 mL aliquots).

Determination of protein concentration

Protein concentrations were determined using the method of Bradford (*1*).

SDS-PAGE denaturing gel

A 15% resolving gel (10 mL, 5 mL per plate)was prepared by mixing the following components in the order shown below:

H₂O	4.0 mL
30% Acrylamide / bis acrylamide mix	3.3 mL
1.5 M Tris (pH 8.8) buffer solution	2.5 mL
10% SDS	0.1 mL
10% Ammonium persulfate	0.1 mL
TEMED	4 μL

This solution (5 mL) of this solution was then applied into each plate (Bio-Rad Mini Protean II system) and the surface of the gel was covered with a thin layer of isopropanol (50%) whilst the gel was allowed to set for 45 min. the thin layer of isopropanol was then removed carefully and a stacking gel was then prepared by mixing the following components in the order shown below:

H₂O	3.4 mL
30% Acrylamide / bis acrylamide mix	0.83 mL
1.5 M Tris (pH 8.8) buffer solution	0.63 mL
10% SDS	0.05 mL
10% Ammonium persulfate	0.05 mL
TEMED	2 μL

This mixture was then applied directly onto the top of the resolving gel and a Teflon comb was inserted into the gel solution. The stacking gel was left to set for 1 hour, after which time the Teflon comb was removed and the wells washed with distilled water.

Samples for analysis by SDS-PAGE were prepared by mixing the required protein solution (20 μL, ~ 2 mg/mL) with sample loading buffer (20 μL, table 5.1). Each sample was then heated to 90 °C for 5 min and then applied onto the gel. Electrophoretic separation was at 180 V in SDS-PAGE running buffer (table 5.2). Gels were stained in Coomaissie brilliant blue stain (table 5.3) and then destained (table 5.4).

Component	Quantity
0.2 M Tris-HCl (pH 6.8)	2.5 mL
DTT	154 mg
SDS	200mg
Bromophenol blue	10 mg
Glycerol	1 mL
Deionised water	Adjust volume to 10 mL

Table 5.1 Sample loading buffer (×1 stock solution).

Component	Quantity
Tris Base	15.1 g
Glycine	94 g
10% SDS solution	50 mL
Deionised water	Adjust volume to 10 mL

Table 5.2 SDS-PAGE running buffer (×5 stock solution).

Component	Quantity
Coomaissie brilliant blue	2.5 g
Methanol:water (1:1)	90 mL
Glacial acetic acid	10 mL

Table 5.3 Coomaissie brilliant blue protein stain.

Component	Quantity
Deionised water	4375 mL
Methanol	375 mL
Glacial acetic acid	250 mL

Table 5.4 Destain solution.

Iron analysis

Iron analysis was carried out according to the method of Fish (*2*).

Sulfide analysis

Sulfide analysis was carried out according to the method of Beinert (*3*).

5.4   Experimental for chapter 2

5.4   Protection of the N^{ε} amino group of lysine with Dde

Preparation of 2-acetyldimedone (Dde)
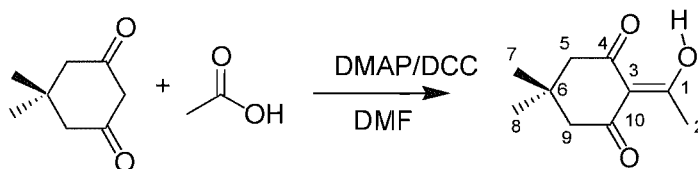
Scheme 5.1 Preparation of 2-acetyldimedone (Dde).

To a stirred solution of acetic acid (6.75 mL, 95 mmol) in DMF (200 mL) were added dimedone (14.08 g, 100 mmol), DCC (18.75 g, 100 mmol) and DMAP (11.50 g, 100 mmol). The mixture was stirred at room temperature for 48 hours. DMF was removed by evaporation and the residue redissolved in ethyl acetate. The resulting solution was washed with 1M $KHSO_4$ (3 × 50 mL) then extracted with sat. $NaHCO_3$ (3 × 50 mL). The aqueous solution was acidified then extracted with DCM, the organic layer was dried over $MgSO_4$ and then the solvent removed under reduced pressure. The product was recrystallised from $MeOH/H_2O$ (1:1) to afford a white crystalline solid (7.25 g, 42 %); R_f 0.27 (ethyl acetate/hexane, 4:1), **ES-MS**: *m/z* 183.2 ([M+H], 100%) ^{1}**H NMR** (300MHz; $CDCl_3$): δ 1.01 (6H, s, H^7, H^8), 2.31 (2H, s, H^{5a}, H^{9a}), 2.50 (2H, s, H^{5b}, H^{9b}), 2.53 (3H, s, H^2); ^{13}**C NMR** (75 MHz, $CDCl_3$) δ 28.2 (C^7, C^8), 28.5 (C^2), 30.6 (C^6), 46.91 (C^5 or C^9), 52.5 (C^5 or C^9), 112.4 (C^3), 195.2 (C^4 or C^{10}), 197.9 (C^4 or C^{10}), 202.4 (C^1).

Preparation of Fmoc-(L)-Lys(Dde)-OH

Dde   +   Fmoc-Lys-OH $\xrightarrow[\text{EtOH}]{\text{0.1\% TFA}}$
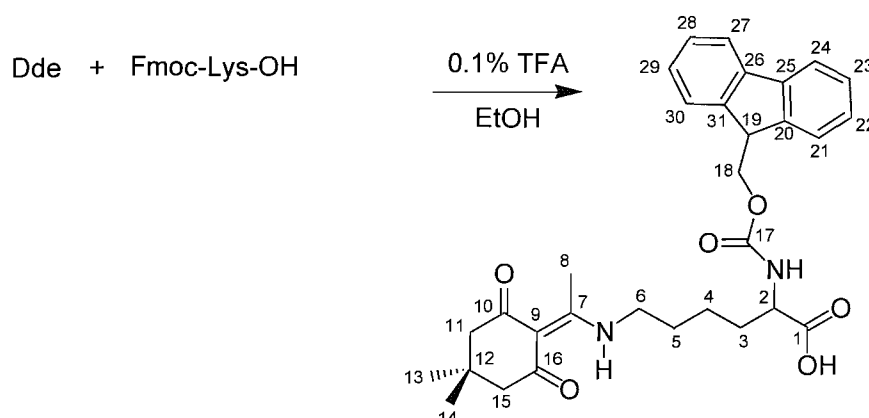
Scheme 5.2 Preparation of Fmoc-(L)-Lys(Dde)-OH.

Fmoc-(L)-Lys(Dde)-OH was prepared according to the method of Bycroft *et. al.* (*4*)..
To a stirred suspension of Fmoc-(L)Lys-OH (1.47 g, 4.0 mmol) and Dde (1.46 g, 4.4 mmol) in ethanol (50 mL) was added TFA (0.03 mL, 0.4 mmol). The resulting mixture was heated under reflux for 72 h. The solvent was removed by evaporation and the resulting orange residue redissolved in ethyl acetate (60 mL). The solution was washed with 1M KHSO$_4$ (2 × 50 mL) then dried over MgSO$_4$. The solvent was removed under reduced pressure to afford a yellow oil which was dissolved in ethyl acetate. Dropwise addition of the resulting solution to ice cold hexane led to precipitation of a white solid which was filtered, washed with hexane then dried *in vacuo* to yield a white solid (1.63 g, 76 %); **Rf** 0.10 (chloroform, methanol, acetic acid, 15:4:1); **ES-MS**: *m/z* 532.6 ([M+Na], 100%); ^{1}**H NMR** (300MHz; CDCl$_3$): δ 1.01 (6H, s, H^{13}, H^{14}), 1.48-1.61 (2H, m, H^4), 1.65-1.89 (3H, m, H^{3a}, H^5), 1.90-2.04 (1H, m, H^{3b}), 2.36 (4H, s, H^{11}, H^{15}), 2.53 (3H, s, H^8), 3.40 (2H, d, J = 6.0 Hz, H^6), 4.19 (1H, t, J = 6.9 Hz, H^{19}), 4.36 (2H, d, J = 6.9 Hz, H^{18}), 4.46 (1H, t J = 3.0 Hz, H^2), 7.29 (2H, dd, J = 1.2, 7.5 Hz, Fmoc), 7.34 (2H, t, J = 7.5 Hz, Fmoc), 7.57 (2H, t, J = 6.7 Hz, Fmoc), 7.73 (2H, d, J = 7.5 Hz, Fmoc); ^{13}**C NMR** (75 MHz, CDCl$_3$) δ 14.2 (C^{12}), 18.1 (C^8), 22.4 (C^4), 28.2 (C^{13} or C^{14}), 28.4 (C^{13} or C^{14}), 30.1 (C^3), 32.0 (C^5), 43.3 (C^{19}), 47.2 (C^6), 52.5 (C^{11}, C^{15}), 53.4 (C^{18},), 67.1 (C^2), 107.9 (C^9), 119.9 (C^{23}, C^{28}), 125.1 (C^{24}, C^{27}), 127.1 (C^{22}, C^{29}), 127.7 (C^{21}, C^{30}), 141.3 (C^{23}, C^{26}), 143.8 (C^{20}, C^{31}), 156.1 (C^{17}), 173.9 (C^7), 174.4 (C^1), 198.2 (C^{10}, C^{16}).

5.4.2 Solid phase peptide synthesis

Peptides were prepared manually, according to standard solid phase protocols (5). Reactions were carried out in a sintered glass bubbler device (5) unless stated otherwise.

Analysis- Qualitative Kaiser (ninhydrin) test (5)

KCN (32 mg) was dissolved in water (50 mL) then 1 mL of this solution diluted to 50 mL with pyridine. Solution A was then prepared by adding this resulting mixture was added to a solution of phenol (20 g) in ethanol (5 mL) to give. Solution B was prepared by dissolving ninhydrin (1.25 g) in ethanol (25 mL). A small resin sample was and rinsed with ethanol then solution A (100 μL) and solution B (25 μL) were added and the mixture heated to 100 °C for 5 minutes. If positive for free amino groups a strong blue colour was seen and if negative a straw colour.

Loading of Fmoc (L)-amino acids onto Wang resin

DIC (0.48 mL) was added to a stirred solution of either Fmoc-(L)-Ile-OH (2.12 g, 6.0 mmol) or Fmoc-(L)-Ala-OH (1.87 g, 6.0 mmol) in DMF (10 mL) in a round bottomed flask. After 10 minutes this solution was added to Wang resin (6) (1.68 g, 0.89 mmol/g) then DMAP (37 mg, 0.3 mmol) was added and the mixture agitated in an ultrasonic bath at room temperature for 3 hours. The resin was then filtered, washed with DCM (3 × 30 mL), DMF (3 × 30 mL) and diethyl ether (3 × 30 ml) and dried in vacuo.

Quantitative Fmoc test

To a known mass (<5 mg) of resin was added a solution of 20% (v/v) piperidine in DMF (1.5 mL) in a 25 mL volumetric flask. The resin was allowed to stand for 15 minutes filtered through a glass pipette with a glass wool plug then the filtrate diluted to 25 mL with 20% piperidine/DMF. The absorbance at 302 nm was recorded against a blank (20% piperidine/DMF) and the loading yield calculated from the following equation:

$$\text{Loading (mmol/g)} = [(A_{302} \times V)/(\varepsilon_{302} \times W)] \times 1000$$

A_{302} = absorbance of the piperidyl-fulvene adduct

V = final volume (25 mL)

W = mass of the resin sample

ε_{302} = molar extinction co-efficient of the adduct at 302 nm (7800 $M^{-1}cm^{-1}$)

Capping of unreacted groups on resin

In a round bottomed flask a solution of benzoyl chloride (0.5 mL) and pyridine (0.5 mL) in DCM (20 mL) was cooled to $0^{\circ}C$ then loaded resin (1.0 g) was added to the solution. The resulting suspension was stirred gently for 30 min at room temperature then filtered and washed with DCM (3 × 30 mL) and diethyl ether (3 × 30 mL). The resin was then dried *in vacuo*.

Removal of the N^{α}-Fmoc protecting group

20% (v/v) piperidine in DMF (10 mL) was added to Fmoc protected peptidyl resins in reaction vessel. The suspended resin was then agitated for 30 min then washed with DMF (5 × 10 mL, 1 min agitation). This process was repeated once then removal of the Fmoc group was confirmed by qualitative Ninhydrin test.

Coupling of Fmoc (L)-amino acids to peptide

Fmoc amino acid (3 equiv with respect to resin loading) and HOBt (3 equiv) were dissolved in DMF then DIC (3 equiv) was added. The resulting solution was stirred at room temperature for 10 min. The activated amino acid solution was added to the peptidyl resin in the reaction vessel and the mixture was agitated for 1hour. The resin was then filtered and washed with DMF (5 × 10 mL, 1 min agitation). The completion of the coupling reaction was confirmed by qualitative Kaiser test.

Dde deprotection

The Dde group was removed with hydroxylamine hydrochloride and imidazole in NMP according to the method of Diaz-Mochon *et al.* (7). Hydroxylamine

hydrochloride (1.25 g, 1.80 mmol) and imidazole (0.92 g, 1.35 mmol) were suspended in N-methylpyrrolidone (5 mL) and the mixture was agitated in an ultrasonic bath until complete dissolution. DMF (1 mL) was added and the solution then added to the peptidyl resin in the reaction vessel. The mixture was then agitated in the reaction vessel for 3 hours. The liquid was then drained and the resin washed with DMF (5 × 10 mL, 1 min agitation). A resin sample was taken for qualitative Kaiser testing to confirm the presence of free amino groups

Coupling of octanoic/(DL)-lipoic acid to peptide

Octanoic acid (5 molar equivalents with respect to resin loading) or (DL)-lipoic acid (5 equiv) was dissolved in DMF (10 mL) then PyBOP (*8*) (4.75 equiv) and DIPEA (0.50 mL) were added and the solution was then added to the resin. The suspended resin was agitated for 1 h then filtered and washed with DMF (5 × 10 mL, 1 min agitation). The completion of the coupling reaction was confirmed by qualitative Kaiser test.

Cleavage of peptides from resin

Peptidyl resins were transferred to a round bottomed flask and a mixture of TFA, anisole and water (10:1:1, 12 mL) was added. The suspended resin was stirred for 2 hours then the liquid was drained and the resin washed with TFA (3 × 5 mL). The combined TFA washings were concentrated in vacuo and the crude peptide precipitated by the addition of diethyl ether.

Preparation of fluorescent peptides 15 (fig. 5.1) and 16 (fig. 5.2)

Labelled octanoyl and (DL)-lipoyl tetrapeptides **15** and **16** were assembled using the above general procedures. Fmoc-(L)-Ile-Wang resin (0.5 g, 0.35 mmol/g) was deprotected then Fmoc-(L)-Lys(Dde)-OH (0.28 g, 3 equiv) was attached. The Dde group was then removed and octanoic acid (0.12 mL, 5 equiv) or (DL)-lipoic acid (0.18 g, 5 equiv) was coupled to the lysine side chain. Following addition of Fmoc-(L)-glutamic acid and appropriate deprotection 5(6)-CFL (0.33 g, 5 eq) and PyBOP (0.43 g, 4.75 equiv) (*8*) were dissolved in DMF (5 mL). Diisopropylethylamine (0.17 mL, 10 equiv) was added and the solution was then applied to the peptidyl resin. The suspended resin was agitated for 1 hour then the liquid drained and the resin washed with DMF (10 mL, 5 x 1 min). This was repeated until Kaiser test was

negative. Peptides were cleaved from the resin to yield 98 mg (64%) of octanoyl peptide and 95 mg (58%) of lipoyl peptide. The crude peptides were dissolved in water/acetonitrile, 9:1 (3.0 mg/mL of peptide) and 200µL aliquots were purified by HPLC on a reversed phase Phenomenex Gemini C18 (5 µm, 150 × 10 mm) column with UV detection at 230 nm. The mobile phase was a mixture of 10 mM ammonium bicarbonate (pump A) and acetonitrile (pump B), beginning with 10 % organic and 90 % aqueous for two minutes at 2 mL/min followed by a 15 min linear gradient to 60 % acetonitrile. This was maintained for 2 min followed by return to initial conditions over 1 min. Each injection was complete in 30 min. This was repeated with further aliquots off crude peptide (19 × 200µL) then the required fractions were pooled and the solvent removed by freeze drying.

Isomeric   mixture   of   (N5-Carboxyfluorescein)-glutamyl-(N6-octanoyl)-lysyl isoleucine and (N6-Carboxyfluorescein)-glutamyl-(N6-octanoyl)-lysyl isoleucine

15a

15b
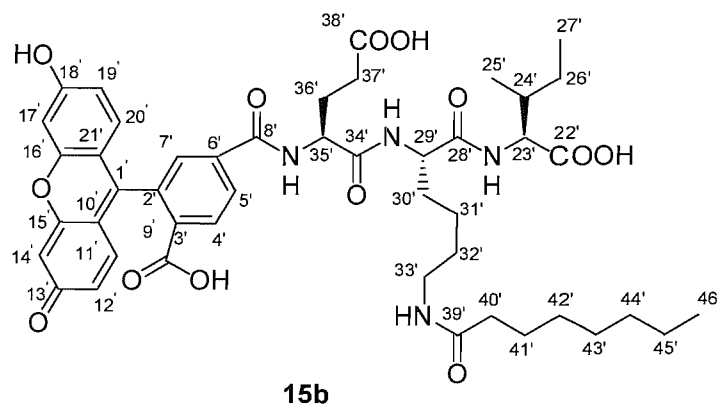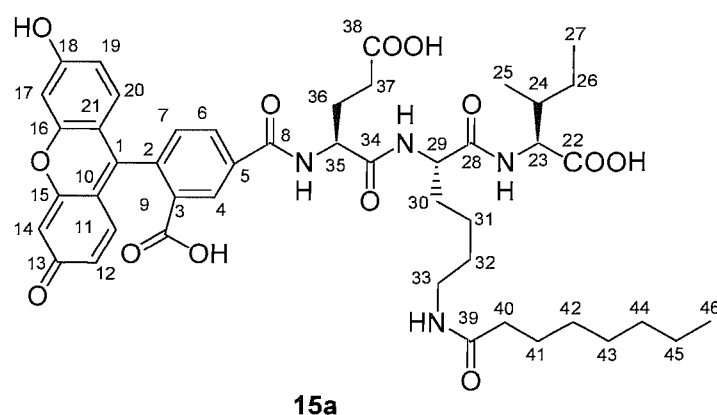
Figure 5.1 Structures of (N5-carboxyfluorescein)-glutamyl-(N6-octanoyl)-lysyl isoleucine and (N6-carboxyfluorescein)-glutamyl-(N6-octanoyl)-lysyl isoleucine.

An orange solid (4.6 mg, 24 %); R_f 0.86 (EtOH/MeOH/H$_2$O/DIPEA, 60:30:20:3); **ES-MS**: *m/z* 873.3 ([M+H]$^+$, 100%); ^{1}**H NMR** (600 MHz, D$_2$O) δ 0.59-0.81 (18H, m, H^{25}, H^{27}, H^{46}, H$^{25'}$, H$^{27'}$, H$^{46'}$), 0.91-1.03 (22H, m, H^{26a}, H^{41}, H^{42}, H^{43}, H^{44}, H^{45}, H$^{26'a}$, H$^{41'}$, H$^{42'}$, H$^{43'}$, H$^{44'}$, H$^{45'}$), 1.12-1.54 (10H, m, H^{26b}, H^{31}, H^{32}, H$^{26'b}$, H$^{31'}$, H$^{32'}$), 1.55-1.87 (6H, m, H^{24}, H^{30}, H$^{24'}$, H$^{30'}$), 1.90-1.95 (2H, m, H^{36a}, H$^{36'a}$), 1.98-2.12 (4H, t, J = 9.1 Hz, H^{40}, H$^{40'}$), 2.19-2.36 (6H, m, H^{36a}, H^{37}, H$^{36a'}$, H$^{37'}$,) 2.95 (2H, t, J=6.0 Hz, H^{33} $^{or\ 33'}$), 3.04 (2H, m, H$^{33\ or\ 33'}$), 3.96 (1H, d, J=6.0 Hz, H$^{23\ or\ 23'}$), 4.01 (1H, d, J= 6.0, H$^{23\ or\ 23'}$) 4.26 (1H, dd, J=9.6, 4.2 Hz, H$^{29\ or\ 29'}$), 4.33 (1H, J=9.6, 4.2 Hz, H$^{29\ or\ 29'}$), 4.39 (1H, dd, J=9.0, 5.4 Hz, H$^{35\ or\ 35'}$) 4.47 (1H, dd, J=9.0, 5.4 Hz, H$^{35\ or\ 35'}$), 6.55 (8H, m, H^{11}, H^{14}, H^{17}, H^{20}, H$^{11'}$, H$^{14'}$, H$^{17'}$, H$^{20'}$), 7.06 (4H, m, H^{12}, H^{19}, H$^{12'}$, H$^{19'}$), 7.32 (1H, d, J = 7.8, H^7), 7.59 (1H, s, H$^{7'}$), 7.86 (1H, d, J = 7.8 Hz, H^6), 7.93 (1H, dd, J = 8.4, 1.2 Hz, H^4), 7.98 (1H, dd, J = 8.4, 1.8 Hz, H$^{5'}$), 8.18 (1H, d, J=1.8 Hz, H^4).

Isomeric mixture of (N5-Carboxyfluorescein)-glutamyl-(N6-lipoyl)-lysyl isoleucine and (N6-Carboxyfluorescein)-glutamyl-(N6-lipoyl)-lysyl isoleucine

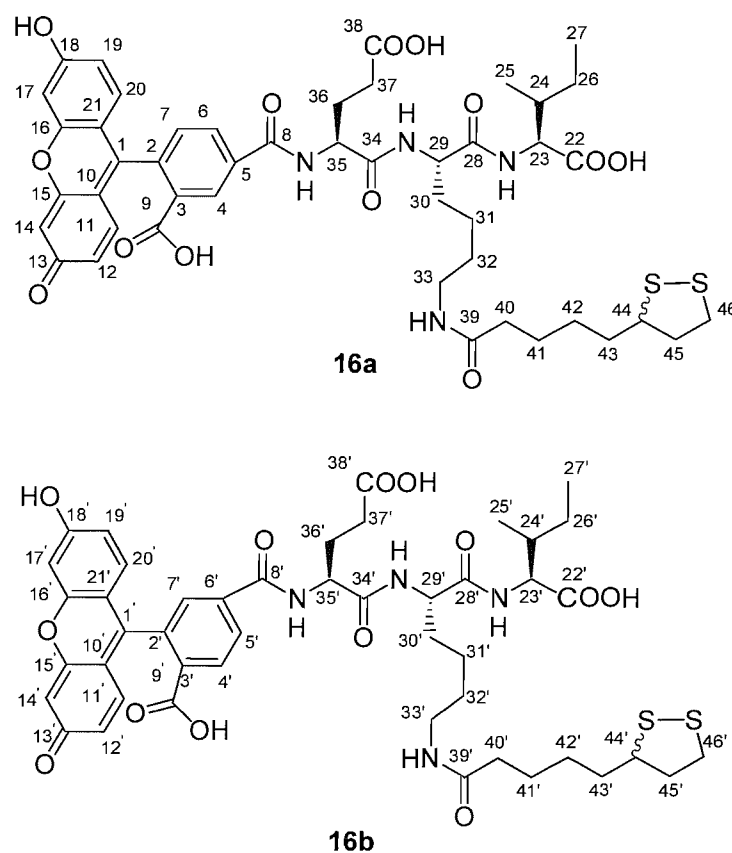**Figure 5.2** Isomeric mixture of (N5-carboxyfluorescein)-glutamyl-(N6-(DL)-lipoyl)-lysyl isoleucine and (N6-carboxyfluorescein)-glutamyl-(N6-(DL)-lipoyl)-lysyl isoleucine.

An orange solid (2.8 mg, 12%); R_f 0.72 (EtOH/MeOH/H$_2$O/DIPEA, 60:30:20:3); **ES-MS**: *m/z* 934.3 ([M+H], 100%); **^{1}H NMR** (600 MHz, D$_2$O) δ 0.71-0.92 (12H, m, H^{25}, H^{27}, H$^{25'}$, H$^{27'}$), 1.05-1.24 (2H, m, H^{26a}, H$^{26'a}$), 1.25-1.49 (18H, m, H^{26b}, H^{31}, H^{32}, H^{41}, H^{42}, H$^{26b'}$, H$^{31'}$, H$^{32'}$, H$^{41'}$, H$^{42'}$), 1.50-1.62 (8H, m, H^{30}, H^{43}, H$^{30'}$, H$^{43'}$), 1.68-1.92 (8H, m, H^{24}, H^{36a}, H^{45}, H$^{24'}$, H$^{36a'}$, H$^{45'}$), 2.03-2.30 (6H, m, H^{36b}, H^{40}, H$^{36b'}$, H$^{40'}$), 2.32-2.49 (4H, m, H^{37}, H$^{37'}$), 3.03 (2H, t, J=6.0, H$^{33 \text{ or } 33'}$), 3.10-3.22 (4H, m, H$^{33 \text{ or } 33'}$, H$^{46 \text{ or } 46'}$), 3.27-3.38 (2H, m, H$^{46 \text{ or } 46'}$), 3.56 (1H, dd, J=7.5, 1.5 Hz, H$^{44 \text{ or } 44'}$), 3.67 (1H, dd, J=7.5, 1.2 Hz, H$^{44 \text{ or } 44'}$), 4.09 (1H, d, J=6.8 Hz, H$^{23 \text{ or } 23'}$), 4.13 (1H, d, J=6.8, H$^{23 \text{ or } 23'}$), 4.38 (1H, m, H$^{29 \text{ or } 29'}$), 4.45 (1H, m, H$^{29 \text{ or } 29'}$), 4.50 (1H, m, H$^{35 \text{ or } 35'}$), 4.59 (1H, m, H$^{35 \text{ or } 35'}$), 6.84 (4H, d, J=9.0 Hz, H^{11,} H^{20,} H$^{11', H20'}$), 6.91 (4H, s, H^{14}, H^{17}, H$^{14'}$, H$^{17'}$), 7.30 (4H, m, H^{12}, H^{19}, H$^{12'}$, H$^{19'}$), 7.50 (1H, dd, J=8.4, 4.2 Hz, H^7), 7.70 (1H, s, H$^{7'}$), 8.07 (1H, d, J=7.8 Hz, H$^{5'}$), 8.10 (1H, d, J=7.8 Hz, H$^{4'}$), 8.34 (1H, s, H^4).

Preparation of tetrapeptides 20 (fig. 5.3) and 21 (fig. 5.4)

Octanoyl and (DL)-lipoyl tetrapeptides **20** and **21** were assembled using the above general procedures. Following deprotection of Fmoc-(L)-Ile-Wang resin (1.00 g, 0.25 mmol/g) Fmoc-(L)-Lys(Dde)-OH (0.40 g, 3 equiv) was coupled. The Dde group was then removed and octanoic acid (0.18 mL, 5 equi) or (DL)-lipoic acid (0.25 g, 5 equiv) was coupled to the lysine side chain. The peptide synthesis was then completed by the addition of Fmoc-(L)-glutamic acid and Fmoc-(L)-threonine with appropriate deprotection. Peptides were cleaved from the resin to yield 146 mg (95%) of octanoyl peptide and 157 mg (93%) of lipoyl peptide. Aliquots of the crude peptides (30 mg) were dissolved in water/acetonitrile (9:1) and purified by reverse phase chromatography on a Supelclean ™ LC-18 solid phase extraction column column. Peptides were eluted in water/acetonitrile (9:1) and the required fractions were pooled then the solvent was removed by freeze drying.

Threnonyl-glutamyl-(N6-octanoyl)-lysyl isoleucine **20**

20
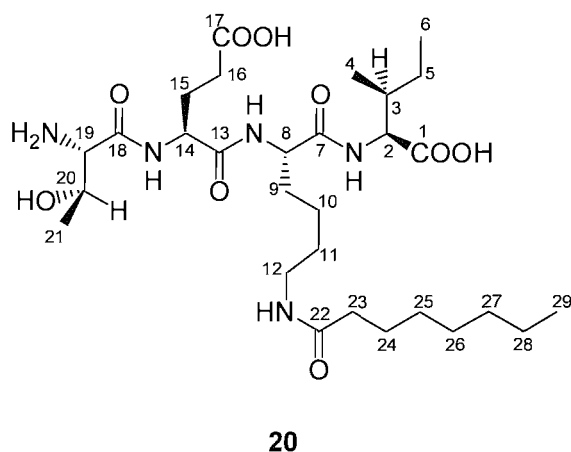
Figure 5.3 Structure of threnonyl-glutamyl-(N6-octanoyl)-lysyl isoleucine.

A white solid (19.4 mg, 68 %); R_f 0.26 (reverse phase, acetonitrile/water 1:9); **ES-MS**: m/z 616.4 ([M+H]$^+$, 100%); **HRES-MS** calculated for $C_{29}H_{53}O_9N_5$ [M+H]: 616.3916; found 616.3910 ^{1}**H NMR** (400 MHz; D_2O): δ 0.91-0.94 (9H, m, H^4, H^6, H^{29}), 1.18 (1H, m, H^{5a}), 1.28-1.35 (13H, m, H^{10}, H^{21}, H^{25}, H^{26}, H^{27}, H^{28},), 1.40-1.49 (1H, m, H^{5b}), 1.53-1.66 (4H, m, H^{11}, H^{24}), 1.76-1.88 (3H, m, H^3, H^9), 1.94-2.05 (1H, m, H^{15a}), 2.07-2.18 (1H, m, H^{15b}), 2.27 (2H, t, J=7.3 Hz, H^{23}), 2.31-2.35 (2H, m, H^{16}), 3.22 (2H, t, J=6.8 Hz, H^{12}), 3.58 (1H, d, J=5.5 Hz, H^{19}), 4.09 (1H, m, H^{20}), 4.15 (1H,

d, J=6.0 Hz, H^2), 4.36 (1H, t, J=8.2 Hz, H^8), 4.41 (1H, dd, J=9.3, 5.0 Hz. H^{14}); ^{13}C

NMR (100 MHz, D$_2$O) δ 13.54 (C^6), 16.13 (C^{29}), 18.03 (C^4), 21.28 (C^{21}), 24.68,

25.18, 27.27, 28.16, 30.55, 30.55, 30.77, 30.80 (C^5, C^{11}, C^{15}, C^{24}, C^{25}, C^{26}, C^{27}, C^{28}),

33.05 (C^3), 33.69 (C^{10}), 36.33 (C^{16}), 38.55 (C^{23}), 39.92 (C^9), 41.75 (C^{12}), 56.34 (C^{14}),

56.63 (C^8), 62.35 (C19), 62.75 (C2), 70.84 (C20), 173.81 (C=O), 175.54 (C=O),

176.17 (C=O), 179.97 (C=O), 181.03 (C=O), 184.14 (C=O).

Threonyl-glutamyl-(N6-(DL)-lipoyl)-lysyl-isoleucine **21**

21

Figure 5.4 Structure of threnonyl-glutamyl-(N6-(DL)-lipoyl)-lysyl isoleucine.

A white solid (14.5 mg, 52 %); **R$_f$** 0.23 (reverse phase, acetonitrile/water 1:9);

ES-MS: *m/z* 678.3 ([M+H]$^+$, 100%); **HRES-MS** calculated for C$_{29}$H$_{51}$O$_9$N$_5$S$_2$

[M+H]: 678.3201; found: 678.3194. ^{1}**H NMR** (400 MHz; D$_2$O) δ 0.83-0.88 (6H, m,

H^4, H^6), 1.12 (1H, m, H^{5a}), 1.30 (3H, d, J=6.3 Hz, H^{21}), 1.33-1.45 (7H, m, H^{5b}, H^{10},

H^{24}, H^{25}), 1.47-1.54 (2H, m, H^{11}), 1.56-1.67 (3H, m, H^{9a}, H^{26}), 1.68-1.88 (2H, m, H^3,

H^{9b}), 1.90-2.02 (2H, m, H^{15a}, H^{28a}), 2.03-2.15 (1H, m, H^{15b}), 2.22 (2H, t, J=7.0 Hz,

H^{23}), 2.34 (2H, m, H^{16}), 2.48 (1H, m, H^{28b}), 3.16 (2H, t, J=6.3 Hz, H^{12}), 3.17-3.25

(2H, m, H^{29}), 3.65-3.71 (1H, m, H^{27}), 3.77 (1H, d, J=6.3 Hz, H^{19}), 4.10-4.14 (2H, m,

H^2, H^{20}), 4.30 (1H, t, J=14.1 Hz, H^8), 4.42 (1H, dd, J=7.0, 5.3 Hz. H^{14}); ^{13}**C NMR**

(100 MHz, D$_2$O) δ 13.49 (C^6), 17.96 (C^4), 21.51 (C^{21}), 25.21 (C^{33}), 27.31 (C^5), 27.84

(C^{32}), 30.09 (C^{15}), 30.54 (C^{10}), 30.61 (C^{11}), 33.16 (C^{34}), 35.06 (C^{16}), 36.44 (C^9),

38.27 (C^{31}), 39.83 (C^3), 40.81 (C^{37}), 41.76 (C^{12}), 43.03 (C^{36}), 56.08 (C^{14}), 56.73 (C^8),

59.29 (C^{35}), 61.36 (C^{19}), 62.43 (C^2), 68.94 (C^{20}), 170.48 (C=O), 175.49 (C=O), 175.59 (C=O), 179.49 (C=O), 180.58 (C=O).

Preparation of tripeptides 25 (fig. 5.5) and 26 (fig. 5.6)

Octanoyl and (DL)-lipoyl tripeptides **25** and **26** were assembled using the above general procedures. Following deprotection of Fmoc-(L)-Ile-Wang resin (0.50 g, 0.50 mmol/g) Fmoc-(L)-Lys(Dde)-OH (0.40 g, 3 equiv) was attached. The Dde group was then removed and octanoic acid (0.18 mL, 5 equiv) or (DL)-lipoic acid (0.25 g, 5 equiv) was coupled to the lysine side chain. The peptide synthesis was then completed by the addition of glutamic acid and appropriate deprotection. Peptides were cleaved from the resin to yield 126 mg (98%) of octanoyl peptide and 117 mg (81%) of lipoyl peptide. Aliquots of the crude peptides (20 mg) were dissolved in water/acetonitrile (9:1) and purified reverse phase chromatography on a Supelclean™ LC-18 solid phase extraction column (10g). Peptides were eluted in water/acetonitrile (9:1) and the required fractions were pooled then the solvent was removed by freeze drying.
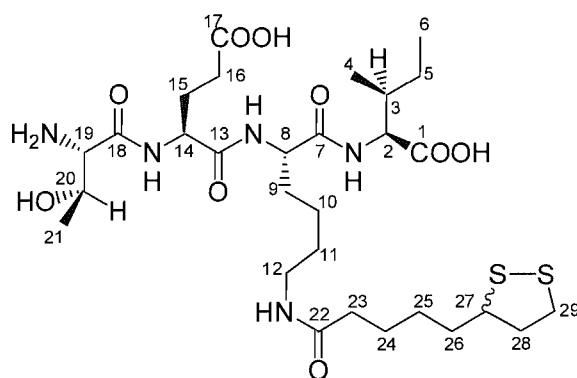
Glutamyl-(N6-octanoyl)-lysyl isoleucine **25**.

25

Figure 5.5 Structure of glutamyl-(N6-octanoyl)-lysyl isoleucine.

A white solid (14.5 mg, 71%) R$_f$ 0.14 (reverse phase, acetonitrile/water 1:9); **ES-MS** *m/z* 515.3 ([M+H]$^+$, 100%); **HRES-MS** calculated for C$_{25}$H$_{46}$O$_7$N$_4$ [M+H]$^+$: 515.3439; found 515.3436; **^{1}H NMR** (400 MHz, D$_2$O) δ 0.80-0.88 (9H, m, H^4, H^6,

H^{25}), 1.02-1.11 (1H, m, H^{5a}), 1.32-1.49 (11H, m, H^{5b}, H^{20},H^{21}, H^{22}, H^{23}, H^{24}), 1.51-1.58 (4H, m, H^{10},H$^{11)}$, 1.72-1.91 (3H, m, H^{3}, H^{9}), 2.06-2.18 (2H, m, H^{15}), 2.36-2.51 (4H, m, H^{16}, H^{19}), 3.08 (2H, t, J=5.8 Hz, H^{12}), 3.52 (1H, t, J=5.5 Hz, H^{14}), 4.03 (1H, d, J=6.3 Hz, H^{2}), 4.25 (1H, t, J=7.8 Hz, H^{8}).

Glutamyl-(N6-(DL)-lipoyl)-lysyl isoleucine **26**

26
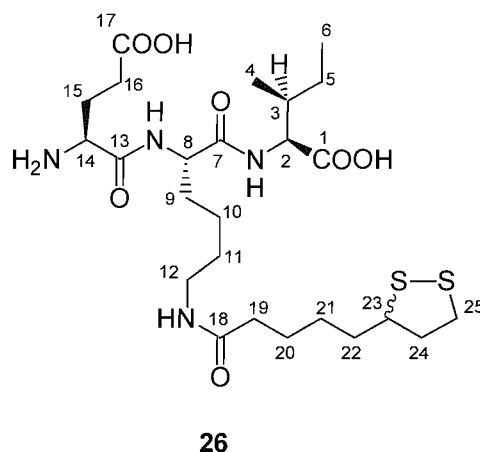
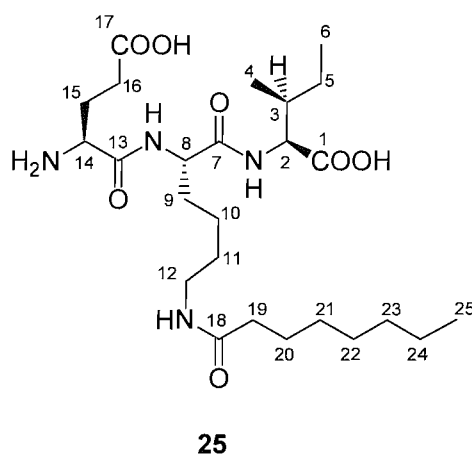**Figure 5.6** Structure of glutamyl-(N6-(DL)-octanoyl)-lysyl isoleucine.

A white solid (10.1 mg, 50 %) R$_f$ 0.17 (reverse phase, acetonitrile/water 1:9); **ES-MS** m/z 577.3 ([M+H]$^{+}$, 100%); **HRES-MS** calculated for C$_{29}$H$_{51}$O$_{9}$N$_{5}$S$_{2}$ [M + H]$^{+}$: 577.2729; found: 577.2724; **^{1}H NMR** (D$_{2}$O): δ 0.69-0.78 (6H, m, H^{4}, H^{6}), 1.01-1.05 (1H, m, H^{5a}), 1.22-1.37 (5H, m, H^{5b}, H^{10}, H^{21}), 1.56-1.71 (6H, m, H^{11}, H^{20}, H^{22}), 1.78-2.00 (5H, m, H^{3}, H^{9}, H^{24}), 2.17-2.23 (2H, m, H^{15}), 2.30 (2H, t, J=7.2 Hz, H^{19}), 2.51 (2H, dt, J=7.6, 2.8 Hz, H^{16}), 3.03 (2H, t, J=7.6 Hz, H^{12}), 3.05-3.10 (2H, m, H^{25}), 3.24 (1H, m, H^{23}), 3.57 (1H, t, J=6.4 Hz, H^{14}), 3.94 (1H, d, J=5.8 Hz, H^{2}), 4.19 (1H, t, J=7.2 Hz, H^{8}).

Preparation of E. coli substrate and product analogue peptides 30 (fig. 5.7)

Octanoyl tripeptide **30** was assembled using the above general procedures. Following deprotection of Fmoc-(L)-Ala-Wang resin (0.75 g, 0.46 mmol/g) Fmoc-(L)-Lys(Dde)-OH (0.55 g, 3 equiv) was attached. The Dde group was then removed and octanoic acid (0.25 mL, 5 equiv) was coupled to the lysine side chain. The peptide synthesis was then completed by the addition of glutamic acid and appropriate deprotection. The peptide was cleaved from the resin to yield 132 mg (83%) of curde octanoyl peptide. The crude peptide was dissolved in water/acetonitrile, 9:1 (2.0 mg/mL of peptide) and 200 µL aliquots were purified by HPLC on a reversed phase Phenomenex Gemini C18 (5 µm, 150 × 10 mm) column with UV detection at 230 nm. The mobile phase was a mixture of 10 mM ammonium bicarbonate (pump A) and acetonitrile (pump B), beginning with 10 % organic and 90 % aqueous for two minutes at 2 mL/min followed by a 15 minute linear gradient to 60 % acetonitrile. This was maintained for 2 minutes followed by return to initial conditions over 1 minute. Each injection was complete in 30 minutes. This was repeated with further aliquots off crude peptide (19 × 200µL) then the required fractions were pooled and the solvent removed by freeze drying.

Aspartyl-(N6-octanoyl)-lysyl alanine **30**

30
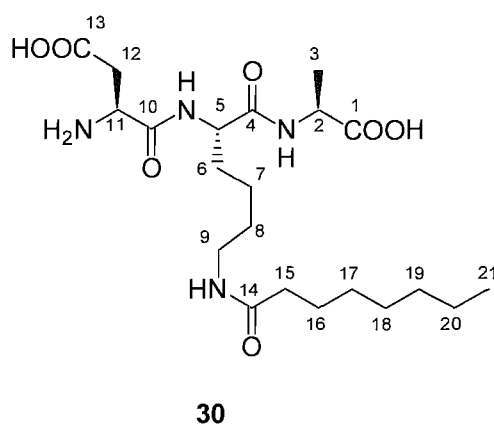
Figure 5.7 Structure of aspartyl-(N6-octanoyl)-lysyl alanine.

A white solid (12.0 mg, 50 %) R_f 0.23 (reverse phase, acetonitrile/water 1:9); **ES-MS** m/z 459.3 ([M+H]$^+$, 100%); **HRES-MS** calculated for $C_{21}H_{38}O_7N_4$ [M+H]$^+$: 459.2813; found 459.2821; ^{1}**H NMR** (400 MHz; D$_2$O) δ 0.91 (3H, t, J = 6.5 Hz, H

^{21}), 1.31-1.33 (8H, m, H^{17}, H^{18}, H^{19}, H^{20}), 1.38 (3H, d, J = 7.3 Hz, H^{3}), 1.44-1.54 (2H, m, H^{7}), 1.56-1.66 (4H, m, H^{8}, H^{16}), 1.73-1.93 (2H, m, H^{6}), 2.27 (2H, t, J = 7.3 Hz), 2.43 (1H, dd, J = 15.8, 8.8 Hz, H^{12a}), 2.66 (1H, dd, J = 15.8, 4.8 Hz, H^{12b}), 3.23 (2H, dt, J = 6.5, 2.5 Hz, H^{9}), 3.77 (1H, dd, J = 8.5, 4.8 Hz, H^{11}), 4.18 (1H, dd, J = 14.6, 7.3 Hz, H^{2}), 4.35 (1H, dd, J = 8.5, 5.8 Hz, H^{5}).

5.4.3   Reconstitution of LipA

Standard procedure for reconstitution of LipA

A NAP-10 column was equilibrated with buffer D (25 mM HEPES, pH 7.5). LipA (1 mL, ~10 mg/mL) was applied to the column then eluted with buffer D. Stock solutions of FeCl$_3$ (100 mM), Na$_2$S.9H$_2$O (30 mM) and DTT (200 mM) in buffer D were prepared. DTT was added (5 mM final concentration) to LipA and the resulting mixture incubated at room temperature for 30 min. Iron chloride (5 mole equiv with respect to LipA) was then added and sodium sulfide (10 mole equiv) was added dropwise. The resultant assay mixtures were incubated at room temperature for 90 min after which time the protein samples were a dark brown colour. Some precipitated iron sulfide was observed and this was removed by centrifugation (10000 rpm, Eppendorf 5415-C microcentrifuge, 5 min). The protein solution was then concentrated using a Millipore microcentrifugal filter (~20 mg/mL). The reconstituted protein was used directly in assays but was desalted using a NAP-10 column prior to iron analysis.

5.4.4   *In vitro* assays for LipA activity with fluorescent substrate 15 (fig. 5.1)

Standard procedure

Reactions were carried out in buffer D (final volume of 250 µL) and contained reconstituted LipA (50 µM), FldA (20 µM), Fpr (5 µM), NADPH (1 mM), SAM tosylate salt (1 mM) and substrate 15 (50 µM) which were added in the order stated. Assays were incubated at 37 °C for 180 mins. Proteins were then precipitated by addition of TCA (0.1 M, 20 µL) and removed by centrifugation (12,000 rpm, Eppendorf 5415-C microcentrifuge, 20 min). The supernatants were taken for HPLC analysis (50 µL aliquots).

Effect of varying protein concentration on lipoyl formation

The standard assay (section 5.7.1) was modified as follows: LipA (50 or 100 μM) was incubated with SAM tosylate salt (1 mM), substrate **15** (50 μM) and FldA (20 μM), Fpr (5 μM), NADPH (1 mM) at 37 °C for 180 mins.

Effect of varying incubation time on lipoyl formation

The standard assay (section 5.7.1) was modified as follows: assays were incubated at 37 °C for 2, 3, 4, 5 or 21 hours. Proteins were then precipitated by addition of TCA (0.1 M, 20 μL) and removed by centrifugation. The supernatants were taken for HPLC analysis (50 μL aliquots).

Effect of using sodium dithionite as reductant on lipoyl formation

The standard assay (section 5.7.1) was modified as follows: FldA (20 μM), Fpr (5 μM), and NADPH (1 mM) were replaced in reaction mixtures by sodium dithionite (1 mM).

5.4.5 *In vitro* assays of *S. solfataricus* LipA with unlabelled substrates 20 (fig. 5.3) and 25 (fig. 5.5)

Standard assay procedure

Reactions were carried out in buffer D (final volume of 250 μL) and contained reconstituted LipA (300 μM), sodium dithionite (1 mM), SAM tosylate salt (1 mM), and either substrate **20** or **25** (150 μM) which were added in the order stated. Assays were incubated at 37 °C for 180 min. Proteins were then precipitated by the addition of TCA (0.1 M, 50 μL), giving a final peptide concentration of 125 μM. Precipitated protein was removed by centrifugation (12,000 rpm, Eppendorf 5415-C microcentrifuge, 20 min), and the supernatants (100 μL) were analyzed by HPLC or LC-MS.

Effect of using FldA/ Fpr/ NADPH as reductant on lipoyl formation

For investigation into the effect of using the FldA/ Fpr/ NADPH on LipA activity the standard assay was modified as follows: sodium dithionite was replaced in reaction mixtures by FldA (20 μM), Fpr (5 μM), and NADPH (1 mM).

Effect of varying LipA concentration on lipoyl formation

The standard assay was modified as follows: reconstituted LipA (75, 150 or 300 μM), sodium dithionite (1 mM), SAM tosylate salt (1 mM), octanoyl substrate **20** (150 μM), were mixed in the order stated and were incubated together at 37 °C for 180 min.

Effect of change in temperature on lipoyl formation

The standard assay was modified as follows: *S. solfataricus* LipA activity reactions were incubated at 6, 23, 37, 50, 60, and 70 °C for 30 min.

5.4.6 Assays using *E.coli* LipA and substrate 24

E. coli LipA was supplied by Dr. Marco Kriek. Assays with *E. coli* LipA used the same general protocol as described above but made use of aspartyl-(N6-octanoyl)-lysyl alanine **30** as substrate.

5.4.7 HPLC analysis of assays

Supernatants were analysed by HPLC using a Hypersil C18 column (5 μm, 150 × 4.6 mm) with UV detection at 230 nm. For analysis of assays using fluorescent peptide **15** (fig. 5.1) excitation and emission wavelengths for fluorescence detection were set at 492 and 517 nm respectively. The mobile phase was a mixture of ammonium bicarbonate (10mM, pump A) and acetonitrile (pump B), beginning with 10% organic and 90% aqueous for 10 min at 1 ml/min, followed by a 25 min linear gradient to 60% acetonitrile. This was maintained for 2 min, followed by a return to initial conditions over 1min. Each injection was complete in 45min. Peak areas were determined by integration using Gilson Unipoint software (Gilson).

5.4.8 LC-MS analysis of assays

Supernatants (100 μL) were analysed by LCMS using a Hypersil C18 column (5 μm, 150 × 4.6mm) column with UV detection at 230 nm. The mobile phase was a mixture of 0.1% TFA in water (Pump A) and 0.1% TFA in acetonitrile (Pump B), beginning with 10% organic and 90% aqueous for 2 min at 0.8 mL/min followed by a 23 min linear gradient to 50% organic followed by a 5 min linear gradient to 100% organic. This was maintained for 5.6 min followed by a return to initial conditions

over 0.1 min. Each injection was complete in 45 min. Mass spectra were recorded using an ES$^+$ ionisation mode.

5.4.9 Construction of standard curve for lipoyl tetrapeptide 21 (fig. 5.4)

Lipoyl tetrapeptides 21 (1 mg) was dissolved in 10 mM ammonium bicarbonate (1 mL) and then standard solutions were prepared in duplicate by dilution of this stock solution (table 5.5). These solutions were then analysed by HPLC using the method for analysis of assays. Peak areas were determined by integration using Gilson Unipoint software (Gilson). The peak areas were then plotted against concentration of peptide to generate standard curves.

[lipoyl tetrapeptide 20] (μM)	Peak Area I	Peak Area II
355	1167369	1200761
284	1028451	1027054
227	888286	869917
182	568814	569241
145	478421	481550
116	347530	352603
93	262650	263518
74	246059	240947

Table 5.5 Peak areas determined by HPLC analysis of standard solutions of lipoyl tetratpeptide 21 (fig. 5.4).

5.4.10 Construction of standard curve for AdoH formation

AdoH was dissolved in 10 mM ammonium bicarbonate (1 mL) and then standard solutions were prepared in duplicate by dilution of this stock solution (table 5.6). These solutions were then analysed by HPLC using the method for analysis of assays. Peak areas were determined by integration using Gilson Unipoint software (Gilson). The peak areas were then plotted against concentration of peptide to generate standard curves.

[AdoH] (μM)	Peak Area I	Peak Area II
500	13296112	12105672
300	8277675	8864021
150	4138801	3757992
100	2759222	3001576
50	1379695	1080821
25	689837	655723
10	275921	210897

Table 5.6 Peak areas determined by HPLC analysis of standard solutions of AdoH.

5.5   Experimental for Chapter 3

5.5.1   Timecourse assays I

Preparation of timecourse reactions of S. solfataricus LipA

Timecourse assay mixtures (125 µL) were prepared by modifying the standard assay procedure as follows: sodium dithionite (1 mM) was added to reconstituted LipA (300 µM) followed by SAM tosylate salt (1 mM) and the resulting mixture incubated at room temperature for 5 min. Reactions were then initiated by addition of octanoyl tripeptide **25** and were incubated at either 23 (room temperature), 30, 37, 45, 50 or 60 °C (water bath). Assays at each temperature were stopped by the addition of TCA (0.1M, 50 µL) at 3 (60 °C only), 5, 10, 15, 20, 25 and 30 mins. Precipitated protein was removed by centrifugation (12,000 rpm, Eppendorf 5415-C microcentrifuge, 20 min), and the supernatants (100 µL) were analyzed by HPLC.

HPLC analysis of timecourse assays I

Supernatants from timecourse assays I were analysed by HPLC using a Hypersil C18 column (5 µm, 150 × 4.6 mm) with UV detection at 230 nm and 259 nm and detector sensitivity set at 0.01. The mobile phase was a mixture of ammonium bicarbonate (10mM, pump A) and acetonitrile (pump B), beginning with 10% organic and 90% aqueous for 10 min at 1 ml/min, followed by a 25 min linear gradient to 60% acetonitrile. This was maintained for 2 min, followed by a return to initial conditions over 1min. Each injection was complete in 55 min. Peak areas were determined by integration using Gilson Unipoint software (Gilson).

Construction of standard curve for octanoyl tripeptide 25 for HPLC analysis

Octanoyl tripeptide **25** (1 mg) was dissolved in 10 mM ammonium bicarbonate (1 mL) and then standard solutions were prepared in duplicate by dilution of this stock solution (table 5.7). These solutions were then analysed by HPLC using the method for analysis of assays with UV detection at 230 nm and detector sensitivity set at 0.01. Peak areas were determined by integration using Gilson Unipoint software (Gilson). The peak areas were then plotted against concentration of peptide to generate standard curves.

[octanoyl tripeptide 25] (µM)	Peak Area I	Peak Area II
200	484470	450427
175	426773	397975
150	361227	382388
125	297506	264460
100	237696	226997
75	162180	164337
50	108836	105942
25	63666	67878

Table 5.7 Peak areas determined by HPLC analysis of standard solutions of octanoyl tripeptide 25.

Construction of standard curve for lipoyl tripeptide 26 for HPLC analysis

Lipoyl tripeptide 26 (1 mg) was dissolved in 10 mM ammonium bicarbonate (1 mL) and then standard solutions were prepared in duplicate by dilution of this stock solution (table 5.8). These solutions were then analysed by HPLC using the method for analysis of assays with UV detection at 230 nm and detector sensitivity set at 0.01. Peak areas were determined by integration using Gilson Unipoint software (Gilson). The peak areas were then plotted against concentration of peptide to generate standard curves.

[lipoyl tripeptide 26] (µM)	Peak Area I	Peak Area II
300	716827	780753
250	610653	665612
200	437422	476790
150	428932	467536
100	316782	345292
75	302033	329216
50	132978	144946
25	77613	84598

Table 5.8 Peak areas determined by HPLC analysis of standard solutions of lipoyl tripeptide 26.

Construction of standard curve for AdoH formation

AdoH was dissolved in 10 mM ammonium bicarbonate (1 mL) and then standard solutions were prepared in duplicate by dilution of this stock solution (table 5.9). These solutions were then analysed by HPLC using the method for analysis of assays with UV detection at 259 nm and detector sensitivity set at 0.01. Peak areas were determined by integration using Gilson Unipoint software (Gilson). The peak areas were then plotted against concentration of peptide to generate standard curves.

[AdoH] (µM)	Peak Area I	Peak Area II
500	50738016	55984196
300	30919480	33449414
150	9347840	9324719
100	6766691	6624913
50	3565325	3206554
25	1605250	1644989
10	904736	683980

Table 5.9 Peak areas determined by HPLC analysis of standard solutions of AdoH.

5.5.2 Timecourse assays II

Preparation of timecourse reactions of S. solfataricus LipA

Reactions were carried out in 10 mM ammonium bicarbonate pH 7.5 (final volume of 250 μL). Sodium dithionite (1 mM) was added to reconstituted LipA (300 μM) followed by SAM tosylate salt (1 mM) and the resulting mixture incubated at room temperature for 5 min. Reactions were then initiated by addition of octanoyl tripeptide **25** and were incubated at either 23 (room temperature), 30, 40, 50 or 60 °C (water bath). Assays at each temperature were stopped by the addition of TFA (20 μL) at 0.5, 1.0, 2.0, 4.0, 6.0, 8.0, 10.0 and 30.0 mins. Precipitated protein was removed by centrifugation (12,000 rpm, Eppendorf 5415-C microcentrifuge, 20 min), and the solvent removed by freeze drying to yield a brown coloured residue.

Derivatisation of assays with iodoacetamide

Residues of freeze dried assay mixtures were dissolved in buffer E (10mM ammonium bicarbonate, 1% NH_3 (aq), pH = 11) (300 μL) under anaerobic conditions. TCEP in buffer E (7.4 μL, 35 mM, 7eq with respect to peptide concentration) was added and mixtures were left for 90 mins. Iodoacetamide in buffer E (14 μL, 55 mM, 20 eq with respect to peptide concentration) was then added and the reaction left for a further 3 hours. Mixtures were then analysed by LC-MS.

LC-MS analysis of iodoacetamide derivatised timecourse assays

Derivatised assays (100 μL) were analysed by LCMS using a Hypersil C18 column (5 μm, 150 × 4.6mm) column with UV detection at 230 nm. The mobile phase was a mixture of 0.1% TFA in water (Pump A) and 0.1% TFA in acetonitrile (Pump B), beginning with 10% organic and 90% aqueous for 7 min at 0.8 mL/min followed by a 23 min linear gradient to 50% organic followed by a 5 min linear gradient to 100% organic. This was maintained for 5 min followed by a return to initial conditions over 1 min. Each injection was complete in 50 min. Mass spectra were recorded using an ES^+ ionisation mode. Peak areas were determined from the UV trace by integration using Gilson Unipoint software (Gilson). The peak areas were then plotted against concentration of peptide to generate standard curves.

Derivatised assays (100 µL) were analysed by HPLC using the method described for LC-MS analysis but with the mass spectrometer disconnected.

6.4.4 Derivatisation of lipoyl tripeptide with iodoacetamide
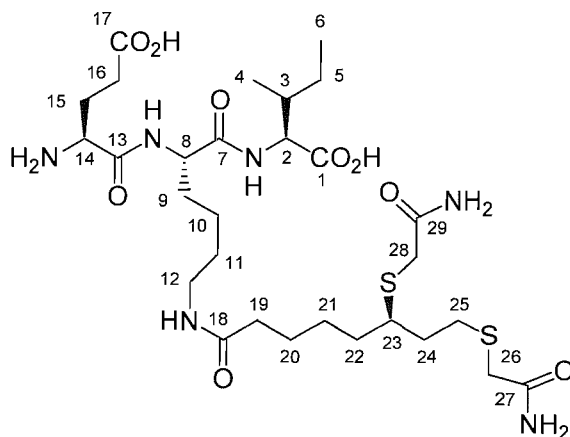
33

Figure 6.1 Structure of synthetic standard of iodoacetamide derivatised lipoyl tripeptide.

Lipoyl tripeptide **26** (10 mg, 17 µmol) was dissolved in buffer E (10mM ammonium bicarbonate, 1% NH3 (aq), pH = 11) (5 mL) under anaerobic conditions and was then treated with TCEP in buffer E (85 µmol). After 1 h iodoacetamide in buffer E (170 µmol) was added and the reaction stirred at room temperature for 3 h. The mixture was freeze dried and the crude product was dissolved in water/acetonitrile, 9:1 (1.0 mg/mL of peptide) then 200 µL aliquots were purified by HPLC on a reversed phase Phenomenex Gemini C18 (5 µm, 150 × 10 mm) column with UV detection at 230 nm. The mobile phase was a mixture of 10 mM ammonium bicarbonate (pump A) and acetonitrile (pump B), beginning with 10 % organic and 90 % aqueous for two min at 2 mL/min followed by a 15 min linear gradient to 60 % acetonitrile. This was maintained for 2 minutes followed by return to initial conditions over 1 min. Each injection was complete in 30 min. This was repeated with further aliquots off crude peptide (19 × 200µL) then the required fractions were pooled and the solvent removed by freeze drying to yield a white solid (1.8 mg, 15 %); R_f 0.23 (reverse phase, acetonitrile/water 1:4); **ES-MS**: m/z 693.3 ([M+H]$^+$, 100%); **HRES-MS** calculated for $C_{29}H_{53}O_9N_5$ [M+H]: 693.3283; found 693.3294 ^{1}H NMR (400 MHz; D$_2$O); δ 0.92-0.97 (6H, m, H^4, H^6), 1.23 (1H, m, H^{5a}), 1.40-1.53 (5H, m, H^{5b}, H^{10}, H^{21}), 1.56-1.71 (6H, m, H^{11}, H^{20}, H^{22}), 1.78-2.00 (5H, m, H^3, H^9,

H^{24}), 2.17-2.23 (2H, m, H^{15}), 2.30 (2H, t, J=7.2 Hz, H^{19}), 2.51 (2H, dt, J=7.6, 2.8 Hz, H^{16}), 2.81 (2H, t, J=7.6 Hz, H^{25}), 2.93 (1H, m, H^{23}), 3.24 (2H, t, J=6.4 Hz, H^{12}), 3.35 (4H, d, J=4.8 Hz, H^{26}, H^{28}), 4.14 (1H, t, J=6.4 Hz, H^{14}), 4.23 (1H, d, J=6.4 Hz, H^{2}), 4.45 (1H, t, J=7.2 Hz, H^{8}).

Construction of standard curve for octanoyl tripeptide 25

Octanoyl tripeptide **25** (1 mg) was dissolved in 10 mM ammonium bicarbonate (1 mL) and then standard solutions were prepared in duplicate by dilution of this stock solution (table 6.4). These solutions were then analysed by LCMS using the method for analysis of derivatised assays with UV detection at 230 nm and detector sensitivity set at 0.002. Peak areas were determined by integration using Gilson Unipoint software (Gilson). The peak areas were then plotted against concentration of peptide to generate standard curves.

[octanoyl tripeptide **25**] (μM)	Peak Area I	Peak Area II
200	2284649	2259017
175	2042341	2000791
150	1795271	1704331
125	1390519	1301355
100	1161473	1102572
75	871648	832576
50	620864	650271
25	317534	385881

Table 5.10 Peak areas determined by LCMS analysis (with UV detection at 230 nm) of standard solutions of octanoyl tripeptide **25**. Peak areas are derived by integration of the UV trace.

Construction of standard curve for derivatised lipoyl tripeptide 38

Iodoacetamide derivatised lipoyl tripeptide **38** (1 mg) was dissolved in 10 mM ammonium bicarbonate (1 mL) and then standard solutions were prepared in duplicate by dilution of this stock solution (table 5.11). These solutions were then analysed by LCMS using the method for analysis of derivatised assays with UV detection at 230n m and detector sensitivity set at 0.002. Peak areas were determined

by integration using Gilson Unipoint software (Gilson). The peak areas were then plotted against concentration of peptide to generate standard curves.

[derivatised lipoyl tripeptide **38**] (μM)	Peak Area I	Peak Area II
300	6637781	7098044
250	5682323	5845160
200	4421488	4550635
175	4029228	4102201
150	3418812	3399360
125	2897613	2917713
100	2702381	2746664
75	2358578	2136334
50	1342858	1343221
25	778658	775066

Table 5.11 Peak areas determined by LCMS analysis (with UV detection at 230 nm) of standard solutions of derivatised lipoyl tripeptide **38**. Peak areas are derived by integration of the UV trace.

5.5.3 Kinetic analysis of timecourse data

Approximation of lipoyl formation quantified from underivatised assays to a single first order process

Changes in lipoyl peptide concentration at 23, 30, 37, 45, 50 and 60 °C quantified by HPLC analysis of underivatised timecourse assays I were approximated to the single first order process shown in scheme 5.3 using DynaFit software (9) (BioKin Ltd., Pullman, WA). Lipoyl peptide concentrations were simulated based on variation of a single rate constant (k_{obs}) for the overall reaction. The initial concentration of octanoyl peptide starting material was set at 125 μM (appendix 1).

$$\text{LipA:SAM:}\mathbf{25} \xrightarrow{\ k_{obs}\ } \mathbf{26}$$

Scheme 5.3 Conversion of an octanoyl substrate to a lipoyl product by *S. solfataricus* LipA with rate constant k_{obs}.

Approximation of lipoyl formation quantified from iodoacetamide derivatised assays to a single first order process

Changes in derivatised lipoyl peptide **38** (fig. 5.8) concentration at 23, 30, 40, 50 and 60 °C quantified by LC-MS or HPLC analysis of iodoacetamide derivatised timecourse assays II were approximated to the single first order process shown in scheme 5.3 using DynaFit software (9) (BioKin Ltd., Pullman, WA). Derivatised lipoyl peptide **38** concentrations were simulated based on variation of a single rate constant (k_{obs}) for the overall reaction. The initial concentration of octanoyl peptide starting material was set at 120 μM (appendix 1).

Approximation of change in octanoyl susbtrate concentration to a single first order process

Changes in octanoyl peptide **25** concentration (quantified from either underivatised or iodoacetamide derivatised assays) at each temperature were approximated to the single first order process shown in scheme 5.4 using DynaFit software (9) (BioKin Ltd., Pullman, WA). Lipoyl peptide concentrations were simulated based on variation of a single rate constant , k_{obs1}, for the conversion of the substrate to a 6MT

intermediate via sulfur insertion at C6. The initial concentration of octanoyl peptide starting material was set at 125 µM or 120 µM for data obtained from underivatised or iodoacetamide derivatised assays respectively (appendix 1).

$$\text{LipA:SAM:}\mathbf{25} \xrightarrow{\ k_{obs1}\ } \text{LipA:}\mathbf{28}$$
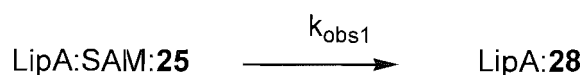
Scheme 5.4 Conversion of LipA bound octanoyl peptide **25** (fig. 3.1) to protein bound 6MT peptide **28** (fig. 3.1).

Approximation of change in lipoyl concentration to two first order processes

Changes in derivatised lipoyl peptide **38** concentration at 23, 30, 40, 50 and 60 °C quantified by LC-MS or HPLC analysis of iodoacetamide derivatised timecourse assays II were approximated to two first order process shown in scheme 5.5 using DynaFit software (*9*) (BioKin Ltd., Pullman, WA). Values for k_{obs1} were set at those derived by analysis of octanoyl peptide concentrations from iodoacetamide derivatised assays (table 5.12). Derivatised lipoyl peptide **38** (fig. 6.1) concentrations were then simulated by varying the rate constant k_{obs2} for the formation of lipoyl product from an intermediate 6MT species. The initial concentration of octanoyl peptide starting material was set at 120 µM (appendix 1).

$$\text{LipA:SAM:}\mathbf{25} \xrightarrow{\ k_{obs1}\ } \text{LipA:}\mathbf{28}$$

$$\text{LipA:}\mathbf{28} \xrightarrow{\ k_{obs2}\ } \mathbf{26}$$
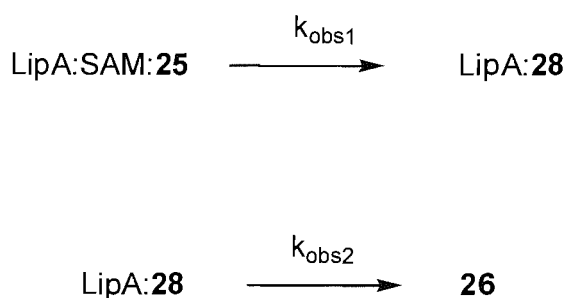
Scheme 5.5 Stepwise formation of lipoyl product by *S. solfataricus* LipA from a protein bound octanoyl peptide substrate.

T	$k_{obs1} \times 10^{-4}$
(°C)	(s^{-1})
23	10.1
30	19.5
40	27.7
50	34.5
60	66.3

Table 6.6 Rate constants (k_{obs1}) calculated for loss of octanoyl peptide **25** over temperature range 23-60 °C. Derived from data obtained from derivatised timecourse assays.

Approximation of change in AdoH concentration to two first order processes

Changes in derivatised AdoH concentration at 23, 30, 40, 50 and 60 °C quantified by HPLC analysis of underivatised timecourse assays I were approximated to two first order process shown in scheme 5.6 using DynaFit software (*9*) (BioKin Ltd., Pullman, WA). Values for k_{obs1} were set at those derived by analysis of octanoyl peptide concentrations from underivatised assays (table 5.13). AdoH concentrations were then simulated by varying the rate constant k_{obs2} for the formation of lipoyl product from an intermediate 6MT species. The initial concentration of octanoyl peptide starting material was set at 150 μM (appendix 1).

$$\text{LipA:SAM:}\textbf{25} \xrightarrow{\ k_{obs1}\ } \text{LipA:}\textbf{28} \ + \ \text{AdoH}$$

$$\text{LipA:}\textbf{28} \xrightarrow{\ k_{obs2}\ } \textbf{26} \ + \ \text{AdoH}$$
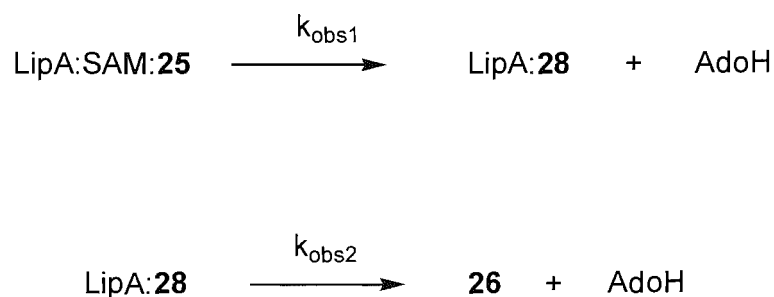
Scheme 5.6 Formation of AdoH by *S. solfataricus* LipA.

T (°C)	$k_{obs1} \times 10^{-4}$ (s⁻¹)
23	9.3
30	15.8
37	24.0
45	25.8
50	42.5
60	60.2

Table 5.13 Rate constants (k_{obs1}) calculated for loss of octanoyl peptide **25** over temperature range 23-60 °C. Derived from data obtained from underivatised timecourse assays.

5.6   Experimental for Chapter 4

5.6.1   UV spectroscopy of *S. solfataricus* LipA

As isolated LipA

Samples of purified *S. solfataricus* LipA (1 mL, ~10 mg/mL) were applied to a NAP-10 column which had been equilibrated with buffer D (25 mM HEPES, pH 7.5). LipA was eluted in buffer D (1.5 mL) and then diluted with further buffer (0.5 mg/mL LipA). The resulting solution was transferred to a quartz cuvette and the UV spectrum recorded.

Reconstituted LipA

S. solfataricus LipA was reconstituted using the standard method The reconstituted protein was then applied to a NAP-10 column which had been equilibrated with buffer D (25 mM HEPES, pH 7.5). LipA was eluted in buffer D (1.5 mL) and then diluted with further buffer (0.5 mg/mL LipA). The resulting solution (1 mL) was transferred to a quartz cuvette and the UV spectrum recorded.

Reconstituted LipA in the presence of SAM

S. solfataricus LipA was reconstituted using the standard method. The reconstituted protein was then applied to a NAP-10 column which had been equilibrated with buffer D (25 mM HEPES, pH 7.5). LipA was eluted in buffer D (1.5 mL) and then diluted with further buffer (0.5 mg/mL LipA). SAM (52 mM, 1.9 µL, final concentration 100 µM) was added then the resulting solution (1 mL) was transferred to a quartz cuvette and the UV spectrum recorded.

Reconstituted LipA under turnover conditions

S. solfataricus LipA was reconstituted using the standard method. The reconstituted protein was then applied to a NAP-10 column which had been equilibrated with buffer D (25 mM HEPES, pH 7.5). LipA was eluted in buffer D (1.5 mL) and then diluted with further buffer (0.5 mg/mL LipA). SAM (52 mM, 1.9 µL, final concentration 100 µM) and octanoyl tripeptide **25** (9.7 mM, 3.0 µL, final concentration 30 µM) was added. This was followed by the addition of sodium dithionite (5.7 mM, 1.7 µL, final concentration 100 µM) and then the resulting

solution (1 mL) was transferred to a quartz cuvette and the UV spectrum recorded at 2, 4, 10, 30 and 60 mins.

5.6.2 EPR spectroscopy of *S. solfataricus* LipA

Stock solutions of sodium dithionite (22 mM), SAM (46 mM) and octanoyl tetrapeptide **20** (16 mM) in anaerobic buffer D were prepared. These were then used in preparation of samples for EPR spectroscopy.

Reconstituted LipA

S. solfataricus LipA (1 mL, 10 mg/mL) was reconstituted using the standard method. A sample of reconstituted LipA (6 mg/mL, 200 µL) was then placed in an EPR tube. The sample was sealed and then removed from the glovebox and frozen with liquid nitrogen. EPR spectra were then recorded at 10 K, 30 K and 60 K under the following conditions: microwave frequency, 9.4340 GHz; microwave power, 2 milliwatts; and field modulation amplitude, 0.4 milliteslas.

Reconstituted LipA following reduction with sodium dithionite

S. solfataricus LipA (1 mL, 10 mg/mL) was reconstituted using the standard method. Sodium dithionite (9 µL, final concentration 1 mM) was then added to a sample of reconstituted LipA (7 mg/mL, 200 µL) and the resulting solution incubated at room temperature for 30 min. The reduced sample was then placed in an EPR tube. The sample was sealed and then removed from the glovebox and frozen with liquid nitrogen. EPR spectra were then recorded at 10 K, 30 K and 60 K under the following conditions: microwave frequency, 9.4340 GHz; microwave power, 2 milliwatts; and field modulation amplitude, 0.4 milliteslas.

Reconstituted LipA in the presence of sodium dithionite and SAM

S. solfataricus LipA (1 mL, 10 mg/mL) was reconstituted using the standard method. The reconstituted LipA (1.2 mL, 7 mg/mL) was split into 6 aliquots (200 µL) and 0.2, 0.5, 1.0, 2.0, 5.0 or 5.0 molar equivalents of SAM with respect to LipA were added. Sodium dithionite (9 µL, final concentration 1 mM) was then added and the resulting solutions were incubated at room temperature for 30 min. Samples were then each placed in an EPR tube which were sealed and then removed from the glovebox and frozen with liquid nitrogen. EPR spectra were then recorded at 10 K, under the

following conditions: microwave frequency, 9.4340 GHz; microwave power, 2 milliwatts; and field modulation amplitude, 0.4 milliteslas.

Reconstituted LipA under turnover conditions

S. solfataricus LipA (1 mL, 10 mg/mL) was reconstituted using the standard method. Reconstituted LipA (0.8 mL, 7 mg/mL) was split into 4 aliquots (200 µL) then SAM (7.6 µL, 2 molar equivalents with respect to LipA) and octanoyl tetrapeptide **20** (27 µL, 10 molar equivalents with respect to LipA) were added. Reactions were initiated by addition of sodium dithionite (9 µL, final concentration 1 mM) and samples were then each placed in an EPR tube which were sealed. Samples were incubated at room temperature for 0, 2, 5 or 20 minutes. and then removed from the glovebox and frozen with liquid nitrogen. EPR spectra were then recorded at 10 K, under the following conditions: microwave frequency, 9.4340 GHz; microwave power, 2 milliwatts; and field modulation amplitude, 0.4 milliteslas.

5.6.3 Assays using ^{34}S reconstituted LipA

Preparation of sodium 34-sulfide

$Na_2{}^{34}S$ was prepared according to the method to described in (*10*). Sodium (28 mg, 1.21 mmol) was placed in the reaction vessel which was maintained under a nitrogen atmosphere. This was cooled in an acetone/CO_2 bath and ammonia (~50 mL) was condensed onto the sodium to give a dark blue solution. Elemental 34-S (42 mg, 1.21 mmol) was then added and after 10 min the blue colour was observed to disappear and a white precipitate could be seen. Ammonia was allowed to evaporate overnight and then the reaction vessel was evacuated under vacuum to yield a white solid which was stored at -20 °C until use in reconstitution of LipA.

Preparation of apo LipA

Apo-LipA was prepared according to the method described previously for preparation of apo-BioB (*11*). A stock solution of EDTA (50 mM) in 25 mM HEPES adjusted to pH 8.0 was prepared and then transferred to the glovebox where it was degassed overnight. A stock solution of sodium dithionite (240 mM) in anaerobic buffer D was also prepared. EDTA (460 µL, 23 mmol) and sodium dithionite (103 µL, 23 mmol) were then added to purified *S. solfataricus* LipA (3 mL, 5 mg/mL, 0.45 mmol) and the resulting mixture incubated at room temperature for 2 h. After this time the UV spectrum of the LipA solution was recorded to confirm decomposition of the iron sulfur clusters.

Reconstitution with $Na_2{}^{34}S$

Apo-LipA was reconstituted according to the standard method (section 5.6) which was modified by replacing $Na_2{}^{32}S$ with $Na_2{}^{34}S$. Formation of iron sulfur cluster(s) was monitored by UV spectroscopy.

Assay using labelled ^{34}S LipA

^{34}S labelled *S. solfataricus* LipA was prepared by removal of the iron sulfur cluster then reconstitution with $Na_2{}^{34}S$ using the methods described above. The resulting sample was then treated again with EDTA and dithionite before repeating the reconstitution step. Reconstituted LipA was then used in assays which made use of

octanoyl tripeptide **25** as a substrate and were prepared according to the standard assay method.

5.7   References

(1)   Bradford, M. M. (1976) A rapid and sensitive method for the quantitation of microgram quantities of protein utilizing the principle of protein-dye binding. *Anal. Biochem. 72*, 248-54.

(2)   Fish, W. W. (1988) Rapid colorimetric micromethod for the quantitation of complexed iron in biological samples. *Methods Enzymol. 158*, 357-64.

(3)   Beinert, H. (1983) Semi-micro methods for analysis of labile sulfide and of labile sulfide plus sulfane sulfur in unusually stable iron sulfur proteins. *Anal. Biochem. 131*, 373-378.

(4)   Bycroft, B. W., Chan, W. C., Chhabra, S. R., Teesdale-Spittle, P. H., and Hardy, P. M. (1993) A novel amino protection deprotection procedure and its application in solid phase peptide-synthesis. *J. Chem. Soc., Chem. Com.*, 776-777.

(5)   Atherton, E., Sheppard, R. C. (1989) *Solid phase peptide synthesis a practicle approach*, IRL Press at Oxford University Press.

(6)   Wang, S. S. (1973) p-alkoxybenzyl alcohol resin and p-alkoxybenzyloxycarbonylhydrazide resin for solid phase synthesis of protected peptide fragments. *J. Am. Chem. Soc. 95*, 1328-33.

(7)   Diaz-Mochon, J. J., Bialy, L., and Bradley, M. (2004) Full orthogonality between Dde and Fmoc: the direct synthesis of PNA--peptide conjugates. *Org. Lett. 6*, 1127-9.

(8)   Coste, J., Le-Nguyen, D., and Castro, B. (1990) PyBOP:A New Peptide coupling reagent devoid of toxic by-product. *Tetrahedron Lett. 31*, 205-208.

(9)   Kuzmic, P. (1996) Program DYNAFIT for the analysis of enzyme kinetic data: application to HIV proteinase. *Anal. Biochem. 237*, 260-73.

(10)   Fehér, F. (1963) *Handbook of Preparative Inorganic Chemistry*, Vol. 1, 2nd ed.

(11)   Tse Sum Bui, B., Florentin, D., Fournier, F., Ploux, O., Mejean, A., and Marquet, A. (1998) Biotin synthase mechanism: on the origin of sulphur. *FEBS Lett. 440*, 226-30.

Appendix 1 – Scripts used for fitting timecourse data using DYNAFIT

1.   Overall lipoyl formation

For data from underivatised assays

```
[task]

    data = progress
    task = fit
    model = overall lipoyl

[mechanism]

  OCT* ---> LIP          :     kobs


[constants]

    kobs = 0.002 ?,

[concentrations]

    OCT*= 125,

[progress]

    directory ./examples/lipoyl
    extension txt

    file lip60      | response LIP = 1


[output]

    directory ./examples/lipoyl/output

[settings]

    <Filter>      | SetSigZero = No    | TMax = 50000
    <Simulate>    | Interpolate = Yes  | Increment = 10

[end]
```

For data from iodoacetamide derivatised assays

```
[task]

    data = progress
    task = fit
    model = overall lipoyl

[mechanism]

  OCT* ---> LIP        :     kobs


[constants]

    kobs = 0.002 ?,

[concentrations]

    OCT*= 120,

[progress]

    directory ./examples/lipoyl
    extension txt

    file lip60der      | response LIP = 1


[output]

    directory ./examples/lipoyl/output

[settings]

    <Filter>      | SetSigZero = No    | TMax = 50000
    <Simulate>    | Interpolate = Yes  | Increment = 10

[end]
```

2.   Change in octanoyl concentration

For data from underivatised assays

```
[task]

    data = progress
    task = fit
    model = octanoyl

[mechanism]

  LipA*O ---> LipA6MT          :    ko1


[constants]

    ko1 = 0.002?,

[concentrations]

    LipA*O =125,

[progress]

    directory ./examples/octanoyl
    extension txt

    file oct60     | response LipA*O = 1

[output]

    directory ./examples/octanoyl/output

[settings]

    <Filter>     | SetSigZero = No    | TMax = 50000
    <Simulate>   | Interpolate = Yes  | Increment = 10

[end]
```

For data from iodoacetamide derivatised assays

```
[task]

    data = progress
    task = fit
    model = octanoyl

[mechanism]

  LipA*O ---> LipA6MT           :     ko1


[constants]

    ko1 = 0.002 ?,

[concentrations]

    LipA*O =120,

[progress]

    directory ./examples/octanoyl
    extension txt

    file oct60der      | response LipA*O = 1


[output]

    directory ./examples/octanoyl/output

[settings]

    <Filter>      | SetSigZero = No     | TMax = 50000
    <Simulate>    | Interpolate = Yes   | Increment = 10

[end]
```

3. Lipoyl formation via a two step process

For data from derivatised assays

```
[task]

    data = progress
    task = fit
    model = lipoyl two step

[mechanism]

  LipA*O ---> LipA6MT          :    ko1
LipA6MT ---> LIP               :    ko2


[constants]

    ko1 = 0.00663 , ko2 = 0.002 ?

[concentrations]

    LipA*O= 120,

[progress]

    directory ./examples/lipoyl
    extension txt

    file lip60der      | response LIP = 1

[output]

    directory ./examples/lipoyl/output

[settings]

    <Filter>       | SetSigZero = No     | TMax = 50000
    <Simulate>     | Interpolate = Yes   | Increment = 10

[end]
```

4. AdoH formation via a two step process

For data from derivatised assays

```
[task]

    data = progress
    task = fit
    model = lipoyl two step

[mechanism]

  SAM*O ---> AdoH + *6MT          :    ko1
SAM*6MT ---> AdoH + LIP           :    ko2


[constants]

    ko1 = 0.00602 , ko2 = 0.002?

[concentrations]

    SAM*O= 125,

[progress]

    directory ./examples/lipoyl
    extension txt

    file AdoH60      | response AdoH = 1
       .

[output]

    directory ./examples/lipoyl/output

[settings]

    <Filter>      | SetSigZero = No    | TMax = 50000
    <Simulate>    | Interpolate = Yes  | Increment = 10

[end]
```